LOW TEMPERATURE HYDROGEN PRODUCTION AND HABITABILITY OF A HYPERALKALINE SERPENTINITE AQUIFER IN THE SAMAIL OPHIOLITE

By

HANNAH MARIE MILLER
B.S., University of Notre Dame, 2012

A thesis submitted to the Faculty of the Graduate School of the University of Colorado
in partial fulfillment of the requirement for the degree of
Doctor of Philosophy
Department of Geological Sciences
2017

Examining Committee:
Alexis S. Templeton, Chair
G. Lang Farmer
Peter E. Kelemen
Stephen J. Mojzsis
John R. Spear

This thesis entitled:

Low temperature hydrogen production and habitability of hyperalkaline serpentine aquifer in Samail ophiolite

written by Hannah Marie Miller

has been approved for the Department of Geological Sciences

_____

Alexis S. Templeton, Thesis Advisor

_____

G. Lang Farmer, Committee Member

_____

Stephen J. Mojzsis, Committee Member

Date_____

The final copy of this thesis has been examined by the signatories, and we find that both the content and the form meet acceptable presentation standards of scholarly work in the above mentioned discipline.

ABSTRACT

Low temperature hydrogen production and habitability of a hyperalkaline serpentinite aquifer in the Samail ophiolite

Hannah Marie Miller (Ph.D., Geological Sciences)

Thesis directed by Associate Professor Alexis S. Templeton

Continental serpentinizing systems, such as the Samail Ophiolite in Oman, are excellent locations to study low-temperature water/rock reactions leading hydrogen production. Hydrogen is a strong electron donor that, along with electron acceptors such as CO_2 or SO_4^{2-}, can sustain microbial life. I performed experimental and analytical work with partially serpentinized peridotite from Oman to determine that Fe(II)-bearing brucite is a key reactive mineral leading to hydrogen production. At 100°C and fluid compositions similar to those found in shallow serpentinizing aquifers, we experimentally observed the destabilization of Fe(II)-brucite to produce hydrogen and Fe(III)-bearing magnetite. These reactions occur quickly over a period of several months. H_2 production is associated with CO_2 reduction into low weight molecular acids, and perhaps solid carbonaceous material. This experimental work was paired with a field study of drill cuttings obtained from subsurface rocks in contact with serpentinizing fluids rich in H_2 and CH_4 at depths ranging from 17m to 262m. Mineralogical and geochemical analysis of drill cuttings showed a similar trend of decreased brucite abundance and increased magnetite formation as the rock became more altered near the surface. CH_4 sampled from subsurface fluids has $\delta^{13}C$ values as positive as +3‰. Although these $\delta^{13}C$ values would traditionally be interpreted as abiotic, we believe it is possible microbial activity may contribute to the CH_4 isotope values because of the presence of methanogens and methanotrophs in the subsurface fluids, as determined by 16S rRNA analysis. Thus, we isolated *Methanobacterium* was from the same subsurface fluids in Oman to investigate the carbon isotope fractionation factors associated

with methanogenesis at high pH, probing if microbiology could be responsible for the unique isotope values found in the fluids. Carbon isotope fractionation during methanogenesis by *Methanobacterium* under conditions of carbon-limitation at pH ~9 is suppressed, leading to $\delta^{13}C_{CH4}$ values as high as -28‰. Such $\delta^{13}C_{CH4}$ values may be mistakenly interpreted as abiotic based on current classifications of "biotic" versus "abiotic" methane isotopic signatures. Thus, we need to carefully evaluate the carbon cycling pathways operating in serpentinizing systems and not automatically assume abiotic or biotic origins for CH_4 until the system is well characterized.

ACKNOWLEDGEMENTS

I am thankful to the entire Templeton lab group for their support. Thanks especially to Lisa Mayhew for being my mentor at the start of my PhD while Alexis was on sabbatical. Lisa graciously shared her hard-earned knowledge about water/rock reactions, culturing methanogens, and synchrotron experimental analysis. Her friendly advice and caring attitude throughout my PhD has made the process much more enjoyable. Nabil Chaudhry was immensely helpful in cultivating methanogens from Oman and running innumerable samples on the GC. Eric Ellison made daily laboratory operations run smoothly and was is an excellent good consultant on data analysis. Alexis has also made my experience here memorable; I respect and admire her not only for her scientific prowess, but also for her integrity in dealing with her students, researchers and colleagues. I am privileged to have worked with such an inspiring woman in science who has cultivated a laboratory group of similarly intelligent and most importantly, kind, people. I feel blessed to have been a member of such a positive work environment and know it will not be easily matched in the future.

I would like to thank the Boulder School of Community for continually pushing me to find deeper meaning in my work. Our weekly Monday meetings helped me to realize that all reality is positive, even when it involves failed experiments, incomplete datasets, and interminable waits for data. This search for meaning has further been augmented by the Graduate Christian Fellowship at CU. Studying the Bible with graduate students gave me a community to commiserate and struggle with in light of our faith, while also exposing me to the diversity of graduate studies on campus and making me fully appreciate my choice in studies.

My parents have always supported my education and valued learning. I am indebted to them for instilling in me a love for reading that blossomed into a general love for learning. As a

goal-oriented independent child, I know I was challenging, but I am thankful and grateful for their love and support. My sisters, Abby and Katie, have always inspired me with their academic abilities, and they gave me a competitive push to surpass their accomplishments. Learning about their respective challenges as mothers has given me good perspective during my PhD. I am excited to share my love of learning and science with my nieces and nephews. Ben has provided me with unwavering support and loyalty, never doubting me or my abilities. He is my go-to adventure partner who has helped me to strengthen my confidence in the mountains, which then translates to my research. He never fails to provide me with random expired food, or steeply discounted Patagonia clothing items to augment my graduate stipend.

I am grateful that I was fully funded, both by the Geology Department and the Department of Energy to pursue basic research. Although I don't intend to continue on the academic path, it truly is amazing that I have been paid for five years to pursue, in its most basic form, truth. Although I intend to do that in more nuanced forms in my future, this has been a special season of life.

CONTENTS

LIST OF TABLES

2. Fractionation factor calculations

LIST OF FIGURES

CHAPTER 1

Introduction

1. Low-temperature hydrogen production by water/rock reactions

Mafic and ultramafic rocks rich in reduced iron generate hydrogen gas as they react with percolating fluids through the process of serpentinization. Hydrogen production from serpentinization occurs extensively and rapidly at high temperatures (>120°C) in mid-ocean ridge environments (Fyfe, 1974; Macdonald and Fyfe, 1985). The reaction products at high temperatures are well characterized and consist of serpentine, brucite, magnetite, and hydrogen (McCollom and Seewald, 2001; Bach et al., 2006; McCollom and Bach, 2009). However, serpentinization can also occur at low temperatures, <120°C, at off-axis ridges or continental ophiolite systems (Barnes et al., 1978; Kelley et al., 2001). At these low temperatures, microbial life can subsist off the water/rock reactions by consuming hydrogen, which is a strong electron donor (Sleep et al., 2004; Nealson et al., 2005; Mayhew et al., 2013), along with electron acceptors like sulfate or nitrate in the fluids. However, the pertinent hydrogen-generating reactions and mechanisms at low temperatures are not well-constrained. These reactions are being investigated in both the laboratory and field in order to better understand the interplay between water/rock reactions and subsurface microbial ecosystems.

1.1 Field sites generating hydrogen at low temperatures

Various environments generate hydrogen from water/rock reactions that can fuel subsurface life. Mid-ocean ridge basalts generate hydrogen from the oxidation of Fe^{2+} to Fe^{3+} in magnetite by the reduction of H_2O during cooling of the magma body (Holloway and O'DAY, 2000). Cold seawater circulating through mid-ocean ridge basalts drives oxidation of Fe in the ocean crust accompanied by hydrogen production (Stein et al., 1995; Bach and Edwards, 2003). These hydrothermal systems (200-400°C) are characterized by iron and sulfide-rich chimneys,

black smokers, which host microbial life on their cooler flanks. Life in hydrothermal systems subsists by harnessing the energy found in the disequilibrium between the hydrothermal fluids containing CO_2, H_2S, H_2, and CH_4 and surrounding seawater (Hannington et al., 1995; Holland, 2002). Additionally, off-axis ridges, like the Lost City Hydrothermal Field, also host water/rock reactions leading to hydrogen generation at low temperatures (40-75°C) where microbial life can harness the hydrogen for metabolic processes (Kelley et al., 2001). Also, continental Precambrian granite can generate significant concentrations of hydrogen through radiolysis (Lollar et al., 2014). Continental rocks, specifically ophiolite sequences with abundant Fe-bearing minerals, can also undergo low-temperature hydration reactions to generate hydrogen. Continental ophiolite sequences rich in hydrogen are found throughout the world, including California, Canada, Turkey, the Philippines, and Oman (Suzuki et al., 2013).

1.2 The Samail ophiolite

The Samail ophiolite is a 500 km mountainous band of upper mantle and oceanic crust exposed along the coast in north-eastern corner of the Arabian Peninsula in the Sultanate of Oman and the United Arab Emirates. The ophiolite is 50-100 km wide, and the mantle rocks are 3-8 km thick (Dewandel et al., 2005). The sequence formed at a medium to fast spreading mid-oceanic ridge, similar to the modern day Juan de Fuca ridge or East Pacific Rise (Hanghøj et al., 2010). As the Tethys seaway closed during the late Cretaceous (~95 million years ago), it was obducted onto the Arabian peninsula in large thrust sheets composed of oceanic crust and upper mantle (Coleman, 1981). The base of the ophiolite consists of mantle peridotite, which comprises ~30% of the ophiolite (Kelemen and Matter, 2008), overlain by crustal gabbros, clearly demarking the Mohorovicic boundary between the crust and mantle. Going up sequence, on top

of the gabbros are dolerites (sheeted dikes) and then pillow lavas (Dewandel et al., 2005). The mantle peridotite is extensively serpentinized due to secondary hydrothermal alteration. These serpentinized harzburgites and dunites are far from equilibrium with the surface conditions and quickly weather, becoming friable at the surface and altering to oxides and clays (Dewandel et al., 2005).

The Samail ophiolite in the Sultanate of Oman is well-suited to coupled field and laboratory experiments examining low-temperature hydrogen production and associated microbiology. It is the largest and best exposed ophiolite sequence on Earth and contains large reserves of peridotite that are currently undergoing serpentinization at low temperatures (~30°C) (Kelemen et al., 2011; Streit et al., 2012). Highly rock-reacted fluids are accessible at surface seeps localized near contact zones between mantle and crustal rocks. Deep fluids can also be sampled by pumping from wells drilled hundreds of meters into peridotite and gabbros by the Ministry of Regional Municipalities and Water Resources. Several such surface seeps and subsurface wells are 2-3 hours from Muscat, the capital and main airport, making it relatively accessible. Additionally, the Samail ophiolite has the potential to provide a large-scale, stable, geological carbon repository (Kelemen et al., 2011). As peridotite undergoes hydration and oxidation during reactions with percolating fluids, it releases Mg^{2+}, Fe^{2+}, and Ca^{2+} into solution. In the presence of fluids enriched in dissolved CO_2, extensive precipitation of carbonate minerals occurs. Extensive carbonate veins are found in the serpentinized peridotite in Oman, which suggests there may be potential to engineer the reactions to occur at a faster rate (Kelemen and Matter, 2008; Kelemen et al., 2011; Mervine et al., 2014). Thus, there are several compelling reasons to study serpentinization, hydrogen-production, and the microbial consortia inhabiting the altered fluids in Oman.

1.3 Carbonation reactions

Mineral carbonation is the precipitation of aqueous carbon dioxide and cations into stable carbonate minerals, such as calcite, dolomite, magnesite, or siderite (Oelkers et al., 2008). Serpentinizing fluids rich in Ca^{2+} and Mg^{2+} from the dissolution of ultramafic minerals have favorable chemistry for mineral carbonation (Kelemen and Matter, 2008), yet there are several barriers to mineral carbonation. Dissolution of the primary olivine and pyroxene minerals is limited by the formation of passivating layers and secondary minerals (Andreani et al., 2009; Béarat et al., 2006; Giammar et al., 2005; Guyot et al., 2011; Saldi et al., 2013). Also, subsurface serpentinizing environments are usually CO_2-limited, but adding excess CO_2 to the system does not ensure carbonation due to complexities inherent in silica dissolution, passivation of mineral surfaces, and carbonate nucleation (Power et al., 2013).

Reaction-driven fracturing has been proposed to achieve complete mineral carbonation in peridotites. The serpentine grain boundaries in partially serpentinized peridotite allow water to migrate deep into the rock and facilitate olivine dissolution (van Noort et al., 2013). As olivine hydrates to form serpentine, its volume expands by ~50%. This bulk expansion generates high stress and strain on the rocks and can cause the formation of fractures in the rock, as well as releasing heat (Macdonald and Fyfe, 1985). This self-propagating reaction has exciting possibilities for ensuring carbonation reactions do not cease after initial surficial weathering. Natural systems document large fractures hypothesized to be generated by self-cracking (Kelemen et al., 2011; Power et al., 2013) in both listwanites (fully carbonated magnesite-quartz rocks) and serpentinites. However, volume expansion and subsequent self-fracturing caused by the formation of new minerals has not been observed in laboratory experiments; instead,

minerals clog the pore space and limit further carbonation (Hövelmann et al., 2012; van Noort et al., 2013; Saldi et al., 2013). *In situ* carbonation of Oman peridotite is more feasible if reaction-induced fracturing due to volume expansion allows the reaction to propagate. Cross-cutting serpentine veins seems to indicate repeated fracturing and hydration (Kelemen et al., 2011). However, reaction-driven fracturing during low-temperature water/rock reactions still needs to be proven.

The ultramafic rocks in the Samail Ophiolite have high carbonation potential. The ^{14}C in carbonate veins in serpentinized outcrops have been dated, and their age spans from 1,600 to 43,000 years, with an average age of ~26,000 years. Thus, carbonation is relatively modern and not related to the formation or emplacement of the ophiolite (Kelemen and Matter, 2008; Mervine et al., 2014). Kelemen and Matter (2008) have estimated that peridotite weathering in Oman converts around 10^4-10^5 tons per year of atmospheric CO_2 into carbonate. Adding just 1 weight percent of CO_2 to the peridotite would consume a quarter of all atmospheric CO_2, bringing levels back to pre-industrial times. However, the optimal method for achieving *in situ* carbonation is still an area of active research. Approaches include drilling and hydraulic fracturing, followed by injecting CO_2-rich fluids, and rates can be greatly enhanced by heating the system (Hansen et al., 2005; Schuiling, 2006; Kelemen and Matter, 2008; Kelemen et al., 2011).

2. Serpentinization and H_2-production in Oman

There are abundant reduced iron species that can facilitate hydrogen generation in Oman peridotite: olivine [$Mg_{1.8}Fe_{0.2}SiO_4$], and orthopyroxene [$(Mg,Fe)_2Si_2O_6$], along with trace amounts of chromite [$FeCr_2O_4$], Fe(III) oxides, Fe(II/III)-bearing serpentine and carbonates.

However, the reactions and mechanisms behind low-temperature serpentinization and hydrogen production in Oman are unknown. Traditionally, serpentinization occurs via the following equation (McCollom and Bach, 2009):

$$Mg_{1.8}Fe_{0.2}SiO_4 + 1.37H_2O = 0.5\ Mg_3Si_2O_5(OH)_4 + 0.3\ Mg(OH)_2 + 0.067Fe_3O_4 + 0.067H_2 \quad \text{(Equation 1)}$$

The oxidized Fe^{3+} in the above reaction is assumed to partition into magnetite. The Mg^{2+} and Fe^{2+} released from the olivine partitions between new mineral phases, leading to Fe-rich minerals, such as MgFe-chrysotile, MgFe-brucite and Fe in awaruite (Ni-Fe alloy) (Sleep et al., 2004). The incorporation of Fe(II) into secondary silicates vs. oxides such as magnetite may lead to reduced H_2 production as Fe(II) is not available for oxidation (McCollom and Bach, 2009). However, at lower temperatures, there is a decreasing thermodynamic drive for magnetite formation (Klein et al., 2013). Instead, Fe(III) substitutes into serpentine structures, so models may be neglecting this important component of H_2 production (Marcaillou et al., 2011)

These water/rock reactions give rise to the unique aqueous geochemistry and mineralogy of serpentinizing systems. Present-day shallow serpentinizing systems were first observed by Barnes et al. (1967) in the Cedars in California when they discovered springs with pH > 11. Barnes et al. (1967) observed two distinct types of waters in serpentinizing systems: Type 1 moderately alkaline waters (~pH 8-9) containing Mg^{2+}-HCO_3^- of meteoric origin and Type II ultrabasic waters (pH > 11) containing Ca^{2+}-OH^- found overlying serpentinized peridotite and dunite. Type I waters are formed from the weathering of serpentine minerals and Mg-bearing minerals that react in the near-surface, whereas Type II waters are derived from serpentinization reactions occurring in the subsurface that are isolated from the atmosphere. The hydration of olivine and pyroxene causes the water to become enriched in OH^-.

$$2Mg_2SiO_4 + 3H_2O = Mg_3Si_2O_5(OH)_4 + Mg^{2+} + 2OH^- \quad \text{(Equation 2)}$$

A similar reaction occurs with Ca-bearing pyroxenes, releasing Ca^{2+} into the fluid. Analysis of fresh peridotites versus serpentinites shows removal of CaO from the rock matrix because CaO is not incorporated into serpentinite, accounting for the large amounts of Ca^{2+} found in these waters (Barnes et al., 1967). However, it is unclear when and where the Type I fluids convert to Type II fluids and how long it takes to form Type II fluids.

3. Abiotic organic carbon synthesis

The highly reducing conditions created by H_2-rich environments may lead to the abiotic reduction of CO_2 to create simple organic compounds that can be an additional source of energy for subsurface microbiology. Experimental work has shown that formate rapidly forms from the reduction of CO_2 in the presence of olivine at 300°C (McCollom and Seewald, 2001). Formate and acetate have been found in the low-temperature Lost City vents (Lang et al., 2010), and formate alone has been detected in surface seeps from the Tablelands Ophiolite (Morrill et al., 2014) and the Coast Range ophiolite (Crespo-Medina et al., 2014). When acetate is detected in fluids, it is generally considered to be a metabolic byproduct or a product of biomass degradation, thus is an encouraging sign of life (Proskurowski et al., 2006; Lang et al., 2010). Additionally, CH_4 is a dominant gas in serpentinizing environments, and isotopic measurements of δD and $\delta^{13}C$ generally indicate it is abiotically formed (Etiope et al., 2011; Etiope and Sherwood Lollar, 2013; Etiope et al., 2013). The abiotic creation of organic matter in serpentinizing systems provides a framework for the formation of prebiotic carbonaceous material, suggesting a favorable environment for the origin of life and sustaining primordial metabolisms (McCollom and Seewald, 2001, p.2006; Russell and Martin, 2004; Proskurowski et

al., 2006; Lang et al., 2010; Russell et al., 2010; Neubeck et al., 2011; Ménez et al., 2012; Pasini et al., 2013).

3.1 Methane formation during serpentinization

There are several abiotic reactions that produce methane, but they are difficult to experimentally reproduce while mimicking environmental conditions. Fischer-Tropsch-type reactions lead to the production of CH_4 and higher chain hydrocarbons by surface-catalyzed reduction and polymerization of a variety of carbon sources, such as CO_2, CO, HCOOH (Berndt et al., 1996; Horita and Berndt, 1999; McCollom and Seewald, 2001; McCollom and Seewald, 2007; Bradley and Summons, 2010). CH_4 can also be produced by the Sabatier reaction which exclusively reduces CO_2 to methane without any other alkane formation (Mccollom and Seewald 2007). Serpentinization of olivine at 300°C and 500 bar was shown to produce CH_4 along with ethane, propane, and a solid carbon phase, presumably through magnetite catalysis (Berndt et al., 1996). However, the carbon was not isotopically labeled, so it is unclear if the hydrocarbons formed during the experiment by reducing headspace CO_2, or if the hydrocarbons were generated by thermal decomposition by reduced carbon already present in reactants (McCollom and Seewald, 2001; McCollom, 2013). This uncertainty about CH_4 formation during serpentinization is enforced by similar experiments conducted with a ^{13}C label that only show small concentrations of labeled CH_4 forming and no higher chain hydrocarbons forming with a ^{13}C label (McCollom and Seewald, 2001; McCollom, 2016). However, it does appear that NiFe-alloys are powerful catalysts to promote the dissolution of CO_2 to CH_4 (Horita and Berndt, 1999); although, the abundance and distribution of these alloys in natural environments is not well constrained.

Low temperature abiotic methane formation (<100°C) also is plagued by inconsistent results in experimental work. Studies at 30°C by Neubeck et al. (2011) report measureable CH_4 formation facilitated by the dissolution of olivine and magnetite catalysis, but the study was not conducted with isotopic labels to verify the reduction of carbon during the experiment. A recent study by Etiope and Ionescu (2015) document CH_4 production from 20-90°C by ruthenium catalysis. These experiments were performed under dry conditions to simulate unsaturated subsurface rocks, and they assume pure ruthenium in contact with gas phase H_2 and CO_2. Most subsurface conditions are water-saturated and do not contain pure ruthenium, thus, it is unclear if these experiments are environmentally relevant. Vapor phase H_2 and CO_2 promotes CH_4 synthesis because it allows the gases to directly contact catalytic mineral surfaces, whereas under saturated conditions, water molecules attach to mineral surfaces that may interfere with catalytic reactions (McCollom, 2016). Truly environmentally relevant experiments, with liquid phase gases, documenting substantial abiotic CH_4 production are limited (McCollom, 2016).

$\delta^{13}C$ of CH_4 values from serpentinizing systems range from approximately -20 to 0‰, with δD values from -450 to -50‰ (Etiope and Sherwood Lollar, 2013). These gases are assumed to be abiotically produced due to these isotope values, and in some cases, corresponding alkane concentrations and isotope values. However, experimental isotope studies of abiotic CH_4 production yield conflicting isotopic signatures. In general, experimental FTT reactions generate CH_4 depleted in D by -35 to -80‰ relative to the initial H_2 (Fu et al., 2007; McCollom et al., 2010). In the same reactions, nearly all hydrocarbons become more depleted in ^{13}C relative to the original carbon source, with a variety of depletions ranging up to 33‰ (McCollom, 2013). This contrasts with recent experiments by Etiope and Ionescu (2015) which report the $\delta^{13}C$ becomes depleted initially, then more ^{13}C enriched. Despite conflicting data, experimental studies do not

successfully reproduce the relatively positive $\delta^{13}C$ values observed from serpentinizing systems, in the range of -20 to 0‰ (Etiope et al., 2013). Thus, this discrepancy needs to be better studied to understand the origin of methane in serpentinizing systems based on isotope values.

3.2 *Organic carbon associated with serpentinites*

Complex organic material has been found associated with serpentinites through high resolution imaging techniques (Ménez et al., 2012; Pasini et al., 2013). Aliphatic and aromatic compounds, along with amides, have been found in association with cavities in hydroandraditic garnets in serpentinized peridotites from the Mid-Atlantic Ridge (Ménez et al., 2012). These hollow cavities may have hosted cryptoendolithic microbes, potentially metabolizing H_2 generated through serpentinization or using Fe(III) in garnets as an oxidant for the H_2. The complex organics can then migrate into the surrounding serpentines and ocean, providing a source of carbon for other microbial life (Pasini et al., 2013). Thermodynamic calculations also suggest that solid carbonaceous material should form in serpentinized fluids under hydrothermal conditions (Milesi et al., 2016). Does carbonaceous material form during experimental H_2-producing water/rock reactions, and if so, what type of organic material forms and in what quantities? How much carbonaceous material is present in modern serpentinizing systems and is it in a useful form for microbial life to utilize?

4. Microbial life

Serpentinizing environments contain abundant electron donors (CH_4, H_2, formate) and electron acceptors (e.g. SO_4^{2-}, NO_3^-) that can be utilized by autotrophic microorganisms (Schrenk et al., 2013) despite the harsh high-pH and carbon limited conditions. DNA extracted from

serpentinizing systems shows a diverse set of microorganisms inhabit hyperalkaline subsurface environments (Blank et al., 2009; Lang et al., 2010; Brazelton et al., 2012; Brazelton et al., 2013; Morrill et al., 2013; Suzuki et al., 2013; Meyer-Dombard et al., 2015; Woycheese et al., 2015). However, most studies have focused on accessing easily accessible surface seeps where hyperalkaline fluids interact with the atmosphere. It is difficult to sample the deep, anoxic subsurface for microbial life, especially life inhabiting the rock matrix. The metabolic processes and energy sources utilized by life intimately associated with minerals is not clearly constrained, but it is pertinent when considering the origins of life on Earth, as well as potential for other planets to harbor microbial life (Boston et al., 1992; Sleep et al., 2004; Blank et al., 2009; Russell et al., 2010).

There are many possible metabolisms supported by the products of water/rock reactions in serpentinizing environments. Cardace and Hoehler (2009) have calculated hydrogen supplies as low as ~100 nM can support the following metabolism utilized by methanogens:

$$CO_2 + 4H_2 = CH_4 + 2H_2O \qquad \text{(Equation 3)}$$

Methanogenesis is just one possible metabolism in serpentinites; other possible metabolisms include hydrogen oxidation tied to iron reduction, anaerobic methanotrophy, fermentation, and sulfate reduction (Schrenk et al., 2013). However, because the field is so broad, this work chooses to focus on CH_4 production, and cursorily investigates and speculates about CH_4 consumption.

4.1 Methanogenesis isotopic signatures

Microbial methanogenesis generates a unique range of $\delta^{13}C$ and δD of CH_4 values (Schoell, 1980; Whiticar, 1999; Valentine et al., 2004; Etiope, 2009; Etiope and Sherwood

Lollar, 2013) which allows scientists to make predictions about microbial activity by investigating the isotopic signature of CH_4 in natural systems. Microbial CO_2 reduction and acetate fermentation generate CH_4 with a $\delta^{13}C$ of -110 to -45‰ and a δD ranging from -375 to -150‰ (Whiticar, 1999; Valentine et al., 2004; Etiope et al., 2013). Biotic, abiotic, and thermogenic CH_4 from a variety of environments on Earth has been isotopically characterized (Whiticar, 1999; Etiope et al., 2013). Isotopic partitioning of CH_4 based on formation mechanism gives insight into geochemical and geomicrobiological processes such as identifying natural gas deposits and characterizing analog methanogenesis habitats on Earth of astrobiological significance (Blank et al., 2009; Etiope et al., 2013). However, the isotopic signature of methanogens under carbon-limited and high pH conditions is not well constrained.

4.2 Methane oxidation

Anaerobic oxidation of methane is prevalent in most anaerobic environments that contain CH_4 such as seafloor and continental margin marine sediments, deep sedimentary and granite aquifers, hydrothermal vents, and oil and natural gas fields (Martens and Berner, 1977; Kotelnikova, 2002; Girguis et al., 2003; Brazelton et al., 2006). Anaerobic oxidation of methane (AOM) is generally explained by the following reaction:

$$CH_4 + {SO_4}^{2-} = {HCO_3}^{-} + HS^{-} + H_2O$$

and yields -25 kJ per mole of methane oxidized (Martens and Berner, 1977; Boetius et al., 2000). This reaction is not very energetically favorable; thus, there must be low concentrations of hydrogen, sulfate and acetate in order for AOM to occur (Boetius et al., 2000), or other more energetically favorable reactions will occur. It is mediated by a consortia of archaea and syntrophic bacterial partners. These bacteria predominately perform sulfate reduction, but

ANME has also been found in association with bacteria performing nitrate-reduction, iron-reduction, and manganese reduction (Orphan et al., 2002; Beal et al., 2009; Haroon et al., 2013).

There is great potential for anaerobic methane oxidizers to be active in serpentinizing systems with their abundant CH_4. The Lost City Hydrothermal Field, a low-temperature serpentinizing oceanic site rich in H_2 and CH_4, contains both ANME-1 and *Methanosarcinales* (Brazelton et al., 2006). Both organisms contain *mcrA*, methyl coenzyme M reductase, but they are not associated with a known sulfate-reducing bacteria. Firmicutes *Desulfotomaculum*, a sulfate-reducer, is pervasive, but not always associated with the ANME-1. Thus this environment is shows evidence of AMO, but the organisms mediating the process are still unknown (Brazelton et al., 2006). The search for anaerobic methane oxidation in serpentinizing sites is ongoing, by looking for: methane consumption, eligible methane-oxidizing organisms, and appropriate electron acceptors.

5. Implications

Low-temperature hydrogen production from serpentinization reactions may provide low concentrations of continuous energy for subsurface microbes. Although hydrogen is the most-cited product of water/rock reactions, the reducing environment created by the hydrogen can then reduce carbon sources to create more energy sources, such as methane, formate, or carbon monoxide. These reactions do not depend on sunlight and instead are driven by disequilibrium between ultramafic rocks and surface conditions. Microbial life is ubiquitous in fluids near the earth's surface, and it is now becoming accepted they are also prevalent in subsurface rock matrices. However, it is challenging for geoscientists to quantitatively measure and model how microscopic organisms may be altering their surrounding aqueous and mineral geochemistry, and

vice versa. Microbes may affect reaction pathways, products, and kinetics for serpentinization and carbonation reactions.

Investigating the connection between microbiology and low-temperature hydrogen production has the potential to provide insights into analogous systems on other planets. The subsurface of Mars contains ultramafic rocks, some of which may be partially hydrated (Ehlmann et al., 2010), and this is an excellent area to search for life because it is shielded from UV radiation and the harsh climate (Oze, 2005). Enceladus also contains oceans with high pH, which likely indicates the presence of serpentinization reactions (Glein et al., 2015). Thus, increasing understanding of products and signs of serpentinization-associated life on Earth can help us to detect and search for life on other rocky bodies.

Furthermore, the carbonation reactions occurring in Oman, perhaps concomitantly with serpentinization, provide the opportunity to sequester carbon in the subsurface. However, the rates and reactions surrounding natural carbon sequestration in ophiolites are poorly constrained. The effect of microbiology on carbon sequestration is also unknown, but it is known that microorganisms rapidly cycle carbon in the subsurface, and may either negatively or positively affect sequestration reactions. Thus, this work will contribute to baseline information about small scale carbon cycling in low-temperature water/rock reactions to help scientists better understand potential processes to sequester greenhouse gases and mitigate the effects of climate change due to anthropogenic carbon energy usage.

6. Dissertation chapters

6.1 Modern water/rock reactions in Oman hyperalkaline peridotite aquifers and implications for microbial habitability

This work was published in *Geochimica et Cosmochimica Acta* in April 2016 (Miller et al., 2016). It characterizes the modern processes associated with the low-temperature hydration of subsurface peridotite in Oman. The work encompasses many aspects of the system: geochemistry of the hyperalkaline fluids, isotopic signatures of the evolved H_2 and CH_4, microbial communities living in the fluids, and mineralogical characterization of drill cuttings from wells that penetrate up to 300 m depth in the peridotite. This data provides the first direct observations of subsurface fluids and mineralogy from a hyperalkaline Oman aquifer, and the potential coupling between geochemical and microbiological processes during low-temperature serpentinization. The paper also received a published comment and subsequent reply concerning the origin of the CH_4, which is also included in the appendices (Etiope, 2016; Miller et al., 2017).

6.2 Low temperature hydrogen production during experimental hydration of partially-serpentinized dunite

This work was submitted to *Geochimica et Cosmochimica Acta* in September 2016 and it has undergone a first round of peer-review and revision (Miller et al., in revision). This manuscript details hydrogen production from 100°C water/rock reactions between partially serpentinized Oman dunite, and artificial seawater and rainwater media. Over a period of 9 months, up to 500 nmol/gram H_2 was produced. Serpentine precipitated, magnetic susceptibility increased, formate was produced, and pH increased from ~6.5 to 9. To identify reactions giving rise to low-temperature hydrogen production, the mineralogy and oxidation state of the Fe-bearing species in the dunite were extensively characterized before and after reaction using Raman spectroscopy, QEMSCAN, powder x-ray diffraction (XRD), magnetic susceptibility and Fe K-edge x-ray absorption near edge structure (XANES) spectroscopic techniques. From this

data, we proposed that the destabilization of Fe(II)-bearing brucite and the subsequent oxidation of the aqueous Fe(II) to form magnetite and Fe(III)-rich serpentine give rise to H_2 production at 100°C. This work demonstrates that dissolved hydrogen and low molecular weight organic acids can be produced during low-temperature serpentinization which may generate sufficient electron donors to fuel in-situ subsurface microbial activity.

6.3 Effects of pH, ionic strength, and temperature on hydrogen production from partially serpentinized Oman dunite

This chapter details multiple water/rock reaction experiments that expand on the previous chapter, but ultimately did not provide conclusive enough material to merit publication. Low-temperature anoxic hydration of Oman dunite was also conducted at 40 and 55°C to more closely mimic shallow subsurface temperatures. The reactions were also conducted from pHs 7-12, and ionic strengths of 0-1.5 M and with various medias to probe the conditions under which hydrogen forms with varying fluid compositions. The development of a gas-tight, non-reactive reaction vessel was also conducted in order to perform these water/rock reactions without any artificially imposed gas production or contaminants. We observed no hydrogen production at low temperatures, but at 100°C, the combination of high pH and Ca^{2+} ions in solution may lead to increased H_2 production. As with 100°C experiments, the destabilization of Fe(II)-brucite and subsequent oxidation of Fe^{2+} appears crucial for hydrogen production. More targeted experiments need to be conducted to understand these results, but this preliminary information is meant to provoke future work.

6.4 Carbon and hydrogen isotope fractionation by Methanobacterium sp. growing at alkaline pHs

This chapter focuses on the growth of the methanogen *Methanobacterium sp.* at a range of pHs (6-11.5) to constrain the isotope systematics of microbially produced methane in fluids that simulate serpentinizing systems. *Methanobacterium* was isolated from hyperalkaline (pH 10.6) fluids from an actively serpentinizing subsurface aquifer in Oman. Organisms were grown in a minimal media made to mimic subsurface fluids with either $NaHCO_3$ or carbonate as the sole provided carbon source over a range of pHs from 6 – 11. The maximum fractionation factor was determined by measured $\delta^{13}C$ of CH_4 from slow-growing cultures, and the minimum fractionation factor was determined by measured $\delta^{13}C$ of CH_4 from fast-growing cultures. The resulting isotopic data can help scientists to better interpret methane isotopes from hyperalkaline conditions.

CHAPTER 2

Modern water/rock reactions in Oman hyperalkaline peridotite aquifers and implications for microbial habitability

Published in *Geochimica et Cosmochimica Acta*, 2016

Co-authors: Jürg M. Matter[a,b], Peter Kelemen[b], Eric T. Ellison[c], Mark E. Conrad[d], Noah Fierer[e,f], Tyler Ruchala[g], Masako Tominaga[g], and Alexis S. Templeton[c]

[a]Department of Ocean and Earth Science, University of Southampton, UK SO14 3ZH
[b]Lamont-Doherty Earth Observatory of Columbia University, 61 Route 9W, Palisades, NY 10964, USA
[c]Department of Geological Sciences, UCB 399, University of Colorado, Boulder, CO 80309, USA
[d]Earth Sciences Division, MS 70A-4418, E.O. Lawrence Berkeley National Laboratory, Berkeley, CA 94720, USA
[e]Department of Ecology and Evolutionary Biology, CIRES 215,-University of Colorado, Boulder, CO 80309, USA
[f]Cooperative Institute for Research in Environmental Sciences, University of Colorado, Boulder, CO 80309
[g]Department of Geology and Geophysics, Texas A&M University, College Station, TX 77843, USA

Abstract

The Samail ophiolite in Oman is undergoing modern hydration and carbonation of peridotite and may host a deep subsurface biosphere. Previous investigations of hyperalkaline fluids in Oman have focused on fluids released at surface seeps, which quickly lose their reducing character and precipitate carbonates upon contact with the O_2/CO_2–rich atmosphere. In this work, geochemical analysis of rocks and fluids from the subsurface provides new insights into the operative reactions in serpentinizing aquifers. Serpentinite rock and hyperalkaline fluids (pH >10), which exhibit millimolar concentrations of Ca^{2+}, H_2 and CH_4, as well as variable sulfate and nitrate, were accessed from wells situated in mantle peridotite near Ibra and studied to investigate their aqueous geochemistry, gas concentrations, isotopic signatures, mineralogy, Fe speciation and microbial community composition.

The bulk mineralogy of drill cuttings is dominated by olivine, pyroxene, brucite, serpentine and magnetite. At depth, Fe-bearing brucite is commonly intermixed with serpentine, whereas near the surface, olivine and brucite are lost and increased magnetite and serpentine is detected. Micro-Raman spectroscopy reveals at least two distinct generations of serpentine present in drill cuttings recovered from several depths from two wells. Fe K-edge x-ray absorption near-edge spectroscopy (XANES) analysis of the lizardite shows a strong tetrahedral Fe coordination, suggesting a mixture of both Fe(II) and Fe(III) in the serpentine. Magnetite veins are also closely associated with this second generation serpentine, and 2-10μm magnetite grains overprint all minerals in the drill cuttings. Thus we propose that the dissolved H_2 that accumulates in the subsurface hyperalkaline fluids was evolved through low temperature oxidation and hydration of relict olivine, as well as destabilization of pre-existing brucite present in the partially serpentinized dunites and harzburgites. In particular, we hypothesize that Fe-

bearing brucite is currently reacting with dissolved silica in the aquifer fluids to generate late-stage magnetite, additional serpentine and dissolved H_2.

Dissolved CH_4 in the fluids exhibits the most isotopically heavy carbon in CH_4 reported in the literature thus far. The CH_4 may have formed through abiotic reduction of dissolved CO_2 or through biogenic pathways under extreme carbon limitation. The methane isotopic composition may have also been modified by significant methane oxidation. 16S rRNA sequencing of DNA recovered from filtered hyperalkaline well fluids reveals an abundance of *Meiothermus, Thermodesulfovibrionaceae* (sulfate-reducers) and *Clostridia* (fermenters). The fluids also contain candidate phyla OP1 and OD1, as well as *Methanobacterium* (methanogen) and *Methylococcus* sp. (methanotroph). The composition of these microbial communities suggests that low-temperature hydrogen and methane generation, coupled with the presence of electron acceptors such as nitrate and sulfate, sustains subsurface microbial life within the Oman ophiolite.

1. Introduction

The Samail ophiolite in the Sultanate of Oman, the largest and best exposed ophiolite sequence on Earth, is well-suited to the study of low temperature serpentinization, which is the aqueous alteration of ultramafic rocks. Over 15,000 km^3 of peridotite is currently undergoing low temperature hydration and oxidation (Barnes et al., 1978; Neal and Stanger, 1983; Neal and Stanger, 1985; Clark and Fontes, 1990; Kelemen and Matter, 2008; Kelemen et al., 2011; Streit et al., 2012; Paukert et al., 2012). Modern serpentinization is inferred from the distribution of hyperalkaline seeps that release hyperalkaline fluids rich in H_2 and CH_4, and poor in dissolved inorganic and organic carbon. However, the water/rock reaction pathways giving rise to H_2 and methane formation at near-surface temperatures are not known. Moreover, no studies have yet explored whether the active hydrogeochemical system hosts a subsurface biosphere.

In Oman, the mantle peridotite consists of olivine, orthopyroxene, and serpentine, with trace amounts of calcic pyroxene, chromite, and Fe-oxides (Hanghøj et al., 2010). The mantle peridotite is 30-70% serpentinized (Boudier et al., 2010) and variably carbonated. Some serpentinization occurred during hydrothermal circulation when the ophiolite was situated at an oceanic spreading ridge, some during thrust emplacement of the ophiolite over pelagic and continental margin sediments, some during late Cretaceous sub-aerial weathering and a subsequent marine transgression, and some during ongoing water/rock reactions (Hanghøj et al., 2010; Kelemen et al., 2011). The proportions and spatial distribution of serpentine and other secondary minerals formed during these different events are unclear. Completely unaltered peridotite is not observed in outcrop in Oman, but the least altered samples are found in deep canyons, whereas the most serpentinized outcrops are in areas of low relief (Kelemen et al., 2011). The peridotite also undergoes carbonation reactions as evidenced by modern carbonate

vein and terrace dates (Clark and Fontes, 1990; Kelemen and Matter, 2008; Mervine et al., 2014) which indicate temperatures of formation from 30-60°C (Kelemen et al., 2011; Streit et al., 2012).

An active hydrological system drives present-day serpentinization and other alteration processes occurring in the subsurface. Groundwater circulation in the peridotite aquifer is controlled by fissure and fracture hydraulic conductivity. Near-surface fissures (perhaps extending to ~ 50 meters depth) accommodate most of the groundwater flow with a hydraulic conductivity of 10^{-7} m/s (Dewandel et al., 2005). The origins of this shallow, hydraulically active zone are not clear, but are probably due to meteoric weathering. The peridotite aquifer contains a network of fractures that began to develop when the ophiolite was hydrothermally altered at the mid-ocean ridge, ~95 million years ago during the Middle Cretaceous (Coleman, 1981). The fractures in the peridotite host serpentine and carbonate veins (Dewandel et al., 2005). Hyperalkaline surface seeps generally discharge at the contact between the mantle and overlying crustal rocks, and along the basal thrust plane of the ophiolite sequence. They release high pH fluids (>11) rich in Ca^{2+}, OH^-, H_2, and CH_4. The surrounding mineralogy is dominated by carbonates that precipitated when the carbon deprived fluids mixed with atmospheric CO_2 (Kelemen and Matter, 2008; Kelemen et al., 2011; Paukert et al., 2012; Chavagnac et al., 2013; Chavagnac et al., 2013).

The origin of dissolved H_2 and CH_4 in Oman are enigmatic. Currently, there is no evidence for modern hydrothermal activity at temperature greater than 200°C of water/rock reactions in the peridotite aquifer, which would correspond to a depth of ~8 km based on a geothermal gradient of 25°C/km. Although serpentinization processes have been extensively studied at temperatures >120°C , the mineral assemblages and alteration processes leading to

formation of dissolved H_2 and CH_4 during serpentinization at lower temperatures are poorly constrained.

Serpentinization leads to the evolution of hydrogen through hydration and the oxidation of reduced iron species found in olivine and pyroxenes. For typical mantle olivine with molar Mg/(Mg+Fe) = 0.9, a simplified reaction above 200°C might be:

$$Mg_{1.8}Fe_{0.2}SiO_4 + 1.37\ H_2O = 0.5\ Mg_3Si_2O_5(OH)_4 + 0.3\ Mg(OH)_2 + 0.067\ Fe_3O_4 + 0.067\ H_2 \quad (1)$$

(e.g. Equation 1; Frost, 1985; McCollom and Bach, 2009). Such water/rock reactions produce fluids rich in H_2. These fluids also commonly contain abundant dissolved CH_4 , which may form abiogenically as the result of Fischer-Tropsch Type or Sabatier reactions (Horita and Berndt, 1999; Etiope et al., 2013), or biologically via methanogenesis (Balch et al., 1979; Sleep et al., 2004).

Hydrogen generation during serpentinization has been modeled from 8-400°C (McCollom and Bach, 2009; Okland et al., 2012; Klein et al., 2013). Experimentally produced H_2 has been generated from 0-100°C (Stevens and McKinley, 1995; Anderson et al., 1998; Stevens and McKinley, 2000; Neubeck et al., 2011; Okland et al., 2012; Mayhew et al., 2013) Comparisons of model and experimental results often yield conflicting results, perhaps because of assumptions included in models. For example, McCollom and Bach (2009) utilize reaction path models to simulate water-rock reactions and resulting mineral assemblages, but they are constrained by the lack of existing thermodynamic data for Mg:Fe solid solutions, the incorporation of Fe(III) into secondary silicates, and the lack of data on mineral compositions that form at low temperature. Also, models assume the reactions have reached equilibrium, and it is unlikely that low-temperature laboratory experiments are fully equilibrated. Thus, detailed

analysis of field samples from low-temperature serpentinizing environments is required to ground-truth modeling efforts.

There is also a lack of data on the detection or characterization of microorganisms in Oman's hyperalkaline aquifers. The high concentrations of H_2 and CH_4 in the hyperalkaline fluids provide electron donors that could be utilized by subsurface chemolithoautotrophic life, which could contribute to carbon cycling in the subsurface (Stevens and McKinley, 1995; Sleep et al., 2004, p.2005; Nealson et al., 2005; Mayhew et al., 2013; Klein et al., 2015). The search for microbial life in other serpentinizing environments has primarily been focused on sequencing the 16S rRNA gene from easily accessible surface springs as windows into the subsurface (Neal and Stanger, 1983; Abrajano et al., 1990; Bruni et al., 2002; Meyer-Dombard et al., 2015; Woycheese et al., 2015), although recent work by Postec et al. (2015) isolated DNA from carbonate chimneys from a low-temperature hydrothermal field. However, all these studies were limited to surface samples collected in oxygenated environments, which allows aerobic organisms to flourish. It is unclear if the microbes inhabiting the surface seeps are similar to those active in the anaerobic subsurface.

This study was designed to assess low temperature serpentinization processes in a peridotite aquifer in Oman and to determine what types of microbial life are hosted in the subsurface. We sampled hyperalkaline, H_2-, CH_4-rich fluids from 10-300 m depth in peridotite and studied their geochemistry, gas concentrations and isotopic signatures. We integrated these data with mineralogical and spectroscopic analysis of mineral chips recovered from depth within two peridotite wells to elucidate the oxidation state, mineralogy, and extent of serpentinization of the rocks in contact with deep subsurface fluids. Magnetic hysteresis analyses on downhole bulk rock samples augment these geochemical and mineralogical analyses by providing the

distribution of different rock magnetic properties within drilled sections, thereby suggesting possible zonation in the serpentinization process. Geochemical data were complemented by high throughput 16S rRNA sequencing of DNA recovered from the well fluids to identify microbial organisms present in the fluid. These data provide the first insights into the modern water/rock reactions in a hyperalkaline Oman aquifer, and the potential coupling between geochemical and microbiological processes during low-temperature serpentinization.

2. Methods

2.1 *Field methods*

The Ministry of Water Resources of the Sultanate of Oman drilled numerous wells into peridotite (~300 meters deep) to investigate water resources for the region. Water samples and drill cuttings were obtained from wells NSHQ14 and NSHQ04 in a peridotite plain in the Samail ophiolite, Oman (Figure 1). NSHQ04 is near a north/south trending fault, with gabbro to the west and mixed dunite and gabbro lenses cut by pyroxenite dikes to the east. NSHQ14 is several kilometers from the crust-mantle boundary; the surrounding rocks are mainly harzburgite with meter-scale dunite bands.

In January 2014, a shallow submersible pump was used to collect water from 18 meters depth in both NSHQ04 and NSHQ14, and a stainless steel bailer was used to collect water from 260 meters in well NSHQ14. Water samples containing dissolved gases were collected in sterile syringes and injected into N_2-purged vials and later used for headspace gas analysis. The vials were acid washed, autoclaved and baked at 400°C in a muffle furnace prior to field work. Samples for ICP-MS analysis were filtered with 0.2µm Millipore filters and acidified in the field with concentrated nitric acid to ~pH 2. The fluid pH, temperature, and conductivity were measured with a conductivity meter (YSI Model#85/10) while pH was measured with a Mettler-Toledo SevenGo2 pH meter calibrated with reference standards of pH 12.46, 10.01, and 7.

Fluids (~5-10L) from the wells were pumped and filtered through 0.2µm Sterivex inline filters to recover biomass for DNA extraction. Filters were transported frozen in liquid nitrogen and stored in a -70°C freezer until extraction.

We also obtained drill cuttings (rock chips recovered during drilling) of the wells from 262, 140, 70, and 17 meters depth at NSHQ14 and from 303, 180, and 120 meters depth at well

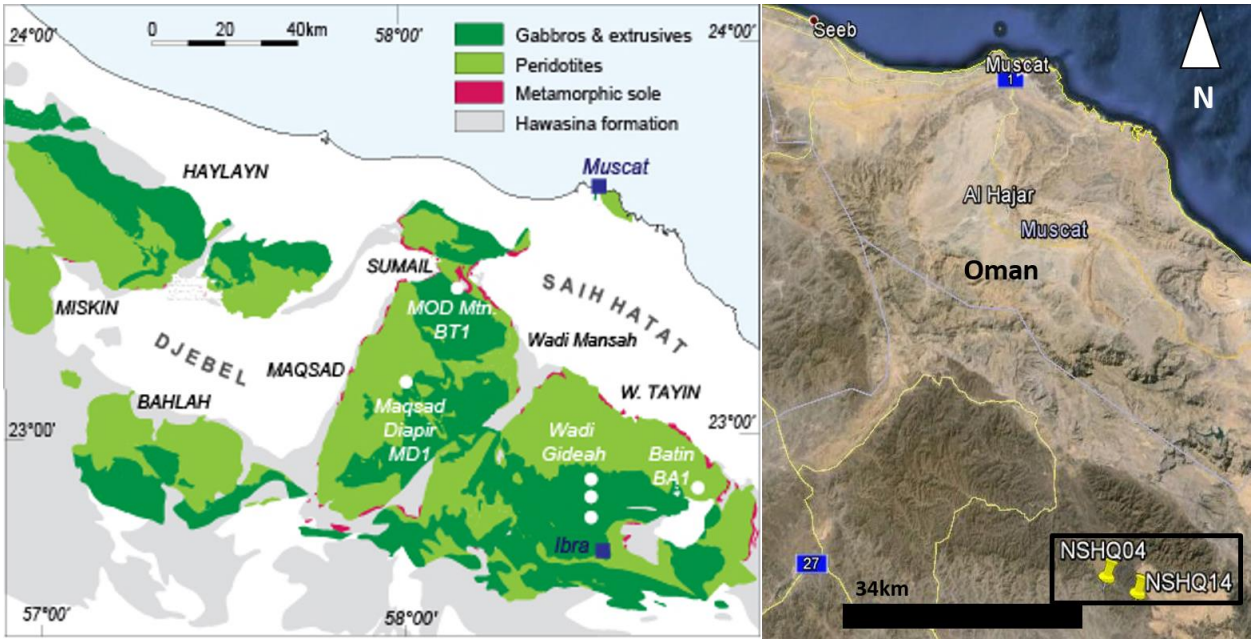

Figure 1. NSHQ04 is located at UTM coordinate 675491 Easting, 2529716 Northing using the WGS-94 datum. NSHQ14 is located at 670975 Easting, 2531692 Northing. The top right picture shows the distribution of the ophiolite in Oman, and the wells are situated in the light green peridotite near the circle labeled Batin (geologic map courtesy of Oman drilling program website).

NSHQ04. These were mounted in epoxy and prepared as 30 µm thick polished thin sections for analysis.

2.2 *Laboratory methods*

Major cations (Na^+, Fe^{2+}, Mg^{2+}, Ca^{2+}, K^+), SiO_2, and trace elements (Ni, As, Se, Cu, Cd, Zn Co, Cr) were analyzed on field-acidified and filtered well waters using Inductively Coupled Plasma-Mass Spectrometry (ICP-MS) on a ThermoScientific X Series 2. Major anions (F^-, Cl^-, Br^-, NO_3^-, PO_4^{3-}, SO_4^{2-}) were analyzed using Ion Chromatography (IC) on a Dionex IC25 with an IonPac column and a 9 mM sodium carbonate eluent. Water samples were collected in acid-washed, autoclaved, and ashed organic free vials and sent to NASA Ames Research Center to measure low weight molecular organic acids on a Shimadzu Prominence LC20AT high-performance liquid chromatograph (HPLC) equipped with a SPD-M20A photodiodearray detector and a flow rate of 1mL per minute.

Drill cuttings were powdered with a mortar and pestle and then x-ray diffraction (XRD) data were obtained using CuKα radiation (λ = 1.5418Å) in the range 15-65° 2θ using a Bruker D2 Phaser operated at 30 kV and 10 mA. A Lynxeye 1D detector with a step size of 0.02° and collection time of 1 s per step were employed. The XRD spectra were semi-quantitatively fit using the Bruker DiffracEva program and results were compared to the RRUFF database (Downs, 2006).

To determine H_2 and CH_4 concentrations (detection limit of 10ppm and analytical error of 5%) in the gases exsolved from the well fluids, we used a SRI 8610C gas chromatograph (GC) with a 2m by 1mm ID micropacked ShinCarbon ST column with N_2 as the carrier gas. 0.5mL of gas was sampled from the headspace of serum vials sealed with blue rubber stoppers and was

injected into a sampling port on the GC. H_2 was measured with a thermal conductivity detector (TCD), and a flame ionization detector (FID) was concurrently used to measure CH_4.

Stable isotope analyses were conducted at the Center for Isotope Geochemistry at the Lawrence Berkeley National Laboratory. The isotopic compositions of H_2 and CH_4 were analyzed using a Thermo Scientific GC Trace Gas Ultra system connected to a Thermo Scientific Delta V Plus Mass Spectrometer (IRMS). Gas samples were injected into a 6-port valve (the loop size varied from 5 L to 250 L depending on the concentration of the analyte in the sample) bypassing the inlet of the GC. After flushing with at least 3 times the volume of the loop, the sample was injected into the GC where the gases were separated chromatographically on an HP-molesieve fused silica capillary column (30 m x 0.320 mm). For H_2, after the samples went through the GC, they were passed through a combustion furnace at room temperature and then into the IRMS. Reproducibility of these analyses is ±2.5‰ (1σ), as determined by repeated analyses of a laboratory gas standard. Carbon isotope ratios of CH_4 were analyzed using the same system with the combustion furnace (a capillary ceramic tube loaded with Ni, Cu, and Pt wires) set at 1030 °C where the CH_4 was converted to CO_2. Produced water was removed, and the carbon isotope ratio of the resulting CO_2 was measured in the IRMS. The reproducibility of these analyses is ±0.2‰. For hydrogen isotopes of CH_4, the sample was passed through a pyrolysis furnace at 1450 °C and the resulting H_2 gas measured with the IRMS. The reproducibility of these analyses is ± 5‰.

Samples with 10-100 micrograms calcite were reacted with 100% H_3PO_4 at 90°C and then used for both carbon and oxygen isotope analyses ($\delta^{13}C$ and $\delta^{18}O$), which were determined using a GV IsoPrime mass spectrometer with Dual-Inlet and MultiCarb systems in the Center for Stable Isotope Biogeochemistry (CSIB) at Department of Integrative Biology, University of

California at Berkeley. Several replicates of one international standard NBS19, and two lab standards $CaCO_3$-I & II were measured along with samples for each run. The overall external analytical precision is about $\pm$0.05‰ for $\delta^{13}C$ and about $\pm$0.07‰ for $\delta^{18}O$.

The isotopic compositions of the water samples were measured using CIG's Los Gatos Research Liquid Water Isotope Analyzer (LWIA). 1 ml of each sample was loaded into 2 ml vials. Using an auto sampler, each sample was injected into the LWIA 8 times where the data for the first 3 injections were discarded and the data for the remaining 5 injections averaged to give the raw isotope values. The data were then compared to a series of 3 standards bracketing the expected isotopic values of the samples analyzed and run multiple times throughout the run. The reproducibility of these analyses based on repeated analyses of the standards is better than ±1‰ for δD and ±0.2‰ for $\delta^{18}O$.

2.3 *Microscale analytical techniques*

Synchrotron-based hard X-ray measurements of Fe K-edge micro-x-ray absorption near edge spectra (μXANES) were conducted at Beamline 2-3 at the Stanford Synchrotron Radiation Lightsource (SSRL). The incident energy was selected with a Si (111) double crystal monochromator with the SPEAR accelerator ring containing ~150-200mA at 3.0 GeV. The beam was focused to approximately 2 by 2 μm using Kirkpatrick Baez mirrors. Data were collected at the Fe K-edge using a Fe^0 foil calibration of 7112 eV with a single-element Vortex detector capable of reading several million counts per second.

Fe K-edge mapping was conducted at 8 energies (7123, 7126, 7128, 7129, 7130, 7131, 7133 keV) chosen to maximize the differences in normalized intensity between representative XANES (Mayhew et al., 2011; Mayhew et al., 2013). These data were coupled with an 11 keV

map of trace element distribution to identify unique areas in the sample. Principle Components Analysis (PCA) on these multiple energy XRF maps were used to identify the location of unique Fe species in the map area using Sam's Microprobe Analysis Kit (SMAK). We then collected representative μXANES spectra from those spots and employed PCA to identify key end member μXANES spectrum that represent the unique chemical forms of Fe in each sample. Finally, multiple-energy maps were fit with the fluorescence intensities of each end member μXANES spectra to show the distribution of Fe-bearing minerals in complex reacted and unreacted samples.

XANES were normalized with Sam's Interface for XAS Package (SIXPACK). XANES spectra were collected from a range of 6882-7152eV. To qualitatively determine Fe speciation and mineralogy, spectra were fit from 7110 to 7150 eV using least squares fitting of Fe model compounds (in SIXPACK) calibrated using the first inflection of a Fe^0 foil at 7112 eV (Mayhew et al., 2011). We also collected the pre-edge (7108-7118eV) region with a step size of 0.1eV and dwell time of 3 seconds and analyzed the pre-edge employing protocols by Andreani *et al.* (2013) and Wilke *et al.* (2001) to determine the ratio of Fe^{2+}/Fe^{3+} in the various generations of serpentine.

Beamline 4-1 at SSRL was used to collect bulk Fe K-edge spectra for seven powdered well chip samples. A Si (220) ϕ= 0 monochromator was used and X-ray absorption spectra (XAS) were collected on a Lytle detector. A Fe^0 foil standard was used and calibrated to 7112eV. Duplicate spectra were collected and averaged for XANES scanning from a range of 6882-7082eV with a step size of 10 points, then from 7092 to 7520 with a 0.35 step size.

Quantum Design MPMS Superconducting Quantum Interface Device (SQUID) magnetometer with the magnetic moment resolution of 10^{-8} emu at Department of Physics and Astronomy at Michigan State University was used to analyze bulk rock powder samples to determine magnetic hysteresis parameters. A total of 7 samples with various weights (40-259 mg) are measured over the range of ± 5 T at 300K.

Micro-Raman spectra and hyperspectral maps for well rock chip samples were collected using a Horiba LabRAM HR Evolution Raman spectrometer equipped with a 532nm frequency-doubled Nd:YAG laser (Laser Quantum, Torus 532 + mpc3000) coupled to an Olympus BXFM optical microscope. The laser beam was focused through a 50x objective lens, yielding a spatial resolution of ~2 µm. A 600 lines/mm grating and adjustable confocal pinhole (100 µm-200 µm) was used to give a spectral resolution full width at half maximum (FWHM) of 4.5-8.4 cm^{-1}. Spectra were collected from 20-1200cm^{-1} using a Si-based CCD detector (1024 x 256 pixels). The spectrometer was calibrated using the 520 cm^{-1} Raman peak of Si daily prior to analysis. Spectral data were corrected for instrumental artifacts and baseline-subtracted using a polynomial fitting algorithm in LabSpec 6 (Horiba Scientific). For the Raman microspectroscopy analyses, the drill cuttings from each depth in NSHQ14 and NSHQ04 were analyzed by generating hyperspectral maps of representative areas in the thin sections, using Multivariate Curve Resolution-Alternating Least Squares (MCR-ALS) and non-negativity constraints on scores and loadings to determine the main spectral components present, then collecting spot Raman spectra to verify the components, and fitting the hyperspectral data set with the end member spectra to generate component maps.

Quantitative chemical analysis of serpentine was performed using the electron microprobe laboratory at the University of Colorado at Boulder on the JEOL JXA-8600

equipped with 4 wavelength-dispersive spectrometers, and a PGT energy-dispersive spectrometer. Spot analyses of polished thin sections were performed at a current of 10 nA, accelerating voltage of 15 keV, and beam diameter of 10 μm to avoid destroying the hydrated serpentine sample to analyze the major element compositions of Si, Al, Mg, Na, Ca, Cr, K, Fe, Mn, and Ti, using natural standards.

TGA measurements were taken in a NETZSCH STA 449 F1 Jupiter. Between 60 and 110 mg of sample in an alumina crucible and a blank alumina crucible were heated in Argon up to 1000°C at a ramp rate of 10 Kelvin per minute. The crucibles were then held at 1000°C for one hour, at which point data collection stopped and the furnace cooled. The derivatives of the data were determined using NETZSCH Proteus.

2.4 *16S rRNA sequencing*

The microbial analyses were conducted as described previously (Bowers et al., 2013; Emerson et al., 2015). DNA was extracted from one quarter of each of the filter samples using the MoBio PowerSoil kit. The V4-V5 region of the 16S rRNA gene was PCR amplified in triplicate reactions using the 515f/806r primer pair. The primers contained the appropriate Illumina adapters and the reverse primer contains a 12-bp error-correcting barcode unique to each sample. The triplicate reactions were composited, amplicon concentrations were determined using the PicoGreen dsDNA assay, and the amplicons from all samples were pooled together in equimolar concentrations. Sequencing was conducted on an Illumina MiSeq at the University of Colorado Genomics Core Facility following the 2 × 250 bp paired-end protocol. Quality filtering of reads and processing of the reads was conducted as described in Barberán et al. (2015). After demultiplexing, reads were quality filtered at an equivalent sequencing depth (6000 reads per

sample) and clustered into phylotypes using the UPARSE pipeline (Edgar, 2013). Reads were assigned to phylotypes at the ≥97% sequence similarity threshold and phylotype taxonomy was determined using the RDP classifier with a confidence threshold of 0.5 (Wang et al., 2007) trained on the Greengenes 13_8 database (McDonald et al., 2012). Multivariate statistical analysis was performed in R, a software environment for statistical computing and graphics (R Development Core Team, 2008).

3. Results

3.1 *Aqueous geochemistry of wells*

Fluids were collected from two wells drilled into peridotite, NSHQ14 (up to a depth of 260m) and NSHQ04 (up to a depth of 50m, below which the well is collapsed). Minimum concentrations of dissolved H_2 and CH_4 were determined by GC. For NSHQ14 at 262m, some gas was lost from the fluids during the transfer from the bailer sampler to gas-tight vials due to rapid exsolution. The calculated dissolved H_2 concentrations range from 0.18 to 0.67 mM H_2, and the methane concentrations range from 0.17 to 1.44 mM (Table 1).

The fluids in both wells are hyperalkaline: NSHQ14 has a pH of 11.5 and NSHQ04 has a pH of 10.6. Major cation and anion analysis for fluids reveals >6mM Ca^{2+}, ≥0.005mM Mg^{2+}, and 6.75-12.30mM Na^+ (Table 1). Low molecular weight organic acids (lactate, acetate, formate, propionate, butyrate and valerate) are below detection limits of ~5.0 µM; thus, there is low dissolved organic carbon in the fluid. Dissolved inorganic carbon (DIC) levels for samples collected from these wells in 2012 were 0.078-0.391 mM (Paukert et al., 2012). Both wells contain high concentrations of Cl^- (>20 mM), which are almost two orders of magnitude higher than the 0.35 mM Cl^- present in Oman rainwater (Weyhenmeyer, 2000; Paukert et al., 2012). The well fluids contain 0.05-0.48 mM SO_4^{2-} and 0.012-0.022 mM NO_3^-. The trace element chemistry of the wells is similar; Ni and Cr are the most abundant metals (average of 0.15 and 0.18 µM, respectively. The only notable difference is NSHQ14 at 262m has more Zn (0.139 µM versus ~0.03 µM) than the other depths.

The fluids in the peridotite wells exhibit similar pH and aqueous geochemistry to surface alkaline springs previously sampled in Oman (Paukert et al., 2012); however, the NSHQ14 and

Table 1. Major and minor elements in wells along with pH, temperature, and conductivity. Oman hyperalkaline spring data is from Paukert et al. (2012) sampling Type II surface waters. Oxidation-reduction potential (ORP) data is from sampling the wells in 2012. Gas concentrations were determined by measuring the headspace of anaerobic vials purged with N_2 filled with site water.

	NSHQ04 18 meters	**NSHQ14 18 meters**	**NSHQ14 260 meters**	**Misbit - Oman hyperalkaline spring**	**Detection limit (µM)**
pH	10.6	11.1	11.5	11.2	-
Temperature (°C)	33.3	34.3	31.5	31.6	-
Conductivity (µS/m)	2386	2430	4300	1640	-
ORP (mV)	-103.4 (70m)	-31.6	-597.3	-	-
Na^+ (mM)	12.136	12.302	6.747	2.12	0.013
Ca^{2+} (mM)	6.424	7.604	9.001	0.017	0.008
Mg^{2+} (mM)	0.005	0.06	0.655	6.54	0.014
K^+ (mM)	0.409	0.422	0.361	-	0.039
$SiO_{2(aq)}$ (mM)	0.011	0.007	0.016	0.04	0.498
Cl^- (mM)	24.942	25.932	21.848	6.97	0.564
SO_4^{2-} (mM)	0.483	0.19	0.05	0.07	0.208
NO_3^- (mM)	0.012	0.022	0.016	<0.01	0.806
Br^- (mM)	0.001	<0.001	0.001	-	0.626
Al^{3+} (mM)	0.098	0.086	0.045	0.023	0.259
Fe^{2+} (mM)	<0.001	<0.001	<0.001	<0.001	0.004
DIC (mM)	0.091	0.078	0.391	-	-
H_2 (mM)	0.18	0.67	0.17	-	0.01
CH_4 (mM)	1.44	0.17	0.04	-	0.01
Ni (µM)	0.147	0.137	0.156	-	0.000
As (µM)	0.042	0.04	0.047	-	0.004
Se (µM)	0.094	0.144	0.166	-	0.002
Cu (µM)	0.032	0.04	0.045	-	0.001
Cd (µM)	<8.90E-05	<8.90E-05	<8.90E-05	-	0.000
Zn (µM)	0.028	0.056	0.139	-	0.001
Co (µM)	0.006	0.005	0.007	-	0.000
Cr (µM)	0.163	0.17	0.19	-	0.005

NSHQ04 well fluids contain more Ca^{2+}, Cl^-, NO_3^- and generally SO_4^{2-}. The dissolved silica concentrations are ~0.01mM $SiO_{2(aq)}$ versus the 0.04mM found in the surface seeps. Oxidation-reduction potential (ORP) values were measured during the January 2012 field season. NSHQ14 fluids exhibit much higher ORP values (-31.6 mV) near the surface at 18 meter, whereas the fluids at 260m are highly reducing (-597.3 mV). The ORP value for fluids collected from NSHQ04 at 70 meters was -103.4 mV.

3.2 *Isotopic composition of fluids, dissolved gases, and carbonates*

The δD values of dissolved H_2 are very low (-680‰ and -686‰ for NSHQ04 and NSHQ14 respectively, Table 2). The $\delta^{18}O$ of the well waters are -3.0‰ and 0.7‰ and the δD values are -15‰ for NSHQ04 and 2‰ for NSHQ14. If the dissolved H_2 formed in isotopic equilibrium with the water, we calculate a temperature of formation of ~50°C using the theoretical geothermometer developed by Bottinga (1969). The δD values of CH_4 are also low, -205‰ and -232‰ for NSHQ04_18m and NSHQ14_262m, respectively. In contrast, the CH_4 is strongly enriched in ^{13}C ($\delta^{13}C$ CH_4 for NSHQ04_18m is +2.4‰; NSHQ14_262m is +3‰) (Table 2). These $\delta^{13}C$ CH_4 and δD CH_4 values from Oman subsurface fluids are notably higher than previously defined isotopic fields for thermogenic, biogenic, and abiotic methane (Figure 2). The carbonate found in the drill cuttings $\delta^{13}C_{VPDB}$ ranges from -1.48 to -7.05‰ while the $\delta^{18}O_{VPDB}$ ranges from -7.73 to -11.49‰ (Table 3). The carbonate concentrations in the rock were low and not quantified.

Table 2. δD H_2, $\delta^{13}C$ CH_4, and δD CH_4 values for subsurface well water in Oman (NSHQ04 and NSHQ14), as well as hyperalkaline surface springs in Oman (Neal and Stanger, 1983), Zambales Ophiolite in the Philippines (Abrajano et al., 1990), Lost City Hydrothermal Vents (Proskurowski et al., 2006), the Precambrian Canadian Shield (Sherwood Lollar et al., 1993), and the Cedars Ophiolite in California (Morrill et al., 2013).

	δD H_2 ‰	δD CH_4 ‰	$\delta^{13}C$ CH_4 ‰
NSHQ04_18m	-680	-205	2.4
NSHQ14_262m	-685	-232	3
Nizwa, Oman	-697		
Bahla, Oman	-699		
Huwayl Qufays, Oman	-699		
B'lad, Oman	-714		
Zambales Ophiolite	-581	-122	-7.34
Lost City Hydrothermal Vents	-609	-127	-10
Precambrian Canadian Shield	-619	-284	-29
Cedars ophiolite	-40 to -50		-68

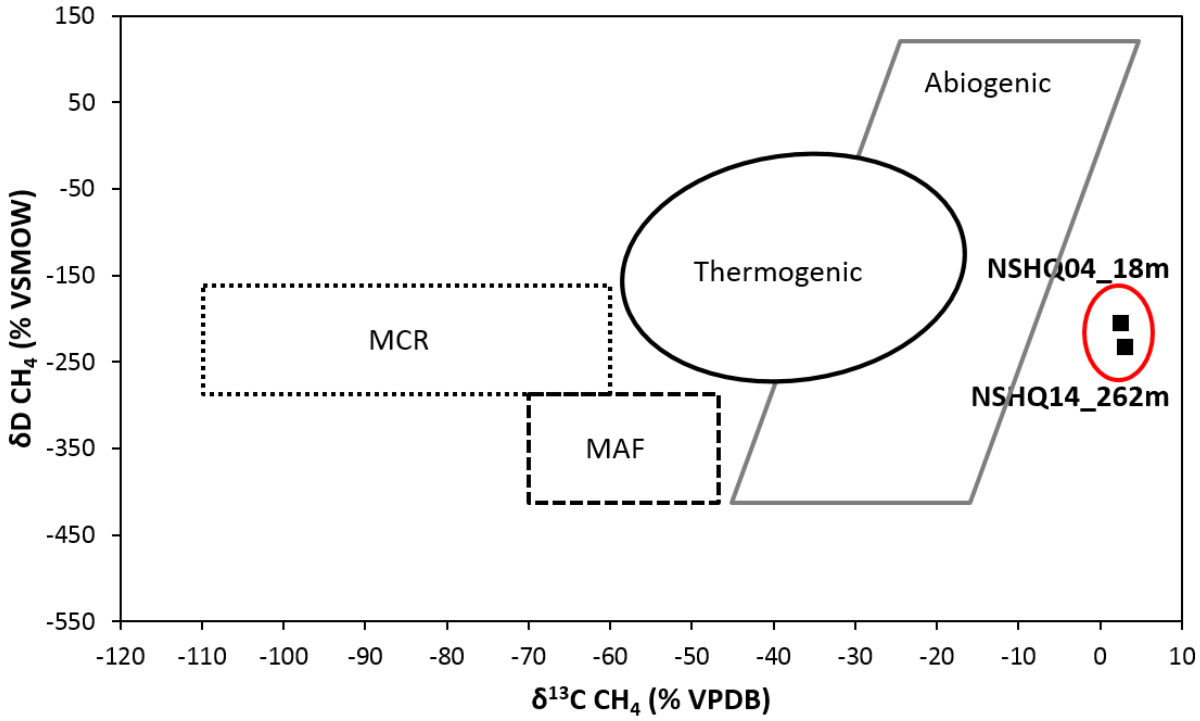

Figure 2. CH_4 isotope variation derived from deuterium and carbon isotopic data. MCR: Microbial CO_2 reduction, MAF: Microbial acetate fermentation (Etiope et al., 2013). Abiogenic red box drawn from variety of abiogenic sources (Abrajano et al., 1990; Sherwood Lollar et al., 1993; Etiope et al., 2011; Laier and Nytoft, 2012; Etiope et al., 2013) Thermogenic methane values encompass range of various thermogenically derived gases (Whiticar, 1990). Yellow circle surrounds values (black squares) obtained from subsurface hyperalkaline wells in Oman.

Table 3. $\delta^{13}C$ and $\delta^{18}O$ values from carbonate found in drill cuttings. The unreported values are due to low carbonate concentrations.

	$\delta^{13}C_{VPDB}$	$\delta^{18}O_{VPDB}$
NSHQ14_17m	-7.05	-7.73
NSHQ14_70m	--	--
NSHQ14_140m	-4.75	-11.07
NSHQ14_262m	-4.69	-11.49
NSHQ04_120m	--	--
NSHQ04_180m	--	--
NSHQ04_303m	-1.48	-10.99

3.3 *Mineralogy of drill cuttings*

Bulk powder XRD spectra are similar between the two wells. They are dominated by lizardite and enstatite and contain magnetite near the surface (Figure 3A,B). In the drill cuttings at 70, 140, and 262m from NSHQ14, there is a brucite peak at 18.8 2θ, but not at the shallow 17m. NSHQ04 drill cutting XRD spectra also contain a brucite peak at depth (180 and 303m), but not at 120m. There is a magnetite peak at 35.5 2θ in the NSHQ14 drill cuttings at 17 and 70m and in the NSHQ04 drill cuttings at 120 and 180m.

Microscale mineralogical structure and chemistry of drill cuttings were determined by a combination of petrologic observations, Raman microspectroscopy, Fe K-edge XANES spectroscopy and electron microprobe analyses. Olivine, diopside, enstatite, chromite, magnetite, brucite, and two-three different generations of serpentine, both chrysotile and lizardite, were detected in the drill cuttings of both wells using Raman microspectroscopy (Figure 4). Brucite and olivine are not detected in the drill cuttings closer to the surface, approximately <120 m. The NSHQ14 drill cuttings become increasingly serpentinized as they approach the surface, showing decreasing relict olivine with proximity to the surface and increasing serpentine (Figure 5). The NSHQ04 drill cuttings also show increased serpentine closer to the surface. There are visually more pyroxenes present in NSHQ04, both diopside and enstatite (Figure 6), and they appear to be partially fractured and altered (lower left corner of Figure 5). Drill cuttings from both wells have magnetite veins and grains (~5 μm) between 17-120 meters deep.

The Raman maps demonstrate that the drill cutting mineralogy is dominated by two to three generations of serpentine. Although chrysotile, lizardite, and antigorite can be identified by Raman spectroscopy from their varying peak positions (Rinaudo et al., 2003; Groppo et al., 2006; Petriglieri et al., 2015), differences in peak position are relatively small and can be obscured by large crystal orientation effects on the relative peak intensities. Furthermore, the

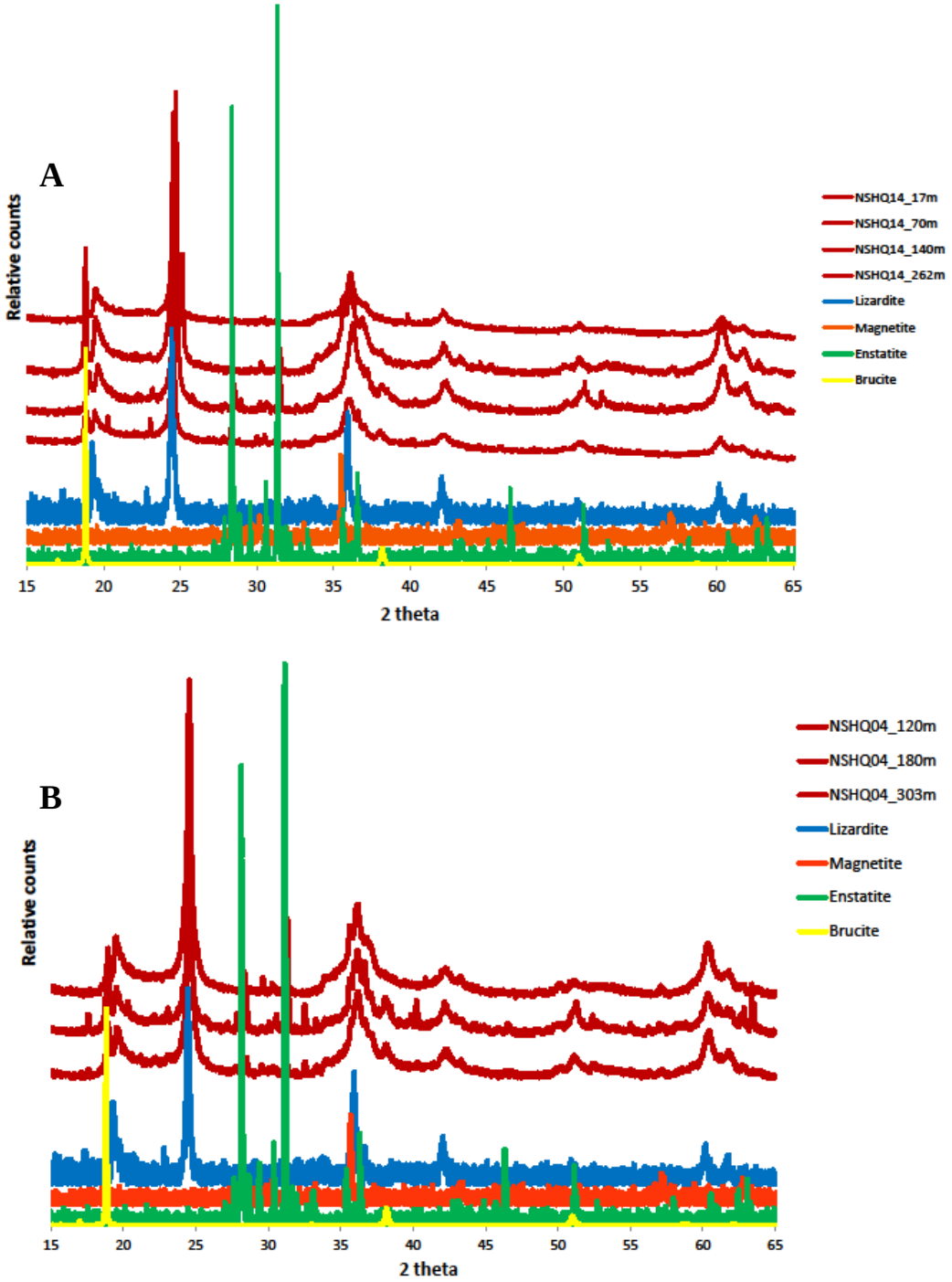

Figure 3. A: NSHQ14 powder XRD data from 4 well chip depths (in red, top 17m down to 262m). Lizardite peaks (blue spectrum) match best to drill cuttings (RRUFFID = 60006). Enstatite peaks (green) also match well (RRUFFID = 040093). Sharp peak centered at 18.8 corresponds to brucite (yellow, RRUFFID=050455). Magnetite (orange, RRUFFID=060656) peak at 35.5 is evident in drill cuttings closer to the surface. B: NSHQ04 powder XRD data from 3 well depths (in blue, 120m well chip on top and go down with depth to 303m). Lizardite peaks (blue spectra) match best to drill cuttings (RRUFFID = 60006). Enstatite peaks (green) also match well (RRUFFID = 040093). Sharp peak centered at 18.8 corresponds to brucite (yellow,

RRUFFID=050455). Magnetite (orange, RRUFFID=060656) peak at 35.5 is evident in drill cuttings closer to the surface. Both powder XRD datasets show increasing magnetite towards surface.

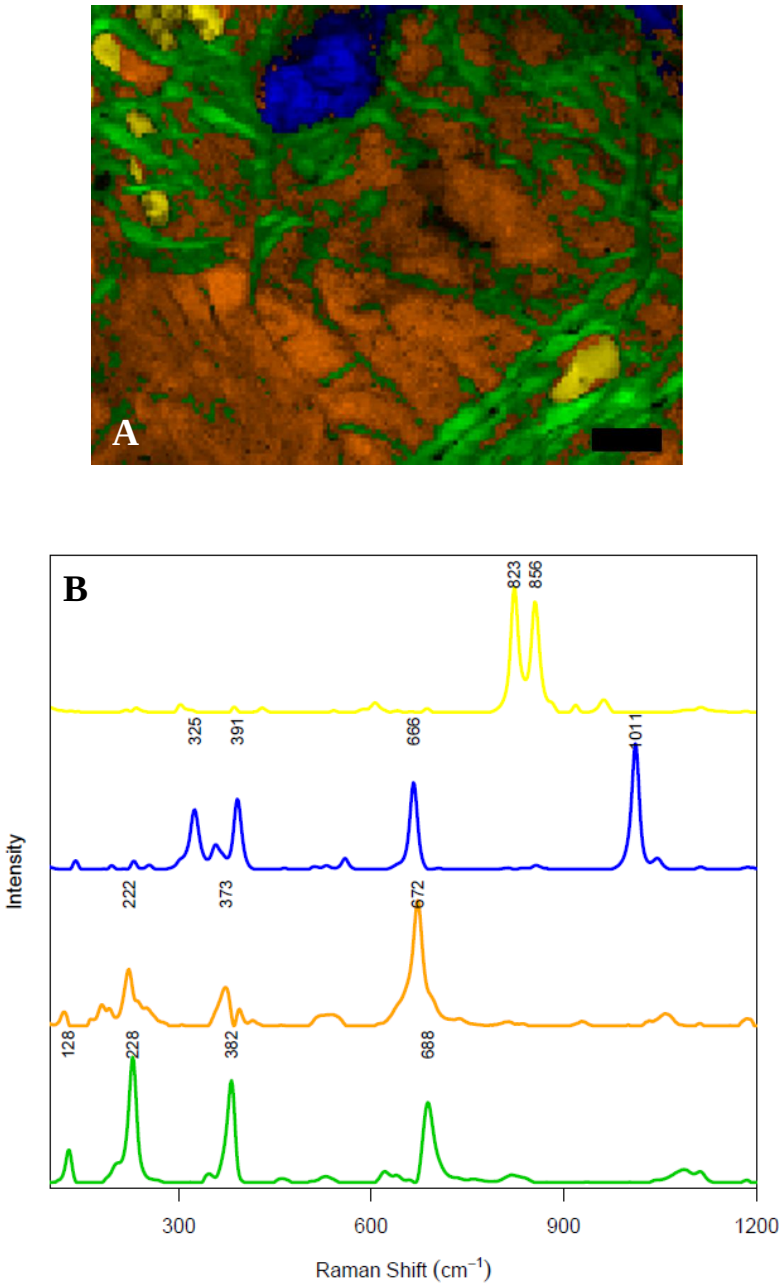

Figure 4. (a) Map of NSHQ14_262m thin section mineralogy generated using Raman spectroscopy and multivariate curve resolution-alternating least square (MCR-ALS). Lizardite (green, 14-gen2) is crosscutting an older generation of lizardite (orange, 14-gen1). Other components in the map include olivine (yellow) and diopside (blue). Scale bar 50 µm (b) Raman spectra for each component shown in map (a). Variation in peak position is due to orientation effects.

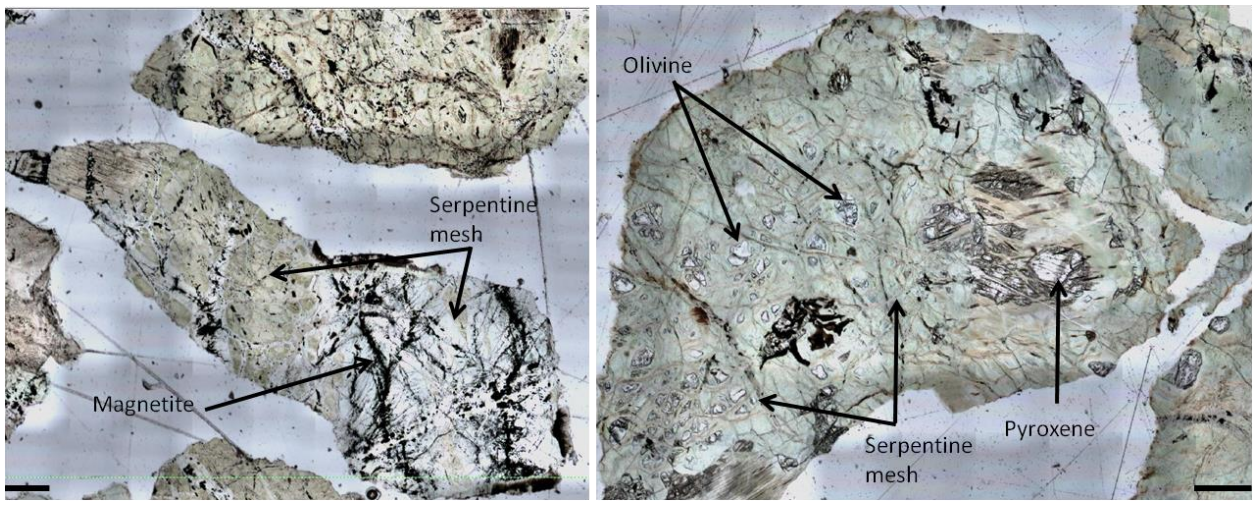

Figure 5. NSHQ14_17m (left) heavily serpentinized mesh texture with extensive magnetite veins compared to NSHQ14_262m with relict olivine (right). Scale bar 400µm

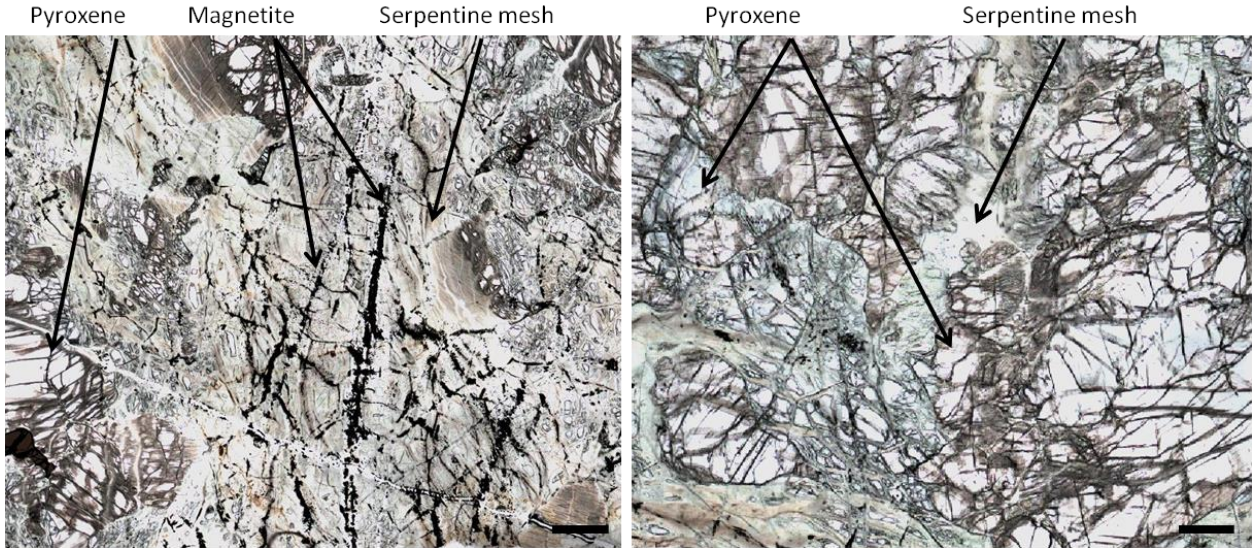

Figure 6. NSHQ04_120m well chip showing relict pyroxene with extensive magnetite veins compared to NSHQ04_180m showing large pyroxene grains and limited magnetite. Scale bar 400µm

effects of varying Mg/(Mg+Fe) and Fe^{3+}/Fe_T on the Raman spectra for the serpentine polytypes are not yet well quantified. Thus, it is difficult to determine the polymorphs of serpentine with certainty when just looking at the fingerprint region from 90-1600cm^{-1}. By mapping the serpentine in both the fingerprint region of 90-1600cm^{-1} and in the more diagnostic O-H stretching region of 3400-3800cm^{-1}, different regions of serpentine have been identified as chrysotile and lizardite (Figure 7C).

Crosscutting relationships reveal distinct generations of serpentine. NSHQ14 at 262 meters contains two generations of lizardite with an older lizardite (14-gen1) crosscut by a younger lizardite (14-gen2) (Figure 4). NSHQ04 at 180 meters has a complex alteration history with a first generation of chrysotile (04-gen1) overprinted by a younger second generation of chrysotile (04-gen2). Brucite is intermixed with third generation lizardite (04-gen3). The intermixed lizardite and brucite are visually apparent in plane polarized light as brown veins (Figure 7). All depths contain multiple generations of serpentine with chrysotile overprinted by lizardite that is variably intermixed with brucite. The drill cuttings closer to the surface contain less chrysotile and more lizardite. There is more brucite at depth than closer to the surface, as evidenced by powder XRD and Raman spectroscopy. Brucite is visually associated with brown serpentine as seen in Figure 7.

Both NSHQ14 and NSHQ04 drill cuttings contain widespread magnetite (Figure 8) as identified by Raman microscopy. The magnetite forms both veins and 2-10μm specks, in some cases in elongate patches or veins cross-cutting all generations of serpentine. Some magnetite is associated in veins with lizardite, but we can use cross-cutting relationships to infer that some of the magnetite postdates formation of all other alteration minerals in these drill cuttings. There is more magnetite observed closer to the surface.

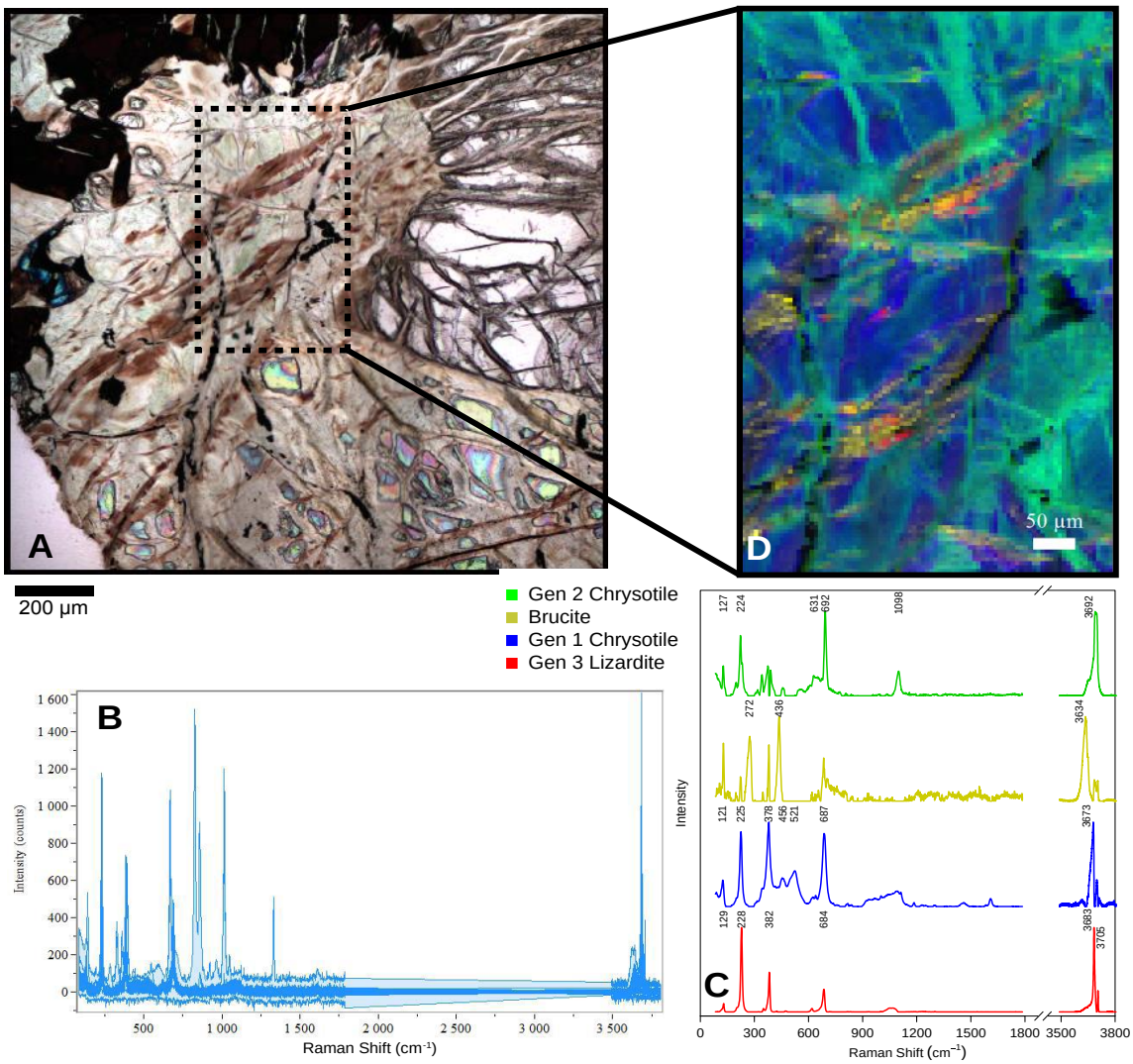

Figure 7. Micro-Raman mapping of well chip NSHQ04 at 180 meters depth. (A) Thin section image in transmitted light shows black magnetite surrounded by brown serpentine crosscutting background lighter serpentine. (B) shows all 14,529 spectra from map in "fingerprint" region between 90-1800 cm^{-1} and the O-H stretch from 3400-3800cm^{-1}. (C) We identified 4 distinct spectra for the major alteration minerals using MCR. Blue is generation 1 chrysotile (04-gen1) overprinted by green generation 2 chrysotile (04-gen2). These are both overprinted by the intermixed red generation 3 lizardite (04-gen3) and yellow brucite (D) These spectra were then fit to the entire map region.

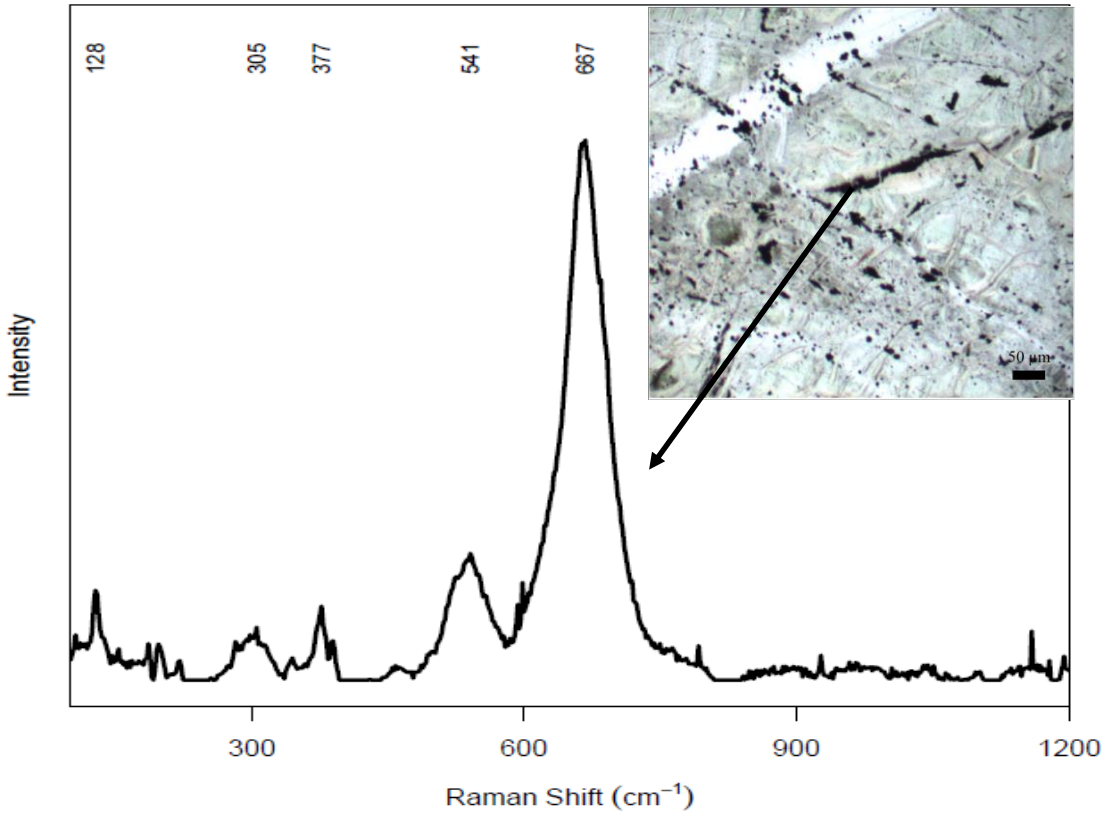

Figure 8. Raman spectra from NSHQ04_120m; magnetite veins (black veins and specks) as identified by Raman spectra. Magnetite is cross-cutting all generations of serpentine.

The chemical variation between generations of serpentine in well chip NSHQ04_180m was quantified with electron microprobe (Table 4). Generations 04gen1 and 04-gen2 chrysotile are chemically identical and contain high amounts of trace metals, notably an average of 0.67 wt% Al_2O_3, 0.22 wt% MnO and 0.33 weight% Cr_2O_3 whereas generation 04-gen3 lizardite has less than 0.07 wt% of those elements. Generation 04-gen3 lizardite has more MgO (40.90 wt% versus 36.06 wt%) and less SiO_2 (34.60 wt% versus 36.87 wt%) than the chrysotile. The totals are low for the serpentine, possibly due to the presence of brucite intermixed with serpentine as well as due to structural water.

We tried to quantify the amount of brucite and serpentine in the drill cuttings with TGA analysis (e.g. Lafay et al., 2012). We first measured known amounts of serpentine and brucite separately, and then mixed the two minerals to verify the method (Supplementary Figure 1). The resulting spectra and mass estimates are found in supplemental information. From this test, we see that mixtures of serpentine and brucite are not reliable for determining the mass of both minerals. Thus, we did not utilize TGA as a technique for quantifying the mass of serpentine and brucite.

3.4 *Fe speciation within the drill cuttings*

When comparing bulk Fe-XANES of the drill cuttings to the bulk spectra of a partially serpentinized dunite (OM95-35) from Oman, the drill cutting spectra are more oxidized as noted by the shift in the spectral features to higher energies (Figure 9). Also, the drill cutting spectra are more oxidized than San Carlos olivine, the type specimen characteristic of unaltered olivine. However, it is difficult to discern differences in the Fe-XANES spectra and Fe-speciation (i.e. average oxidation states and mineralogy) between well depths (Figure 9).

Table 4. Electron microprobe weight % data for serpentine generations from well chip NSHQ04_180m corresponding to varying generations of serpentine identified with Raman spectroscopy. Numbers refer to various analysis spots on the well chip thin section.

Generation 1 and 2 chrysotile (04-gen1,2)						
Sample	**3**	**5**	**6**	**9**	**10**	**average**
Na_2O	0.00	0.00	0.00	0.00	0.04	0.01
MgO	36.41	35.22	36.17	36.86	35.63	36.06
Al_2O_3	0.40	0.99	0.82	0.31	0.85	0.67
SiO_2	38.21	35.97	36.40	36.70	37.05	36.87
CaO	0.40	0.54	0.44	0.30	0.47	0.43
FeO	7.29	8.50	7.51	8.12	8.20	7.92
MnO	0.20	0.26	0.18	0.14	0.32	0.22
TiO_2	0.00	0.00	0.00	0.00	0.00	0.00
Cr_2O_3	0.09	0.61	0.51	0.00	0.42	0.33
Total	82.99	82.09	82.03	82.43	82.99	82.51
Mg #	0.83	0.81	0.83	0.82	0.81	0.82
Generation 3 lizardite intermixed with brucite (04-gen3)						
Sample	**7**	**8**	**11**	**12**	**13**	**average**
Na_2O	0.00	0.00	0.00	0.00	0.00	0.00
MgO	41.00	41.01	40.93	40.74	40.84	40.90
Al_2O_3	0.00	0.00	0.08	0.14	0.03	0.05
SiO_2	33.58	34.51	35.74	34.63	34.54	34.60
CaO	0.06	0.07	0.12	0.15	0.12	0.10
FeO	8.12	7.41	6.07	6.13	7.24	6.99
MnO	0.00	0.00	0.11	0.09	0.15	0.07
TiO_2	0.00	0.00	0.00	0.00	0.00	0.00
Cr_2O_3	0.00	0.00	0.00	0.00	0.00	0.00
Total	82.76	83.00	83.05	81.88	82.93	82.72
Mg #	0.83	0.85	0.87	0.87	0.85	0.85

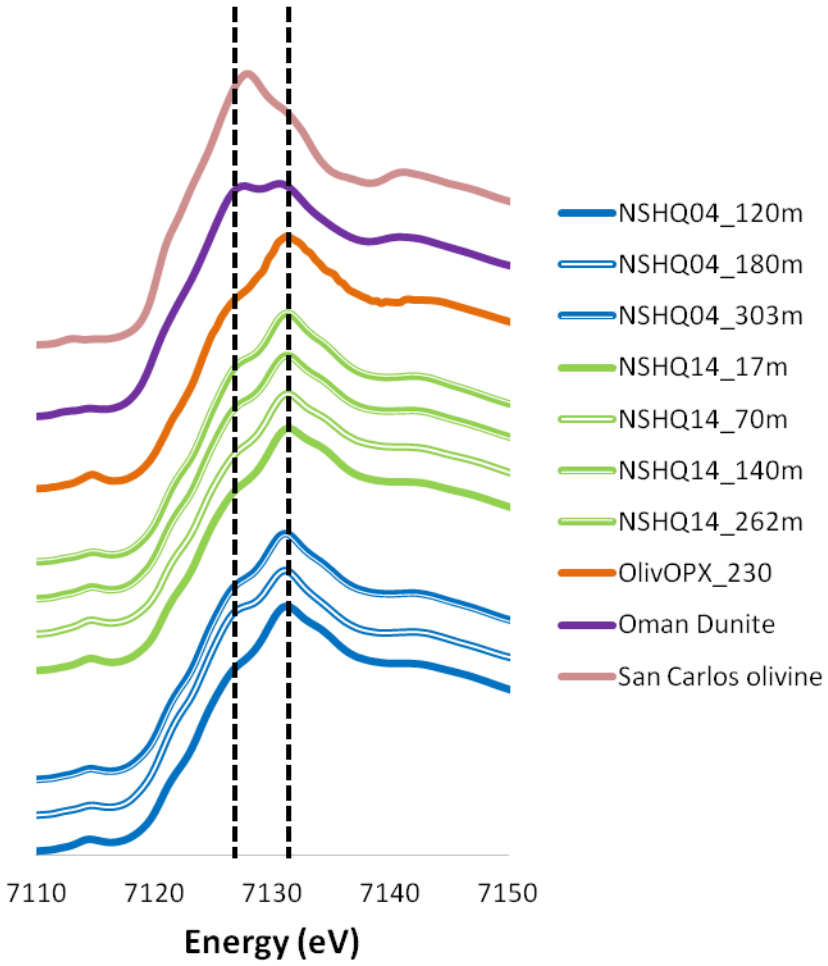

Figure 9. Bulk Fe K-edge XANES data for all depths of NSHQ14 and NSHQ04. Representative spectra of partially serpentinized dunite from Oman, XANES spectra of San Carlos olivine (type specimen of unaltered olivine), and OlivOPX_230 (serpentine formed during laboratory alteration of olivine and pyroxene with water at 230°C) are also shown.

The bulk Fe-XANES spectra of the drill cutting samples were fit by Fe XANES model spectra (e.g. Mayhew et al., 2011) of known minerals in the sample: olivine, pyroxene, brucite, magnetite, and serpentine. The linear-combination fits to the data show that serpentine increases in the higher drill cuttings, and olivine and brucite decreases, while pyroxene remains relatively constant (Supplementary Table 3). The changes in bulk Fe speciation are small and due to the number of Fe-bearing phases present, the bulk Fe XANES data is relatively insensitive to noted mineralogical changes such as increased magnetite. We did not collect a highly resolved pre-edge for the bulk XANES data; thus, it was not possible to quantify a shift in Fe(II)/Fe(III) with depth.

We obtained Fe K-edge μXANES spectra from the multiple generations of serpentine (as identified from Raman spectroscopy) to determine variations in Fe-oxidation state and coordination within serpentines across samples. Three distinct Fe K-edge serpentine spectra with varying oxidation states are shown in Figure 10. Focusing on the pre-edge (7108-7118eV) reveals the unoccupied states of the Fe 2p orbital, giving insight into both oxidation state and coordination (Wilke et al., 2001; Andreani et al., 2013a). The serpentine spectra have a shift in the centroid position in the pre-edge to higher energy, which reveals that there is a significant Fe(III) component. In addition, the increase in the fluorescence intensity at higher energy indicates that some of this Fe(III) is tetrahedrally coordinated. The spectra with the prominent second peak at 7130eV most closely aligns with the lizardite generation identified by Raman, whereas the most shifted spectrum (prominent peak ~7130.5eV) is associated with the chrysotile. The spectrum most shifted to lower energy is San Carlos olivine - a reduced spectrum that contains only Fe^{2+} (Figure 10). The ferric to ferrous iron ratio could not be quantitatively calculated using the method of Wilke et al. (2001), Muñoz et al. (2013), and Andreani et al. (

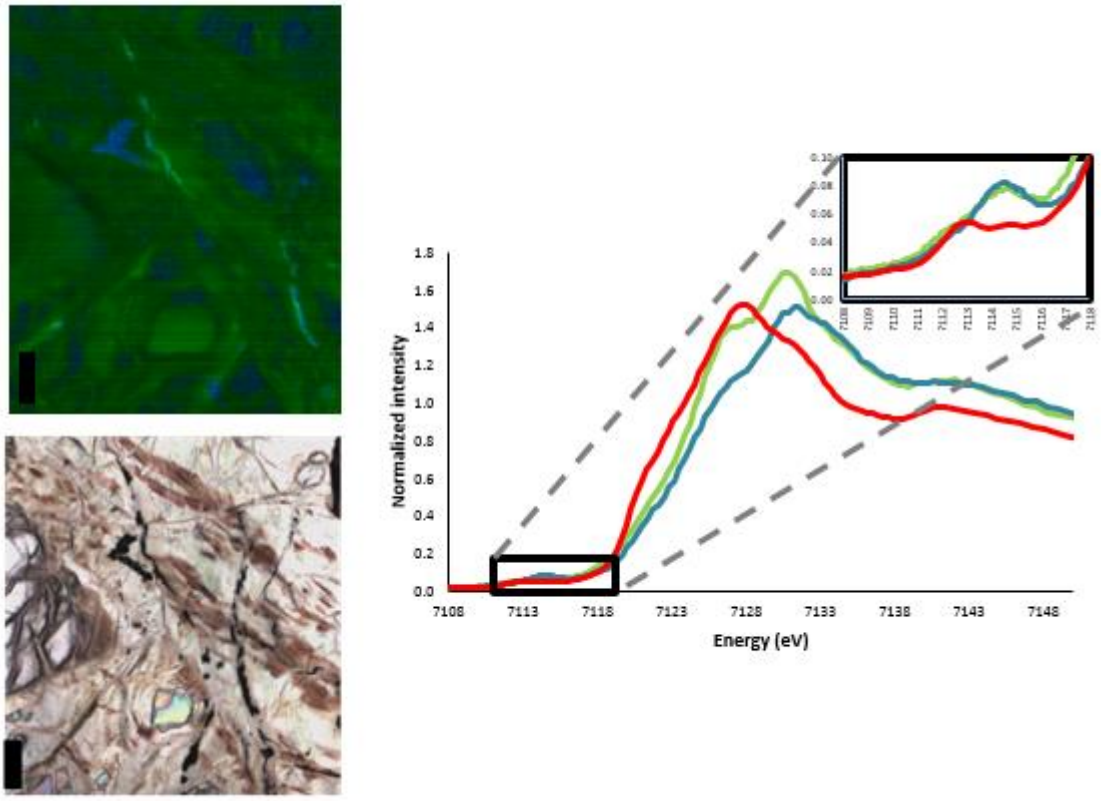

Figure 10. NSHQ04_180m Multiple energy Fe-K edge fitted map of serpentine variation. Two distinct serpentine Fe K-edge XANES spectra (green, blue) from 7108-7148eV, red spectra shows San Carlos olivine. The inset shows a zoomed-in pre-edge (7108-7118eV) environment, revealing that the blue and green spectra contain oxidized Fe(III) with tetrahedral component as seen by the prominent peak around 7114.5eV. Black scale bar is 90µm.

2013a) because these data were collected on a Beamline 2-3 at SSRL using a Si 110 vs. 311 monochromator, resulting in poorer energy resolution. This shifts and broadens the pre-edge features relative to published standards. However, such quantification will be possible in the future by measuring the same standards across multiple beamlines through inter-laboratory exchange.

3.5 *Magnetic hysteresis analysis of the drill cuttings*

The drill cuttings exhibit two distinctive types of hysteresis behavior. Drill cuttings deeper than 120m are paramagnetic while those shallower than 120m are ferromagnetic (Table 5). The ferromagnetic samples (NSHQ14_17m, NSHQ14_70m, and NSHQ04_120m) also show superparamagnetic behavior, indicating that a population of the magnetic minerals in the samples are smaller than magnetically stable single-domain size particles, likely < 20 nm (Dunlop, 1973; Butler and Banerjee, 1975; Worm, 1998). We also note a large increase in the saturation magnetization values in the drill cuttings closer to the surface than at depth in both NSHQ04 and NSHQ14 samples (Table 5).

3.6 *16S rRNA analysis of DNA collected from well fluids*

We sequenced the hypervariable V4-V5 region of the 16S rRNA gene from DNA extracted from filters that were loaded with biomass by pumping fluids from each well. Analysis of the 16S rRNA data shows that the NSHQ14 16S sequences were 99.5% bacteria and 0.05% archaea. Similar dominance of bacterial sequences was observed in NSHQ04 (99.4% bacteria and 0.06% archaea). The Bacteria are dominated by members of the Deinococcus-Thermus, Nitrospirae, Firmicutes, Chloroflexi, and Proteobacteria phyla. Fluids from both wells contain

Table 5. Room temperature magnetic hysteresis measurements. Grain size is detected from the hysteresis curve of each sample; hysteresis parameters obtained from modeled curve by QuickMagIC (Tauxe, 2010).

Well depth	Magnetic types	Hysteresis behavior	Saturation magnetization($A*m^2$)	Remanent magnetization($A*m^2$)	Saturation coercivity (T)	Coercivity (T)
NSHQ14_17m	Ferromagnetic	Super-paramagnetic	0.000151	0.000021	0.034300	0.011600
NSHQ14_70m	Ferromagnetic	Super-paramagnetic	0.000277	0.000023	0.034300	0.007960
NSHQ14_140m	Paramagnetic		0.000028	0.000004	0.033900	0.012900
NSHQ14_262m	Paramagnetic		0.000033	0.000004	0.036000	0.013550
NSHQ04_120m	Ferromagnetic	Super-paramagnetic	0.000359	0.000031	0.032900	0.008517
NSHQ04_180m	Paramagnetic		0.000057	0.000011	0.030500	0.014260
NSHQ04_303m	Paramagnetic		0.000191	0.000025	0.033600	0.011200

candidate phylum OP1 (1.1 and 2.8%, respectively), and NSHQ04 additionally has candidate phylum OD1. The species richness, as determined by the number of OTUs from each well, is 1737 for NSHQ04 fluids vs. 710 for NSHQ14. NSHQ04 is more diverse than NSHQ14.

We found that *Meiothermus* (phylum Deinococcus-Thermus, class Deinococci) comprises 8.6% (NSHQ04) and 46.1% (NSQH14) of the operational taxonomic units (OTUs) in both wells. *Thermodesulfovibrionaceaea* (phylum Nitrospirae), a sulfate-reducer, comprises 21.6% of NSHQ14 and 1.4% of NSHQ04. Chloroflexi is prominent in NSHQ04, 5.3%, but only 0.1% in NSHQ14 (Table 6). Both wells contain Firmicutes (class Clostridia family Anaerobrancaceae), fermentative microorganisms, and Proteobacteria (genus Hydrogenophaga), hydrogen-oxidizing bacteria found in other serpentinizing systems (Brazelton et al., 2013; Suzuki et al., 2013). The fluids from both wells notably contain methanogen *Methanobacterium*, which can utilize hydrogen and variable carbon sources such as formate to produce methane. *Methylococcus*, a methanotroph, is also present.

Table 6. Heat map of relative abundance of top OTUs from 16S rRNA sequencing of filtered well water from NSHQ04 and NSHQ14. Red indicates the highest number of OTUs, green indicates the lowest number of OTUs. Phyla, class, and order of best-fit OTUs are shown. The "other bacteria" correspond to OTUs that could not be matched to any known bacteria. The "remaining bacteria and archaea" corresponds to all OTUs that comprise <1.0% of the total OTUs.

NSHQ04	NSHQ14	Phyla	Class	Order
8.6%	46.1%	Deinococcus-Thermus	Deinococci	Thermales
1.4%	21.6%	Nitrospirae	Nitrospira	Nitrospirales
7.2%	0.0%	Firmicutes	Clostridia	Natranaerobiales
5.8%	0.4%	Proteobacteria	Gammaproteobacteria	Methylococcales
6.0%	0.0%	Proteobacteria	Betaproteobacteria	Burkholderiales
4.7%	0.0%	Bacteroidetes	Bacteroidia	Bacteroidales
3.5%	0.1%	Chloroflexi	TK17	mle1-48
2.4%	1.2%	Proteobacteria	Alphaproteobacteria	Rhodospirillales
2.3%	0.6%	Proteobacteria	Deltaproteobacteria	Desulfovibrionales
0.6%	2.2%	GAL15		
2.8%	0.0%	OP1	OPB14	
2.3%	0.1%	Proteobacteria	Gammaproteobacteria	Chromatiales
2.4%	0.0%	Proteobacteria	Betaproteobacteria	Rhodocyclales
0.6%	1.8%	Proteobacteria	Betaproteobacteria	Burkholderiales
2.2%	0.0%	Firmicutes	Clostridia	Desulforudales
0.2%	1.7%	Firmicutes	Clostridia	Natranaerobiales
1.9%	0.0%	Proteobacteria		
1.8%	0.0%	Chloroflexi	Anaerolineae	Anaerolineales
0.7%	0.9%	Proteobacteria	Betaproteobacteria	Burkholderiales
1.2%	0.0%	Other bacteria (unclassified)		
0.0%	1.1%	OP1	MSBL6	
1.0%	0.0%	Thermus-Deinococcus	Deinococci	Deinococcales
1.0%	0.0%	Firmicutes	Clostridia	
1.0%	0.0%	Other bacteria (unclassified)		
38.4%	22.4%	Remaining bacteria and archaea <1.0%		

4. Discussion

This study explores the mineralogy and aqueous geochemistry of modern water/rock reactions associated with low temperature serpentinization and hydrogen production in Oman and how these processes may give rise to habitable conditions for microbial life in the peridotite aquifer. We then use 16S rRNA sequencing of DNA extracted from subsurface fluids to investigate the phylogenetic diversity of the fluid microbial communities and infer potential microbial metabolisms sustained in-situ.

4.1 *Fluid chemistry of low temperature serpentinization*

Modern alteration of primary minerals in the aquifer is evident from the abundant Ca^{2+} and OH^- in peridotite hosted well waters NSHQ04 and NSHQ14 (Neal and Stanger, 1983; Neal and Stanger, 1984; Neal and Stanger, 1985). Neal and Stanger (1983, 1984,1985) extensively studied the hydrogeology of Oman's fluids and coined these hyperalkaline waters (pH > 11) containing Ca^{2+}-$2OH^-$ as Type II fluids, following the initial observation of Barnes and O'Neil (1969). They are situated in serpentinized dunite and harzburgite and are derived from serpentinization reactions with subsurface fluids that are isolated from the atmosphere. The hydration of olivine and pyroxene causes the water to become enriched in Ca^{2+}-OH^- (Barnes and O'Neil, 1969; Neal and Stanger, 1984; Bruni et al., 2002; Kelemen et al., 2011):

$$4\,Mg_2SiO_4 + CaMgSi_2O_6 + 7H_2O = 3\,Mg_3Si_2O_5(OH)_4 + Ca^{2+} + 2OH^- \quad (2)$$

The Ca^{2+} is released from diopside (present in all drill cuttings), and then accumulates in the water because Ca^{2+} is not incorporated into serpentine minerals (Barnes et al., 1967). These Type II fluids are carbon-depleted and when they emerge at surface springs, they rapidly mix with atmospheric carbon dioxide to precipitate carbonate minerals (Stanger, 1986; Kelemen and

Matter, 2008; Kelemen et al., 2011; Paukert et al., 2012; Mervine et al., 2014). The Ca^{2+} values we measure in the deeper subsurface fluids are ~1mM higher than those reported from hyperalkaline springs, presumably because Ca^{2+} in the subsurface has not been depleted through the precipitation of carbonate minerals. Thus, sampling the Type II fluids in wells before they interact with atmospheric CO_2 in the unsaturated zone or on the surface provides a more direct assessment of the water composition in the aquifer.

The subsurface well water contains more Cl^- than found in Oman rainwater and hyperalkaline surface seeps (Paukert et al., 2012) which provides additional proof that modern water/rock interaction is occurring. We infer that the high Cl^- concentrations are due to the presence of Cl^- that was incorporated in the Oman peridotite during initial, high-temperature serpentinization near an oceanic spreading ridge, and dissolved in groundwater during ongoing weathering (Stanger, 1986). The Cl^- is presumably at lower concentrations at the surface seeps than in the wells because it is precipitating with carbonates in salt.

The wells only contain Type II fluids; however, the shallow peridotite aquifer in Oman also hosts Mg^{2+}-$2HCO_3^-$ as observed by Barnes and O'Neil (1969). These are termed Type I fluids (Neal and Stanger, 1983; Kelemen et al., 2011) and are moderately alkaline fluids of a Mg^{2+}-$2HCO_3^-$ composition found in the shallow groundwater (~pH 8-9). In Oman, Type I fluids are typically found in wadi (channel that is dry except during rainy seasons) pools, ultramafic wadi gravels, and water wells (e.g., Neal and Stanger, 1985; Paukert et al., 2012) and form through the following simplified reaction (e.g. Kelemen et al., 2011):

$$Mg_2SiO_4 + 4\,CO_2 + 2\,H_2O = 2Mg^{2+} + 4HCO_3^- + SiO_2 \quad (3)$$

Atmospheric carbon dioxide dissolves in the water and forms bicarbonate as olivine and serpentine minerals in the near-surface react with the waters and release magnesium ions and

silica. Although we did not observe Type I fluids in this study, their mixing and interaction with Type II fluids may be influencing water/rock reactions and microbial diversity in the subsurface. In particular, the presence of oxygenated Type I fluids in the highly fractured upper portion of the aquifer may explain the aerobic organisms detected by 16S rRNA sequencing.

4.2 *Mineral assemblages associated with low temperature hydrogen production*

We investigated the mineralogy of the subsurface aquifer to see if the mineral assemblages give insight into the water/rock reactions and mechanisms that produce hydrogen at low-temperature. The drill cuttings contain serpentine, brucite, and magnetite, as is common in partially serpentinized peridotites. Although the drill cuttings are heavily serpentinized, they still contain relict olivine at depth that diminishes towards the surface, which suggests olivine may be the dominant mineral reacting with the in-situ fluids. There is a significant portion of unaltered pyroxene that could also be reacting; however, few zones of pyroxene alteration have been observed. Pyroxene alteration can be a dominant reaction in other serpentinizing sites (Klein et al., 2009; Marcaillou et al., 2011; Andreani et al., 2013a). A common alteration product of pyroxene is talc [$Mg_3Si_4O_{10}(OH)_2$] under conditions of high silica activity (Frost and Beard, 2007; McCollom and Bach, 2009; Klein et al., 2013). We do not observe any talc formation; thus, we do not believe pyroxene alteration is dominating the water/rock reactions, although the high concentrations of Ca^{2+} in the fluids do suggest that at least some pyroxene dissolution is occurring in the hyperalkaline aquifer.

The multiple generations of serpentine observed in the drill cuttings reveal that the mantle peridotite experienced multiple periods of water/rock alteration. The mantle section of the ophiolite was first serpentinized near an oceanic spreading ridge, during emplacement of the

ophiolite onto the Arabian continental margin, and/or during subaerial erosion and a subsequent marine transgression in the late Cretaceous (Kelemen and Matter, 2008; Hanghøj et al., 2010; Mervine et al., 2014). These events may have caused formation of the extensive chrysotile matrix seen in the drill cuttings. The chrysotile is overprinted by lizardite veins; however, we cannot infer a formation temperature due to the fact that chrysotile is metastable relative to lizardite (Evans, 2004).

We characterized the Fe content and speciation of the serpentine to investigate reservoirs of Fe in the system. Both the lizardite and chrysotile contain ~7-8 wt.% FeO_T (considering all Fe as Fe^{2+}). In average natural samples, chrysotile contains 3 wt.% FeO_T, while lizardite ranges from 2-8 mol.% Fe (Evans et al., 2009; Streit et al., 2012). Thus, the chrysotile in Oman is Fe-rich while the lizardite is average. Characterization of serpentine in our samples with electron microprobe and XANES confirms the presence both Fe(II) and Fe(III) in the serpentine. Fe(III) can substitute into both the octahedral and tetrahedral sites, replacing Si^{4+}, to form cronstedtite, $(Mg_2,Fe^{3+})_3(Fe^{3+},Si)_2O_5(OH)_4$ (Frost and Beard, 2007; Klein et al., 2009; Evans, 2010; Streit et al., 2012). The formula for chrysotile inferred during early alteration of the peridotite is $(Mg_{2.79}Fe^{II}_{0.10}Fe^{III}_{0.11})(Si_{1.89}Fe^{III}_{0.11})O_5(OH)_4$ while the younger lizardite formula is difficult to determine because it is intermixed with brucite. It contains less Si (perhaps due to intergrown brucite) than the chrysotile, but has high Fe concentrations (6-8 wt% FeO_T), with Fe occupying both tetrahedral and octahedral sites.

Fe(III) rich serpentine forms at low temperatures (<200°C) (Streit et al., 2012; Klein et al., 2013) and may have played an important role in hydrogen generation in Oman because it is another reservoir of oxidized Fe (besides magnetite), that can form during Fe(II)-driven reduction of water to form hydrogen. Generally, the oxidized Fe(III) is assumed to partition into

magnetite (equation 1). However, at lower temperatures, there is a decreasing thermodynamic drive for magnetite formation (Klein et al., 2013), and indeed magnetite may redissolve into serpentine at low temperature (Streit et al. 2012). Thus, Fe(III)-rich serpentine becomes an important mineral to consider as an indicator of hydrogen production during serpentinization (Klein et al., 2009; Marcaillou et al., 2011; Andreani et al., 2013b). The average oxidation state of Fe in the drill cuttings is greater than that of partially serpentinized dunite from Oman and San Carlos olivine (Figure 9). This reveals rocks interacting with hyperalkaline fluids have been altered after their initial formation when they contained mostly Fe(II). Moreover, spatially-resolved Fe K-edge XANES data on drill cuttings reveal the presence of Fe(III)-rich serpentine. Our observation of Fe(III) rich serpentine is consistent with observations from Streit et al. (2012) of Fe(III)-rich serpentine in Oman rocks undergoing low-temperature alteration processes, and from Andreani et al. (2013) during serpentinization at mid-ocean ridges (<150-200°C).

We find that in addition to Fe(III)-rich serpentine, magnetite is also formed during low-temperature serpentinization in Oman in the upper portions of the two wells studied. The simplified unbalanced equation (6) presented in Klein et al. (2013b) shows how magnetite and Fe(III)-rich serpentine can accommodate hydrogen production:

$$(MgFe)_2SiO_4 + vH_2O = w(MgFe^{II})OH_2 + x(MgFe^{II/III})_3(SiFe^{III})_2O_5(OH)_4 + yFe_3O_4 + zH_2 \quad (4)$$

Such reactions may contribute to the high levels of H_2 found in the subsurface fluids. As noted above, and demonstrated in Figure 8, there is extensive magnetite in our samples, with some of it forming veins that cross-cut all of the serpentine assemblages.

Downhole bulk sample magnetic hysteresis analyses indicate that the drill cuttings above 70 and 120 meters in NSHQ14 and NSHQ04 wells (respectively) are ferromagnetic (i.e. minerals

that retain remnant magnetization) and have superparamagnetic grain sizes, further confirming that there is increased magnetite in drill cuttings closer to the surface. The drill cuttings at depth, on the other hand, have a paramagnetic signature (i.e. no retainable magnetic properties without applied field). The hysteresis behavior (Tauxe et al., 2014) shows there are multiple size populations of magnetite in these rocks (micron-scale and nanoscale magnetite), or the visible magnetite particles must consist of aggregations of nano-scale magnetite.

The measured changes in magnetic character augment the petrological observation of increased magnetite population closer to the surface. It is possible to calculate an approximate mass of magnetite in the sample using an empirically derived constant of 92 $A.m^2/kg$ to correlate the saturation magnetization with the amount of magnetite (Malvoisin et al. 2012). However, such a quantification of magnetite assumes that the magnetic carrier in the sample is equal to and/or larger than single-domain size magnetite particles. This assumption may be false in our samples. Hysteresis analysis of each sample clearly exhibits significant contribution from superparamagnetic particles, which means the field will never be fully saturated, which effectively underestimates the amount of magnetite present in the drill cuttings. In addition, there is a prevalence of FeII/III-bearing serpentine grains also mixed within the matrix. Instead, we simply utilize the suite of magnetic data to show several lines of evidence indicating increased magnetite formation at shallow depths.

Brucite can accommodate Fe(II) in its structure that can then be oxidized during subsequent alteration to produce hydrogen at low temperatures (Klein et al., 2013). Typically, brucite forms mesh rims around olivine and traps Fe(II) in a stable mineral structure and prevents hydrogen generation (Klein et al., 2009; Evans, 2010). However, in our drill cutting samples, and in our comparison Oman dunite sample, we observe brucite intimately intermixed with lizardite.

It is not possible to determine an iron content for the brucite due to the fact that it is not present in large enough, serpentine-free areas for analysis. Electron microprobe measurements were not used to constrain Fe-contents of brucite intermixed with serpentine because Fe can substitute into Si sites in serpentine (particularly in Fe(III) rich serpentine) as well as Mg sites in brucite, thus an estimate of brucite calculated from electron microprobe would be inaccurate. However, Raman analysis shows a distinct change in the brucite spectrum from that of the pure $Mg(OH)_2$ endmember. Additionally, brucite in serpentinizing systems commonly contains iron; brucite can include greater than 10 wt% FeO_T, with increasing Fe content at lower temperatures in the same bulk composition (Moody, 1976; Klein et al., 2009). Yet brucite is not thermodynamically stable at the silica activities measured in our fluid samples (Table 1). Thus, we propose that brucite should react with silica-rich fluids in the aquifer (Bach et al., 2006), driving Fe(II) to undergo oxidation to form Fe(III)-rich serpentine and/or magnetite while concurrently reducing H_2O to make H_2 (see equation 7 below).

There are several possible reasons for the high silica activity in our fluid samples. First, the fluids in the wells are high in Ca^{2+}. Well NSHQ04 is close to the Moho, the zone of contact between peridotite and gabbro. Thus, it is possible gabbro-equilibrated fluids are interacting with the peridotite aquifer. Fluid that has equilibrated with gabbro has higher silica activity, and it will destabilize and consume brucite (Frost and Beard, 2007). However, there is insufficient hydrological information about the region surrounding the wells to test this hypothesis, and the similarity of fluids in wells NSHQ04 (near the Moho) and NSHQ14 (kilometers from the Moho) seems inconsistent with this hypothesis.

Bach et al. (2006) suggest that high Si fluids are generated when olivine nears exhaustion in the host rock and pyroxene alteration becomes a more important control on fluid chemistry. This is plausible given the low amount of relict olivine remaining in the drill cuttings.

A third possibility, as shown in equation 3, is that the generation of Type I waters in the shorter residence fluid-flow pathways can lead to fluids with high silica activities. Subsequently, we may be observing the destabilization of brucite in the host rock when Type I waters mix with Type II fluids within the shallow subsurface. This is supported by the observation of decreasing brucite in the highly serpentinized samples near the surface where Type I waters may be present.

There is increased extent of serpentinization in the drill cuttings near the surface as opposed to at depth, which suggests varying hydrological pathways in the subsurface. The top tens of meters below the surface could be subject to more variable conditions with higher water/rock ratios and/or interaction with Type I fluids than rock at depth due to rainwater recharge. This can lead to increased fracture permeability (e.g., Kelemen and Hirth, 2012) and periodic exposure to oxygen, as well as shorter fluid residence times. Thus, the fluids will not be equilibrated with the mineral assemblages, leading to more rapid destabilization and alteration, as well as increased oxidation and drive to form magnetite.

4.3 *Hydrogen generating reactions*

Based on our observations, we infer that three different hydrogen generating reactions have occurred in the subsurface. An initial serpentinization stage prior to modern water/rock reactions produced hydrogen from alteration of olivine and led to the production of Fe(II)-bearing brucite and Fe(III) rich serpentine (chrysotile generation):

$$(MgFe^{II})_2SiO_4 + H_2O = x(MgFe^{II})(OH)_2 + y\left(MgFe^{II/III}\right)_3(SiFe^{III})_2O_5(OH)_4 + zH_2 \quad (5)$$

There is relict olivine in the deep drill cuttings that is replaced by serpentine at shallower depths, so similar H_2 generating reactions could occur today. Moreover, less brucite might form because modern silica activities in the fluids are too high for brucite stability. Thus we suggest that relict olivine is now reacting to form new Fe(III)-bearing lizardite and hydrogen at low temperatures:

$$(MgFe^{II})_2SiO_4 + H_2O = x\left(MgFe^{II/III}\right)_3(SiFe^{III})_2O_5(OH)_4 + yH_2 \quad (6)$$

Currently, a high silica fluid is interacting with the rock, destabilizing the Fe(II)-bearing brucite (as modeled in Geochemist Workbench). This leads to the formation of magnetite and lizardite, with the production of hydrogen:

$$(MgFe^{II})(OH)_2 + SiO_2 = x(Fe^{II}Fe^{III}{}_2)O_4 + y\left(MgFe^{II/III}\right)_3(SiFe^{III})_2O_5(OH)_4 + zH_2 \quad (7)$$

The destabilization of Fe(II)-bearing brucite to form magnetite and serpentine, and the alteration of olivine to Fe(III) rich serpentine, should both produce hydrogen at low temperatures. This model of alteration and hydrogen generation is consistent with observations by Andreani et al. (2013b) that serpentinites from mid-ocean ridges contain both Fe(III)-serpentine and more magnetite as the degree of serpentinization increases.

4.4 Isotopic signature of hydrogen and methane

The isotopic signature of the H_2 serves as a valuable indicator of formation temperature, which complements mineralogical observations of serpentinization leading to hydrogen production. (Neal and Stanger, 1983) collected gas samples from surface hyperalkaline seeps and observed low δD H_2 values (-697‰ and -714‰) similar to those measured from our well samples (-680‰ and -686‰). They noted that H_2- and CH_4-rich gases (H_2 as high as 99% and CH_4 as high as 4.3%) emerge at hyperalkaline surface seeps, whereas the well fluids provide access to dissolved gases in the host rock itself. Sherwood Lollar et al. (1993), Proskurowski et

al. (2006), and Abrajano et al. (1990) also found negative δD gases that formed at low temperatures (<200°C) at other serpentinizing sites (both continental and oceanic), as shown in Table 4.

The dissolved gases from Oman subsurface wells uniformly contain some of the most negative δD hydrogen gas found in nature. We calculate a formation temperature of ~50°C by applying the geothermometer of Bottinga (1969) to the coupled δD H_2 and δD H_2O in the well fluids. Assuming the geothermal gradient at NSHQ14 is approximately 25°C/km (Paukert et al., 2012), the gases are hypothesized to form at a depth of less than 2km. A formation temperature of ~50°C supports the hypothesis that low-temperature serpentinization and hydrogen formation is occurring in the Oman aquifer, rather than H_2 being physically released from hydrogen inclusions that formed during higher temperature serpentinization events (McCollom and Seewald, 2001). We verified the lack of gas-rich inclusions in relict olivine by extensively probing the olivine grains by confocal Raman spectroscopy. However, the mantle section of the ophiolite is up to 8 km thick (Ravaut et al., 1997); thus, the H_2 could be generated at temperatures as high as 200°C and then migrate upwards to the surface. In this case, the current negative δD of the H_2 could instead represent isotopic exchange and re-equilibration between the H_2 and H_2O after formation of the H_2 as the waters circulate to shallower, cooler depths.

NSHQ04 fluids contain millimolar amounts of CH_4, which may be produced abiotically due to the highly reducing conditions reflected in the abundant H_2 in the system. In olivine dissolution reactions at 30+°C, (Neubeck et al., 2011) observed measureable CH_4, potentially through the oxidation of H_2 and reduction of CO_2 (Sleep et al., 2004). However, the CH_4 detected by Neubeck et al. (2011) could have been released from fluid inclusions, or produced by reaction of fluid with the experimental reaction vessel. At higher temperature (>120°C), CH_4

production can occur abiotically through Fischer-Tropsch-type or Sabatier reactions, through catalysis by magnetite and awaruite (Ni-Fe alloy) commonly found in serpentinites (Frost, 1985; Lorand, 1987; Horita and Berndt, 1999). Etiope et al. (2013) suggested catalysts such as ruthenium or chromite produce methane at temperatures <50°C. Such low temperature methane production may be possible in Oman due to the abundance of magnetite, chromite and awaruite found in the partially serpentinized mantle peridotites. Alternatively, methane formation could be biologically mediated by methanogens.

The $\delta^{13}C$ CH_4 signatures are the highest values reported in the literature thus far despite the wide range of methane isotopic compositions compiled in the past 30+ years. Plots comparing the ranges of $\delta^{13}C$ CH_4 and δD CH_4 found in various geologic environments (Whiticar, 1990; Etiope et al., 2013) give context to methane isotopic compositions measured in the peridotite-hosted wells in Oman. Thermogenic natural gas has been extensively studied, as have gases from extreme environments like hyperalkaline lakes and Antarctic ice sheets (Whiticar, 1990). The previously highest documented $\delta^{13}C$ CH_4 values (-1.6‰) were found from the Ilimaussaq inclusions Greenland (Laier and Nytoft, 2012; Etiope et al., 2013). That methane was hypothesized to have a biological origin, and subsequent sediment burial and partial loss by diffusion during uplift and erosion enriched the gas in isotopically heavy methane (Laier and Nytoft, 2012). A similar explanation is plausible for the high $\delta^{13}C$ CH_4 values in Oman. Alternatively, if the methane we observe in Oman formed abiotically at 50°C at a depth of ~2km, similar to the H_2, slow diffusion upwards from depth could fractionate and enrich the remaining methane in isotopically heavy carbon after the lighter ^{12}C CH_4 has diffused away. However, this should have a similar effect on the hydrogen isotopic composition of the methane as well, which

we did not observe. The methane-hydrogen D/H fractionation can be used to estimate temperature of formation of methane (Horibe and Craig, 1995) at ~70° +/- 3°C.

The isotopic composition of methane collected from wells in Oman falls near the traditionally defined abiotic range. Abiotic methane tends to have $\delta^{13}C$ CH_4 values greater than -50‰ and δD of CH_4 can range from -450 to -50‰ (Etiope and Sherwood Lollar, 2013; Etiope et al., 2013). Bacterial reduction of CO_2 to methane gives negative $\delta^{13}C$ CH_4 values as low as -110‰ and δD CH_4 down to -531‰ (Whiticar, 1999); thus, methane from Oman does not have a traditional bacterial signature. Low temperature CH_4 production has been experimentally demonstrated with ruthenium and rhodium catalysts (Jacquemin et al., 2010). Platinum group metal inclusions, including Ru and Rh, are found in chromites (e.g, Jacquemin et al., 2010). Platinum group metals in chromites in Oman could be catalyzing low temperature methane formation and leading to a heavy $\delta^{13}C$ CH_4 signature, but there are no experimental data to confirm this hypothesis. High ^{13}C CH_4 can also be produced by extensive biological oxidation of biogenic or abiogenic methane that enriches the residual methane in ^{13}C (Whiticar and Faber, 1986; Whiticar, 1999); however, this would also be expected to enrich δD in the residual methane. Thus, if methane cycling is active in the subsurface aquifer, the isotopic signature of CH_4 may not be an unequivocal marker of the methane formation pathway (Whiticar and Faber, 1986; Templeton et al., 2006).

The processes giving rise to the heavy $\delta^{13}C$ CH_4 in Oman cannot be elucidated without further investigation of the microbial and low-temperature abiotic pathways that are giving rise to the production of mM concentrations of CH_4. First, the source of carbon must be assessed. The $\delta^{13}C$ signature of carbonates mineralized in Oman peridotites provide some insights into the isotopic signature of the carbon pool. The carbonate found in the drill cuttings $\delta^{13}C$ ranges from -

1.48 to -7.05‰ while the $\delta^{18}O$ is -7.73 to -11.49‰. These values are similar to the Mg-rich carbonate veins from outcrops and roadcuts that have $\delta^{13}C$ ranging from -25.98 to 0.98‰ and $\delta^{18}O$ from -7.04 to 5.56‰ (Clark and Fontes, 1990; Kelemen and Matter, 2008; Kelemen et al., 2011; Mervine et al., 2014). The negative $\delta^{13}C$ values as low as -26‰ probably formed through a mechanism dominated by kinetic isotope fractionation during carbonate precipitation. Both the values from the drill cuttings and outcrops are still lighter than $\delta^{13}C$ in the CH_4, suggesting that even if the entire DIC pool was converted to methane under extreme carbon limitation, processes such as further $\delta^{13}C$ enrichment by diffusion or partial oxidation of the methane must be invoked.

4.5 *Potential metabolic pathways supported by hyperalkaline fluids*

The hyperalkaline fluids in Oman contain electron donors and acceptors to sustain anaerobic microbial metabolisms. There are millimolar amounts of H_2 and CH_4 to serve as electron donors, but dissolved organic acids were not detected at the micromolar detection limit. NSHQ04 notably contains high levels of SO_4^{2-}, which may be a source of critical electron acceptors for microorganisms (ex. sulfate reducers). Nitrate found in both wells is another potential electron acceptor that can be coupled with oxidation of H_2, CH_4 and Fe(II).

The aqueous geochemistry of the well fluids can support several potential metabolic pathways. Well fluids contain more sulfate and nitrate than samples from hyperalkaline seeps with comparable pH, and elevated H_2 and CH_4 (Paukert et al., 2012). Thus, nitrate and sulfate reduction at depth, tied to hydrogen oxidation, is likely. The high methane concentrations in NSHQ04 can support anaerobic oxidation of methane (AOM) (Hoehler et al., 1994; Joye et al., 2004), especially considering AOM consortia are often syntropically associated with sulfate-

reducing microorganisms. The following reactions are often invoked for serpentinizing systems and may be relevant metabolisms for microbial life in the subsurface of Oman:

$a.\ CO_{2(aq)} + 4H_{2(aq)} = CH_{4(aq)} + 2H_2O_{(l)}$

$b.\ 2NO_3^- + 10Fe^{2+} + 24H_2O_{(l)} = 10Fe(OH)_3 + N_2 + 18H^+$

$c.\ NO_3^- + 2.5H_{2(aq)} + H^+ = 0.5\ N_{2(aq)} + 3H_2O_{(l)}$

$d. SO_4^{2-} + 4H_{2(aq)} + 2H^+ = H_2S_{(aq)} + 4H_2O_{(l)}$

$e. CH_{4(aq)} + SO_4^{2-} = HCO_3^- + HS^- + H_2O_{(l)}$

$f. CH_{4(aq)} + 4NO_3^- = CO_{2(aq)} + 4NO_2^- + 2H_2O_{(l)}$

(Hoehler et al., 1994; Nielsen and Nielsen, 1998; Chapelle et al., 2002; Cardace and Hoehler, 2009; Haroon et al., 2013; Cardace et al., 2015). These metabolic strategies provide the energy to generate an electrochemical gradient to produce ATP. However, it is energetically taxing to generate a traditional hydrogen pump at high pH (Hicks et al., 2010; Suzuki et al., 2014). Microorganisms in Oman may be employing a sodium or calcium motive force to generate ATP instead of a proton pump. Many microorganisms pump H^+ ions outside the cell to create an energy gradient, but in a high pH environment, this H^+ quickly combines with abundant OH^- in the environment and cannot be utilized by the cell. Microorganisms can adapt to hyperalkaline conditions by generating a sodium motive force instead of pumping protons onto the surface of a cell inundated with OH^-. There is ample Na^+ in the fluids, so organisms in Oman may use a sodium motive force to cope with high pH environments. Alternatively, recent work has shown that some organisms can utilize a proton motive force, even under alkaline conditions (Mulkidjanian et al., 2008; Hicks et al., 2010; Suzuki et al., 2014). The pH in NSHQ04 is slightly lower than in NSHQ14, potentially making it more habitable for microorganisms. NSHQ04 also

has more abundant electron donors, nitrate and sulfate, than NSHQ14, further increasing its habitability.

4.6 *Organisms detected in fluids from 16S rRNA sequencing*

Predictions about potential metabolic pathways in serpentinizing systems aid in interpreting 16S rRNA data from the fluids and allow us to place the phylogeny of the organisms detected in the subsurface fluids within a context of potential functional activities. There is a curious mixture of both aerobic and strictly anaerobic microorganisms in the subsurface. DNA extracted from well fluids shows the presence of aerobic organisms *Meiothermus* and *Hydrogenophaga* that require oxygen as an electron acceptor. *Meiothermus* is considered to be obligately aerobic and chemoorganotrophic, capable of utilizing a range of carbon sources from glucose to acetate (Tindall et al., 2010). *Hydrogenophaga* is chemoorganotrophic or chemolithoautotrophic, and it oxidizes hydrogen and reduces organic material or heterotrophically denitrifies nitrate (Willems et al., 1989). We also found members of the Clostridia class and *Methanobacterium* genera, which are strict anaerobic fermenters and methanogens, respectively. Anaerobes *Thermodesulfovibrionaceaea* are also present, which are sulfate reducing bacteria that use hydrogen as electron donors and ferment pyruvate or other organics (Haouari et al., 2008). We likely significantly mixed the deep and shallow well fluids during pumping, so there may be internal variation in the fluid Eh as a function of depth, and intervals of variable permeability, that affect microbial community composition and function in ways that we cannot yet identify. The near-surface fluids probably have a shorter residence time and more recent interaction with ambient atmospheric oxygen. The mixture of organisms may

point to an upper zone of more oxidized fluids in the wells (e.g. Type I fluids), leading to an interesting geochemical interfaces that microorganisms can exploit.

Methanobacterium, a methanogen, is present in NSHQ04 and NSHQ14. This may explain the abundant CH_4 in the wells. It is a strict anaerobe that oxidizes H_2 and reduces formate, CO, or CO_2 to produce methane (Balch et al., 1979). Similar *Methanobacterium* sequences have also been observed in the Zambales ophiolite seeps (Woycheese et al., 2015). Methanogenesis is oftentimes invoked as a metabolic pathway in serpentinizing environments due to the abundant hydrogen and methane in the fluids (Chapelle et al., 2002; Cardace and Hoehler, 2009; Cardace et al., 2015). In order to determine *Methanobacterium*'s contribution to the CH_4 in the wells, it will be necessary to investigate the abundance and activity of the methanogens along with the isotopic signature of the CH_4 that they produce.

Candidate phylum OP1 was first detected in hot springs, but curiously it is present in the mesophilic, hyperalkaline conditions of the Oman subsurface. OP1 was first found in a neutral hot spring (75-95°C) in Yellowstone rich in iron, sulfide, carbon dioxide, and hydrogen (Kumar and Saravanan, 2011). There is a nearly complete genome for the OP1 *Candidatus* 'Acetothermus autotrophicum' that suggests it is one of the earliest bacteria to branch from the last universal common ancestor (Takami et al., 2012). 13 of the OP1 OTUs from NSHQ14 have 100% identity to this genome, whereas the other 250 OP1 OTUs are other species from candidate phylum OP1. The genome for *Candidatus* 'Acetothermus autotrophicum' has a high GC content (61.9%), and this organism is estimated to have an ideal growth temperature of 84.7°C. It also is phylogenetically similar to the members of the Deinococcus-Thermus clade, which is interesting giving the high concentrations of *Meiothermus* (phylum Deinococcus-Thermus) in the wells. The proposed metabolism of 'A. autotrophicum' is acetogenesis through the acteyl CoA pathway

utilizing CO_2 and H_2, which is an ancient C-fixation pathway (Takami et al., 2012). Candidate phyla by definition are phyla with no cultured and formally described representative strains, so little to nothing is known about their metabolic requirements and physiology. Future microbiological studies of Oman subsurface fluids may provide more insight into the function of these organisms, particularly if they can be cultured and studied in the laboratory.

A diverse range of phyla were identified from the well fluids. Clostridia and *Hydrogenophaga* are abundant in the fluids, supporting the idea that previous studies probing hyperalkaline seeps were identifying organisms that are indeed present in the subsurface (Brazelton et al., 2013; Suzuki et al., 2013). The *Hydrogenophaga* sequences detected here were 100% identical to *Serpentinomonas* (Suzuki et al., 2014), a bacterium cultured and characterized from the Cedars ophiolite. This organism is an obligate alkaliphile with an optimum growth pH of 11. It utilizes H_2, $CaCO_3$, and O_2 for growth. Clostridia, specifically members of the *Erysipelothrix* group, found in these samples were also found in the Tablelands Ophiolite, and this group is known to contain abundant fermentation-associated hydrogenases, suggesting that it uses organic compounds to survive (Brazelton et al., 2013). Lipids extracted from brucite-calcite veins at the Iberia margin, a Lost-City type hydrothermal field, are also hypothesized to correspond to *Desulfotomaculum* and *Clostridium* (Klein et al., 2015); thus, Clostridia are widespread in serpentinizing systems. Additionally, these anaerobic organisms contain [FeFe]-hydrogenases that can catalyze hydrogen production from the reduction of organic materials like acetate and formate (Brazelton et al., 2012). Clostridia are also endospore-forming, which may allow them to persist in these fluids during nutrient-poor periods (Madigan, 2012).

The metabolic pathways of the 16S rRNA correspond to predictions of potential metabolisms in the fluids that are derived from the in-situ geochemistry. Chloroflexi have a

range of metabolic strategies which include fermentation, CO_2 fixation, and acetogenesis (Hug et al., 2013). *Thermodesulfovibrionaceaea* is a sulfate-reducer, and some species of Clostridia may also be capable of sulfate reduction (Madigan, 2012). There are several Gammaproteobacteria in the fluids that may be denitrifiers (e.g. the extensively studied *Psuedomonoas stutzeri*) (Madigan, 2012). The other predicted metabolisms, such as methane oxidation and sulfate reduction, may be facilitated by Methylococcales and Desulfovibrionales.

The two wells host different microbial communities. This is most likely dictated by the varying geochemistry and pH between the subsurface systems. NSHQ04 has a lower pH (10.5) and more electron acceptors such as nitrate and sulfate to make it more habitable and diverse. NSHQ04 also has higher concentrations of CH_4 than NSHQ14, which is reflected by the fact that it contains methane oxidizers. Although our method of 16S rRNA amplicon sequencing does not reflect the quantity of organisms in the system, it does reveal that geochemistry strongly modulates microbial ecology in hyperalkaline subsurface fluids.

4.7 *Carbon sources in hyperalkaline fluids*

The well fluids from 2012 are carbon-poor with DIC concentrations that vary from 0.078-0.391mM. It is possible that the highly reducing conditions produced by high levels of H_2 in serpentinizing environments lead to the abiogenic formation of low weight molecular acids (Lang et al., 2010; Schrenk et al., 2013). McCollom and Seewald (2001) observed formation of formate during 300°C olivine serpentinization experiments:

$$CO_2 + H_2 = HCOOH \quad (8)$$

High concentrations of formate (36-158 μm/kg) are observed at the Lost City Hydrothermal Field, and isotopic data suggest that the formate formed abiotically (Proskurowski et al., 2006;

Lang et al., 2010). However, low molecular weight organic acids were not detected above the micromolar detection limit for the species measured in our samples, suggesting that they are not extensively produced under in-situ conditions. Alternatively, the absence of formate and other organic acids could be due to their rapid consumption by subsurface microorganisms.

We searched for complex organic carbon in the Oman drill cuttings as a potential carbon source and indicator of microbial life, but no accumulations of macromolecular carbon were detected in the well chips by Raman spectroscopy. Raman spectroscopic mapping has successfully been used to search for signs of life within serpentinized peridotites from the Mid-Atlantic Ridge, where complex organic carbon has been found in association with cavities in hydroandraditic garnets (Ménez et al., 2012). These hollow cavities are thought to host cryptoendolithic microbes, metabolizing H_2 generated through serpentinization or using Fe(III) in garnets as an oxidant for H_2. Complex organic molecules from these organisms might then migrate into the surrounding serpentines and ocean, providing a source of carbon for other microbial life (Pasini et al., 2013).

We also measured total organic carbon (TOC) in the drill cuttings through combustion techniques, but the results are likely overestimates because residual magnesite may be present (Supplementary Table 1). Organic carbon could derive from a rock-hosted biome, but these concentrations of organic carbon could also be a relic of drilling contamination or abiotic reduction of CO_2. Further information about molecular structure and distribution of organic carbon are necessary to characterize its source.

Heavily altered Oman peridotites contain extensive carbonate vein networks (Kelemen and Matter, 2008; Kelemen et al., 2011; Streit et al., 2012; Paukert et al., 2012; Mervine et al., 2014) which may provide an unconventional carbon source to microorganisms in the subsurface.

Previous work by Suzuki et al. (2014) shows the *Serpentinomonas* can utilize $CaCO_3$ as a carbon source. However, we do not detect the presence of carbonate veins in the drill cuttings, but they are most likely a small component (aqueous carbonic acid was not measured) so would not be easily detected by bulk powder XRD. We did a simple test for carbonate by adding HCl and measuring change in mass and observe about 1% carbonate in the drill cuttings; this is also a low estimate, since the analysis is neglecting to measure magnesite. Thus, carbonate veins in the rocks may be a carbon source for organisms in the subsurface.

Finally, Type I, Mg-HCO_3-rich waters are abundant in Oman, and contain 1-10 mM total carbon (e.g., compiled data in Supplement of Kelemen and Matter, 2008). Type I waters could supply carbon for growth of micro-organisms by infiltration into more heavily reacted rocks hosting Type II waters.

5. Conclusions

Subsurface mantle peridotites from the Samail Ophiolite in Oman are highly serpentinized and oxidized, and are in contact with hyperalkaline (>pH 10) fluids high in Ca^{2+}, OH^-, dissolved H_2 and CH_4. High concentrations of very negative δD H_2 values are inferred to have formed or equilibrated at ~50°C. The coupled δD and positive $\delta^{13}C$ of the dissolved CH_4 would traditionally be interpreted as abiotic, and dissolved CH_4 has the most isotopically heavy $\delta^{13}C$ CH_4 reported in the literature thus far. We suggest that the methane isotopic signature is in part modulated by significant oxidation, whether it was produced through biotic or abiotic pathways.

We hypothesize that these gas-rich hyperalkaline fluids have evolved through an ongoing stage of low temperature serpentinization in the peridotite. Olivine hydration during early hydrothermal alteration and obduction formed Fe(II,III) serpentine, Fe(II) brucite and hydrogen. During the current phase of low temperature water/rock interaction, brucite is destabilized in the fluids with high SiO_2 activity, generating H_2 when it is converted to magnetite and additional Fe(III)-rich serpentine. The relict olivine is also further reacting to form Fe(III)-rich serpentine and hydrogen. The formation mechanism for methane remains enigmatic, and could involve low temperature abiotic CO_2 reduction by mineral catalysts, or in-situ biological activity.

Our study of drill cuttings and fluids reveals that the timing and extent of various stages of serpentinization in Oman remain unconstrained. It is difficult to tease apart mineral parageneses formed during hydrothermal alteration near an oceanic spreading ridge, emplacement of the ophiolite, Late Cretaceous weathering, and modern water/rock reactions. Future studies that can connect rock alteration histories along reaction paths with varying fluid sources and residence times will be a valuable next step in assessing the mechanisms and extent

of modern, low-temperature H_2 and CH_4 generation. Continuous physical and magnetic properties measurements downhole and on bulk core samples will help delineate sections with hydrology *in situ* where serpentinization has been extensive.

16s rRNA data of DNA extracted from the hyperalkaline fluid microbial communities indicate an abundance of both aerobic and anaerobic organisms, including abundant *Meiothermus*, *Thermodesulfovibrionaceae* (sulfate-reducers), Clostridia (fermentors), and *Hydrogenophaga* (H_2-oxidizers). Although not abundant, the methanogen *Methanobacterium* and candidate phylum OP1 are notably present. We hypothesize that the subsurface microbial communities are harnessing the H_2 produced by water/rock reactions, and coupling the oxidation of H_2 to electron acceptors such as SO_4^{2-}, CO_2 and Fe(III)-bearing phases at depth, and episodically with O_2 and nitrate in the upper fractured part of the aquifer.

Probing the microbial community composition in these fluids provides a first glimpse into the complex subsurface peridotite-hosted microbiome. The rock-hosted communities may be quite different than those established in the fluids, due to strong gradients in redox potential, electron acceptor and donor availability, porosity, permeability, fluid residence times, and mineral reactivity. Moreover, this initial 16S rRNA gene sequence data are just an initial perspective within the broader efforts to fully understand feedbacks between microbial activity, aqueous geochemistry and mineralogy. Isolating and culturing the peridotite-hosted organisms will be an important step in understanding their true metabolic activities and how they adapt to the carbon-depleted, hyperalkaline fluid environment. The microorganisms may be utilizing carbonate veins as a carbon source, leading to mineral dissolution and potential methane production. Additionally, microbial consumption of hydrogen from water/rock reactions may increase the rate of hydrogen-producing reactions. Furthermore, in-situ microbes may be

generating distinct organic, mineral and/or isotopic biosignatures in serpentinizing environments that can be used to identify microbial activity remotely.

Examining the functional activity of microbial life in the subsurface will be important to fully understand the coupling between the water/rock reactions, production of reduced gases, and changes in aquifer chemistry and hydrology. A next step for studying the coupling between the hydrological and geochemical processes and the distribution and activity of subsurface microbial life will be to focus on process rate measurements of in-situ hydrogen generation and consumption, pathways of C assimilation and uptake, and rates of methanogenesis, sulfate reduction, and nitrate reduction. Intensive culturing of peridotite-adapted microorganisms in the laboratory will also be necessary to elucidate the operative metabolic pathways. All of these efforts will be greatly facilitated by the International Continental Drilling Program (ICDP) project in Oman (https://www.ldeo.columbia.edu/gpg/projects/icdp-workshop-oman-drilling-project). The results from this scientific endeavor will give further insight into predicted mineralogy, microbiology, gas generation and C cycling of planetary systems undergoing active alteration of peridotite in the shallow subsurface.

Acknowledgements: The authors would like to thank Tori Hoehler and Mike Kubo (NASA Ames) for providing exploratory organic acid analyses; Said Nasser Al-Habsi and Salim Mohammed Al Khanbashi of the Ministry of Regional Municipalities and Water Resources Sultanate of Oman for granting access to well fluids and drill cuttings; Amelia Paukert for providing supporting information and samples. We would also like to thank numerous colleagues at the University of Colorado at Boulder: Julien Allaz and the electron microprobe lab, the Raman lab, Fred Luiszer at the Laboratory for Environmental and Geological Studies, the Barger lab with their total organic carbon analyzer, the Fierer lab for their sequencing help, Lisa Mayhew for valued discussions and Kaitlin Rempfert for help collecting samples in 2015. Raman imaging and spectroscopy was conducted at the Raman Microspectroscopy Laboratory at the Department of Geological Sciences, University of Colorado-Boulder. Use of the Stanford Synchrotron Radiation Lightsource, SLAC National Accelerator Laboratory, is supported by the U.S. Department of Energy, Office of Science, Office of Basic Energy Sciences under Contract No. DE-AC02-76SF00515, in collaboration with staff scientists Sam Webb, Courtney Krest, and Ryan Davis. This research was funded by the Department of Energy (DE-SC0006886), the NASA Astrobiology Institute (Cooperative Agreement NNA15BB02A), Alfred P. Sloan Foundation Grant 2014-3-01, and NSF EAR-1049905.

References

Abrajano T. A., Sturchio N. C., Kennedy B. M., Lyon G. L., Muehlenbachs K. and Bohlke J. K. (1990) Geochemistry of reduced gas related to serpentinization of the Zambales ophiolite, Philippines. *Appl. Geochem.* **5**, 625–630.

Anderson R. T., Chapelle F. H. and Lovley D. R. (1998) Evidence Against Hydrogen-Based Microbial Ecosystems in Basalt Aquifers. *Science* **281**, 976–977.

Andreani M., Muñoz M., Marcaillou C. and Delacour A. (2013a) μXANES study of iron redox state in serpentine during oceanic serpentinization. *Lithos* **178**, 70–83.

Andreani M., Muñoz M., Marcaillou C. and Delacour A. (2013b) μXANES study of iron redox state in serpentine during oceanic serpentinization. *Lithos* **178**, 70–83.

Bach W., Paulick H., Garrido C. J., Ildefonse B., Meurer W. P. and Humphris S. E. (2006) Unraveling the sequence of serpentinization reactions: petrography, mineral chemistry, and petrophysics of serpentinites from MAR 15°N (ODP Leg 209, Site 1274). *Geophys. Res. Lett.* **33**. Available at: http://doi.wiley.com/10.1029/2006GL025681 [Accessed May 19, 2015].

Balch W. E., Fox G. E., Magrum L. J., Woese C. R. and Wolfe R. S. (1979) Methanogens: reevaluation of a unique biological group. *Microbiol. Rev.* **43**, 260–296.

Barberán A., Ladau J., Leff J. W., Pollard K. S., Menninger H. L., Dunn R. R. and Fierer N. (2015) Continental-scale distributions of dust-associated bacteria and fungi. *Proc. Natl. Acad. Sci.* **112**, 5756–5761.

Barnes I., LaMarche V. C. and Himmelberg G. (1967) Geochemical Evidence of Present-Day Serpentinization. *Science* **156**, 830–832.

Barnes I. and O'Neil J. R. (1969) The Relationship between Fluids in Some Fresh Alpine-Type Ultramafics and Possible Modern Serpentinization, Western United States. *Geol. Soc. Am. Bull.* **80**, 1947–1960.

Barnes I., O'Neil J. R. and Trescases J. J. (1978) Present day serpentinization in New Caledonia, Oman and Yugoslavia. *Geochim. Cosmochim. Acta* **42**, 144–145.

Bottinga Y. (1969) Calculated fractionation factors for carbon and hydrogen isotope exchange in the system calcite-carbon dioxide-graphite-methane-hydrogen-water vapor. *Geochim. Cosmochim. Acta* **33**, 49–64.

Boudier F., Baronnet A. and Mainprice D. (2010) Serpentine Mineral Replacements of Natural Olivine and their Seismic Implications: Oceanic Lizardite versus Subduction-Related Antigorite. *J. Petrol.* **51**, 495–512.

Bowers R. M., Clements N., Emerson J. B., Wiedinmyer C., Hannigan M. P. and Fierer N. (2013) Seasonal Variability in Bacterial and Fungal Diversity of the Near-Surface Atmosphere. *Environ. Sci. Technol.* **47**, 12097–12106.

Brazelton W. J., Morrill P. L., Szponar N. and Schrenk M. O. (2013) Bacterial Communities Associated with Subsurface Geochemical Processes in Continental Serpentinite Springs. *Appl. Environ. Microbiol.* **79**, 3906–3916.

Brazelton W. J., Nelson B. and Schrenk M. O. (2012) Metagenomic Evidence for H2 Oxidation and H2 Production by Serpentinite-Hosted Subsurface Microbial Communities. *Front. Microbiol.* **2**. Available at: http://www.frontiersin.org/Journal/10.3389/fmicb.2011.00268/full [Accessed January 30, 2014].

Bruni J., Canepa M., Chiodini G., Cioni R., Cipolli F., Longinelli A., Marini L., Ottonello G. and Vetuschi Zuccolini M. (2002) Irreversible water–rock mass transfer accompanying the generation of the neutral, Mg–HCO3 and high-pH, Ca–OH spring waters of the Genova province, Italy. *Appl. Geochem.* **17**, 455–474.

Butler R. and Banerjee S. (1975) Theoretical Single-Domain Grain Size Range m Magnetite and Titanomagnetite. *J. Geophys. Res.*, 4049–4058.

Cardace D. and Hoehler T. M. (2009) Serpentinizing Fluids Craft Microbial Habitat. *Northeast. Nat.* **16**, 272–284.

Cardace D., Meyer-Dombard D. R., Woycheese K. M. and Arcilla C. A. (2015) Feasible metabolisms in high pH springs of the Philippines. *Front. Microbiol.* **6**. Available at: http://journal.frontiersin.org/Article/10.3389/fmicb.2015.00010/abstract [Accessed May 21, 2015].

Chapelle F. H., O'Neill K., Bradley P. M., Methé B. A., Ciufo S. A., Knobel L. L. and Lovley D. R. (2002) A hydrogen-based subsurface microbial community dominated by methanogens. *Nature* **415**, 312–315.

Chavagnac V., Ceuleneer G., Monnin C., Lansac B., Hoareau G. and Boulart C. (2013) Mineralogical assemblages forming at hyperalkaline warm springs hosted on ultramafic rocks: A case study of Oman and Ligurian ophiolites. *Geochem. Geophys. Geosystems* **14**, 2474–2495.

Chavagnac V., Monnin C., Ceuleneer G., Boulart C. and Hoareau G. (2013) Characterization of hyperalkaline fluids produced by low-temperature serpentinization of mantle peridotites in the Oman and Ligurian ophiolites. *Geochem. Geophys. Geosystems* **14**, 2496–2522.

Clark I. D. and Fontes J.-C. (1990) Paleoclimatic reconstruction in northern Oman based on carbonates from hyperalkaline groundwaters. *Quat. Res.* **33**, 320–336.

Coleman R. G. (1981) Tectonic setting for ophiolite obduction in Oman. *J. Geophys. Res. Solid Earth* **86**, 2497–2508.

Dewandel B., Lachassagne P., Boudier F., Al-Hattali S., Ladouche B., Pinault J.-L. and Al-Suleimani Z. (2005) A conceptual hydrogeological model of ophiolite hard-rock aquifers in Oman based on a multiscale and a multidisciplinary approach. *Hydrogeol. J.* **13**, 708–726.

Downs R. T. (2006) The RRUFF Project: an integrated study of the chemistry, crystallography, Raman and infrared spectroscopy of minerals. In *Program and Abstracts of the 19th General Meeting of the International Mineralogical Association in Kobe, Japan* pp. O03–13.

Dunlop D. J. (1973) Superparamagnetic and single-domain threshold sizes in magnetite. *J. Geophys. Res.* **78**, 1780–1793.

Edgar R. C. (2013) UPARSE: highly accurate OTU sequences from microbial amplicon reads. *Nat. Methods* **10**, 996–8.

Emerson J. B., Keady P. B., Brewer T. E., Clements N., Morgan E. E., Awerbuch J., Miller S. L. and Fierer N. (2015) Impacts of Flood Damage on Airborne Bacteria and Fungi in Homes after the 2013 Colorado Front Range Flood. *Environ. Sci. Technol.* **49**, 2675–2684.

Etiope G., Ehlmann B. L. and Schoell M. (2013) Low temperature production and exhalation of methane from serpentinized rocks on Earth: A potential analog for methane production on Mars. *Icarus* **224**, 276–285.

Etiope G., Schoell M. and Hosgörmez H. (2011) Abiotic methane flux from the Chimaera seep and Tekirova ophiolites (Turkey): Understanding gas exhalation from low temperature serpentinization and implications for Mars. *Earth Planet. Sci. Lett.* **310**, 96–104.

Etiope G. and Sherwood Lollar B. (2013) Abiotic Methane on Earth. *Rev. Geophys.* **51**, 276–299.

Evans B. W. (2010) Lizardite versus antigorite serpentinite: Magnetite, hydrogen, and life (?). *Geology* **38**, 879–882.

Evans B. W. (2004) The Serpentinite Multisystem Revisited: Chrysotile Is Metastable. *Int. Geol. Rev.* **46**, 479–506.

Evans B. W., Kuehner S. M. and Chopelas A. (2009) Magnetite-free, yellow lizardite serpentinization of olivine websterite, Canyon Mountain complex, N.E. Oregon. *Am. Mineral.* **94**, 1731–1734.

Frost B. R. (1985) On the stability of sulfides, oxides, and native metals in serpentinite. *J. Petrol.* **26**, 31–63.

Frost B. R. and Beard J. S. (2007) On Silica Activity and Serpentinization. *J. Petrol.* **48**, 1351–1368.

Groppo C., Rinaudo C., Cairo S., Gastaldi D. and Compagnoni R. (2006) Micro-Raman spectroscopy for a quick and reliable identification of serpentine minerals from ultramafics. *Eur. J. Mineral.* **18**, 319–329.

Hanghøj K., Kelemen P. B., Hassler D. and Godard M. (2010) Composition and Genesis of Depleted Mantle Peridotites from the Wadi Tayin Massif, Oman Ophiolite; Major and Trace Element Geochemistry, and Os Isotope and PGE Systematics. *J. Petrol.* **51**, 201–227.

Haouari O., Fardeau M.-L., Cayol J.-L., Fauque G., Casiot C., Elbaz-Poulichet F., Hamdi M. and Ollivier B. (2008) Thermodesulfovibrio hydrogeniphilus sp. nov., a new thermophilic sulphate-reducing bacterium isolated from a Tunisian hot spring. *Syst. Appl. Microbiol.* **31**, 38–42.

Haroon M. F., Hu S., Shi Y., Imelfort M., Keller J., Hugenholtz P., Yuan Z. and Tyson G. W. (2013) Anaerobic oxidation of methane coupled to nitrate reduction in a novel archaeal lineage. *Nature* **500**, 567–570.

Hicks D. B., Liu J., Fujisawa M. and Krulwich T. A. (2010) F1F0-ATP synthases of alkaliphilic bacteria: Lessons from their adaptations. *Biochim. Biophys. Acta BBA - Bioenerg.* **1797**, 1362–1377.

Hoehler T. M., Alperin M. J., Albert D. B. and Martens C. S. (1994) Field and laboratory studies of methane oxidation in an anoxic marine sediment: Evidence for a methanogen-sulfate reducer consortium. *Glob. Biogeochem. Cycles* **8**, 451–463.

Horibe Y. and Craig H. (1995) DH fractionation in the system methane-hydrogen-water. *Geochim. Cosmochim. Acta* **59**, 5209–5217.

Horita J. and Berndt M. E. (1999) Abiogenic Methane Formation and Isotopic Fractionation Under Hydrothermal Conditions. *Science* **285**, 1055–1057.

Hug L. A., Castelle C. J., Wrighton K. C., Thomas B. C., Sharon I., Frischkorn K. R., Williams K. H., Tringe S. G. and Banfield J. F. (2013) Community genomic analyses constrain the distribution of metabolic traits across the Chloroflexi phylum and indicate roles in sediment carbon cycling. *Microbiome* **1**, 22.

Jacquemin M., Beuls A. and Ruiz P. (2010) Catalytic production of methane from CO2 and H2 at low temperature: Insight on the reaction mechanism. *Catal. Today* **157**, 462–466.

Joye S. B., Boetius A., Orcutt B. N., Montoya J. P., Schulz H. N., Erickson M. J. and Lugo S. K. (2004) The anaerobic oxidation of methane and sulfate reduction in sediments from Gulf of Mexico cold seeps. *Chem. Geol.* **205**, 219–238.

Kelemen P. B. and Hirth G. (2012) Reaction-driven cracking during retrograde metamorphism: Olivine hydration and carbonation. *Earth Planet. Sci. Lett.* **345–348**, 81–89.

Kelemen P. B. and Matter J. (2008) In situ carbonation of peridotite for CO2 storage. *Proc. Natl. Acad. Sci.* **105**, 17295–17300.

Kelemen P. B., Matter J., Streit E. E., Rudge J. F., Curry W. B. and Blusztajn J. (2011) Rates and Mechanisms of Mineral Carbonation in Peridotite: Natural Processes and Recipes for Enhanced, in situ CO2 Capture and Storage. *Annu. Rev. Earth Planet. Sci.* **39**, 545–576.

Klein F., Bach W., Humphris S. E., Kahl W.-A., Jons N., Moskowitz B. and Berquo T. S. (2013) Magnetite in seafloor serpentinite--Some like it hot. *Geology* **42**, 135–138.

Klein F., Bach W., Jöns N., McCollom T., Moskowitz B. and Berquó T. (2009) Iron partitioning and hydrogen generation during serpentinization of abyssal peridotites from 15°N on the Mid-Atlantic Ridge. *Geochim. Cosmochim. Acta* **73**, 6868–6893.

Klein F., Bach W. and McCollom T. M. (2013) Compositional controls on hydrogen generation during serpentinization of ultramafic rocks. *Lithos* **178**, 55–69.

Klein F., Humphris S. E., Guo W., Schubotz F., Schwarzenbach E. M. and Orsi W. D. (2015) Fluid mixing and the deep biosphere of a fossil Lost City-type hydrothermal system at the Iberia Margin. *Proc. Natl. Acad. Sci.*, 201504674.

Kumar M. R. and Saravanan V. S. (2011) Candidate OP Phyla: Importance, Ecology and Cultivation Prospects. *Indian J. Microbiol.* **50**, 474–477.

Lafay R., Montes-Hernandez G., Janots E., Chiriac R., Findling N. and Toche F. (2012) Mineral replacement rate of olivine by chrysotile and brucite under high alkaline conditions. *J. Cryst. Growth* **347**, 62–72.

Laier T. and Nytoft H. P. (2012) Bitumen biomarkers in the Mid-Proterozoic Ilímaussaq intrusion, Southwest Greenland – A challenge to the mantle gas theory. *Mar. Pet. Geol.* **30**, 50–65.

Lang S. Q., Butterfield D. A., Schulte M., Kelley D. S. and Lilley M. D. (2010) Elevated concentrations of formate, acetate and dissolved organic carbon found at the Lost City hydrothermal field. *Geochim. Cosmochim. Acta* **74**, 941–952.

Lorand J. (1987) A New Occurrence of Native Iron in a Serpentinized Mantle Peridotite - Maqsad, Sumail Massif, Semail Ophiolite (Southern Oman). *Comptes Rendus Acad. Sci. Ii* **304**, 703–6.

Madigan M. T. (2012) *Brock biology of microorganisms*., Benjamin Cummings, San Francisco.

Malvoisin B., Carlut J. and Brunet F. (2012) Serpentinization of oceanic peridotites: 1. A high-sensitivity method to monitor magnetite production in hydrothermal experiments. *J. Geophys. Res. Solid Earth* **117**, B01104.

Marcaillou C., Muñoz M., Vidal O., Parra T. and Harfouche M. (2011) Mineralogical evidence for H2 degassing during serpentinization at 300 °C/300 bar. *Earth Planet. Sci. Lett.* **303**, 281–290.

Mayhew L. E., Ellison E. T., McCollom T. M., Trainor T. P. and Templeton A. S. (2013) Hydrogen generation from low-temperature water–rock reactions. *Nat. Geosci.* **6**, 478–484.

Mayhew L. E., Webb S. M. and Templeton A. S. (2011) Microscale Imaging and Identification of Fe Speciation and Distribution during Fluid–Mineral Reactions under Highly Reducing Conditions. *Environ. Sci. Technol.* **45**, 4468–4474.

McCollom T. M. and Bach W. (2009) Thermodynamic constraints on hydrogen generation during serpentinization of ultramafic rocks. *Geochim. Cosmochim. Acta* **73**, 856–875.

McCollom T. M. and Seewald J. S. (2001) A reassessment of the potential for reduction of dissolved CO2 to hydrocarbons during serpentinization of olivine. *Geochim. Cosmochim. Acta* **65**, 3769–3778.

McDonald D., Price M. N., Goodrich J., Nawrocki E. P., DeSantis T. Z., Probst A., Andersen G. L., Knight R. and Hugenholtz P. (2012) An improved Greengenes taxonomy with explicit ranks for ecological and evolutionary analyses of bacteria and archaea. *ISME J.* **6**, 610–8.

Ménez B., Pasini V. and Brunelli D. (2012) Life in the hydrated suboceanic mantle. *Nat. Geosci.* **5**, 133–137.

Mervine E. M., Humphris S. E., Sims K. W. W., Kelemen P. B. and Jenkins W. J. (2014) Carbonation rates of peridotite in the Samail Ophiolite, Sultanate of Oman, constrained through 14C dating and stable isotopes. *Geochim. Cosmochim. Acta* **126**, 371–397.

Meyer-Dombard D. R., Woycheese K. M., YargÄ±Ã§oÄŸlu E. N., Cardace D., Shock E. L., GÃ¼leÃ§al-Pektas Y. and Temel M. (2015) High pH microbial ecosystems in a newly discovered, ephemeral, serpentinizing fluid seep at YanartaÅŸ (Chimera), Turkey. *Front. Microbiol.* **5**. Available at: http://journal.frontiersin.org/article/10.3389/fmicb.2014.00723/abstract [Accessed March 7, 2015].

Moody J. B. (1976) Serpentinization: a review. *Lithos* **9**, 125–138.

Morrill P. L., Kuenen J. G., Johnson O. J., Suzuki S., Rietze A., Sessions A. L., Fogel M. L. and Nealson K. H. (2013) Geochemistry and geobiology of a present-day serpentinization site in California: The Cedars. *Geochim. Cosmochim. Acta* **109**, 222–240.

Mulkidjanian A. Y., Dibrov P. and Galperin M. Y. (2008) The past and present of sodium energetics: May the sodium-motive force be with you. *Biochim. Biophys. Acta BBA - Bioenerg.* **1777**, 985–992.

Muñoz M., Vidal O., Marcaillou C., Pascarelli S., Mathon O. and Farges F. (2013) Iron oxidation state in phyllosilicate single crystals using Fe-K pre-edge and XANES spectroscopy: Effects of the linear polarization of the synchrotron X-ray beam. *Am. Mineral.* **98**, 1187–1197.

Neal C. and Stanger G. (1984) Calcium and magnesium hydroxide precipitation from alkaline groundwaters in Oman, and their significance to the process of serpentinization. *Miner. Mag* **48**, 237–241.

Neal C. and Stanger G. (1983) Hydrogen generation from mantle source rocks in Oman. *Earth Planet. Sci. Lett.* **66**, 315–320.

Neal C. and Stanger G. (1985) Past And Present Serpentinisation of Ultramafic Rocks; An Example from the Semail Ophiolite Nappe of Northern Oman. In *The Chemistry of Weathering* (ed. J. I. Drever). Nato ASI Series. Springer Netherlands. pp. 249–275. Available at: http://link.springer.com/chapter/10.1007/978-94-009-5333-8_15 [Accessed June 17, 2015].

Nealson K. H., Inagaki F. and Takai K. (2005) Hydrogen-driven subsurface lithoautotrophic microbial ecosystems (SLiMEs): do they exist and why should we care? *Trends Microbiol.* **13**, 405–410.

Neubeck A., Duc N. T., Bastviken D., Crill P. and Holm N. G. (2011) Formation of H2 and CH4 by weathering of olivine at temperatures between 30 and 70 C. *Geochem. Trans.* **12**, 6.

Nielsen J. L. and Nielsen P. H. (1998) Microbial Nitrate-Dependent Oxidation of Ferrous Iron in Activated Sludge. *Environ. Sci. Technol.* **32**, 3556–3561.

Okland I., Huang S., Dahle H., Thorseth I. H. and Pedersen R. B. (2012) Low temperature alteration of serpentinized ultramafic rock and implications for microbial life. *Chem. Geol.* **318-319**, 75–87.

Pasini V., Brunelli D., Dumas P., Sandt C., Frederick J., Benzerara K., Bernard S. and Ménez B. (2013) Low temperature hydrothermal oil and associated biological precursors in serpentinites from Mid-Ocean Ridge. *Lithos* **178**, 84–95.

Paukert A. N., Matter J. M., Kelemen P. B., Shock E. L. and Havig J. R. (2012) Reaction path modeling of enhanced in situ CO2 mineralization for carbon sequestration in the peridotite of the Samail Ophiolite, Sultanate of Oman. *Chem. Geol.* **330-331**, 86–100.

Petriglieri J. R., Salvioli-Mariani E., Mantovani L., Tribaudino M., Lottici P. P., Laporte-Magoni C. and Bersani D. (2015) Micro-Raman mapping of the polymorphs of serpentine. *J. Raman Spectrosc.*, n/a–n/a.

Postec A., Quéméneur M., Bes M., Mei N., Benaïssa F., Payri C., Pelletier B., Monnin C., Guentas-Dombrowsky L., Ollivier B., Gérard E., Pisapia C., Gérard M., Ménez B. and Erauso G. (2015) Microbial diversity in a submarine carbonate edifice from the serpentinizing hydrothermal system of the Prony Bay (New Caledonia) over a 6-year

period. *Front. Microbiol.* **6**. Available at: http://www.ncbi.nlm.nih.gov/pmc/articles/PMC4551099/ [Accessed November 20, 2015].

Proskurowski G., Lilley M. D., Kelley D. S. and Olson E. J. (2006) Low temperature volatile production at the Lost City Hydrothermal Field, evidence from a hydrogen stable isotope geothermometer. *Chem. Geol.* **229**, 331–343.

R Development Core Team (2008) *R: A language and environment for statistical computing*., R Foundation for Statistical Computing, Vienna, Austria. Available at: http://www.R-project.org.

Ravaut P., Bayer R., Hassani R., Rousset D. and Yahya'ey A. A. (1997) Structure and evolution of the northern Oman margin: gravity and seismic constraints over the Zagros-Makran-Oman collision zone. *Tectonophysics* **279**, 253–280.

Rinaudo C., Gastaldi D. and Belluso E. (2003) Characterization of Chrysotile, Antigorite and Lizardite by Ft-Raman Spectroscopy. *Can. Mineral.* **41**, 883–890.

Schrenk M. O., Brazelton W. J. and Lang S. Q. (2013) Serpentinization, Carbon, and Deep Life. *Rev. Mineral. Geochem.* **75**, 575–606.

Sherwood Lollar B., Frape S. K., Weise S. M., Fritz P., Macko S. A. and Welhan J. A. (1993) Abiogenic methanogenesis in crystalline rocks. *Geochim. Cosmochim. Acta* **57**, 5087–5097.

Sleep N. H., Meibom A., Fridriksson T., Coleman R. G. and Bird D. K. (2004) H2-rich fluids from serpentinization: geochemical and biotic implications. *Proc. Natl. Acad. Sci. U. S. A.* **101**, 12818–12823.

Stanger G. (1986) The hydrogeology of the Oman Mountains. Open University London.

Stevens T. O. and McKinley J. P. (2000) Abiotic Controls on H_2 Production from Basalt−Water Reactions and Implications for Aquifer Biogeochemistry. *Environ. Sci. Technol.* **34**, 826–831.

Stevens T. O. and McKinley J. P. (1995) Lithoautotrophic Microbial Ecosystems in Deep Basalt Aquifers. *Science* **270**, 450–455.

Streit E., Kelemen P. and Eiler J. (2012) Coexisting serpentine and quartz from carbonate-bearing serpentinized peridotite in the Samail Ophiolite, Oman. *Contrib. Mineral. Petrol.* **164**, 821–837.

Suzuki S., Ishii S., Wu A., Cheung A., Tenney A., Wanger G., Kuenen J. G. and Nealson K. H. (2013) Microbial diversity in The Cedars, an ultrabasic, ultrareducing, and low salinity serpentinizing ecosystem. *Proc. Natl. Acad. Sci.* **110**, 15336–15341.

Suzuki S., Kuenen J. G., Schipper K., van der Velde S., Ishii S., Wu A., Sorokin D. Y., Tenney A., Meng X., Morrill P. L., Kamagata Y., Muyzer G. and Nealson K. H. (2014) Physiological and genomic features of highly alkaliphilic hydrogen-utilizing Betaproteobacteria from a continental serpentinizing site. *Nat. Commun.* **5**. Available at: http://www.nature.com/ncomms/2014/140521/ncomms4900/full/ncomms4900.html [Accessed November 19, 2014].

Takami H., Noguchi H., Takaki Y., Uchiyama I., Toyoda A., Nishi S., Chee G.-J., Arai W., Nunoura T., Itoh T., Hattori M. and Takai K. (2012) A Deeply Branching Thermophilic Bacterium with an Ancient Acetyl-CoA Pathway Dominates a Subsurface Ecosystem. *PLoS ONE* **7**, e30559.

Tauxe L., Banerjee S. K., Butler R. F. and van der Voo R. (2014) Essentials of Paleomagnetism, 3rd Web Edition.

Telling J., Boyd E. S., Bone N., Jones E. L., Tranter M., MacFarlane J. W., Martin P. G., Wadham J. L., Lamarche-Gagnon G., Skidmore M. L., Hamilton T. L., Hill E., Jackson M. and Hodgson D. A. (2015) Rock comminution as a source of hydrogen for subglacial ecosystems. *Nat. Geosci.* **8**, 851–855.

Templeton A. S., Chu K.-H., Alvarez-Cohen L. and Conrad M. E. (2006) Variable carbon isotope fractionation expressed by aerobic CH4-oxidizing bacteria. *Geochim. Cosmochim. Acta* **70**, 1739–1752.

Tindall B. J., Sikorski J., Lucas S., Goltsman E., Copeland A., Glavina Del Rio T., Nolan M., Tice H., Cheng J.-F., Han C., Pitluck S., Liolios K., Ivanova N., Mavromatis K., Ovchinnikova G., Pati A., Fähnrich R., Goodwin L., Chen A., Palaniappan K., Land M., Hauser L., Chang Y.-J., Jeffries C. D., Rohde M., Göker M., Woyke T., Bristow J., Eisen J. A., Markowitz V., Hugenholtz P., Kyrpides N. C., Klenk H.-P. and Lapidus A. (2010) Complete genome sequence of Meiothermus ruber type strain (21T). *Stand. Genomic Sci.* **3**, 26–36.

Wang Q., Garrity G. M., Tiedje J. M. and Cole J. R. (2007) Naive Bayesian classifier for rapid assignment of rRNA sequences into the new bacterial taxonomy. *Appl. Environ. Microbiol.* **73**, 5261–7.

Weyhenmeyer C. (2000) Origin and evolution of groundwaters in the alluvial aquifer of the Eastern Batinah Coastal Plain, Sultanate of Oman. *PhD Thesis Univ. Bern Switz.*

Whiticar M. J. (1990) A geochemial perspective of natural gas and atmospheric methane. *Org. Geochem.* **16**, 531–547.

Whiticar M. J. (1999) Carbon and hydrogen isotope systematics of bacterial formation and oxidation of methane. *Chem. Geol.* **161**, 291–314.

Whiticar M. J. and Faber E. (1986) Methane oxidation in sediment and water column environments—Isotope evidence. *Org. Geochem.* **10**, 759–768.

Wilke M., Farges F., Petit P.-E., Brown G. E. and Martin F. (2001) Oxidation state and coordination of Fe in minerals: An Fe K-XANES spectroscopic study. *Am. Mineral.* **86**, 714–730.

Willems A., Busse J., Goor M., Pot B., Falsen E., Jantzen E., Hoste B., Gillis M., Kersters K., Auling G. and others (1989) Hydrogenophaga, a new genus of hydrogen-oxidizing bacteria that includes Hydrogenophaga flava comb. nov.(formerly Pseudomonas flava), Hydrogenophaga palleronii (formerly Pseudomonas palleronii), Hydrogenophaga pseudoflava (formerly Pseudomonas pseudoflava and "Pseudomonas carboxydoflava"), and Hydrogenophaga taeniospiralis (formerly Pseudomonas taeniospiralis). *Int. J. Syst. Bacteriol.* **39**, 319–333.

Worm H.-U. (1998) On the superparamagnetic—stable single domain transition for magnetite, and frequency dependence of susceptibility. *Geophys. J. Int.* **133**, 201–206.

Woycheese K. M., Meyer-Dombard D. R., Cardace D., Argayosa A. M. and Arcilla C. A. (2015) Out of the dark: transitional subsurface-to-surface microbial diversity in a terrestrial serpentinizing seep (Manleluag, Pangasinan, the Philippines). *Front. Microbiol.* **6**. Available at: http://journal.frontiersin.org/Article/10.3389/fmicb.2015.00044/abstract [Accessed May 21, 2015].

CHAPTER 3

Low temperature hydrogen production during experimental hydration of partially-serpentinized dunite

Submitted to and under first round of revisions in *Geochimica et Cosmochimica Acta*, 2016-7

Co-authors: Lisa E. Mayhew[a], Eric T. Ellison[a], Peter Kelemen[b], Mike Kubo[c], Alexis S. Templeton[a,*]

[a]Department of Geological Sciences, UCB 399, University of Colorado, Boulder, CO 80309, USA

[b]Lamont-Doherty Earth Observatory of Columbia University, 61 Route 9W, Palisades, NY 10964, USA

[c]Carl Sagan Center for Life in the Universe, SETI Institute, Mountain View, CA 94043, USA,

Abstract

Dissolved hydrogen is common in mafic and ultramafic aquifers; however, the water/rock reactions that give rise to hydrogen production at near-surface temperatures are enigmatic. Similarly, mineral hydration experiments have not yet unequivocally demonstrated whether H_2 can be produced at low-temperatures at significant rates from reaction of aqueous fluids with basalts and peridotites for prolonged amounts of time. We conducted laboratory-based water/rock reactions between partially serpentinized Oman dunite and a simulated Oman rainwater (RW) media, as well as a simulated seawater (SW) media, to quantify H_2 generation rates at 100°C. Throughout more than 9 months of water/rock reaction, extensive hydrogen production and consumption were observed in RW and SW media. In the first 24 hours of reaction in anoxic fluids containing only dissolved N_2 and CO_2, the room-temperature pH in both RW and SW media increased from 6.5 to ~9, and the average pH then remained relatively constant at pH 8.5 (+/- 0.5 pH) for the duration of the experiments. We also measured some of the highest hydrogen concentrations observed in experimental low-temperature serpentinization reactions. The maximum measured H_2 concentrations in SW media were 470 nmol H_2 per gram mineral after ~3 months, while RW media H_2 concentrations reached 280 nmol/gram H_2 after ~3 months. After reaching micromolar dissolved $H_{2(aq)}$, the H_2 concentrations notably declined, and CO_2 was almost fully consumed. We measured the formation of formate (up to 98 µM) and acetate (up to 91 µM) associated with a drawdown of H_2 and CO_2 in the experiments. No CH_4 or carbonate formation was observed. To identify reactions giving rise to low-temperature hydrogen production, the mineralogy and oxidation state of the Fe-bearing species in the dunite were extensively characterized before and after reaction using Raman spectroscopy, Quantitative Evaluation of Minerals by SCANning electron microscopy (QEMSCAN), powder x-ray

diffraction (XRD), magnetic susceptibility, scanning electron microscopy (SEM), and Fe K-edge x-ray absorption near edge structure (XANES) spectroscopic techniques. The mineralogy of the solid starting material was dominated by olivine and serpentine with minor brucite, pyroxene and spinel. After reaction, additional serpentine and magnetite could be detected as reaction products, and pre-existing brucite was consumed. No changes were observed in the abundance or grain sizes of olivine or pyroxene. Thus, we propose that the destabilization of Fe(II)-bearing brucite and the subsequent oxidation of the aqueous Fe(II) to form magnetite and Fe(III)-rich serpentine give rise to H_2 production at 100°C. This work demonstrates that dissolved hydrogen and low molecular weight organic acids can be produced by the reaction of labile Fe(II)-bearing minerals generated during a prior stage of water/rock reactions. In particular, progressive alteration of partially-serpentinized peridotites containing brucite may generate sufficient electron donors to fuel in-situ subsurface microbial activity.

1. Introduction

Serpentinization, the hydration and oxidation reaction of ultramafic rocks and minerals, can produce hydrogen at low temperatures which can support H_2-fueled microbial life (Sleep et al., 2004; Nealson et al., 2005; Mayhew et al., 2013). Low-temperature reactions can be classified as those occurring ≤ 122°C (Takai et al., 2008), which is the highest temperature of observed microbial growth. Serpentinization reactions are predicted to produce less hydrogen at temperatures relevant for microbial life, but still enough to sustain subsurface microbial ecosystems, which can utilize H_2 concentrations as low as 13 nM (Kral et al., 1998; Nealson et al., 2005). H_2-fueled metabolisms are diverse and include anaerobic methanotrophy, fermentation, sulfate reduction and hydrogen oxidation tied to iron reduction (Schrenk et al., 2013). H_2 produced by serpentinization reactions may have fueled the first life on Earth at low-temperature off-axis hydrothermal fields (Russell et al., 2010; Russell et al., 2013; Shibuya et al., 2016). Additionally, serpentinization reactions have likely occurred on Enceladus and Mars, which may provide a favorable environment for H_2-utilizing microbial life (Ehlmann et al., 2010; Glein et al., 2015; Sekine et al., 2015).

However, the mechanisms and reaction pathways giving rise to hydrogen production at low temperatures are unclear (Stevens and McKinley, 1995; Anderson et al., 1998; Neubeck et al., 2011a; Mayhew et al., 2013; Neubeck et al., 2014; Okland et al., 2014; Telling et al., 2015), whereas high temperature (>200°C) hydrogen production is well-characterized through both experimental and modeling efforts (Fyfe, 1974; McCollom and Seewald, 2001; McCollom and Bach, 2009; Klein et al., 2009; Evans et al., 2009; Malvoisin, Carlut, et al., 2012; Klein et al., 2013; Frost et al., 2013; Klein et al., 2015; McCollom et al., 2016). Thus, further work on low-temperature serpentinization and associated hydrogen production is necessary to better constrain

reaction pathways and mechanisms (Mayhew et al., 2013; Bach, 2016; McCollom and Donaldson, 2016).

Although extensive thermodynamic modeling of hydrogen production has been conducted at high temperatures, these results cannot be easily extrapolated to lower temperatures. Several thermodynamic models have been used to infer that water/rock reactions at low temperatures will generate much less hydrogen than at temperatures from 200-350°C (McCollom and Bach, 2009; Klein et al., 2009; Klein et al., 2013). Hydrogen production at temperatures <120°C is predicted to strongly decrease because Fe(II) released from olivine will be sequestered into secondary brucite, resulting in less Fe oxidation. Magnetite formation is also thermodynamically inhibited at low temperatures (McCollom and Bach, 2009; Klein et al., 2013). Instead, the formation of Fe(III)-rich serpentine may be the central reaction accommodating low-temperature hydrogen generation. Thermodynamic models also assume systems reach a state of equilibrium, and this may not occur during fluid flow through peridotite aquifers (Paukert et al., 2012). Also, the kinetics and mechanisms of the key mineral dissolution, precipitation and Fe(II)-oxidation reactions are poorly constrained, along with the thermodynamic data for Fe(III) secondary phases that form at low temperatures.

Although recent kinetic-thermodynamic modeling of reactions between peridotite and water at 25°C (Bach, 2016) addresses some of these issues, it is clear that these models need to be experimentally verified. Further mechanistic studies are needed to reveal the rates and reactions involved in H_2 production during low temperature peridotite alteration. New models by Bach (2016) better capture the complexity of these low-temperature reactions by allowing the precipitation of several possible Fe(III) reaction

products to accommodate H_2 production. Notably, these new models predict that more H_2 could be produced at low temperatures than has been observed experimentally (e.g. in Mayhew et al. 2013, Neubeck et al. 2011, etc.). Experiments coupled with new models may help to explain how continental ophiolite systems contain high concentrations of dissolved hydrogen at near surface temperatures (Neal and Stanger, 1983; Abrajano et al., 1990; Etiope et al., 2011; Morrill et al., 2013; Szponar et al., 2013; Suda et al., 2014; Miller et al., 2016).

Several experimental studies of water/rock reactions have investigated the rates and extent of low-temperature H_2 generation (Stevens and McKinley, 1995; Anderson et al., 1998; Neubeck et al., 2011a; Mayhew et al., 2013; Neubeck et al., 2014; Okland et al., 2014; Telling et al., 2015), yet they have encountered numerous challenges and have produced inconsistent results (Table 1). It is difficult to reproduce results as a variety of conditions can affect the amount of hydrogen production (Stevens and McKinley, 1995; Anderson et al., 1998; Stevens and McKinley, 2000). These factors include water/rock ratio, fluid chemistry, pH, temperature, silica activity, surface passivation, mineral surface area, composition of the reaction vessel, and Fe(II/III) partitioning into secondary mineral phases (Béarat et al., 2006; Frost and Beard, 2007; McCollom and Bach, 2009; Klein et al., 2009; Mayhew et al., 2013; Andreani et al., 2013a). Challenges arise from the fact that reactions are oftentimes conducted in silica serum vials with butyl stoppers that generate small amounts of hydrogen (Anderson et al., 1998; Mayhew et al., 2013; McCollom and Donaldson, 2016). Additionally, incomplete serpentinization of starting material and slow reaction rates make it difficult to judge the true hydrogen-generating potential of the minerals and rocks reacted (Neubeck et al., 2011b; Okland et al., 2012; Mayhew et al., 2013; Okland et al., 2014; Neubeck et al., 2015). The low extent of reaction also makes it difficult to quantify mass changes and determine the operative Fe-

Table 1. Comparison of maximum experimental hydrogen generation measured at temperature <100°C.

Study	Temperature (°C)	Max. H_2 generation (nmol/gram mineral)	Rock/Mineral reacting	pH	water:rock ratio	Mineral surface area (m^2/g) or mineral diameter (mm)
Stevens and McKinley 1995	22	~80	Umtanum Ridge Basalt	6	1 to 1	<0.25mm
Anderson et al. 1998	22	500	Snake River Plain basalt Reference	6	1 to 1	0.53-0.125mm
Stevens and McKinley 2000	60	~60	Umtanum Collonade basalt	5	1 to 1	1 m^2/g
Neubeck et al. 2011	30	0.24	Olivine (Forsterite 91)	9.07	2.3 to 1	0.125-1.0mm
Mayhew et al. 2013	100	300	San Carlos peridotite	~7	7 to 1	0.34 m^2/g
Okland et al. 2014	25	~110	Highly altered Leka ophiolite dunite	9.56	2 to 1	7.1 m^2/g
Telling et al. 2015	0	~10	Elsworth quartzite	NA	1 to 1	~1-4 m^2/g
Telling et al. 2015	35	~60	Engabreen schist	NA	1 to 1	~6-12 m^2/g
McCollom and Donaldson 2016	90	39.6	Harzburgite	6.8	4 to 1	0.59 m^2/g
This study	100	500	Partially serpentinized Oman dunite	9	7 to 1	0.47-0.60 m^2/g

oxidation pathways (Mayhew et al., 2013). Thus, experimental studies of low-temperature serpentinization which encompass the entire, complex reactions involved in water/rock reactions with environmentally relevant, partially altered rocks are needed.

1.1 This study

This study investigates hydrogen production from laboratory water/rock reactions between partially serpentinized dunite from Oman and anoxic fluids at low temperatures (100°C). The dunite is ~50% serpentinized, which constitutes some of the least-altered rocks from the Samail ophiolite. This is the world's largest and best exposed ophiolite, which contains large reserves of peridotite and an extensive aquifer system where deep subsurface hyperalkaline fluids contain millimolar amounts of dissolved hydrogen at temperatures <50°C (Barnes et al., 1978; Neal and Stanger, 1984; Kelemen et al., 2011; Streit et al., 2012; Miller et al., 2016).

We simulated serpentinization reactions between anoxic fluids and Oman dunite, and observed extensive H_2 production and consumption over >9 months of water rock reaction at 100ºC. Partially serpentinized dunite OM95-35 was chosen for this work as representative of a typical dunite obtained from a surface outcrop in Oman; there are numerous olivine-rich dunite lenses in the mantle section of the Samail ophiolite (Kelemen et al., 1997; Hanghøj et al., 2010). We probed the changes in mineralogy and aqueous geochemistry of the minerals and fluids to infer the reactions associated with H_2 generation. The whole rock mineralogy of the dunite, as well as the mineralogy of the rock powders after water/rock reaction, have been characterized with powder XRD, XANES spectroscopy, Raman spectroscopy, QEMSCAN, magnetic susceptibility techniques, and thermogravimetric analysis (TGA). By coupling this data with

changes in dissolved ions, gases and organic acid concentrations, we identify the key reactions that give rise to H_2 production in our experimental system.

2. Methods

2.1 Experimental set-up

We prepared 70 mL silica serum vials of medium-only blanks and water/rock reactions (Figure 1). The experiments were conducted with two different solution compositions: an artificial seawater medium (SW) and a simulated Oman rainwater medium (RW, Table 2). The artificial SW medium contained 27.5 g/L NaCl, 1.4 g/L $CaCl_2$, 0.72 g/L KCl, 0.2 g/L $NaHCO_3$, 1.0 g/L NH_4Cl, 0.05 g/L K_2HPO_4, and 5.38 g/L $MgCl_2$ and is identical to the solution composition in Mayhew et al. (2013). The simulated Oman RW medium contained 9.89 mg/L NaCl, 11.10 mg/L $CaCl_2$, 5.06 KNO_3, 7.41 $Ca(OH)_2$, 30.83 $CaSO_4*H_2O$, 12.32 $Mg(SO_4)_2*7H_2O$, and 10.17 mg/L $MgCl_2$ (from Paukert et al., 2012). Five grams of partially serpentinized Oman dunite were mixed with 35 mL of the specified medium to achieve a water/rock ratio of 7 (Mayhew et al., 2013). The vials were purged with 80% N_2: 20% CO_2 to achieve anoxic conditions and placed in a 100°C oven to react. This temperature was chosen to ensure reaction along reasonable time-scales in temperature ranges relevant to microbial life. Additionally, two vials containing Oman dunite, filled with SW and RW media, respectively, were purged with 100% N_2 gas to investigate low-weight molecular acid formation without added headspace CO_2 (Figure 1).

Prior to use, the silica serum vials were heated to 550°C for 3 hours to remove any combustible carbon species. The vials were capped with an airtight butyl rubber stopper boiled 3 times in 0.1 N NaOH media following the protocol of Oremland et al. (1987) to reduce contamination by volatile organic compounds in the butyl stoppers. Vials, rubber stoppers, and the media were autoclaved before the experiment began.

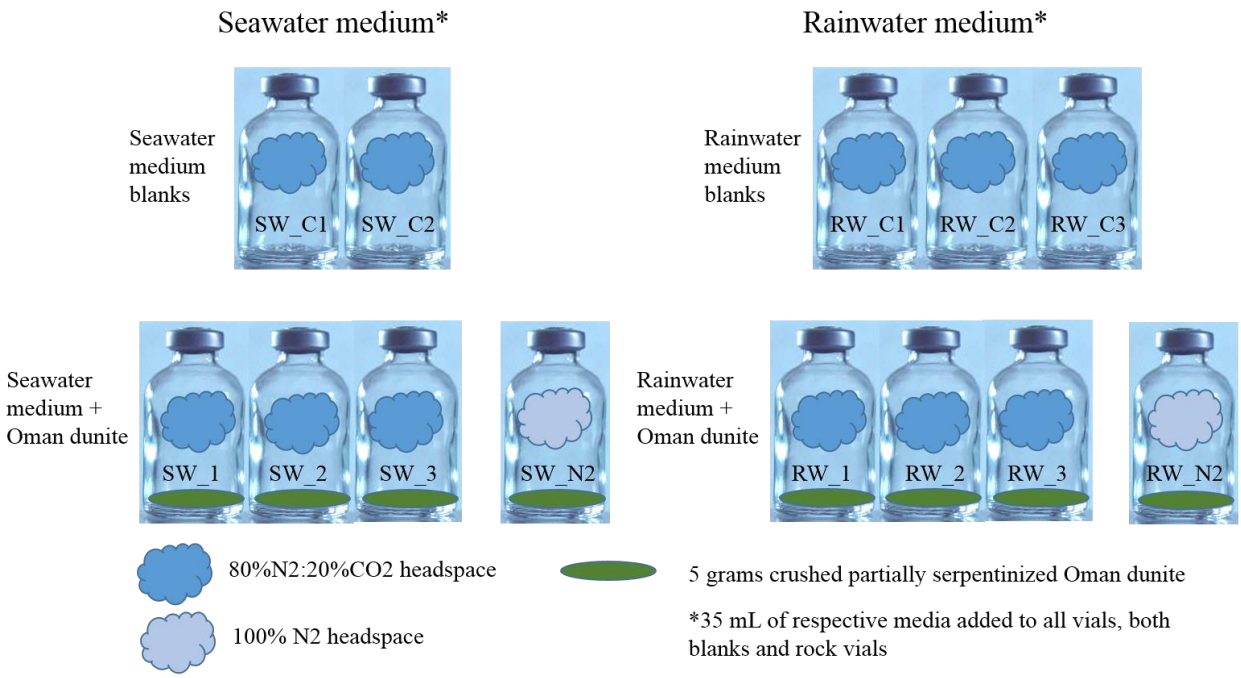

Figure 1. Experimental matrix for water/rock reactions and blanks. 13 vials total were prepared and monitored over the lifespan of the experiments.

Table 2. Composition of initial SW and RW media prior to water/rock reaction, as calculated from media formulation. This fluid was equilibrated with a 80% N_2: 20% CO_2 headspace. Concentration of HCO_3^- in media includes solid bicarbonate included in media and HCO_3^- generated from the dissolution and speciation of headspace CO_2.

	Starting composition (mM)	
	SW media	RW media
pH	7	6.5
Na^+	470.57	0.20
Ca^{2+}	12.61	0.50
K^+	10.23	0.05
Mg^{2+}	26.46	0.15
Cl^-	577.08	0.50
NO_3^-	0.00	0.05
SO_4^{2-}	0.00	0.30
HCO_3^-	2.41	0.02
NH_4^+	18.69	0.00
HPO_4^{2-}	0.29	0.00

The Oman dunite was cut with a diamond-blade saw; the outer weathered portions of the rock were removed and only the unweathered interior was used in experiments. The rock was tumbled with silicon carbide in a rock tumbler with de-ionized water, rinsed, and then tumbled again with fresh silicon carbide to remove any residual steel fragments from sampling/sawing, which could produce hydrogen by the reaction of Fe(0) with water. The cleaned material was crushed with a ceramic mortar and pestle and wet-sieved with deionized water to a size fraction of 53-212 μm. The surface area (SA) of the unreacted and reacted minerals was determined with the Brunauer_Emmett_Teller (BET) method using a Micromeritics Gemini V machine with N_2 gas.

H_2 in SW experiments was measured for 203 days, but the vials continued to react in the 100°C oven after regular H_2 analysis ended, which allowed us to sample pH, fluid, and mineral grains at later time points (Table 3). H_2 in RW experiments was measured for 97 days, and these vials also continued to react in the 100°C oven after this time period. Small amounts of fluid (<0.5 mL) were sampled from SW vials periodically to measure pH, whereas 2 mL of fluid was sampled periodically from RW vials to fully analyze aqueous geochemistry and pH. When 2 mL of fluid was removed from RW vials, it was replaced with equal volumes of fresh N_2-purged RW medium to preserve the water/rock ratio of 7.

Sampling for H_2 gas, water chemistry, and reacted mineral products was not uniform across experimental sets. Thus, the information is summarized in Table 3 to clearly show when various samples were extracted. H_2 gas monitoring stopped after 203 or 97 days because the H_2 concentrations were no longer increasing or noticeably changing. The experiments were maintained at 100°C to allow for sampling of the reacted rock at later times. As a result, most of the reacted samples were obtained after hydrogen monitoring was complete. Mineral grains were

Table 3. Sampling timeline for all analyses. The SW & RW days columns indicate when the sample was collected with respect to days from the start of the water/rock reactions. Samples were extracted at different times from SW and RW vials in an attempt to thoroughly characterize all geochemical changes during reaction.

Sample	Analysis performed	SW vials (days)	RW vials (days)	Data figure
Gas and aqueous samples				
H_2 gas sampling (0.5 mL headspace gas)	Gas chromatography for H_2	0-203$^+$	0-97$^+$	figure 5, tables 6 and 7
CO_2 gas sampling (single time point, 0.5 mL headspace gas)	Gas chromatography for CO_2	304	171	supplemental table 5
Fluid for aqueous geochemistry (2 mL)	ICP-OES ($SiO_{2(aq)}$, Mn^{2+}, Fe^{2+}, Mg^{2+}, Ca^{2+}) ICP-MS (Ni, Cr) IC (SO_4^{2-})	Only 287	0-155	figure 6
Fluid for pH sampling (<0.5mL)	pH measurement	0-287	0-366	supplemental figure 3
Fluid for organic acid sampling* (5 mL)	HPLC measurement for low weight molecular organic acids	525	992	table 8

$^+$continued reacting the vials in the oven, but did not monitor regularly after this time period

*100% N_2 purged vials were both sampled after 308 days of reaction with same protocol

Mineral samples				
Unreacted rock samples				
Thin section of unreacted Oman dunite	QEMSCAN, Raman spectroscopy, µXANES mapping, electron microprobe	0	0	figures 3,4, table 5, supplementary figures 2 & 5, table
Unreacted mineral grain mount	XANES, electron microprobe	0	0	Supplementary figure 5, table 5
Unreacted mineral grains	Quantitative powder XRD, bulk XANES, BET, TGA, SQUID magnetometer, TOC	0	0	Tables 4 & 9, figures 2, 10
Reacted rock samples				
Mineral sample extracted from vials	Raman spectroscopy, BET, SEM, XRD, µXANES, electron microprobe, length of olivine grains analyzed	111 & 330**	NA	Figure 9, supplementary table 3
Mineral sample extracted from vials	Raman spectroscopy, BET, TGA, µXANES (bulk and microscale), length of olivine grains analyzed	NA	275	Figure 9, 10, supplementary table 3
White mineral precipitate extracted	Powder XRD (only SW sample), Micro-Raman spectroscopy, SEM	111	90	Figures 7, 8, supplementary figures 2, 4
Vial opened and all 5 grams of mineral extracted	Quantitative powder XRD, Total organic carbon analysis, mass spectrometer to quantify CO2, SQUID magnetometer, bulk XANES, Raman spectroscopy	>730	>365	Figure 2, supplementary figure 5, supplementary table 2, table 4

**the second SW sample extracted at 330 days was only analyzed with µXANES and electron microprobe techniques

not all sampled at the same time because additional analyses were performed as needed to fully characterize the mineralogical and geochemical changes. Grains removed from the water/rock reactions were extracted with a 23 gauge needle and rinsed 3 times with de-ionized (DI) water before analysis. Some of this material was mounted in epoxy for microscale analysis, while some remained in dried loose powder form. We are aware there was likely size discrimination during this removal process, but it was the best method available to us to allow continued reaction of the additional rock.

H_2 in the experiments was measured on an SRI 310C gas chromatograph with an Alltech Molecular Sieve (5A 80/100) 6000-8500 ID column and thermal conductivity detector using N_2 as the carrier gas. 0.5 mL of headspace gas was sampled for this analysis, thus, vials developed a partial vacuum over time because the headspace samples were not replaced with any additional gas. The H_2 standard concentrations were calibrated each time the machine was used which led to some of the variability observed in the H_2 concentrations between measurements. However, the standard values varied by less than 5%, so overall trends are valid. A separate GC was used to measure CH_4 and CO_2. Methane was measured using a flame ionization detector and CO_2 was measured using a thermal conductivity detector on an SRI 8610C gas chromatograph with a PORAPAK Q 60_0:085" I.D. column using He as the carrier gas. H_2 and CH_4 detection limit is ~10 nmol and the overall measurements have a variability of 5%.

To test the rate of H_2 diffusion out of the butyl stoppers, we incubated three empty silica serum vials purged with 10%H_2:90%N_2 at 100°C for 425 days and periodically measured H_2 headspace concentrations (Supplementary Figure 1). This test shows an average of 20 nanomoles of headspace H_2 leaks from the vials per day. However, the amount of hydrogen in the headspace of these test measurements is much larger (158 µmoles) than the hydrogen in our experiments

(2.4 µmoles). Thus, we scaled the rate of hydrogen diffusion down to match the experimental hydrogen levels (Supplementary Figure 1), which then shows a prediction that approximately 1 nanomole of H_2 would be lost per day. A similar control experiment was conducted to document the release of Si from serum vials over time. Three serum vials were filled with 35 mL of artificial SW medium and incubated for 51 days, with periodic sampling for aqueous Si (Supplementary Table 1). The results show an increase of ~2.7 µM aqueous Si daily, which we acknowledge when discussing some of the mineral dissolution and precipitation reactions .

2.2 Aqueous geochemistry of the water/rock reactions

Major and minor elemental data was only collected for RW vials during water/rock reaction, and all fluid samples were replaced by an equal volume of the anaerobic media. Trace elements (Ni, Cr) were analyzed on acidified and filtered fluid from the water/rock reactions using Inductively Coupled Plasma-Mass Spectrometry (ICP-MS) on a Perkin Elmer SCIEX Elan DRC-e. Major cations ($SiO_{2(aq)}$, Mn^{2+}, Fe^{2+}, Mg^{2+}) were analyzed using Inductively Coupled Optical Emission Spectrometry (ICP-OES) on an ARL 3410+ with a Meinhard nebulizer. The detection limits were 0.345 µM for Si, 0.026 µM for Mn, and 0.111 µM for Mg. These analyses were conducted at the Laboratory for Environmental and Geological Studies (LEGS) at the University of Colorado at Boulder. Water samples (5 mL) for both SW and RW vials were collected in acid-washed, autoclaved, and ashed organic free vials and sent to NASA Ames Research Center to measure low weight molecular organic acids on a Shimadzu Prominence LC20AT high-performance liquid chromatograph (HPLC) equipped with a SPD-M20A photodiode array detector and a flow rate of 1 mL per minute. pH was measured with a Thermo Scientific Orion PerpHecT ROSS Combination pH Micro Electrode calibrated with reference

standards of pH 4, 7, and 10. The pH was measured at 25°C, whereas the water/rock reactions were incubated at 100°C. We are unable to report the in situ pH at 100°C because of incomplete aqueous geochemical and gas headspace data for each corresponding pH measurement. However, we did explore pH re-speciation based on temperature using the React module in Geochemist Workbench v8 with the standard thermodynamic dataset. The resulting pH varied from 6-7.8 depending on whether we suppressed the formation of carbonate minerals. Thus the in-situ pH values cannot be determined with the available data, but the in-situ pH will be lower than the pH measured at 25C.

2.3 Characterizing the mineralogy of the partially serpentinized dunite pre- and post-reaction

The surface area (SA) of the unreacted and reacted crushed Oman dunite was determined with the Brunauer_Emmett_Teller (BET) method using a Micromeritics Gemini V machine with N_2 gas at the University of Colorado at Boulder. Quantitative powder XRD analyses were conducted on the unreacted dunite and a serpentine standard to determine initial modal mineralogy at the Campbell laboratory at the Boulder United States Geological Survey. Samples were prepared for XRD using a modified method based on Eberl (2003). One gram of homogenized sample was mixed with 20% corundum and ground in a McCrone micronizing mill with 4mL ethanol for 5 minutes, generating particle sizes on the order of 10-30μm. The resulting sample was dried at 50°C in an oven overnight and then combined with 500 mL of DuPont™ Vertrel® and mixed for 10 minutes with 3 delrin balls in a Spex SamplePrep 8000D Mixer/mill to preserve random crystal orientations during the packing step. The powder was passed through a 250 μm sieve to break up larger aggregates, and loaded into a side-mounted XRD sample holder (Eberl, 2003). Samples were analyzed using a Siemens D500 X-ray diffractometer from 5

to 65° 2Θ using Cu Kα X-ray radiation, with a step size of 0.02 degrees and a dwell time of 2 seconds per step. The sample rotates during the scanning process at 30 rpm, thus ensuring a representative scan of the sample's surface. Fitting was determined with USGS software, RockJock, a program that quantifies the mineralogy of powdered samples by comparing the integrated XRD intensities of minerals in mixtures to intensities of an internal corundum standard (Eberl, 2003).

TGA measurements were taken in a NETZSCH STA 449 F1 Jupiter at the University of Colorado at Boulder. Between 60 and 110 mg of sample in an alumina crucible and a blank alumina crucible were heated in Argon up to 1000°C at a ramp rate of 10 °Celsius per minute. The crucibles were held at 1000°C for one hour, at which point data collection stopped and the furnace cooled. The derivatives of the data were determined using NETZSCH Proteus.

QEMSCAN, at Colorado School of Mines, was also used to identify the mineralogy and textural relationships of a thin section of unreacted dunite. QEMSCAN integrates scanning electron microscope (SEM) analysis with energy dispersive X-ray spectrometry (EDS) and calibrated backscatter electron (BSE) intensity levels to generate a mineralogy map of the thin section (Hoal et al., 2009). The instrument operated at 25 kV accelerating voltage, 5 nA sample current, 1 μm beam size with a step size of 5 μm.

Micro-Raman spectra of unreacted and reacted grains, and a hyperspectral map of the unreacted dunite thin section were collected using a Horiba LabRAM HR Evolution Raman spectrometer at the Department of Geological Sciences at the University of Colorado at Boulder equipped with a 532 nm frequency-doubled Nd:YAG laser coupled to an Olympus BXFM optical microscope. The laser beam was focused through a 50x (0.75NA) objective lens, yielding a spatial resolution of ~2μm. A 600 lines/mm grating and adjustable confocal pinhole (100 μm-

200 μm) were used to give a spectral resolution full width at half maximum (FWHM) of 4.5-8.4 cm^{-1}. Spectra were collected using a Si-based CCD detector (1024 x 256 pixels). The spectrometer was calibrated daily using the 520 cm^{-1} Raman peak of Si prior to analysis. Spectral data were corrected for instrumental artifacts and baseline-subtracted using a polynomial fitting algorithm in LabSpec 6 (Horiba Scientific). A hyperspectral map of a representative area in the thin section was generated using Multivariate Curve Resolution-Alternating Least Squares (MCR-ALS). Non-negativity constraints on scores and loadings were determined for the main spectral components present, then spot Raman spectra were collected to verify the components, and the hyperspectral data set was fit with the end member spectra to generate component maps.

Synchrotron-based hard X-ray measurements of Fe K-edge micro-x-ray absorption near edge spectra (μXANES) were conducted at Beamline 2-3 at the Stanford Synchrotron Radiation Lightsource (SSRL). The incident energy was selected with a Si (111) double crystal monochromator with the SPEAR accelerator ring containing ~350-500mA at 3.0 GeV. The beam was focused to approximately 2 by 2 μm using Kirkpatrick Baez mirrors. Data were collected at the Fe K-edge using a Fe^0 foil calibration of 7112 eV with a single-element Vortex detector capable of counting several million counts per second. Fe K-edge XANES spectra were collected from 6882-7505 eV with a high resolution (step size of 0.1 eV) through the pre-edge (7108-7118 eV) region and a dwell time of 3 seconds. The acquisition time is 16 minutes, thus some photo-oxidation may have occurred, which may result in slightly over-estimated Fe^{3+}/Fe_{total} ratios (Debret et al., 2014). Crystal orientation leads to varying measurements of pre-edge centroids, which can also shift Fe^{3+}/Fe total ratios by 0.1 in antigorite (Muñoz et al., 2013). XANES were background subtracted and normalized with Sam's Interface for XAS Package (SIXPACK). Analysis of the pre-edge to determine the ratio of Fe^{2+}/Fe_T employed protocols from Andreani *et*

al. (2013) and Wilke *et al.* (2001). Measurement, analysis, and comparison of the pre-edge of standards with known Fe(II)/(III) ratios and Fe coordination states (staurolite, andradite, sanidine and siderite provided and previously characterized by Dr. Manuel Muñoz) to unknown samples allows us to constrain the Fe(II)/(III) ratio in primary and alteration phases in order to assess the extent of Fe oxidation and the distribution of Fe(II) vs. Fe(III) between different mineral phases.

Beamline 4-1 at SSRL was used to collect bulk Fe K-edge spectra for powdered samples. A Si (220) ϕ= 0 monochromator was used and X-ray absorption spectra (XAS) were collected on a Lytle detector. A Fe^0 foil standard was used and calibrated to 7112eV. Duplicate spectra were collected and averaged for XANES scanning from a range of 6882-7082eV with a step size of 10 eV, then from 7092 to 7520 with a 0.35 eV step size. Calibration of the Fe pre-edge was not conducted.

The Quantum Design MPMS Superconducting Quantum Interference Device (SQUID) magnetometer with magnetic moment resolution of 10^{-8} emu at the Department of Physics and Astronomy at Michigan State University was used to analyze two bulk rock powder samples to determine magnetic hysteresis parameters over the range of ± 5 T at 300K.

Quantitative chemical analysis of serpentine was performed using the electron microprobe laboratory at the University of Colorado at Boulder on the JEOL JXA-8600 equipped with 4 wavelength-dispersive spectrometers, and a PGT energy-dispersive spectrometer. Spot analyses of polished thin sections were performed at a current of 10 nA, accelerating voltage of 15 keV, and beam diameter of 10 µm to avoid destroying the hydrated serpentine sample to analyze the major element compositions of Si, Al, Mg, Na, Ca, Cr, K, Fe, Mn, and Ti, using natural standards.

Samples were reacted with 100% H_3PO_4 at 90°C and then used for carbonate quantification, along with carbon and oxygen isotope analyses ($\delta^{13}C$ and $\delta^{18}O$), which were

determined using a GV IsoPrime mass spectrometer with Dual-Inlet and MultiCarb systems in the Center for Stable Isotope Biogeochemistry (CSIB) at Department of Integrative Biology, University of California at Berkeley. Several replicates of one international standard NBS19, and two lab standards $CaCO_3$-I & II were measured along with samples for each run. The overall external analytical precision is about $\pm$0.05‰ for $\delta^{13}C$ and about $\pm$0.07‰ for $\delta^{18}O$.

Total organic carbon (TOC) analysis was conducted in the Kiowa laboratory at University of Colorado at Boulder with a FLASH EA 1112 Series CHN analyzer, which consists of the system unit, a MAS 200 autosampler, and analysis with Eager 300 software.

3. Results

3.1 Mineralogy and Fe-content of unreacted rock

The Oman dunite used in the water/rock experiments was extensively characterized to accurately quantify how the mineralogy and Fe speciation changed through the course of reaction at 100°C. The mineralogy of our partially-serpentinized Oman dunite sample is dominated by olivine (51%), lizardite (43%), and brucite (6%); these peaks were identifiable with powder XRD (Figure 2) and quantified using the USGS RockJock software (Table 4).

To further quantify mineralogy, as well as document its spatial relationships at the microscale, we employed two imaging techniques, QEMSCAN and Raman microspectroscopy. Spatially-resolved imaging (1 μm beam size at surface) with QEMSCAN of a ~13 mm by 23 mm heterogeneous area shows the complex structure of serpentine intermixed with olivine, and trace minerals: pyroxene, carbonate, Mg-Fe-Ca silicates, Mg-Ca carbonates, chlorite, and chromite (Figure 3). Brucite was not detected with QEMSCAN. Raman hyperspectral maps verify the extensive presence of serpentine, specifically lizardite based off the shape and position of the OH peak near 3700 cm^{-1} (Rinaudo et al., 2003; Groppo et al., 2006; Petriglieri et al., 2015). In addition, Raman microspectroscopy reveals that serpentine is intimately intermixed with brucite, at a scale of <1 μm. Brucite can be clearly detected in the OH stretch region at 3640 cm^{-1} even though it is obscured by serpentine in the fingerprint region of 80-1600 cm^{-1}. Figure 4 shows the intermixed serpentine and brucite spectra, along with a pure serpentine spectrum. Nearly all of the serpentine in the dunite contained this mixture of brucite and serpentine. Other discrete mineral phases detected include diopside, enstatite, magnetite, chromite, and olivine (Figure 4). Confocal Raman spectroscopy was also used to look for fluid inclusions in mineral grains. We found small (~1 μm) magnetite grains inside some olivine grains, but no evidence of H_2 or CH_4

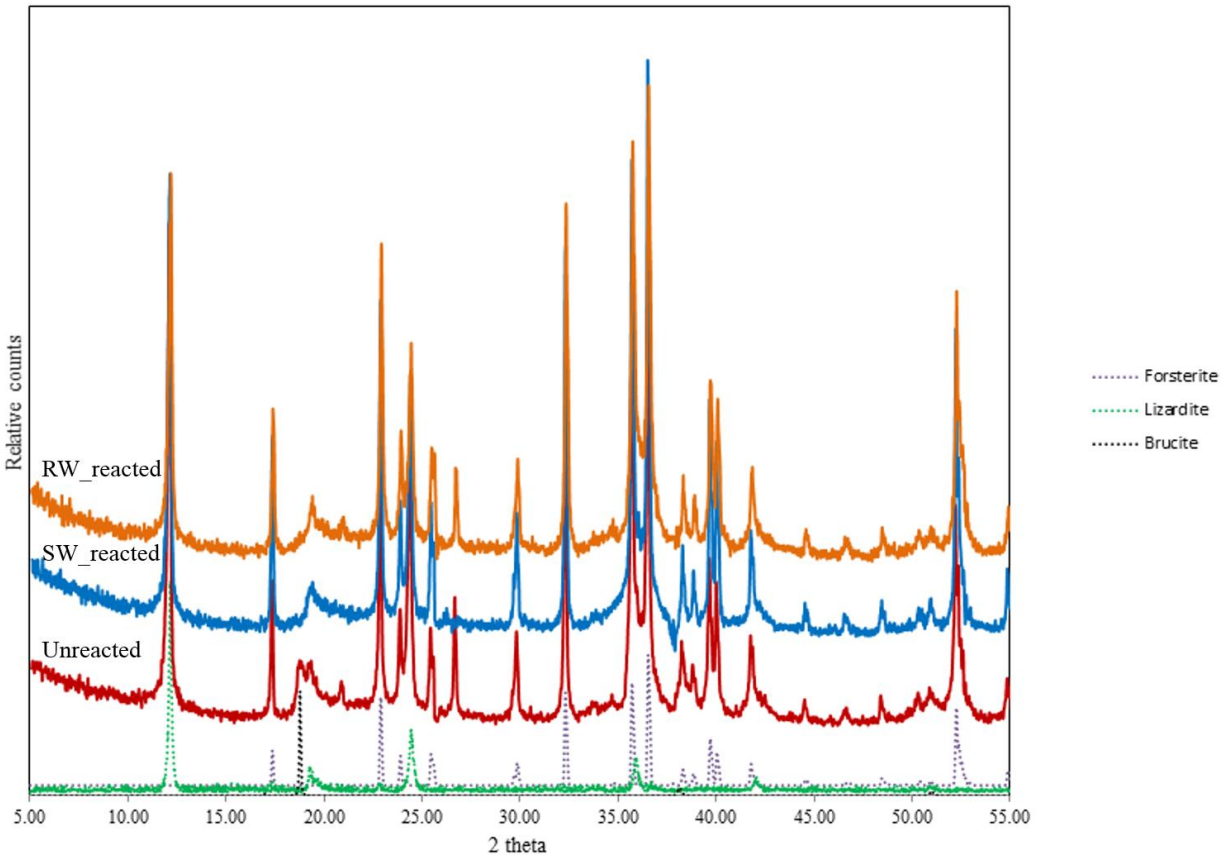

Figure 2. Powder XRD of unreacted and reacted Oman dunite with SW and RW media. Unreacted rock (red) contains lizardite (green dashed, RRUFFID = 60006), forsterite (purple dashed, RRUFFID = 100099), and brucite (black dashed, RRUFFID = 050455). Lizardite and forsterite are in the SW reacted rock (blue) and RW reacted rock (orange), but brucite is no longer present. The main magnetite peak overlaps forsterite at ~36 2 theta, thus it is hard to identify magnetite with powder XRD.

Table 4. Quantitative powder XRD measurements determined by RockJock of unreacted Oman dunite.

	Unreacted Oman dunite	
Mineral	**Weight %**	**Normalized weight %**
Forsterite	53	51
Brucite	6	6
Serpentine (Chrysotile + Lizardite)	46	43
Total	105	100
Full pattern degree of fit	**0.1393**	

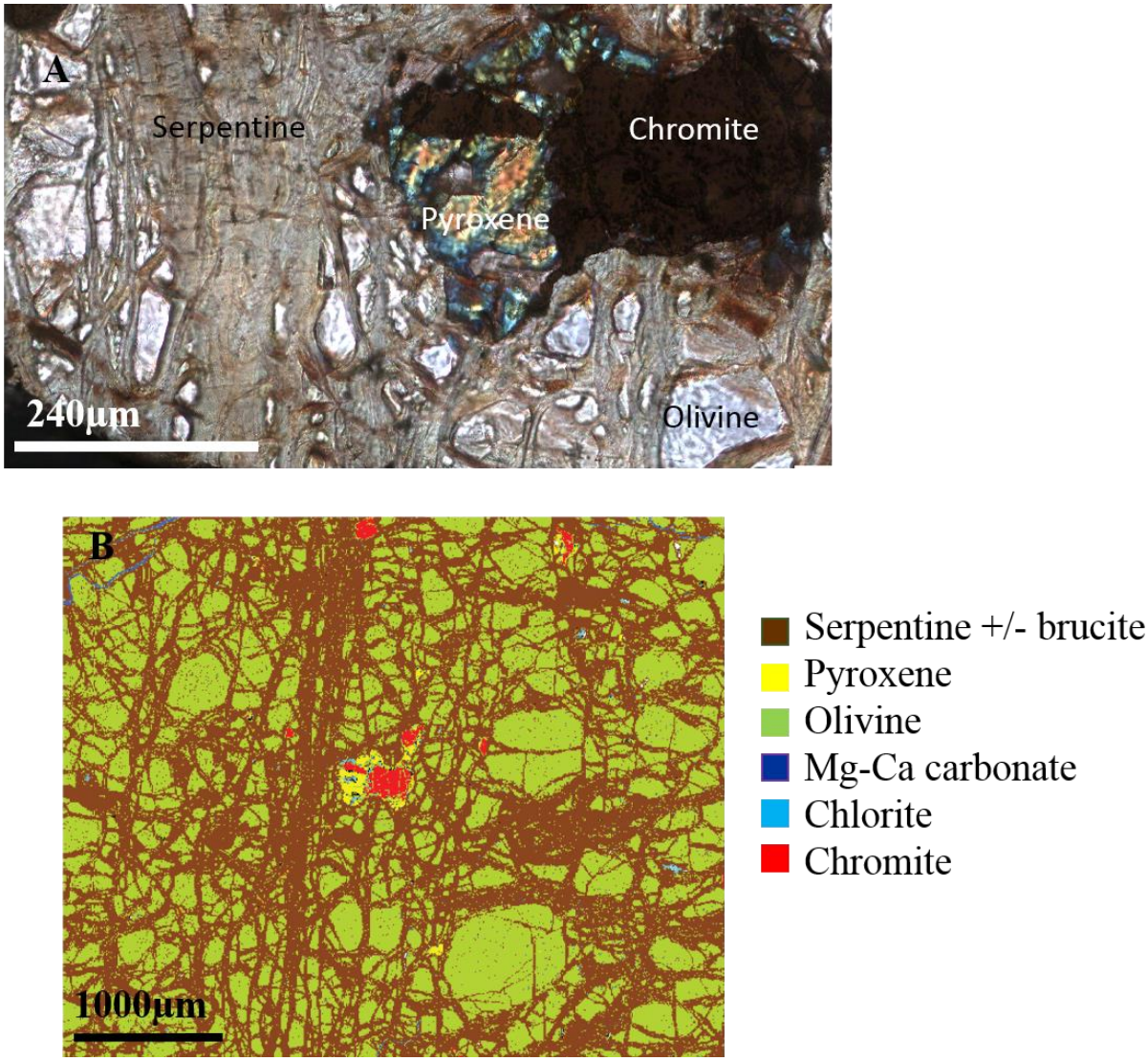

Figure 3. A: Transmitted light image of Oman dunite with key minerals labeled. B: QEMSCAN image of grain mount of unreacted Oman dunite. Serpentine +/- brucite (dark brown) encompasses ~50% of thin section, while other ~50% of minerals detected include olivine (light green), pyroxene (yellow), chromite (red), chlorite (dark green), Mg-Fe-Ca silicates (light blue) and unidentified Mg-Ca carbonates (purple).

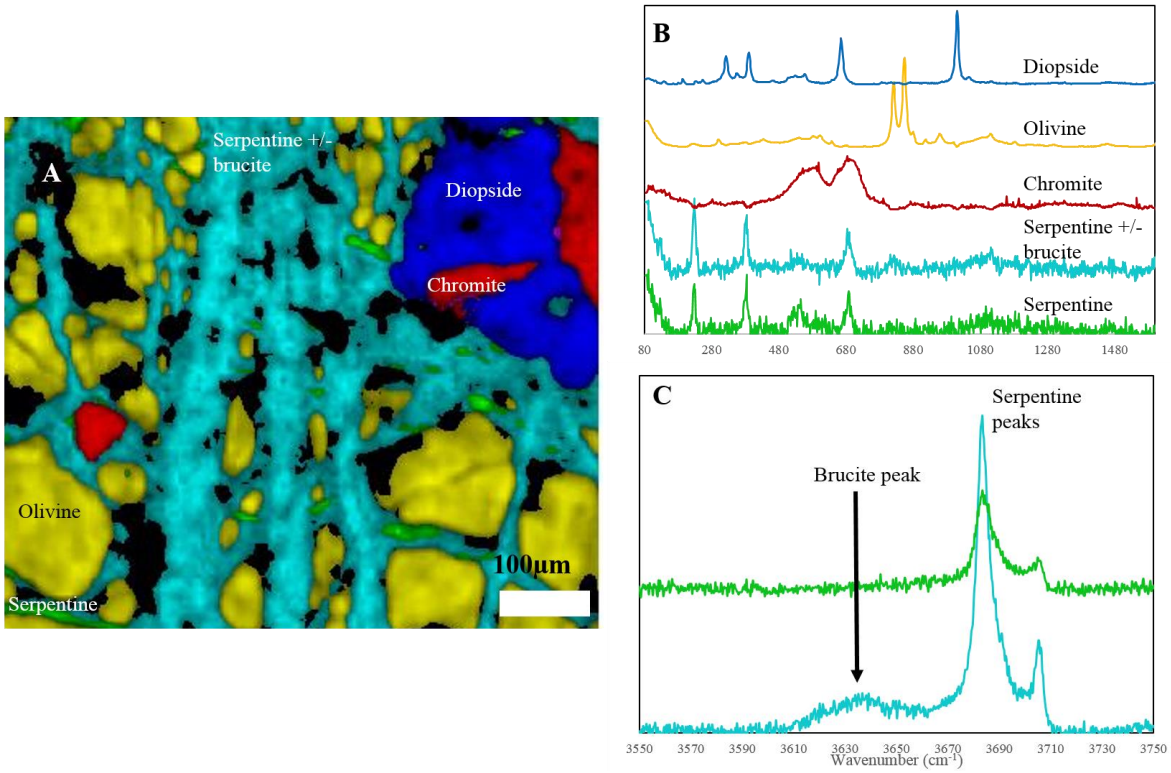

Figure 4. A: Hyperspectral MicroRaman map of Oman partially serpentinized dunite. Olivine (yellow) grains are surrounded by serpentine intermixed with brucite (cyan) and some serpentine with no brucite (green). There is a large chromite grain in the right corner (red), along with diopside (blue). Black regions indicate serpentine spectra intermixed with an epoxy signal. B: Spectra in fingerprint region (80-1600cm^{-1}) corresponding to colors on map. C: OH stretch region for hydrous minerals in the map. The serpentine peaks are evident at 3680 and 3700 cm^{-1}, whereas the brucite peak is present mixed with the serpentine in the cyan spectrum at 3640 cm^{-1} (see arrow).

bearing fluids. The dunite contains 0.24% carbonate, as measured by the amount of CO_2 evolved from acidification, which is approximately 0.012 grams of the total weight of the original 5 gram sample (Supplementary Table 2).

Electron microprobe analyses were used to determine the composition of the olivine grains and infer the chemical composition of the serpentine/brucite mixtures in Oman dunite. The average olivine formula in the Oman dunite sample is $(Mg_{1.80}Fe_{0.20})SiO_4$. The Fe concentration in the serpentine/brucite varied from 4.47 to 7.64 wt % FeO (Table 5) and the weight percent oxide totals were low (71-84 wt %). These total weight percent oxide values fall between predicted total weight percent oxide for serpentine (87%) and brucite (69%) due to intermixing of these phases (Supplementary Text 1).

We estimated the Fe-content of the brucite to be 18 weight % FeO using Raman spectroscopy. The Fe-content was calculated by determining the position of the OH peak of the brucite spectrum near 3650 cm^{-1}. This peak shifts to lower wavenumbers when Fe substitutes into brucite (Reynard et al., 2015). We prepared a calibration from a suite of 20 natural and synthetic brucites with a range of iron concentrations that showed the position of the OH peak decreases by ~0.9 cm^{-1} per weight % FeO. This slope was used to calculate the 18 weight % FeO in our brucite, or in terms of wt % MgO, 53, with a Mg # of 0.86.

We quantified the oxidation state of Fe-bearing minerals in the unreacted and reacted rock powders because Fe-oxidation drives hydrogen production during serpentinization. Pre-edge multiple energy mapping of serpentine and brucite in a thin section of Oman dunite was conducted at BL2-3 at SSRL to determine Fe^{3+}/Fe_{Total} prior to laboratory water/rock reaction. Following the work of Wilke et al. (2001) and Andreani et al. (2013b), the range of pre-edge centroids and intensities of unreacted serpentine and brucite XANES were plotted on a Fe

Table 5. Electron microprobe data from serpentine in Oman dunite prior to reaction and after reaction in SW medium. Columns represent 6 different analysis points. The Si/(Mg+Fe) ratio should be 0.67 for a pure serpentine. % Brucite is calculated from the following equation: Si/(Mg+Fe) ratio = x*(0) + (1-x)*(0.67), where 0 is the theoretical ratio of Si/(Mg+Fe) for pure brucite and 0.67 is the theoretical ratio of Si/(Mg+Fe) for pure serpentine. Large standard deviations reflect the variability of brucite abundance in serpentine.

Unreacted serpentine areas from Oman dunite							**Average (standard deviation)**
Na_2O	0.00	0.00	0.00	0.00	0.00	0.00	0 (0.00)
MgO	36.84	36.45	39.86	39.29	39.00	38.29	38.29 (1.26)
Al_2O_3	0.00	0.00	0.00	0.00	0.00	0.00	0 (0.00)
SiO_2	37.31	30.45	35.10	36.19	36.44	35.10	35.10 (2.22)
CaO	0.05	0.04	0.08	0.05	0.05	0.05	0.05 (0.02)
FeO	5.91	4.47	6.66	5.97	7.64	6.13	6.13 (.0.95
MnO	0.14	0.11	0.09	0.09	0.11	0.11	0.11 (0.02)
Total	80.25	71.51	81.79	81.59	83.24	79.68	79.68 (3.83)
SW Reacted serpentine areas							**Average (standard deviation)**
Na_2O	0.00	0.04	0.00	0.04	0.04	0.00	0.02 (0.02)
MgO	38.87	37.61	37.13	37.74	36.41	40.51	38.05 (1.33)
Al_2O_3	0.00	0.00	0.00	0.00	0.00	0.00	0 (0.00)
SiO_2	41.16	39.27	39.24	39.83	38.43	35.81	38.96 (1.63)
CaO	0.00	0.08	0.08	0.07	0.07	0.07	0.06 (0.03)
FeO	4.33	5.42	6.57	4.38	8.48	6.21	5.90 (1.43)
MnO	0.00	0.10	0.00	0.00	0.16	0.12	0.06 (0.07)
Total	84.36	82.51	83.02	82.05	83.59	82.72	83.04 (0.75)

variogram to quantify the Fe(II)/(III) ratios (Supplementary Figure 2). The Fe(III) content of intermixed serpentine and brucite ranged from ~40-80% of the total Fe in each analysis (error of +/- 10%).

3.2 Hydrogen production

Both SW and RW water/rock reactions begin making small amounts (12 - 34 nmol/gram mineral) of hydrogen after reacting for 2 days (Tables 6 & 7, Figure 5). The reaction with SW media produced the highest measured total H_2 concentrations (summed from both the fluid and the headspace) of 470 nmol/gram mineral after 92 days of reaction. Hydrogen is partitioned into different reservoirs (headspace vs. aqueous phase), and thus we report the concentrations of H_2 in nanomoles in fluid and headspace, nmol (total in fluid and headspace)/gram mineral, and nM in fluid (Tables 6 & 7). The H_2 in the SW experiment decreased to 270 - 310 nmol H_2/gram mineral after 203 days (Table 6, Figure 5). The RW media also produced significant H_2, with peak concentrations at 37 days with a maximum 280 nmol H_2/gram mineral (Table 7). H_2 concentrations in RW media then decreased to 96 – 110 nmol H_2/gram mineral at 97 days (Table 7, Figure 5).

Control vials with RW or SW solutions equilibrated with N_2:CO_2 were also regularly analyzed, since incubating silica serum vials with fluids and butyl stoppers produces small amounts of H_2 (Mayhew et al., 2013; McCollom and Donaldson, 2016). In these experiments, the controls all exhibit H_2 concentrations of 200 nmol or less in the fluid plus headspace throughout the lifetime of the experiment. Although this pathway for generation of small amounts of hydrogen complicates calculations of the amount of H_2 generation by reaction of aqueous fluids with minerals from the Oman dunite sample, the effect is minimal because the observed

Table 6. Concentrations of H_2 in water/rock reactions when reacting with artificial sulfate-free seawater (SW) media, presented in terms of total amount H_2 per reaction (nmoles), amount normalized to mineral mass (nmol/g), and aqueous H_2 concentration (nM) for convenience. Significant figures reflect an uncertainty of 5% in the original H_2 headspace measurement by GC in µmol/mL. SW_C1 and SW_C2 are control vials without minerals. Blanks are in duplicate and reactions in triplicate.

Total H_2 in fluid and headspace (nmoles)

Day	SW_C1	SW_C2	SW_1	SW_2	SW_3
0	0	0	0	0	0
2	0	0	87	73	69
48	48	38	850	850	920
92	190	200	2400	2000	2000
203	180	80	1500	1400	1550

Total H_2 in fluid and headspace (nmol/g mineral)

Day	SW_C1	SW_C2	SW_1	SW_2	SW_3
0	0	0	0	0	0
2	0	0	17	15	14
48	10	8	170	170	180
92	38	41	470	400	400
203	36	16	310	270	310

H_2 in fluid (nM)

Day	SW_C1	SW_C2	SW_1	SW_2	SW_3
0	0	0	0	0	0
2	0	0	46	39	37
48	39	35	740	570	610
92	100	100	1300	1100	1100
203	96	43	810	720	820

Table 7. Concentrations of H_2 in water/rock reactions when reacting with artificial rainwater (RW) media presented in terms of total amount H_2 per reaction (nmoles), amount normalized to mineral mass (nmol/g), and aqueous H_2 concentration (nM) for convenience. Significant figures reflect an uncertainty of 5% in the original H_2 headspace measurement by GC in μmol/mL. RW_C1, RW_C2, and RW_C3 are control vials without minerals.

Total H_2 in fluid and headspace (nmoles)

Day	RW_C1	RW_C2	RW_C3	RW_1	RW_2	RW_3
0	0	0	0	0	0	0
2	0	0	0	59	130	170
13	35	52	73	530	630	760
37	76	110	180	900	1100	1400
97	94	100	94	480	530	500

Total H_2 in fluid and headspace (nmol/g mineral)

Day	RW_C1	RW_C2	RW_C3	RW_1	RW_2	RW_3
0	0	0	0	0	0	0
2	0	0	0	12	26	34
13	7	10	15	110	130	150
37	15	23	37	180	220	280
97	19	21	19	96	110	100

Total H_2 in fluid (nM)

Day	RW_C1	RW_C2	RW_C3	RW_1	RW_2	RW_3
0	0	0	0	0	0	0
2	0	0	0	31	70	90
13	19	28	39	280	340	400
37	41	61	98	480	580	740
97	50	55	50	250	280	270

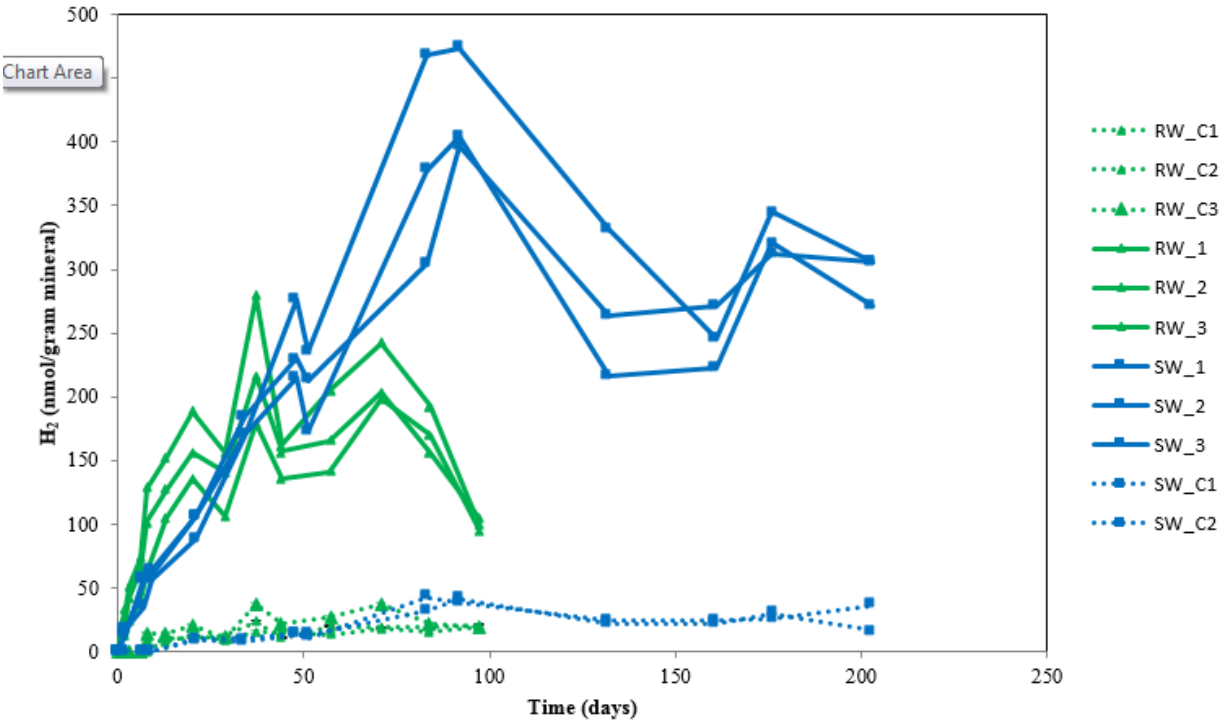

Figure 5. Hydrogen production at 100°C from reaction of partially serpentinized Oman dunite with SW media (blue lines) and Oman RW media (green lines), conducted in triplicate. Controls (vials filled with fluids, no minerals, purged with N_2:CO_2) are shown with dashed lines, respectively. Net H_2 concentrations increase for 50-100 days and then decrease.

concentrations of H_2 from the 100°C reactions are an order of magnitude higher than the concentrations of H_2 in the controls.

3.3 Aqueous chemistry

Within 24 hours of the onset of the reaction at 100°C, the pH increases from ~5-6.5 to 8.5-9 in both SW and RW media, and then decreases slightly to 8-8.5 for the lifetime of the experiments (Supplementary Figure 3). As discussed in methods, these values reflect the pH measured at 25°C, not the in situ pH values, which are expected to be 1-2 pH units lower. The headspace CO_2 concentration decreases over time in both media. Unfortunately, the initial headspace CO_2 concentration in the water/rock reactions was not measured, but we did measure the headspace CO_2 concentration in the control vials after 171 days (RW) and 304 days (SW). As the control vials are non-reactive, this headspace CO_2 concentration approximates the initial headspace CO_2 concentration in the vials with rock. From this assumption, the $CO_{2(aq)}$ concentrations in the RW experiments begin at ~7.0 µmol/mL and decreased to ~1.0 µmol/mL after 6 months. The $CO_{2(aq)}$ concentrations in the SW experiments start at ~4.0 µmol/mL and decreased to ~0.03 µmol/mL after 10 months. No CH_4 was detected in any of the vials with a gas chromatograph detection limit of ~10 nmol.

The final aqueous geochemistry measurement was on day 155 for RW experiments and day 287 for SW experiments. In addition, samples were also analyzed from early time-points in the RW media experiment. The composition of the reacted fluid was measured after 24 hours of reaction and showed a rapid increase in the concentration of Mg^{2+}, Fe^{2+} and Mn^{2+} ions in solution. Then, concentrations of Fe^{2+} and Mn^{2+} decreased rapidly to near initial concentrations, while Mg^{2+} decreased more gradually over time (Figure 6). Silica gradually increased over time.

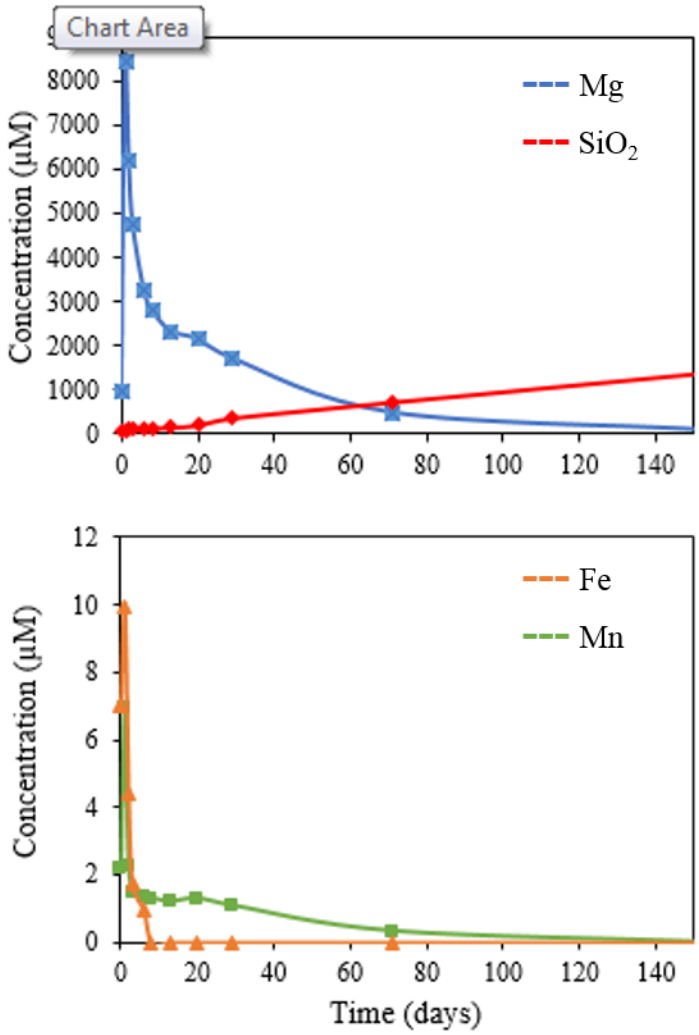

Figure 6. Water chemistry of RW media reacting with Oman dunite over 50 day period; later time points were not included because concentrations do not vary significantly after 50 days. Initial release of Mg^{2+}, Fe^{2+}, and Mn^{2+} results in maximum cation concentrations after 24 hours of reaction, then levels decline over time. Release of $SiO_{2(aq)}$ is not detected in the first 10 days, but $SiO_{2(aq)}$ does slowly increase over the course of the experiment. Other major cations, anions, and trace metals (Ca^{2+}, Ni, Cr, SO_4^{2-}) were measured but did not change significantly with time.

Most of the increase concentration of silica is due to the dissolution of the silica serum vials, as seen by similar silica concentrations in control and water/rock vials (Supplemental Table 1). The aqueous chemistry of the SW experiments was not measured at early time points.

3.4 Low molecular weight organic acids

Dissolved low molecular weight organic acids were measured in the water/rock reactions and controls (Table 8). The fluids were extracted from the experiments after decreases in the H_2 headspace concentration were observed, on day 525 for SW and 392 for RW. 40.2-98.1 µM of formate and 38.2-91.2 µM of actetate were observed in the RW and SW experiments. Less than 13.5 µM of propionate, butyrate, valerate, and lactate were detected in the products of the SW and RW experiments (Table 8). We believe the control experiments have small amounts of organic acids due to contamination from the butyl rubber stoppers. Organic acid concentrations in the water/rock experiments are significantly higher than in mineral-free controls (Table 6). Thus, we infer that formate and acetate were generated in the SW and RW water/rock reactions as H_2 and CO_2 were consumed. Formate was more abundant in the RW experiments while acetate was more abundant in the SW experiments.

To confirm that CO_2 was required to generate organic acids, separate SW- and RW-dunite experiments were conducted with only N_2 in the headspace (see Figure 1). These experiments serve as controls because without CO_2 in the headspace, there is little carbon to react with H_2 to make low molecular weight organic acids. SW and RW media do contain small amounts of HCO_3^-, 2.41 and 0.02 mM, respectively. However, this carbon does not appear to transform into organic acids. The N_2-only reactions generated similar levels of H_2 to the SW and RW reactions, but contained much lower concentrations of organic acids, similar to the controls

Table 8. Organic acid measurements (μM) of 100°C water/rock reactions. C indicates "control" vials with no minerals present, and N_2 indicates vials purged with only N_2 gas, whereas all the others were purged with N_2:CO_2. ND indicates no detection, while BDL indicates below the limit of detection, but a signal is still present. SW fluids were sampled after 525 days of reaction and RW fluids after 392 days of reaction with N_2:CO_2. N_2-only purged samples were measured after 308 days of reaction. The low concentrations of propionate, butyrate, lactate, and valerate are not statistically significant.

Sample	Formate	Acetate	Lactate	Propionate	Butyrate	Valerate
Limit of detection (μM)	3.3	5.1	1.8	0.1	4.1	0.3
SW_C1	21.9	15.4	ND	10.4	ND	ND
SW_C2	18.4	12.9	ND	13.5	ND	ND
SW_1	40.2	81.7	BDL	11.8	ND	ND
SW_2	57.4	50.4	BDL	13.6	ND	1.7
SW_3	52.9	69.9	ND	12.1	ND	1.5
RW_C1	19.0	7.6	ND	0.2	BDL	ND
RW_C2	57.5	7.6	ND	0.4	ND	ND
RW_C3	54.1	12.2	ND	0.3	ND	0.9
RW_1	98.1	38.8	ND	0.8	ND	1.4
RW_2	73.4	38.2	ND	0.6	BDL	ND
RW_3	82.5	91.2	ND	1.1	ND	0.4
SW_N2	13.1	18.5	BDL	1.5	ND	ND
RW_N2	7.7	16.3	BDL	1.5	ND	ND

with no minerals. These experiments were not run in triplicate, so their H_2 generation results are not reported. They contained <13.1 µM formate, <18.5 µM acetate, and <1.5 µM lactate, propionate, butyrate, and valerate, confirming that the elevated levels of organic acids are only observed when dissolved CO_2 is provided as a reactant.

3.5 Mineralogy and Fe-content of reacted rock

Minerals were sampled from the RW and SW experiments one or more times after extensive water/rock reaction; the exact sampling times are detailed in Table 3. A secondary, white mineral precipitate formed during both the SW and RW water/rock reaction after ~30 days of reaction. Several techniques were used to try to quantify the mineralogy and Fe-content of this mineral. Secondary precipitate was collected from SW media after ~90 days of reaction to analyze with powder XRD. The diffraction peaks most closely align with lizardite (Figure 7). However, olivine peaks were also present, showing that the secondary mineral was not fully separated from the primary olivine. There was not sufficient material available to conduct powder XRD on the secondary mineral formed in the RW medium. Raman spectra of single grains of the secondary mineral in both samples (SW_reacted and RW_reacted) fit the spectrum of serpentine (Figure 8). The serpentine created during the water/rock reactions is clearly visible in grain mounts of reacted SW and RW minerals, which also demonstrate that serpentine and olivine are the dominant minerals (Figure 9). Scanning electron microscopy was used to image the newly-formed serpentine and acquire EDS spectra for both the SW and RW reacted grains (Supplementary Figure 4). The serpentine is variably platy and globular, coating olivine grains. Electron dispersive spectroscopy data indicate that the serpentine contains Mg, Si, and O with trace amounts of Al and Fe (Supplementary Figure 4). The presence of carbon cannot be

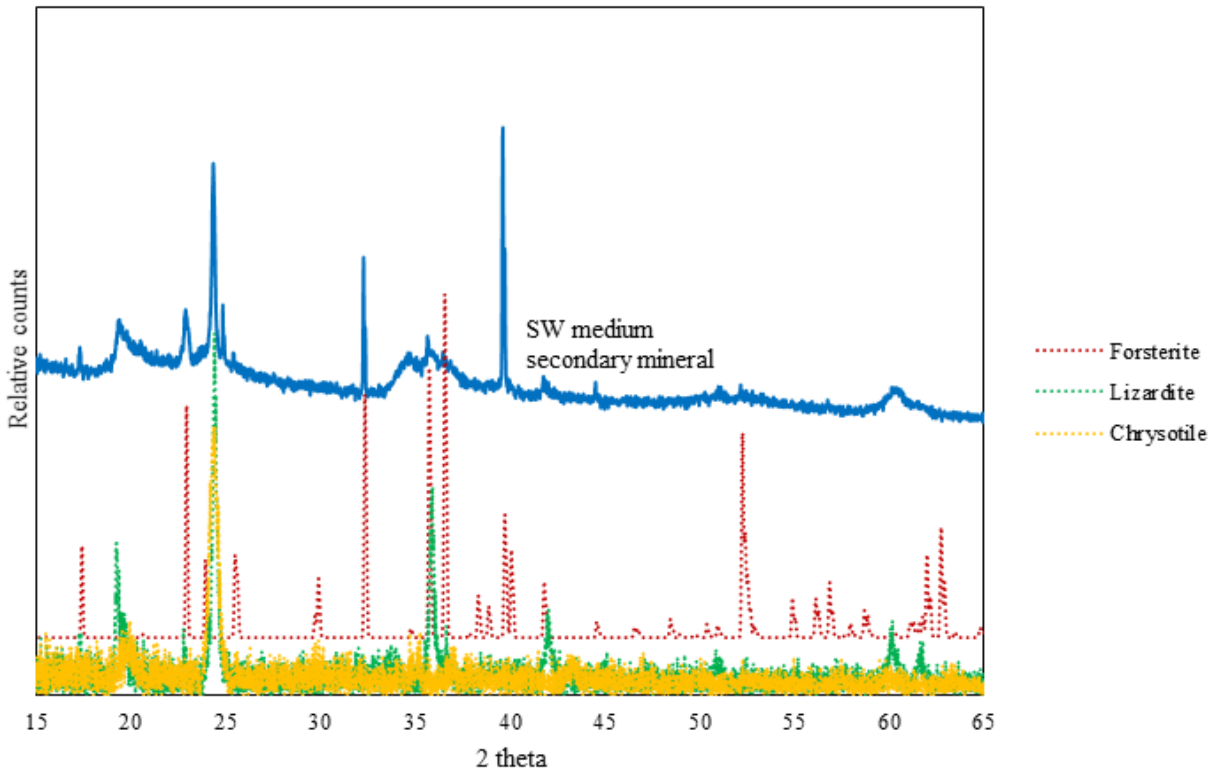

Figure 7. Powder XRD spectrum of secondary mineral (blue) that forms in SW medium reaction. The spectrum fits most strongly to lizardite (green dashed), but also has traces of olivine (red dashed) due to difficulty in completely separating the grains. Chrysotile (yellow dashed) was added to show the spectrum more closely fits lizardite.

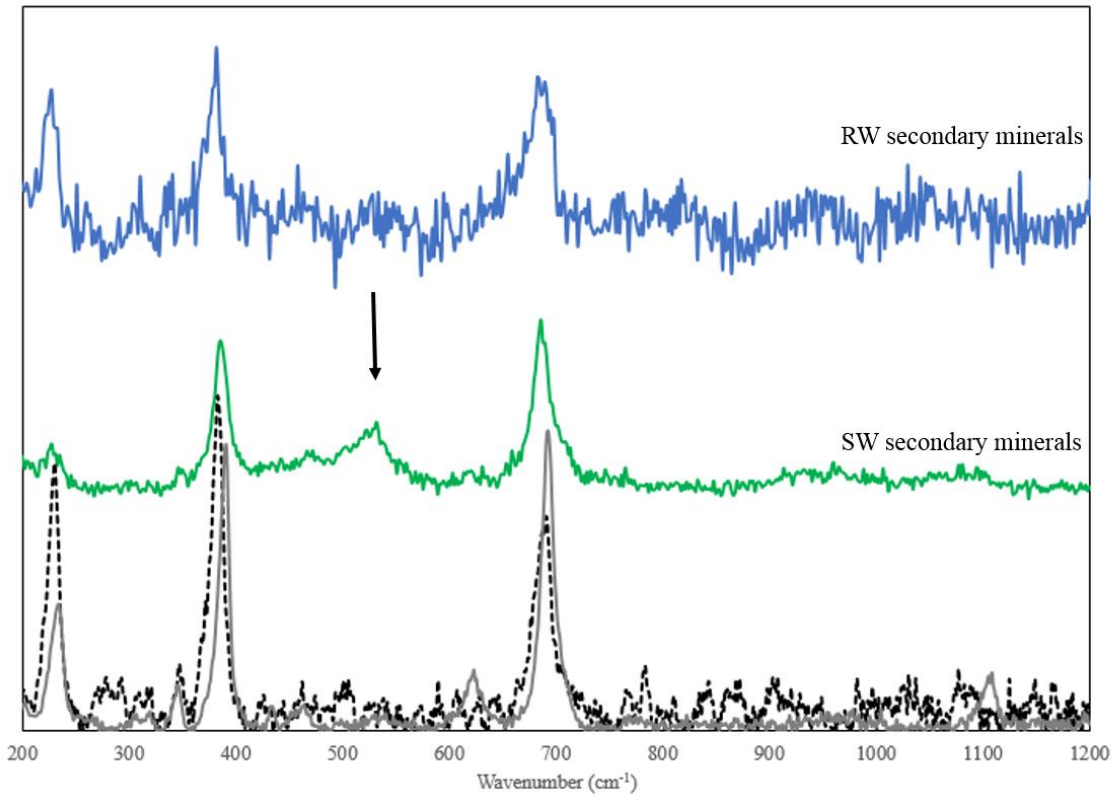

Figure 8. Raman spectra of SW secondary minerals (green) and RW secondary minerals (blue) compared to a lizardite Raman spectrum (black dashed, RRUFFID = R060006) and chrysotile Raman spectrum (gray, RRUFFID = R070088). Secondary minerals are not fully crystalline, thus do not produce high signal to noise spectra. The black arrows above the small peak at 550 cm^{-1} (black arrow) in green is a common occurrence in serpentine from Oman; however, the exact chemical composition leading to that peak is unclear.

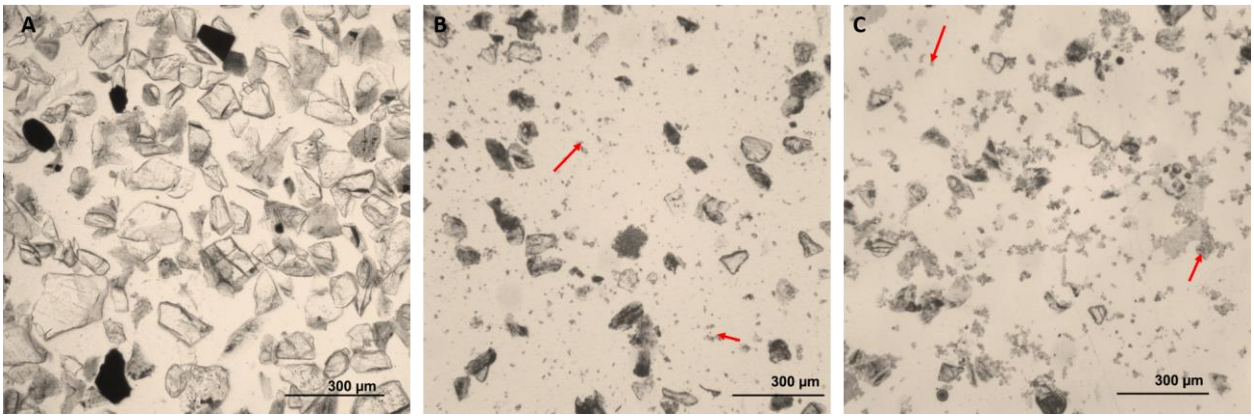

Figure 9. Image of unreacted Oman dunite grain mount **(A)** with clear olivine, serpentine, and opaque chromites. The serpentine was extracted with a 23 gauge needle from the anaerobic serum vials, along with other fine-grained particles from RW reacted **(B)** and SW reacted **(C)** experiments and mounted on grain mounts. The amorphous serpentine can be seen dispersed throughout the epoxy (see red arrows), along with clear olivine grains and dark serpentine grains.

assessed because both samples were carbon coated. However, no carbonate formation was observed by probing the grains with Raman spectroscopy, powder XRD, and SEM. We analyzed the reacted SW and RW grains with a mass spectrometer to quantify any trace carbonate formation, but the amount of CO_2 evolved from acidification of the samples was less than or equal to that of the unreacted dunite (Supplementary Table 2). We also analyzed the grains for total organic carbon (TOC) by combustion techniques, but all organic carbon values were less than the lowest standard run (0.109 mg of 70% carbon); the organic carbon is not quantifiable by this technique for our samples.

The average surface area of the mineral grains increased by more than an order of magnitude during the course of the reactions, which is attributed to the formation of the amorphous serpentine. The unreacted rock had a surface area of 0.47-0.60 m^2/gram. After reaction with RW, average surface area increased to 6.31 m^2/gram, while the average surface area of the mineral grains reacted with SW increased to 10.17 m^2/gram. The length of olivine grains in unreacted and reacted grains was measured (Supplementary Table 3), and did not change throughout the experiment. Thus, the surface area increase is due to the precipitation of new serpentine and not to the fragmentation of existing olivine.

Changes in magnetic susceptibility were quantified for the rock reacting in the RW media. The results show an increase in magnetite content after water/rock reaction. Both the unreacted and reacted dunite powders are paramagnetic; they only demonstrate magnetic properties in the presence of an applied magnetic field. The remanent magnetization (residual magnetism remaining after external magnetic field is removed) in the unreacted rock is 0.1353 $A.m^2$ (emu), whereas the remanent magnetization in the reacted rock is 0.1828 $A.m^2$ (emu). The

saturation magnetization is 0.0036 $A.m^2$ (emu) for the unreacted rock and 0.0101 $A.m^2$ (emu) for the reacted rock (Table 9).

Notably, brucite was not present in the Oman dunite samples after reaction with SW and RW. Powder XRD reveals a brucite peak at 18.8 2θ in unreacted rock that is no longer present in the SW and RW reacted products. The lack of brucite in the reaction products was confirmed by analyzing the reacted grains with Raman spectroscopy and noting the absence of the brucite OH stretch at ~3640 cm^{-1} from both SW and RW media after >1 year of reaction. In contrast, brucite is pervasive in the unreacted mineral grains (Figure 4).

Electron microprobe was used to quantify the % FeO concentration in the olivine and serpentine from the SW experiments to determine any changes during the reaction (Table 5). The SW reacted olivine FeO values were similar to the unreacted olivine at ~10 weight % FeO. A range of 4.33-8.48 weight % FeO in serpentine was observed, similar to the unreacted serpentine.

The bulk iron speciation of the dunite was also assessed before and after reaction using Fe K-edge XANES spectroscopy. Least squares fitting of bulk XANES spectra was employed to show that the Fe speciation of the XANES spectra from both the unreacted dunite and the reaction products from the RW experiments can be fit using approximately 50% serpentine and 50% olivine, with a sensitivity of ±10%. There was no discernible shift in the overall Fe XANES spectrum for the unreacted and reacted rock (Supplementary Figure 5). In addition, Fe pre-edge XANES analyses were conducted at the microscale for the newly-formed serpentine in RW experiments to determine the $Fe(III)/Fe_T$ ratio. These measurements were challenging because the newly-formed serpentine contains low iron concentrations. For the spectra obtained, the centroids and intensities of the pre-edge spectra were plotted in the $Fe(III)/Fe_T$ variogram (Supplementary Figure 2) and compared to the range of $Fe(III)/Fe_T$ ratios found in serpentine

Table 9. Magnetic susceptibility measurements for powdered Oman dunite, before and after water/rock reaction with rainwater (RW) media.

Sample	Magnetic type	Remanent magnetization(Mr) ($A.m^2/emu$)	Saturation magnetization(Ms) ($A.m^2/emu$)	Coercivity (Hc)
RW_unreacted	Paramagnetic	0.1353	0.0036	116.6438
RW_reacted	Paramagnetic	0.1828	0.0101	108.9219

from unreacted Oman dunite obtained from a multiple energy pre-edge map (Wilke et al., 2001; Mayhew et al., 2013; Muñoz et al., 2013; Andreani et al., 2013b). Some newly-formed serpentine falls within the range of pre-existing serpentine Fe(III)/Fe_T ratios, which vary from 40-80% Fe(III)/Fe_T. However, some spot analyses show >90% Fe(III), which is more oxidized than any of the pre-existing serpentine. Unfortunately, we could not conduct the same analysis on the newly-formed serpentine in SW media because it was difficult to separate it from grains of olivine.

3.6 Mass balance of Fe during the water/rock reactions

TGA analysis of the minerals from the unreacted and reacted RW experiments was used to quantify changes in the total mass of serpentine and brucite during water/rock reaction. The TGA data for the unreacted Oman dunite indicated that brucite made up ~5 wt % of the initial mineralogy, and serpentine was 38 wt % of the unreacted rock (Figure 10). After the RW reactions, serpentine remained 38 wt % of the mineralogy, while brucite was not detected. We have reservations about TGA analysis because we have tested how well TGA can estimate a known mixture of brucite and serpentine, and the analysis underestimated the amount of brucite and overestimated the amount of serpentine (explained in detail in Miller et al., 2016). Despite these reservations, the TGA data affirms the presence of both brucite and serpentine in the unreacted rock. It also shows that brucite is not present in the reacted product and provides an approximation of mass change during water/rock reaction.

Bulk powder XRD measurements show the loss of the brucite peak at 18.8 2θ for both RW and SW reacted grains (Figure 2). The dominant olivine and serpentine peaks were similar pre- and post-reaction. The initial mineralogy of Oman dunite was quantified using the USGS

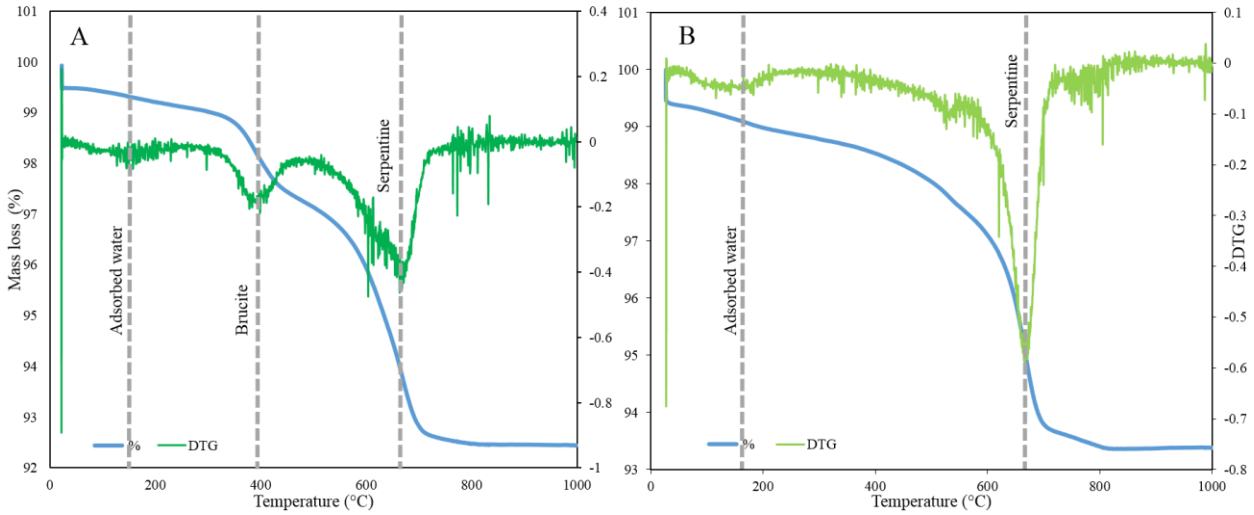

C.

Unreacted Oman dunite	mass % OH lost as measured by TGA	% mass of mineral in total rock
Brucite	1.7	5%
Chrysotile	4.9	38%
RW reacted Oman dunite		
Brucite	0.0	0%
Chrysotile	6.6	38%

Figure 10. A: TGA of unreacted Oman dunite shows brucite and serpentine present. **B:** TGA of RW reacted dunite shows the absence of brucite peak and presence of larger serpentine peak. **C:** Quantification of mass % brucite and mass % serpentine for unreacted dunite and RW reacted dunite derived from TGA.

RockJock software. The results from this technique are consistent with TGA results: 44% serpentine, 6% brucite, and 46% forsterite (Table 4). Quantification of SW and RW reacted grains was attempted with RockJock, but reasonable data were not obtained because the amount of olivine present appeared to increase after water/rock reaction. This likely indicates that a representative sample was not used, perhaps due to the abundance of amorphous precipitated serpentine that did not homogenize well with the more durable olivine grains. However, the brucite peak disappears in the RW and SW bulk powders. This is consistent with corresponding data collected from Raman spectroscopy and TGA thus, it is reasonable to conclude that brucite was entirely consumed during water/rock reactions.

The maximum mass of magnetite generated during the RW water/rock reaction was calculated using a proportionality constant of 92 $A.m^2/kg$ to empirically correlate the saturation magnetization to the amount of magnetite using the methods of Malvoisin et al. (2012). This calculation yields a total of 1.1 milligrams of magnetite in unreacted Oman dunite and 2.7 milligrams of magnetite after reaction in RW media, per 5 grams of dunite reacted. Thus a maximum of 1.6 milligrams of magnetite was produced, which is equivalent to 0.31 mmoles of magnetite. This estimate assumes the sole magnetic carrier in the sample is magnetite, which may not be true due to the prevalence of Fe(II & III)-bearing serpentine. Also, it is possible that maghemite formed, which oftentimes forms when magnetite is oxidized at low-temperatures (Oufi et al., 2002). The powder XRD peaks of the two minerals overlap (Kim et al., 2012) and XANES spectra are also similar (Espinosa et al., 2012), thus it is difficult to certainly state the mineral product. Maghemite has a proportionality constant of 65.3 $A.m^2/kg$ (Özdemir and Dunlop, 2010), which would correspond to 1.6 mg of maghemite in unreacted Oman dunite and 3.8 mg of maghemite formed in RW vials. This is discussed in more detail later.

4. Discussion

4.1 Hydrogen production at 100°C

Our experimental low-temperature water/rock reactions with Oman dunite produce sufficient hydrogen over prolonged time-scales to sustain subsurface microbial activity. Methanogens grow in a variety of environments with low levels of hydrogen comparable to this study, with dissolved aqueous concentration of up to 1.3 µM H_2 at pH ~9: rice paddies (28 nM H_2), lake sediment (36 nM H_2), sewage sludge (203 nM H_2), and hot springs (>300 nM H_2) (Zinder, 1993; Spear et al., 2005). Other hydrogenotrophic anaerobes, such as *Desulfovibrio* and *Acetobacterium*, require even less H_2 (<10 nM H_2) to sustain growth (Zinder, 1993).

Partially serpentinized dunite has the capability to produce large quantities of H_2, even when the primary olivine and pyroxene are already partially serpentinized. The experiments described herein gave rise to some of the highest concentrations reported in the literature for H_2 generated at low-temperatures (Table 1). A maximum of 470 nmol H_2/gram mineral was measured after several months of water/rock reaction at 100°C in SW media. However, the maximum hydrogen generated is likely greater than the reported value because we did not correct for the H_2 removed from the headspace during sampling. Comparable amounts of H_2, up to 500 nmol/gram H_2, were produced by reaction of Snake River Plain basalt at 22°C at a pH of 6 (Anderson et al., 1998). However, when the pH was increased to 8 in subsequent experiments, a more environmentally realistic condition that is also more similar to this study, the basalt did not dissolve and no H_2 was detected. Previous studies conducted with variably altered dunite from the Leka ophiolite produced up to 110 nmol/gram H_2, which was particularly notable given the low reaction temperature of 25°C (Okland et al., 2012). Our work also uses partially

serpentinized dunite, but at higher reaction temperatures. Under these conditions, we generated more H_2 than recent experiments on the hydration of individual Fe(II)-bearing rocks and minerals, such as olivine, pyroxene, magnetite, as well as fresh San Carlos peridotite where a maximum of 300 nmol/gram mineral H_2 was observed at 100°C (Mayhew et al., 2013).

We believe the rapid increase in pH, concurrent with cation release, is due to brucite dissolution. The RW vials have a notable spike in Mg^{2+}, Fe^{2+}, and Mn^{2+} after 24 hours of reaction (Figure 6), that is attributed to the dissolution of (Mg,Fe) brucite containing small amounts of Mn^{2+}. The concentration of these cations decreases after the initial dissolution of brucite, possibly because the cations are incorporated into newly crystallized magnetite, serpentine, or trace secondary phases. There is no evidence of increased silica due to dissolution of any silicate phase.

Fluid composition exerts a strong influence on the extent of H_2 production. Reactions in SW produced more H_2 compared to reactions in RW media. Phosphate and bicarbonate are inorganic ligands in the SW media that can promote brucite dissolution by attacking surface metal-oxygen bonds (Pokrovsky et al., 2005). Additionally, the presence of Ca^{2+} in SW media (0.01 M Ca^{2+} in SW media versus 0.0005 M Ca^{2+} in RW media) may have led to increased brucite dissolution as inferred from experiments where the addition of 0.01 M Ca^{2+} to a brucite suspension resulted in an increase in brucite dissolution at pH 4.9 (Pokrovsky et al., 2005). The simulated SW is a higher ionic strength media (0.73 M) versus RW media (0.005 M). However, dissolution rates of brucite, the key mineral releasing Fe(II) for oxidation, are not dependent on ionic strength, likely due to the double-layered brucite sheets that can accommodate high charge densities (Pokrovsky, et al. 2004). In summary, a combination of increased inorganic ligands and

divalent cations in SW vs. RW media appears to have caused faster rates of brucite dissolution in SW, affecting Fe(II) release and subsequent hydrogen generation.

4.2 Mineralogical changes during water/rock reaction

We investigated the changes between the initial and final mineralogy of the Oman dunite sample to determine which mineral/water reactions contribute to low-temperature hydrogen production. The unreacted and reacted rock powders were characterized by bulk powder XRD, Raman spectroscopy, TGA, chemical separation and magnetic susceptibility measurements to quantify mass balance (Table 3).

Mass balance calculations show that oxidation of only ~0.001% of the total Fe(II) in the dunite is required to explain the observed levels of H_2 production (Supplementary Table 4). It is very difficult to document such a small change. In addition, the water/rock reactions do not go to completion, nor are the minerals and aqueous solutions in equilibrium with each other. Thus, mineral analyses are dominated by the unreacted starting mineralogy. Any changes are likely on the order of milligrams of material that are heterogeneously distributed throughout the sample. Thus, we found it challenging to robustly quantify the small reservoirs of Fe(II) and Fe(III) that undergo a net change in these reactions. However, the combined suite of analytical techniques that we utilized did provide direct evidence for some changes in mineralogy and allowed us to estimate changes in modal abundance or chemical composition to partially constrain low-temperature serpentinization and H_2 production pathways.

The Oman dunite used for these experiments had already undergone at least one episode of serpentinization. The Fe-bearing phases in the partially serpentinized dunite are dominated by Fe(II)-bearing olivine, Fe(II) & Fe(III)-bearing serpentine, and Fe(II)-rich brucite, along with

trace amounts of pyroxene, chromite, and magnetite. The serpentine and brucite are intimate mixtures presumably formed while the ophiolite was exposed to hydrothermal fluids at the mid-ocean ridge or during the process of obduction onto the Arabian Peninsula (Coleman, 1981; Boudier et al., 2010; Hanghøj et al., 2010), or during low temperature subaerial alteration (Barnes et al., 1978; Neal and Stanger, 1983, 1985; Kelemen and Matter, 2008; Kelemen et al., 2011; Miller et al., 2016). Thus, the starting mineral assemblage in Oman dunite contains several reservoirs of Fe(II) that may lead to hydrogen production in addition to, or instead of, serpentinization of the remaining olivine.

We do not observe significant olivine dissolution at 100°C during the experiments. However, the detection limit of powder XRD is approximately 5% by weight, so some olivine could have dissolved without detection. This observation is supported by the slow rates of olivine dissolution at low temperatures; example rates from prior studies include 1.68×10^{-12} mol cm^{-2} s^{-1} at 120°C and pH 8.33 (Prigiobbe et al., 2009) and 2.10×10^{-12} mol cm^{-2} s^{-1} at 120°C and pH 9.44 (Hänchen et al., 2006). Another potentially reactive reservoir of Fe(II) in the dunite is pyroxene. However, as for olivine, there is little evidence for pyroxene dissolution during the course of these water/rock reactions. Serpentine is another reservoir of both ferric and ferrous iron that may react with water, leading to hydrogen production. Thus, the oxidation of existing Fe(II,III)-bearing serpentine can lead to the precipitation of newly-formed serpentine more enriched in Fe(III). However, given the initial abundance of serpentine in these experiments, it is difficult to detect changes in abundance or bulk chemistry. The pre-existing serpentine in the Oman dunite contains up to 10 weight % FeO, and this Fe may be >50% Fe(III) (Supplementary Figure 2). Therefore, based on the analyses we were able to conduct, it remains unclear if the

pre-existing serpentine quantitatively changes Fe(II/III) ratios during the experiments. However, the white precipitate that formed during water/rock reactions is unequivocally new serpentine.

Another reservoir of Fe(II) in the starting mineral assemblage is Fe(II)-bearing brucite that is intermixed with the serpentine. The brucite contains approximately 18 weight % FeO, making it a viable source of Fe(II) in solution. Ferrous hydroxide substituted into the brucite structure can give rise to H_2 production by the following end-member reaction (McCollom and Bach, 2009):

$$3Fe(OH)_2 = Fe_3O_4 + H_2 + 2H_2O \qquad (1)$$

which results in the formation of magnetite as the sole Fe(III)-bearing mineral associated with hydrogen production. Reactions dissolving Fe-brucite and producing magnetite, similar to reaction (1), are likely to be the main cause of H_2 generation in our experiments, although there are other Fe(II)-bearing minerals present in the unreacted mineral assemblage. Reaction (1) indicates the importance of Fe(II)-bearing brucite, and is consistent with the observed, significant consumption of brucite and production of magnetite during our experiments. Additional, possible reactions that consume the Fe-component in brucite could produce additional H_2 in combination with Fe-oxyhydroxides such as bernalite ($Fe(OH)_3$) and goethite (FeO(OH)), or in combination with Fe(III) bearing serpentine. These can be approximated, as:

$$2Fe(OH)_2 + 2H_2O = 2Fe(OH)_3 + H_2 \text{ , } 2Fe(OH)_2 = 2FeO(OH) + H_2 \quad (2,3)$$

$$2Fe(OH)_2 + Mg_2SiO_4 + H_2O = Mg_2Fe^{3+}SiFe^{3+}O_5(OH)_4 + H_2 \qquad (4)$$

Three mineralogical changes were observed in the 100°C water/rock reactions: the disappearance of Fe-bearing brucite, the production of magnetite, and the precipitation of new Fe(III)-bearing serpentine. The new amorphous serpentine probably accounts for the increase in surface area from the unreacted to reacted products. Energy dispersive spectroscopy analyses

suggest that the newly formed serpentine has similar Fe-content to the unreacted serpentine, with a Mg:Fe ratio of 7.8:1 to 5.9:1 in the new serpentine versus an average of 5.7:1 in unreacted serpentine. However, the new serpentine estimate is only based on two measurements. Although we could not quantify the mass of new serpentine formed, it was a small fraction of the initial mass, likely less than 1%. Although it is probably not a substantial reservoir for Fe(II) or Fe(III), the newly-formed serpentine in RW media does contain up to 95% Fe(III) compared to the 40-80% Fe(III) in the initial serpentine in the unreacted Oman dunite (Supplementary Figure 2). This observation of Fe(III)-bearing serpentine corresponds to observations of Fe(III)-rich serpentine in highly altered Oman serpentinites (Streit et al., 2012) and the hypothesis that Fe(III)-bearing serpentine forms in other low-temperature water/rock experiments (Neubeck et al., 2014).

The source of silica to precipitate new serpentine may be small amounts of olivine or pyroxene dissolution, or the dissolution of the borosilicate serum vials in which the experiments were conducted (Supplementary Figure 1). The addition of silica from the serum vials may also have contributed to brucite dissolution in the reactions (Ogasawara et al., 2013), however, it is still a relevant aqueous species in serpentinizing environments (Jöns et al., 2010; Miller et al., 2016). The newly-precipitated serpentine provides proof that Fe(III)-rich serpentine forms at low temperatures. However, we cannot determine whether or not serpentine formation is an important source of hydrogen generation in these experiments.

4.3 Proposed pathway and mass-balance for H_2 generation

We propose that the destabilization of Fe(II)-bearing brucite and subsequent oxidation of aqueous Fe(II) to form magnetite drives H_2 production in our low temperature laboratory

water/rock experiments. This aligns with previous work in recognizing the importance of dissolution of Fe-bearing species (Stevens and McKinley, 2000; Mayhew et al., 2013; Neubeck et al., 2014; Okland et al., 2014), but varies because dissolution of Fe-bearing brucite, rather than olivine, is the most important source of Fe(II). There are several alternative pathways of low-temperature hydrogen however, they do not seem likely to have been important in our experiments (e.g. formation of silica surface radicals through rock communition (Telling et al., 2015) but this process does not explain hydrogen production over the observed 3 month time period); H_2 within fluid inclusions released during mineral dissolution (e.g. Neubeck et al., 2011a) however, fluid inclusions were not detected using confocal Raman spectroscopy).

To assess our hypothesis regarding brucite reactivity, we made a simple calculation to test whether the Fe(II) originally contained in brucite, $Mg_{0.86}Fe_{0.14}(OH)_2$, could account for the maximum H_2 produced in the SW water/rock reactions. Based on our estimate of brucite abundance and iron content (Supplementary Table 4), and the stoichiometric reaction (1), we estimate that 251 µmol of H_2 could be produced if this reaction went to completion. This maximum amount of H_2 is 2 orders of magnitude higher than the production of H_2 we observed, 2.4 µmol. It is possible that more H_2 was produced than observed, for example if H_2 consumption was concurrent with H_2 production as organic acids were made, or if H_2 diffusion out of the experimental vials was significant. However, the total organic acids would only require 1.9 µmol of H_2. Another possibility is that a large fraction of the Fe(II) released from the dissolution of brucite was not oxidized and instead was sequestered into a Fe(II & III)-bearing serpentine.

The estimated mass of magnetite generated, as inferred from magnetic susceptibility data, can also be used to estimate the total H_2 produced during 100°C water/rock reactions. Assuming

all of the iron oxidation involved in magnetite production led to H_2 production, the formation of 13 µmoles of Fe^{3+} in magnetite indicates that 6.5 µmoles of H_2 were produced in our water/rock reaction experiments. Our maximum H_2 measurements were slightly lower, 2.4 µmoles of H_2 (Table 6). It is possible that maghemite, another Fe^{3+}-bearing spinel, formed instead of magnetite. We cannot confirm the mineralogy of the paramagnetic mineral in our sample. If we make the same calculation as above assuming maghemite is the Fe(III)-bearing end product instead of magnetite, using a maghemite proportionality constant of 65.3 $A*m^2/kg$ (Özdemir and Dunlop, 2010), we estimate 62.6 µmoles of H_2 would be produced. This is much larger than the amount of H_2 observed.

This discrepancy between measured and calculated H_2 values may be due to errors with measuring nanoscale magnetite and applying the proportionality constant used to calculate mass of magnetite generated based on saturation magnetization (Malvoisin et al., 2012). The error may also come from the fact that this method assumes magnetite is the sole magnetic carrier in the sample and neglects the potential importance of magnetite-spinel solid solutions (Shibuya et al., 2015), maghemite, and Fe(II & III)-bearing serpentine (Coey et al., 1981; Elmaleh et al., 2012). Unfortunately, we do not have measurements of magnetization as a function of temperature, to determine the exact source of the paramagnetic contribution.

Calculations suggest the water/rock reactions did not consume all of the Fe present in brucite to make H_2. Hydrogen may have been consumed before it accumulated in the headspace gas. We do not consider hydrogen diffusion out of the experimental vials to be a significant sink because the timing and rates of hydrogen production and loss are well replicated in these RW and SW experiments. The magnetite mass estimates closely align with maximum H_2 measurements, but they do suggest larger H_2 production than we observe.

4.4 Fate of carbon in water/rock reactions

We find compelling evidence for the formation of low molecular weight organic acids, specifically formate and acetate during our experiments. We briefly address these observations because of the significance of the synthesis and accumulation of low molecular weight organic acids in serpentinizing systems as potential energy sources for microbial metabolisms (e.g. methanogens, sulfate reducers, and metal-reducers (Jetten et al., 1992; Zinder, 1993; McCollom and Seewald, 2001). Organic acids may be a carbon source for microbial biosynthesis when inorganic carbon is limiting under hyperalkaline conditions. Inorganic low weight molecular synthesis is possibly as an important process for the origin of life (Russell and Martin, 2004; Russell et al., 2010). Additionally, formate and acetate have been observed in many actively serpentinizing systems (e.g. (Lang et al., 2010; Morrill et al., 2014; Crespo-Medina et al., 2014; McDermott et al., 2015).

Headspace carbon dioxide, along with H_2, decreases significantly over the course of the water/rock reactions (Supplementary Table 5). Thus, it is feasible that the hydrogen is reacting with CO_2 to form low molecular weight organic acids via the following reaction (McCollom and Seewald, 2003):

$$HCO_3^- + H_2 = CHOO^- + H_2O \quad (6)$$

Equation 6 is dependent on high concentrations of H_2, and a relatively alkaline pH (8-10) for HCO_3^- to be an important carbonate species in solution, conditions met by our experimental system. However, this reaction is only experimentally shown to equilibrate rapidly from 175-300°C (McCollom and Seewald, 2001; McCollom and Seewald, 2003; Seewald et al., 2006), not at 100°C as observed in our experiments.

The formation of acetate is more enigmatic. Modeling of acetate, propionate, and butyrate formation shows it is thermodynamically favored when cold, oxidized seawater rich in bicarbonate mixes with hot, reduced hydrothermal fluids (Shock and Schulte, 1998). Yet our batch water/rock reactions do not have a compositional gradient characterized by disequilibrium between two fluids thus we suggest that our tentative findings must be replicated and verified with a $NaH^{13}CO_3$ tracer (McCollom and Seewald, 2001) to investigate all possible sinks of carbon in the system.

The water/rock reactions produced insufficient H_2 to produce the concentrations of formate and acetate observed, thus we assume organic acid production was concurrent with H_2 generation (Supplementary text 2). An alternative explanation would be that the observed organic acids were released from fluid inclusions that preserved products of earlier high-temperature serpentinization. However, we did not observe fluid inclusions in olivine, and significant olivine dissolution is not observed during the 100°C reactions. Additionally, control experiments, with partially serpentinized Oman dunite, SW and/or RW media, only N_2 in the headspace and <3 mM of HCO_3^- in the fluid produced only 10-20% of the organic acid concentrations in the N_2:CO_2 headspace experiments while generating similar concentrations of H_2. It appears Fe-oxidation reactions were occurring in both experiments, but much less carbon was available in the N_2-only controls.

The production of low molecular weight organic molecules does not account for all of the carbon lost from the headspace; there is a missing sink of carbon (Supplementary Text 3). We do not observe abiotic formation of CH_4 at 100°C. CH_4 has been observed as a product in water/rock reaction experiments at 30, 50 and 70°C in previous studies, but it is unclear if such CH_4 formed as the result of the water/rock reactions or was released from fluid inclusions or the

butyl stoppers used in the experiment (Neubeck et al., 2011b; Okland et al., 2014). Nor do we observe carbonate formation (Supplementary Table 2). This may be due to kinetic limitations in precipitating dolomite and magnesite at low temperatures (Giammar et al., 2005; Hänchen et al., 2008), the high water/rock ratios in our experiments, or the pervasive reduction of carbon during ongoing H_2 production. Another possible sink of carbon in these experiments is abiotic solid carbonaceous material (Milesi et al., 2016). It is challenging to spectroscopically identify because it can be concentrated in rare blebs or coating mineral surfaces as a small fraction of a weight % compared to the mineral components. Using our mass-balance calculations, there could be ~14 millimoles of particulate carbon forming in SW experiments and ~20 millimoles of carbon forming in RW experiments. Such a small amount of carbon is difficult to measure by standard total organic carbon combustion techniques, which analyze <100 mg of sample at a time. Therefore, although our TOC analysis does not show the presence of solid carbon, it is below the detection limit.

5. Conclusions

The hydration of Oman dunite in anoxic, CO_2-bearing fluids produces as much or more H_2 as similar, previous low-temperature laboratory experiments (Neubeck et al., 2011b; Okland et al., 2012; Mayhew et al., 2013; Okland et al., 2014). A key control on the amount of hydrogen generated is the solubility of Fe(II)-bearing phases such as brucite, which can be sensitively modulated by the fluid chemistry. The reacted mineral assemblage in our experiments still contains abundant Fe(II), thus it stores significant reducing potential and long-term reactivity. We predict that Oman dunite is capable of producing one to two orders more H_2 than we observed based on remaining Fe(II). However, the conditions under which the additional Fe can be released and oxidized are enigmatic. Additionally, although significant CO_2 consumption occurs, no carbonate minerals form and not all of the lost C is sequestered into observed quantities of organic acids. Amorphous solid carbon species may have also formed; however, such carbon has not been directly verified.

It remains challenging to conduct low-temperature anoxic water/rock reactions due to the slow reaction rates and small amounts of reaction products. Silica serum vials capped with butyl rubber stoppers are not ideal for continuously measuring low levels of hydrogen production. They contribute background concentrations of hydrogen and organic compounds, as well as dissolved silica, which can alter the reaction products. Follow-up work should focus on conducting similar peridotite hydration experiments in gas-tight, non-reactive vessels that allows periodic sampling of the aqueous and mineral components. These experiments should also use HCO_3^- with a ^{13}C label to track the fate of dissolved C and unequivocally demonstrate the presence, or absence, of organic synthesis reactions. Moreover, the effects of pH, silica activity, ionic strength, and temperature need to be clearly constrained and experimentally tested at low

temperatures to better pinpoint the operative hydrogen-producing reactions in subsurface serpentinizing systems.

Overall, partially-serpentinized rocks have the potential to generate significant amounts of hydrogen due to oxidation of Fe(II)-bearing brucite, as well as produce organic acids at low temperatures. The H_2 and organic acids produced during the alteration of partially-serpentinized dunite could support subsurface rock-hosted life. Low levels of dissolved HCO_3^- and oxidants can fuel metabolisms such as methanogenesis, acetogenesis, sulfate reduction and metal-reduction pathways.

Acknowledgements

The authors would like to thank numerous colleagues at the University of Colorado at Boulder: Julien Allaz and the electron microprobe lab, Fred Luiszer at the Laboratory for Environmental and Geological Studies. We also thank Masako Tominaga (TAMU), who conducted the magnetic susceptibility analyses, and Mark Conrad (LBNL) who contributed the carbonate quantification and $\delta^{13}C$ measurements. Raman imaging and spectroscopy was conducted at the Raman Microspectroscopy Laboratory at the Department of Geological Sciences, University of Colorado-Boulder. This research was funded primarily by the Department of Energy (DE-SC0006886), with supporting work conducted through the Rock-Powered Life NASA Astrobiology Institute (Cooperative Agreement NNA15BB02A). Use of the Stanford Synchrotron Radiation Lightsource, SLAC National Accelerator Laboratory, is supported by the U.S. Department of Energy, Office of Science, Office of Basic Energy Sciences under Contract No. DE-AC02-76SF00515, in collaboration with staff scientists Sam Webb, Courtney Krest, and Ryan Davis. We also thank Franck Bourdelle (Université des Sciences et Technologies de Lille 1) and Manuel Munoz (Institut des Sciences de la Terre, Universite Joseph Fourier) for providing standards for our Fe(II/III) analysis.

References

Abrajano T. A., Sturchio N. C., Kennedy B. M., Lyon G. L., Muehlenbachs K. and Bohlke J. K. (1990) Geochemistry of reduced gas related to serpentinization of the Zambales ophiolite, Philippines. *Appl. Geochem.* **5**, 625–630.

Anderson R. T., Chapelle F. H. and Lovley D. R. (1998) Evidence Against Hydrogen-Based Microbial Ecosystems in Basalt Aquifers. *Science* **281**, 976–977.

Andreani M., Muñoz M., Marcaillou C. and Delacour A. (2013a) µXANES study of iron redox state in serpentine during oceanic serpentinization. *Lithos* **178**, 70–83.

Andreani M., Muñoz M., Marcaillou C. and Delacour A. (2013b) µXANES study of iron redox state in serpentine during oceanic serpentinization. *Lithos* **178**, 70–83.

Bach W. (2016) Some Compositional and Kinetic Controls on the Bioenergetic Landscapes in Oceanic Basement. *Extreme Microbiol.*, 107.

Barnes I., O'Neil J. R. and Trescases J. J. (1978) Present day serpentinization in New Caledonia, Oman and Yugoslavia. *Geochim. Cosmochim. Acta* **42**, 144–145.

Béarat H., McKelvy M. J., Chizmeshya A. V. G., Gormley D., Nunez R., Carpenter R. W., Squires K. and Wolf G. H. (2006) Carbon Sequestration via Aqueous Olivine Mineral Carbonation: Role of Passivating Layer Formation. *Environ. Sci. Technol.* **40**, 4802–4808.

Boudier F., Baronnet A. and Mainprice D. (2010) Serpentine Mineral Replacements of Natural Olivine and their Seismic Implications: Oceanic Lizardite versus Subduction-Related Antigorite. *J. Petrol.* **51**, 495–512.

Coey J. M. D., Ballet O., Moukarika A. and Soubeyroux J. L. (1981) Magnetic properties of sheet silicates; 1:1 layer minerals. *Phys. Chem. Miner.* **7**, 141–148.

Coleman R. G. (1981) Tectonic setting for ophiolite obduction in Oman. *J. Geophys. Res. Solid Earth* **86**, 2497–2508.

Crespo-Medina M., Twing K. I., Kubo M. D. Y., Hoehler T. M., Cardace D., McCollom T. and Schrenk M. O. (2014) Insights into environmental controls on microbial communities in a continental serpentinite aquifer using a microcosm-based approach. *Front. Microbiol.* **5**. Available at: http://www.ncbi.nlm.nih.gov/pmc/articles/PMC4231944/ [Accessed September 1, 2015].

Debret B., Andreani M., Muñoz M., Bolfan-Casanova N., Carlut J., Nicollet C., Schwartz S. and Trcera N. (2014) Evolution of Fe redox state in serpentine during subduction. *Earth Planet. Sci. Lett.* **400**, 206–218.

Eberl D. D. (2003) *User Guide to RockJock - A Program for Determining Quantitative Mineralogy from X-Ray Diffraction Data*., U.S. Geological Survey. Available at: http://pubs.er.usgs.gov/publication/ofr200378 [Accessed January 29, 2016].

Ehlmann B. L., Mustard J. F. and Murchie S. L. (2010) Geologic setting of serpentine deposits on Mars: SERPENTINE ON MARS. *Geophys. Res. Lett.* **37**, n/a-n/a.

Elmaleh A., Tarantino S. C., Zema M., Devouard B. and Fialin M. (2012) The low-temperature magnetic signature of Fe-rich serpentine in CM2 chondrites: Comparison with terrestrial cronstedtite and evolution with the degree of alteration. *Geochem. Geophys. Geosystems* **13**, Q05Z42.

Espinosa A., Serrano A., Llavona A., Morena J. J. de la, Abuin M., Figuerola A., Pellegrino T., Fernández J. F., Garcia-Hernandez M., Castro G. R. and Garcia M. A. (2012) On the discrimination between magnetite and maghemite by XANES measurements in fluorescence mode. *Meas. Sci. Technol.* **23**, 15602.

Etiope G., Schoell M. and Hosgörmez H. (2011) Abiotic methane flux from the Chimaera seep and Tekirova ophiolites (Turkey): Understanding gas exhalation from low temperature serpentinization and implications for Mars. *Earth Planet. Sci. Lett.* **310**, 96–104.

Evans B. W., Kuehner S. M. and Chopelas A. (2009) Magnetite-free, yellow lizardite serpentinization of olivine websterite, Canyon Mountain complex, N.E. Oregon. *Am. Mineral.* **94**, 1731–1734.

Frost B. R. and Beard J. S. (2007) On Silica Activity and Serpentinization. *J. Petrol.* **48**, 1351–1368.

Frost B. R., Evans K. A., Swapp S. M., Beard J. S. and Mothersole F. E. (2013) The process of serpentinization in dunite from New Caledonia. *Lithos* **178**, 24–39.

Fyfe W. S. (1974) Heats of Chemical Reactions and Submarine Heat Production. *Geophys. J. R. Astron. Soc.* **37**, 213–215.

Giammar D. E., Bruant Jr. R. G. and Peters C. A. (2005) Forsterite dissolution and magnesite precipitation at conditions relevant for deep saline aquifer storage and sequestration of carbon dioxide. *Chem. Geol.* **217**, 257–276.

Glein C. R., Baross J. A. and Waite Jr. J. H. (2015) The pH of Enceladus' ocean. *Geochim. Cosmochim. Acta* **162**, 202–219.

Groppo C., Rinaudo C., Cairo S., Gastaldi D. and Compagnoni R. (2006) Micro-Raman spectroscopy for a quick and reliable identification of serpentine minerals from ultramafics. *Eur. J. Mineral.* **18**, 319–329.

Hänchen M., Prigiobbe V., Baciocchi R. and Mazzotti M. (2008) Precipitation in the Mg-carbonate system—effects of temperature and CO2 pressure. *Chem. Eng. Sci.* **63**, 1012–1028.

Hänchen M., Prigiobbe V., Storti G., Seward T. M. and Mazzotti M. (2006) Dissolution kinetics of fosteritic olivine at 90–150 °C including effects of the presence of CO2. *Geochim. Cosmochim. Acta* **70**, 4403–4416.

Hanghøj K., Kelemen P. B., Hassler D. and Godard M. (2010) Composition and Genesis of Depleted Mantle Peridotites from the Wadi Tayin Massif, Oman Ophiolite; Major and Trace Element Geochemistry, and Os Isotope and PGE Systematics. *J. Petrol.* **51**, 201–227.

Hoal K. O., Appleby S. K., Stammer J. G. and Palmer C. (2009) SEM-based quantitative mineralogical analysis of peridotite, kimberlite, and concentrate. *Lithos* **112**, **Supplement 1**, 41–46.

Jetten M. S., Stams A. J. and Zehnder A. J. (1992) Methanogenesis from acetate: a comparison of the acetate metabolism in Methanothrix soehngenii and Methanosarcina spp. *FEMS Microbiol Rev* **88**, 181–197.

Jöns N., Bach W. and Klein F. (2010) Magmatic influence on reaction paths and element transport during serpentinization. *Chem. Geol.* **274**, 196–211.

Kelemen P. B., Hirth G., Shimizu N., Spiegelman M. and Dick H. J. (1997) A review of melt migration processes in the adiabatically upwelling mantle beneath oceanic spreading ridges. *Philos. Trans. R. Soc. Lond. Math. Phys. Eng. Sci.* **355**, 283–318.

Kelemen P. B. and Matter J. (2008) In situ carbonation of peridotite for CO2 storage. *Proc. Natl. Acad. Sci.* **105**, 17295–17300.

Kelemen P. B., Matter J., Streit E. E., Rudge J. F., Curry W. B. and Blusztajn J. (2011) Rates and Mechanisms of Mineral Carbonation in Peridotite: Natural Processes and Recipes for Enhanced, in situ CO2 Capture and Storage. *Annu. Rev. Earth Planet. Sci.* **39**, 545–576.

Kim W., Suh C.-Y., Cho S.-W., Roh K.-M., Kwon H., Song K. and Shon I.-J. (2012) A new method for the identification and quantification of magnetite–maghemite mixture using conventional X-ray diffraction technique. *Talanta* **94**, 348–352.

Klein F., Bach W., Jöns N., McCollom T., Moskowitz B. and Berquó T. (2009) Iron partitioning and hydrogen generation during serpentinization of abyssal peridotites from 15°N on the Mid-Atlantic Ridge. *Geochim. Cosmochim. Acta* **73**, 6868–6893.

Klein F., Bach W. and McCollom T. M. (2013) Compositional controls on hydrogen generation during serpentinization of ultramafic rocks. *Lithos* **178**, 55–69.

Klein F., Grozeva N. G., Seewald J. S., McCollom T. M., Humphris S. E., Moskowitz B., Berquó T. S. and Kahl W.-A. (2015) Experimental constraints on fluid-rock reactions during incipient serpentinization of harzburgite. *Am. Mineral.* **100**, 991–1002.

Kral T. A., Brink K. M., Miller S. L. and McKay C. P. (1998) Hydrogen Consumption by Methanogens on the Early Earth. *Orig. Life Evol. Biosph.* **28**, 311–319.

Lang S. Q., Butterfield D. A., Schulte M., Kelley D. S. and Lilley M. D. (2010) Elevated concentrations of formate, acetate and dissolved organic carbon found at the Lost City hydrothermal field. *Geochim. Cosmochim. Acta* **74**, 941–952.

Malvoisin B., Brunet F., Carlut J., Rouméjon S. and Cannat M. (2012) Serpentinization of oceanic peridotites: 2. Kinetics and processes of San Carlos olivine hydrothermal alteration. *J. Geophys. Res. Solid Earth* **117**, n/a–n/a.

Malvoisin B., Carlut J. and Brunet F. (2012) Serpentinization of oceanic peridotites: 1. A high-sensitivity method to monitor magnetite production in hydrothermal experiments. *J. Geophys. Res. Solid Earth* **117**, B01104.

Mayhew L. E., Ellison E. T., McCollom T. M., Trainor T. P. and Templeton A. S. (2013) Hydrogen generation from low-temperature water–rock reactions. *Nat. Geosci.* **6**, 478–484.

McCollom T. M. and Bach W. (2009) Thermodynamic constraints on hydrogen generation during serpentinization of ultramafic rocks. *Geochim. Cosmochim. Acta* **73**, 856–875.

McCollom T. M. and Donaldson C. (2016) Generation of Hydrogen and Methane during Experimental Low-Temperature Reaction of Ultramafic Rocks with Water. *Astrobiology*. Available at: http://online.liebertpub.com/doi/abs/10.1089/ast.2015.1382 [Accessed June 6, 2016].

McCollom T. M., Klein F., Robbins M., Moskowitz B., Berquó T. S., Jöns N., Bach W. and Templeton A. (2016) Temperature trends for reaction rates, hydrogen generation, and partitioning of iron during experimental serpentinization of olivine. *Geochim. Cosmochim. Acta* **181**, 175–200.

McCollom T. M. and Seewald J. S. (2001) A reassessment of the potential for reduction of dissolved CO2 to hydrocarbons during serpentinization of olivine. *Geochim. Cosmochim. Acta* **65**, 3769–3778.

McCollom T. M. and Seewald J. S. (2003) Experimental constraints on the hydrothermal reactivity of organic acids and acid anions: I. Formic acid and formate. *Geochim. Cosmochim. Acta* **67**, 3625–3644.

McDermott J. M., Seewald J. S., German C. R. and Sylva S. P. (2015) Pathways for abiotic organic synthesis at submarine hydrothermal fields. *Proc. Natl. Acad. Sci.*, 201506295.

Milesi V., McCollom T. M. and Guyot F. (2016) Thermodynamic constraints on the formation of condensed carbon from serpentinization fluids. *Geochim. Cosmochim. Acta* **189**, 391–403.

Miller H. M., Matter J. M., Kelemen P., Ellison E. T., Conrad M. E., Fierer N., Ruchala T., Tominaga M. and Templeton A. S. (2016) Modern water/rock reactions in Oman hyperalkaline peridotite aquifers and implications for microbial habitability. *Geochim. Cosmochim. Acta* **179**, 217–241.

Morrill P. L., Brazelton W. J., Kohl L., Rietze A., Miles S. M., Kavanagh H., Schrenk M. O., Ziegler S. E. and Lang S. Q. (2014) Investigations of potential microbial methanogenic and carbon monoxide utilization pathways in ultra-basic reducing springs associated with present-day continental serpentinization: the Tablelands, NL, CAN. *Front. Microbiol.* **5**. Available at: http://www.ncbi.nlm.nih.gov/pmc/articles/PMC4230201/ [Accessed January 6, 2015].

Morrill P. L., Kuenen J. G., Johnson O. J., Suzuki S., Rietze A., Sessions A. L., Fogel M. L. and Nealson K. H. (2013) Geochemistry and geobiology of a present-day serpentinization site in California: The Cedars. *Geochim. Cosmochim. Acta* **109**, 222–240.

Muñoz M., Vidal O., Marcaillou C., Pascarelli S., Mathon O. and Farges F. (2013) Iron oxidation state in phyllosilicate single crystals using Fe-K pre-edge and XANES spectroscopy: Effects of the linear polarization of the synchrotron X-ray beam. *Am. Mineral.* **98**, 1187–1197.

Neal C. and Stanger G. (1984) Calcium and magnesium hydroxide precipitation from alkaline groundwaters in Oman, and their significance to the process of serpentinization. *Miner. Mag* **48**, 237–241.

Neal C. and Stanger G. (1983) Hydrogen generation from mantle source rocks in Oman. *Earth Planet. Sci. Lett.* **66**, 315–320.

Nealson K. H., Inagaki F. and Takai K. (2005) Hydrogen-driven subsurface lithoautotrophic microbial ecosystems (SLiMEs): do they exist and why should we care? *Trends Microbiol.* **13**, 405–410.

Neubeck A., Duc N. T., Bastviken D., Crill P. and Holm N. G. (2011a) Formation of H2 and CH4 by weathering of olivine at temperatures between 30 and 70 C. *Geochem. Trans.* **12**, 6.

Neubeck A., Duc N. T., Bastviken D., Crill P. and Holm N. G. (2011b) Formation of H2 and CH4 by weathering of olivine at temperatures between 30 and 70 C. *Geochem. Trans.* **12**, 6.

Neubeck A., Duc N. T., Hellevang H., Oze C., Bastviken D., Bacsik Z. and Holm N. G. (2014) Olivine alteration and H2 production in carbonate-rich, low temperature aqueous environments. *Planet. Space Sci.* **96**, 51–61.

Neubeck A., Nguyen D. T. and Etiope G. (2015) Low-temperature dunite hydration: evaluating CH4 and H2 production from H2O and CO2. *Geofluids*, n/a-n/a.

Ogasawara Y., Okamoto A., Hirano N. and Tsuchiya N. (2013) Coupled reactions and silica diffusion during serpentinization. *Geochim. Cosmochim. Acta* **119**, 212–230.

Okland I., Huang S., Dahle H., Thorseth I. H. and Pedersen R. B. (2012) Low temperature alteration of serpentinized ultramafic rock and implications for microbial life. *Chem. Geol.* **318**–**319**, 75–87.

Okland I., Huang S., Thorseth I. H. and Pedersen R. B. (2014) Formation of H2, CH4 and N-species during low-temperature experimental alteration of ultramafic rocks. *Chem. Geol.* **387**, 22–34.

Oremland R. S., Miller L. G. and Whiticar M. J. (1987) Sources and flux of natural gases from Mono Lake, California. *Geochim. Cosmochim. Acta* **51**, 2915–2929.

Oufi O., Cannat M. and Horen H. (2002) Magnetic properties of variably serpentinized abyssal peridotites. *J. Geophys. Res. Solid Earth* **107**, EPM 3-1.

Özdemir Ö. and Dunlop D. J. (2010) Hallmarks of maghemitization in low-temperature remanence cycling of partially oxidized magnetite nanoparticles. *J. Geophys. Res. Solid Earth* **115**, B02101.

Paukert A. N., Matter J. M., Kelemen P. B., Shock E. L. and Havig J. R. (2012) Reaction path modeling of enhanced in situ CO2 mineralization for carbon sequestration in the peridotite of the Samail Ophiolite, Sultanate of Oman. *Chem. Geol.* **330**–**331**, 86–100.

Petriglieri J. R., Salvioli-Mariani E., Mantovani L., Tribaudino M., Lottici P. P., Laporte-Magoni C. and Bersani D. (2015) Micro-Raman mapping of the polymorphs of serpentine. *J. Raman Spectrosc.*, n/a-n/a.

Pokrovsky O. S., Schott J. and Castillo A. (2005) Kinetics of brucite dissolution at 25°C in the presence of organic and inorganic ligands and divalent metals. *Geochim. Cosmochim. Acta* **69**, 905–918.

Pokrovsky, Oleg S. J. S. (2004) Experimental study of brucite dissolution and precipitation in aqueous solutions: Surface speciation and chemical affinity control. *Geochim. Cosmochim. Acta* **68**, 31–45.

Prigiobbe V., Costa G., Baciocchi R., Hänchen M. and Mazzotti M. (2009) The effect of and salinity on olivine dissolution kinetics at. *Chem. Eng. Sci.* **64**, 3510–3515.

Reynard B., Bezacier L. and Caracas R. (2015) Serpentines, talc, chlorites, and their high-pressure phase transitions: a Raman spectroscopic study. *Phys. Chem. Miner.* **42**, 641–649.

Rinaudo C., Gastaldi D. and Belluso E. (2003) Characterization of Chrysotile, Antigorite and Lizardite by Ft-Raman Spectroscopy. *Can. Mineral.* **41**, 883–890.

Russell M. J., Hall A. J. and Martin W. (2010) Serpentinization as a source of energy at the origin of life: Serpentinization and the emergence of life. *Geobiology* **8**, 355–371.

Russell M. J. and Martin W. (2004) The rocky roots of the acetyl-CoA pathway. *Trends Biochem. Sci.* **29**, 358–363.

Russell M. J., Nitschke W. and Branscomb E. (2013) The inevitable journey to being. *Phil Trans R Soc B* **368**, 20120254.

Schrenk M. O., Brazelton W. J. and Lang S. Q. (2013) Serpentinization, Carbon, and Deep Life. *Rev. Mineral. Geochem.* **75**, 575–606.

Seewald J. S., Zolotov M. Y. and McCollom T. (2006) Experimental investigation of single carbon compounds under hydrothermal conditions. *Geochim. Cosmochim. Acta* **70**, 446–460.

Sekine Y., Shibuya T., Postberg F., Hsu H.-W., Suzuki K., Masaki Y., Kuwatani T., Mori M., Hong P. K., Yoshizaki M., Tachibana S. and Sirono S. (2015) High-temperature water–rock interactions and hydrothermal environments in the chondrite-like core of Enceladus. *Nat. Commun.* **6**, 8604.

Shibuya T., Russell M. J. and Takai K. (2016) Free energy distribution and hydrothermal mineral precipitation in Hadean submarine alkaline vent systems: Importance of iron redox reactions under anoxic conditions. *Geochim. Cosmochim. Acta* **175**, 1–19.

Shibuya T., Yoshizaki M., Sato M., Shimizu K., Nakamura K., Omori S., Suzuki K., Takai K., Tsunakawa H. and Maruyama S. (2015) Hydrogen-rich hydrothermal environments in the Hadean ocean inferred from serpentinization of komatiites at 300 °C and 500 bar. *Prog. Earth Planet. Sci.* **2**, 46.

Shock E. L. and Schulte M. D. (1998) Organic synthesis during fluid mixing in hydrothermal systems. *J. Geophys. Res. Planets* **103**, 28513–28527.

Sleep N. H., Meibom A., Fridriksson T., Coleman R. G. and Bird D. K. (2004) H2-rich fluids from serpentinization: geochemical and biotic implications. *Proc. Natl. Acad. Sci. U. S. A.* **101**, 12818–12823.

Spear J. R., Walker J. J., McCollom T. M. and Pace N. R. (2005) Hydrogen and bioenergetics in the Yellowstone geothermal ecosystem. *Proc. Natl. Acad. Sci. U. S. A.* **102**, 2555–2560.

Stevens T. O. and McKinley J. P. (2000) Abiotic Controls on H_2 Production from Basalt−Water Reactions and Implications for Aquifer Biogeochemistry. *Environ. Sci. Technol.* **34**, 826–831.

Stevens T. O. and McKinley J. P. (1995) Lithoautotrophic Microbial Ecosystems in Deep Basalt Aquifers. *Science* **270**, 450–455.

Streit E., Kelemen P. and Eiler J. (2012) Coexisting serpentine and quartz from carbonate-bearing serpentinized peridotite in the Samail Ophiolite, Oman. *Contrib. Mineral. Petrol.* **164**, 821–837.

Suda K., Ueno Y., Yoshizaki M., Nakamura H., Kurokawa K., Nishiyama E., Yoshino K., Hongoh Y., Kawachi K., Omori S., Yamada K., Yoshida N. and Maruyama S. (2014) Origin of methane in serpentinite-hosted hydrothermal systems: The CH4–H2–H2O hydrogen isotope systematics of the Hakuba Happo hot spring. *Earth Planet. Sci. Lett.* **386**, 112–125.

Szponar N., Brazelton W. J., Schrenk M. O., Bower D. M., Steele A. and Morrill P. L. (2013) Geochemistry of a continental site of serpentinization, the Tablelands Ophiolite, Gros Morne National Park: A Mars analogue. *Icarus* **224**, 286–296.

Takai K., Nakamura K., Toki T., Tsunogai U., Miyazaki M., Miyazaki J., Hirayama H., Nakagawa S., Nunoura T. and Horikoshi K. (2008) Cell proliferation at 122°C and isotopically heavy CH4 production by a hyperthermophilic methanogen under high-pressure cultivation. *Proc. Natl. Acad. Sci.* **105**, 10949–10954.

Telling J., Boyd E. S., Bone N., Jones E. L., Tranter M., MacFarlane J. W., Martin P. G., Wadham J. L., Lamarche-Gagnon G., Skidmore M. L., Hamilton T. L., Hill E., Jackson M. and Hodgson D. A. (2015) Rock comminution as a source of hydrogen for subglacial ecosystems. *Nat. Geosci.* **8**, 851–855.

Wilke M., Farges F., Petit P.-E., Brown G. E. and Martin F. (2001) Oxidation state and coordination of Fe in minerals: An Fe K-XANES spectroscopic study. *Am. Mineral.* **86**, 714–730.

Zinder S. H. (1993) Physiological Ecology of Methanogens. In *Methanogenesis* (ed. D. J. G. Ferry). Chapman & Hall Microbiology Series. Springer US. pp. 128–206. Available at: http://link.springer.com/chapter/10.1007/978-1-4615-2391-8_4 [Accessed November 11, 2015].

CHAPTER 4

Effects of pH, ionic strength, and temperature on hydrogen production from partially serpentinized Oman dunite

Abstract

High concentrations of hydrogen have been found exsolving from low-temperature fluids in continental ophiolites, but it is unclear under what temperatures, conditions and timescales the hydrogen is being generated. Low-temperature anoxic hydration of Oman dunite was conducted at 40 and 55°C, as well as across a range of pHs, ionic strengths and media compositions, to probe the conditions under which hydrogen forms at low temperatures. The development of a gas-tight, non-reactive reaction vessel was also conducted in order to perform these water/rock reactions without any artificially imposed gas production or contaminants. Neither the 55°C nor the 40°C water/rock reactions produced significant H_2 gas, in contrast to similar experiments conducted at 100°C. Highly reactive components of the rock mineralogy, such as Fe(II)-bearing brucite, were still intermixed with serpentine at the termination of these reactions. Additionally, $Ca(OH)_2$ was added to 100°C experiments with Oman dunite to increase the pH, which led to increased H_2 production, along with CO_2 consumption linked with CO production. The hydrogen appears to form through the dissolution and subsequent oxidation of Fe(II)-bearing brucite, but the exact reasons for the brucite instability are unknown. Water/rock reactions were also performed with subsurface, reducing fluids from Oman, but they did not produce any hydrogen. More targeted experiments need to be conducted to understand these results, but this preliminary information is meant to provoke future work.

Introduction

Chapter 3 detailed many unanswered questions regarding the key reactions giving rise to low-temperature hydrogen production and also highlighted the difficulty of conducting water/rock reactions with low blanks (e.g. low H_2, silica etc. in control). Studying water/rock reactions at 100°C with a partially serpentinized Oman dunite raised multiple questions about the effects of pH, ionic strength, and temperature on hydrogen-producing reactions in subsurface serpentinizing systems. Additionally, the paper made it clear that silica serum vial with butyl rubber stoppers are not ideal for conducting reactions.

The following work details preliminary experiments to test the reactivity of Oman dunite at low temperatures and under varying aqueous geochemical conditions. Not only can this work provide insights into low-temperature hydrogen generation that may sustain subsurface microbial life, but it also specifically investigates the conditions under which H_2 may be produced in the modern peridotite aquifer in Oman. Specifically, this chapter investigates hydrogen production during water/rock reactions with partially serpentinized Oman dunite and harzburgite. The reactions are conducted over a range of temperatures (100, 55 and 40°C), and at various ionic strengths (0, 0.005, 0.73, and 1.5 M) and pHs (8.85, 9.04, 10.36, 11.68, and 12.48). Additionally, this chapter describes efforts to develop a non-reactive, gas-tight vessel to perform low-temperature water/rock reactions by detailing the development of a new reaction vessel.

Overall, the data in this chapter is preliminary and does not extensively characterize the mineralogy of the reaction products, nor does it attempt to mass balance the system. However, it does inform future work on low-temperature water/rock reactions by identifying that the extent of hydrogen production is highly sensitive to the aqueous geochemistry, particularly increasing pH by adding Ca^{2+} ions at 100°C. However, temperatures below 100°C do not lead to

appreciable H_2 production. This work also confirms that brucite as a key reactive mineral, as identified in other chapters of this thesis, while simultaneously underscoring the complex nature of water/rock reactions leading to hydrogen production at near-surface conditions.

Methods

Experimental set-up

Oman dunite, OM95_35, is the same rock used in Miller et al. 2017. Oman harzburgite, OM14-05, was collected during January 2014 in the Samail ophiolite and is representative of the harzburgite found throughout the region. All water/rock reactions were performed in silica serum vials capped with an airtight blue butyl rubber stopper, boiled and soaked according to Oremland et al. (1982). Vials, rubber stoppers, and the media soaked in an acid bath, were rinsed, and then autoclaved before the experiment began. The vials were either incubated in an oven or water bath.

To determine H_2, CH_4, CO and CO_2 concentrations in the water/rock experiments, we used a SRI 8610C gas chromatograph (GC) with a 2m by 1mm ID micropacked ShinCarbon ST column with N_2 as the carrier gas. 0.5mL of gas was sampled from the headspace of serum vials sealed with blue rubber stoppers and was injected into a sampling port on the GC. H_2 was measured with a thermal conductivity detector (TCD), and a flame ionization detector (FID) was concurrently used to measure CO, CO_2, and CH_4. All sampling drew a vacuum; the headspace was not replaced with N_2. Experiments, including media-only controls were conducted in triplicate at 40 and 55°C.

100 µL of fluid was removed from reaction, and pH was measured with a Thermo Scientific Orion PerpHecT ROSS Combination pH Micro Electrode calibrated with reference standards of pH 4, 7, and 10. After each sampling, an equal volume of the anaerobic media was replaced. When measuring the fluid from the pH water/rock experiments, the electrode was calibrated with reference standards of pH 4, 7, 10, 11, and 12.45.

Micro-Raman spectra of reacted grains were collected using a Horiba LabRAM HR Evolution Raman spectrometer equipped with a 532 nm frequency-doubled Nd:YAG laser coupled to an Olympus BXFM optical microscope. The laser beam was focused through a 50x (0.75NA) objective lens, yielding a spatial resolution of ~2 µm. A 600 lines/mm grating and adjustable confocal pinhole (100 µm-200 µm) were used to give a spectral resolution full width at half maximum (FWHM) of 4.5-8.4 cm^{-1}. Spectra were collected using a Si-based CCD detector (1024 x 256 pixels). The spectrometer was calibrated daily using the 520 cm^{-1} Raman peak of Si prior to analysis. Spectral data were corrected for instrumental artifacts and baseline-subtracted using a polynomial fitting algorithm in LabSpec 6 (Horiba Scientific).

55° and 40°C methods

The 55°C and 40°C reactions were performed with a simulated Oman pH 9 medium (all values reported per liter: 50 mg NaCl, 6 mg $CaCl_2$, 0.3 mg H_4SiO_4, 178 mg $MgSO_4*7H_2O$, 10 mg KNO_3, 0.2 mg NaBr). The reactions had a water/rock ratio of 1:7; 5 grams of OM95_35 dunite were put in a 80% N_2:20% CO_2 purged 70 mL serum vial and then mixing with 35 mL of media that had been purged with N_2:CO_2. Prior to use, vials were heated to 550C for 3 hours to remove any combustible carbon species. A harzburgite from Oman, OM14_05, was also reacted at 55°C to see the effect of increased pyroxenes on hydrogen production. There were 3 media-only controls at both temperatures in addition to triplicate vials of water/rock reactions.

Ionic strength methods

To test the effect of ionic strength on hydrogen production, we reacted 1 gram of OM95_35 dunite with 7 mL of media of 0.0 M (deionized water), 0.005 M (Oman rainwater),

0.73 M (seawater), and 1.5 M (very saline) at 100°C in 35 mL glass serum vials purged with 80% N_2:20% CO_2. The ionic strength was modulated with $MgCl_2$.

pH experiment methods

The 100°C pH reactions were performed with a simulated Type I fluid found in Oman, which represents relatively unreacted surface fluids (all values reported per liter: 174 mg NaCl, 5 mg KNO_3, 7.7 mg $CaSO_4*H_2O$, 178 mg $MgSO_4*7H_2O$, 4.5 mg $Mg(NO_3)_2$, 244.5 mg $MgCO_3$, 0.02 mg H_4SiO_4). The reactions had a water/rock ratio of 1:7; 3 grams of OM95_35 dunite were put in a 100% N_2 purged 30mL serum vial and then mixed with 21 mL of media that had been purged with N_2. The pH was then adjusted by adding various amounts of a 0.1M NaOH solution until the desired pH range was achieved. The range of pHs was 8.85, 9.04, 10.36, 11.68, and 12.48, with 2 media-only control vials containing Type I media at the unadjusted pH of 8.86 and the high pH of Type I media at 12.53. After the pH held steady in the vials for 24 hours, the media was transferred into fresh vials containing OM95_35 through a 0.2 µm filter to remove any precipitates. The combined water/rock anaerobic vials were then purged with N_2 again to purge any residual atmospheric gas. Vials, rubber stoppers, and the media were autoclaved before the experiment began.

NSHQ14 water/rock experiment methods

The 40°C pH reactions were performed with a 0.2 µm filtered site water from subsurface well NSHQ14 in Oman at a pH of 11.45. The reactions had a water/rock ratio of 1:7; 2 grams of rock were put in a 100% N_2 purged 30mL serum vial and then mixed with 14 mL of NSQH14 fluid that had been purged with N_2 to remove any residual H_2 or CH_4 that was in the fluid. One

vial contained crushed OM95_35 dunite, while the other contained crushed drill cuttings from a depth of 262 meters from well NSHQ14.

Results

55°C experiments

Water/rock reactions with both Oman dunite and harzburgite did not produce consistent concentrations of H_2 over the 336 day duration of the experiment. Vials reacting at 55°C with Oman dunite did not start making appreciable hydrogen until 170 days. We observed 230-400 nmol/gram H_2 after 170 days, for all 3 dunite vials, but decreased to 20-30 nmol/gram H_2 by 336 days (Figure 1). However, a vial with harzburgite produced 54 nmol/gram H_2 after 13 days and peaked at 440 nmol/gram H_2 at 232 days, but the other 2 harzburgite vials showed limited, or no, hydrogen generation. At 170 days, one harzburgite vial made 230 nmol/gram H_2, but that value decreased to 0 nmol/gram H_2 when measured at 232 days. The controls record no hydrogen produced over the lifetime of the experiment.

The pH for 55°C experiments started from 7.1-7.3 and increased to pH 8.3 after 24 hours. The pH then slightly increased to 8.6-8.8 after 2 days and remained steady throughout the experiments for both the dunite and harzburgite vials (Figure 2). The controls started with a pH of 7.6, with an anomalous reading of 9.96 for one, then slowly decreased to 6.3-6.7 over time.

40°C experiments

Water/rock experiments at 40°C also did not produce consistent H_2 (Figure 3). There was zero hydrogen production by 122 days. In response to this lack of activity, we modified the original three vials with Oman dunite on day 213: one of the vials was inoculated with a consortia containing *Methanobacterium* from Oman and purged with 80%H_2:20%CO_2 in the headspace, one vial was unmodified, and one vial received 0.1M $Ca(OH)_2$, raising the pH to 12.2

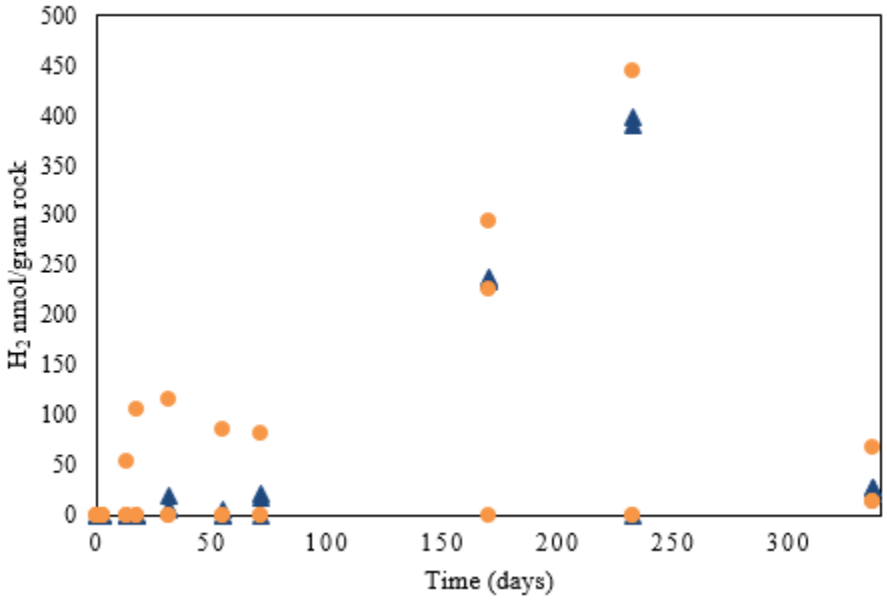

Figure 1. Hydrogen production from 55°C water/rock reactions with Oman dunite (blue triangles), and Oman harzburgite (green circles). Control data is not included because all 3 controls produced no hydrogen over the 336 day lifetime of the experiment.

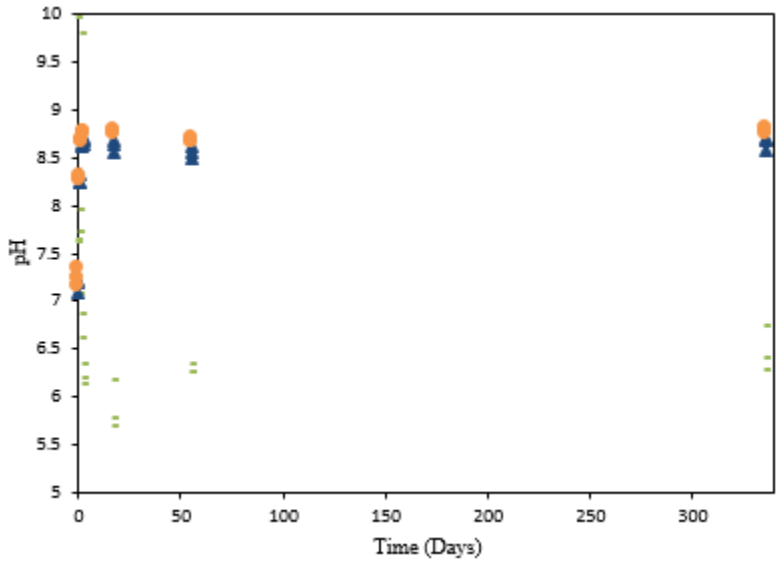

Figure 2. pH vs time of reaction for 55°C water/rock reactions, Oman harzburgite (orange circles), Oman dunite (blue triangles), controls (green lines).

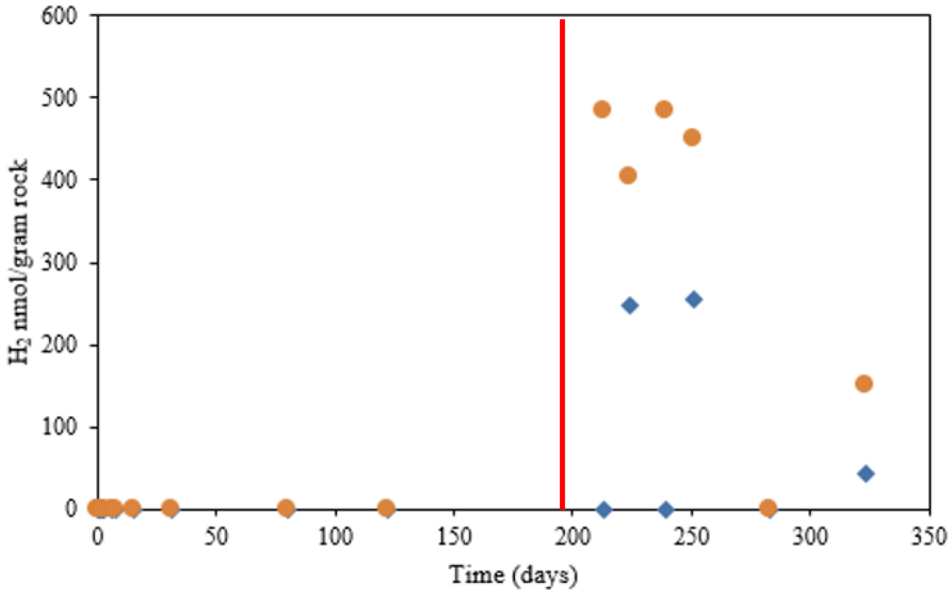

Figure 3. H_2 production at 40°C water/rock reactions with Oman dunite. Control data is not included because all 3 controls produced no hydrogen over the lifetime of the experiment. At ~200 days (red line), the pH for the orange circles (vial 1) was increased to ~pH 12 by adding 0.1 M $Ca(OH)_2$. The blue triangles shows the unmodified water/rock reaction. The experiment was initially run in triplicate, but then the third vial was inoculated with a methanogen consortia along with adding 80% H_2: 20%CO_2 to the headspace, so the data is not included.

(Figure 4). Thus, there are only two measurements of H_2 production in Figure 3. When we measured the H_2 again at 213 days, the vial with a high pH had 480 nmol/gram H_2. The hydrogen values stayed relatively constant until 282 days, where the H_2 dropped to 0, and then at 323 days, we measured 150 nmol/gram H_2. The unmodified vial showed modest H_2 production, 260 nmol/gram from at 251 days, but the H_2 measurement was not constant, and dropped to zero, then back to 250 nmol/gram H_2.

The pH for the controls was around 5.8-6.7 for the life of the experiments, except for an anomalously high reading on day 8 of 7.1-8.2. The two vials initially unmodified and measured for H_2 production began at pH 6.6 and increased to 7.9-8.1 after 24 hours. After 7 days, the pH increased to 9.1 and stayed there, or slightly lower at pH 8.8 for the duration of the experiment. After 213 days, the pH in one vial was increased to 12.2 by adding 0.1M $Ca(OH)_2$.

Ionic strength results

Hydrogen production from all 4 ionic strengths (de-ionized water (DIW), 0.0005 M, 0.73 M, and 1.5 M) did not occur for the first 18 days. At 35 days, the first DIW, 0.0005 M, and 0.73 M made 45-55 nmol/gram H_2, wherease 1.5 M produced 140 nmol/gram H_2. However, after 117 days, all experiments measured zero hydrogen (Figure 5), so we increased the pH in all vials by adding 0.1 M $Ca(OH)_2$. $Ca(OH)_2$ is very insoluble; thus, these experiments were then filled with white Ca-hydroxide precipitates. A week after increasing the pH with $Ca(OH)_2$, the H_2 production surged to >1000 nmol/gram mineral (Figure 5) for all vials, reaching as high as 2000 nmol/gram H_2 in 0.005 M and DIW. However, at 329 days, the H_2 values all had greatly decreased, down to 0 for 1.5 M, 56 for 0.0005 M, 310 for 1.5 M, and 960 nmol/gram H_2 for DIW.

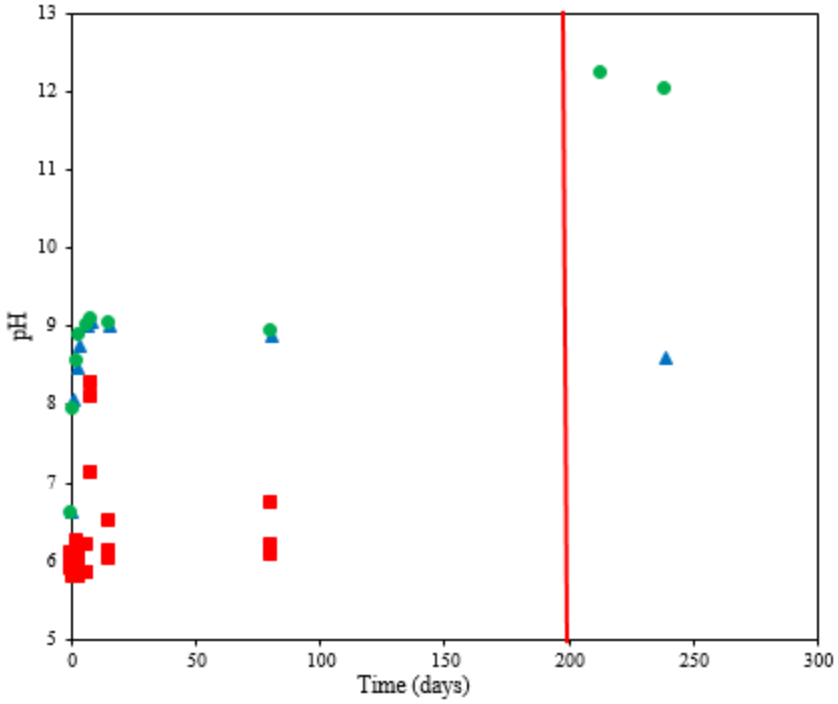

Figure 4. pH of water/rock reactions with Oman dunite at 40°C. Red line shows when increased green pH by adding 0.1 M $Ca(OH)_2$. Blue markers show water/rock reaction with unmodified pH. Red markers are 3 control pHs.

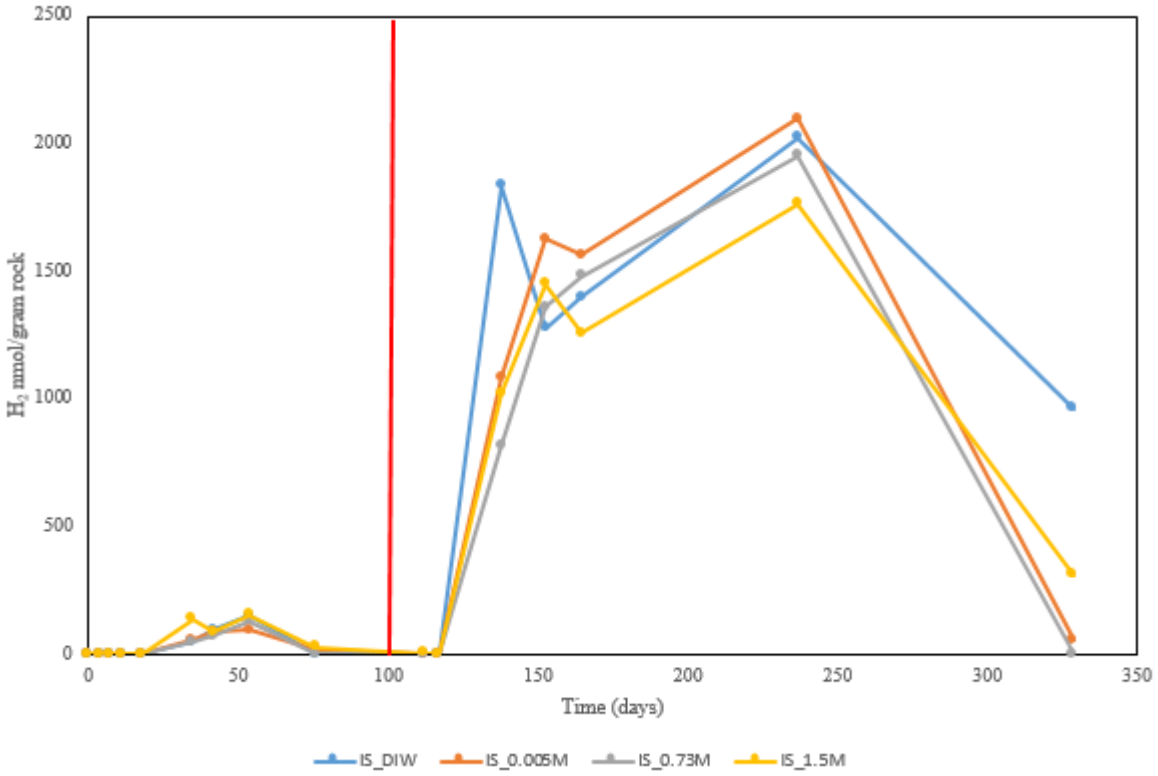

Figure 5. H_2 production from Oman dunite ionic strength experiments at 100°C; ionic strength modulated with $MgCl_2$. Red line shows when increased pH by adding 0.1M $Ca(OH)_2$ to all vials.

The initial pH for the vials was 6.7-7.7, but as soon as the 0.1M $Ca(OH)_2$ was added at 117 days, the pH rapidly increased to 12 for DIW and 0.005 M, 11.3 for 0.73 M, and 9.6 for 1.5 M (Figure 6). The lower ionic strength vials (0.0M and 0.005M) retained a higher pH throughout the course of the experiment, stabilizing around pH 10.3-11.3 after 329 days, while the 2 high ionic strength experiments stabilized at pH 6.8-8.3 after 329 days.

CO concentrations were measured in concert with H_2, and after the pH was increased at 117 days, up to 6000 nmol/gram CO was formed in the 0.73 M and 1.5 M experiments (Figure 7), whereas the background levels of CO before the pH increase were a maximum of 200 nmol/gram. Up to 1800 nmol/gram CO was formed in the 1.5 M and 0.73 M experiments.

CO_2 concentrations in the water/rock reactions quickly decreased from ~160,000 nmol/gram CO_2 to <100,000 nmol/gram CO_2 after one day of reaction (Figure 8), which is standard for these experiments. After the pH was increased at 117 days, the CO_2 rapidly decreased to a concentration of <500 nmol/gram mineral.

pH results

We observed that water/rock reactions with a pH greater than 9 led to significant hydrogen production. Therefore, to test the effect of pH on hydrogen production, we conducted water/rock experiments with Oman dunite and various concentrations of NaOH at 100°C. NaOH was used instead of $Ca(OH)_2$ because it is more soluble and will not precipitate. Various amounts of NaOH were added to the vials to produce a range of pHs: 8.57, 9.36, 10.15, 11.22, and 12.12 (Figure 9).

No hydrogen production was observed in the first 12 days, then 19 nmol/gram H_2 was observed only in the pH 8.86 vial at 13 days (Figure 9). After 68 days, this vial contained the

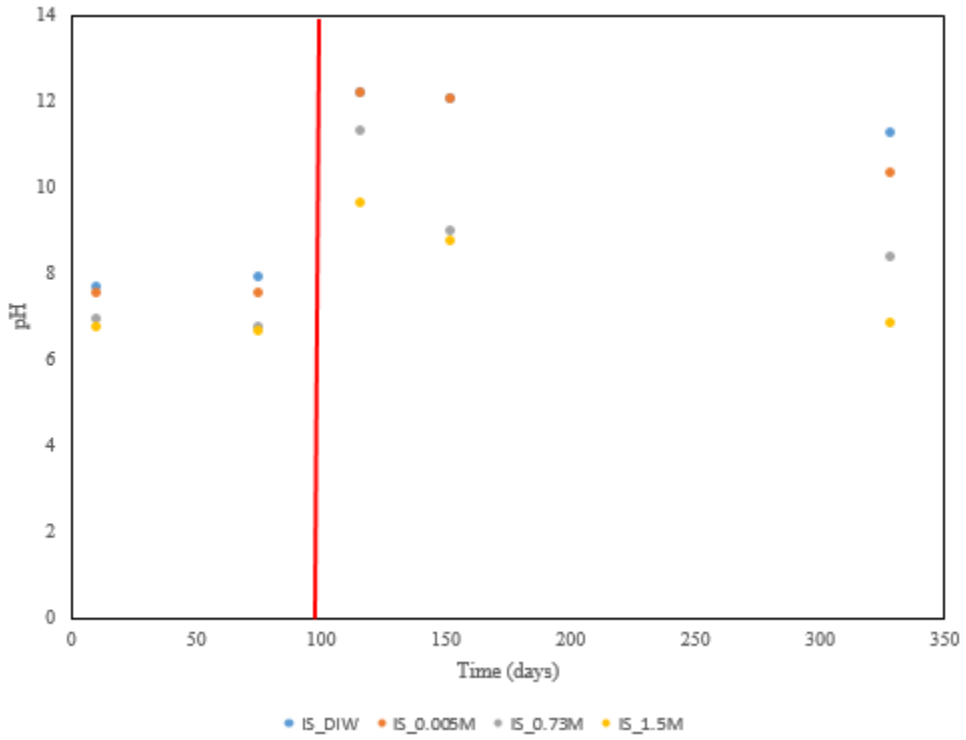

Figure 6. pH versus time in ionic strength experiments with OM95_35 dunite at 100°C. Red line shows where pH was increased in the experiments with the addition of 0.1M $Ca(OH)_2$.

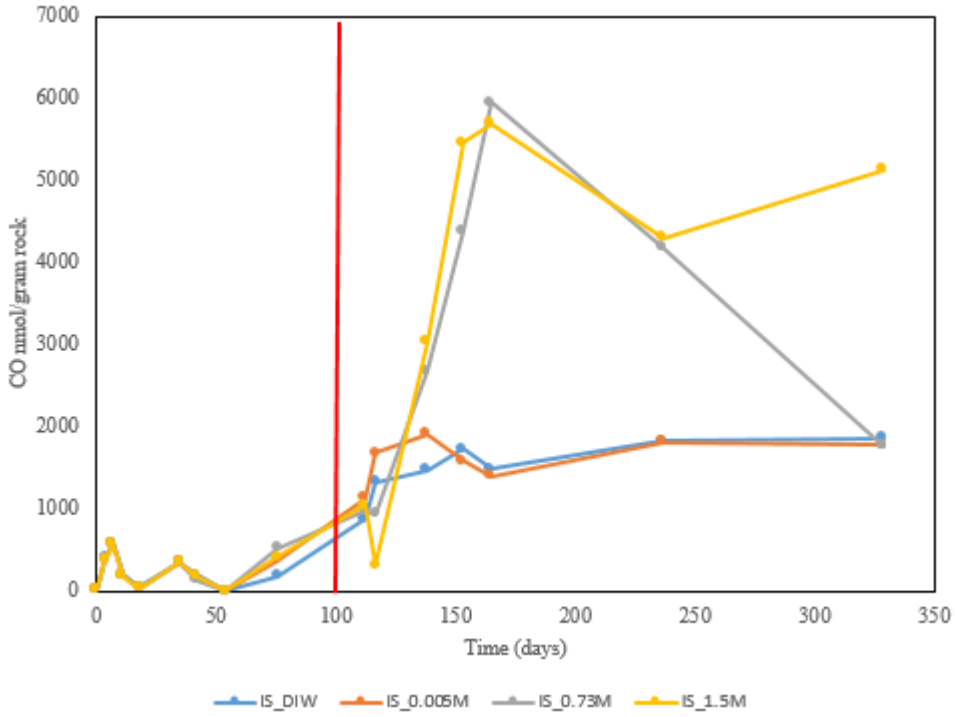

Figure 7. CO concentrations in ionic strength water/rock reactions with Oman dunite at 100°C. Red line shows where pH was increased.

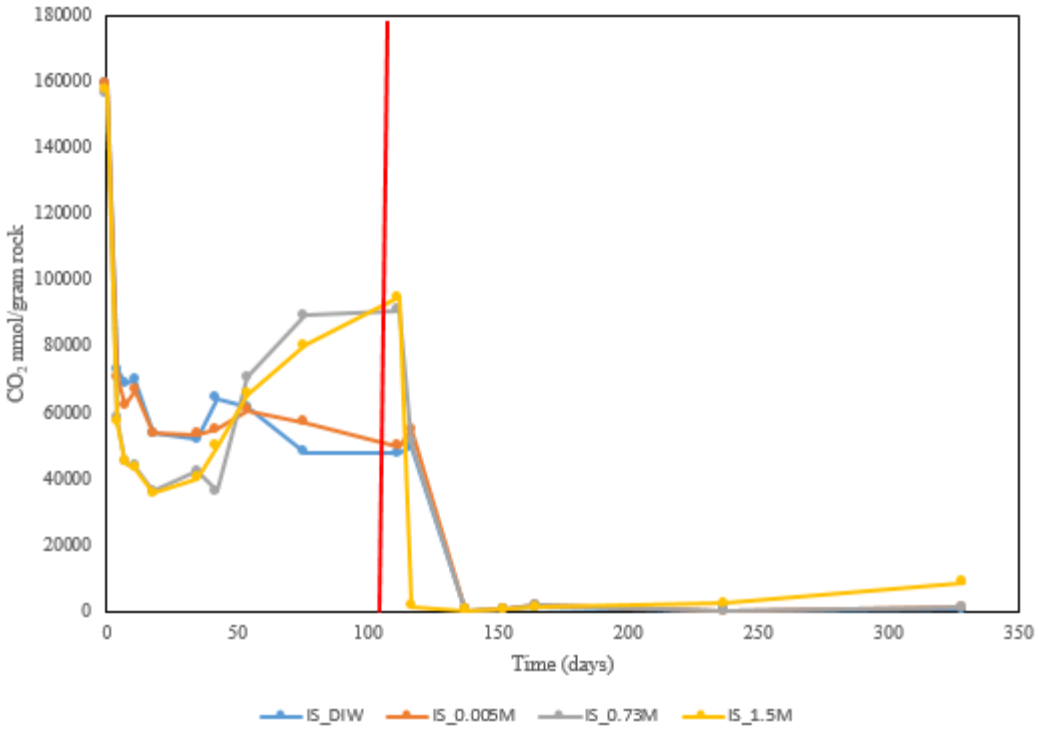

Figure 8. CO_2 concentrations in ionic strength water/rock reactions with Oman dunite at 100°C. Red line shows where pH was increased.

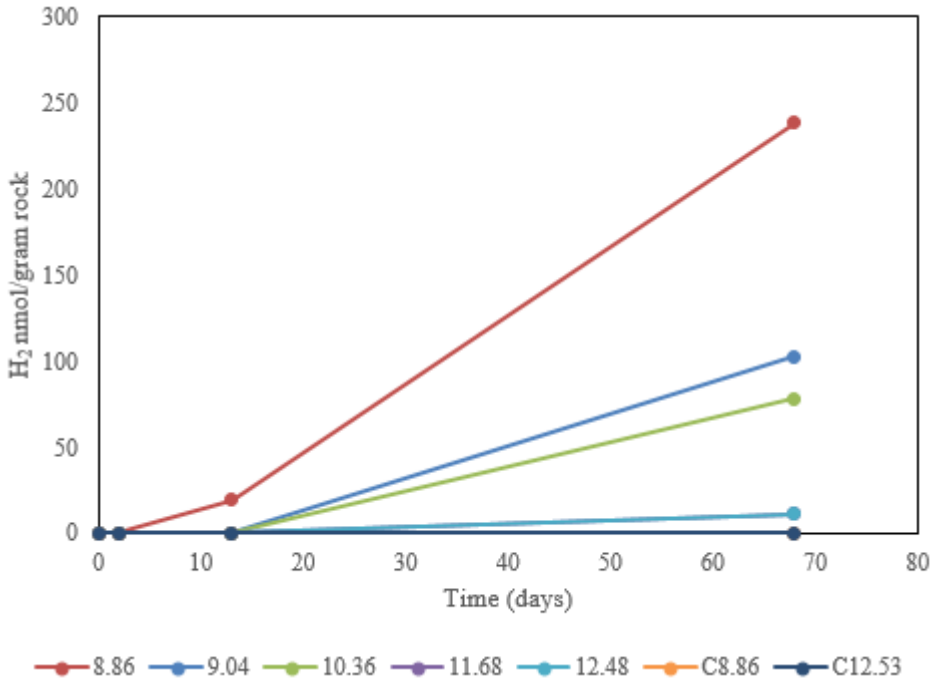

Figure 9. H_2 headspace concentrations in pH water/rock reactions with Oman dunite at 100°C. 11.68 overlaps with 12.48.

most H_2 at 240 nmol/gram. The other vials did not exceed 100 nmol/gram H_2 during 68 days. pH stayed steady throughout the experiments (Figure 10).

NSHQ14 fluid water/rock reaction results

Drill cuttings were obtained from a subsurface, hyperalkaline well (NSHQ14) with mM amounts of H_2 and CH_4. Two grams of drill cuttings obtained from a depth of 262 meters were crushed to 53-212 µm and then reacted with 14 mL of filter-sterilized NSHQ14 fluid. The fluid was originally collected from well NSHQ14 with a submersible pump and injected into a sterile 1 liter bottle, which was then stored at 40°C in the laboratory. It was then filter-sterilized before added to the water/rock reactions with a 2 µm filter. Two grams of Oman dunite were also reacted with this same filter-sterilized fluid, and there was a control with just filter-sterilized NSHQ14 fluid. The filter fluid pH was 11.45 initially, and it was purged with N_2 gas to remove the residual H_2 and CH_4 originally found in the fluid.

After reacting for 116 days, the water/rock reactions produced less than 100 nmol/gram H_2 (Figure 11). The control, with just NSHQ14 fluid, made the most hydrogen with 86 nmol/gram H_2 at 61 days, which then decreased to 0 at 116 days. This value was run twice on the GC to verify its accuracy. At 116 days, the vial with crushed NSHQ14_262m rock made 26 nmol/gram H_2. pH dropped during the reactions from 11.45 to ~9 (Figure 12).

Reaction vessel

Incubating silica serum vials with butyl stoppers produces small amounts of H_2 (<50 nmol). This may confound the actual amount of H_2 generation by minerals; however, the observed concentrations of H_2 from the 100°C reactions is an order of magnitude above

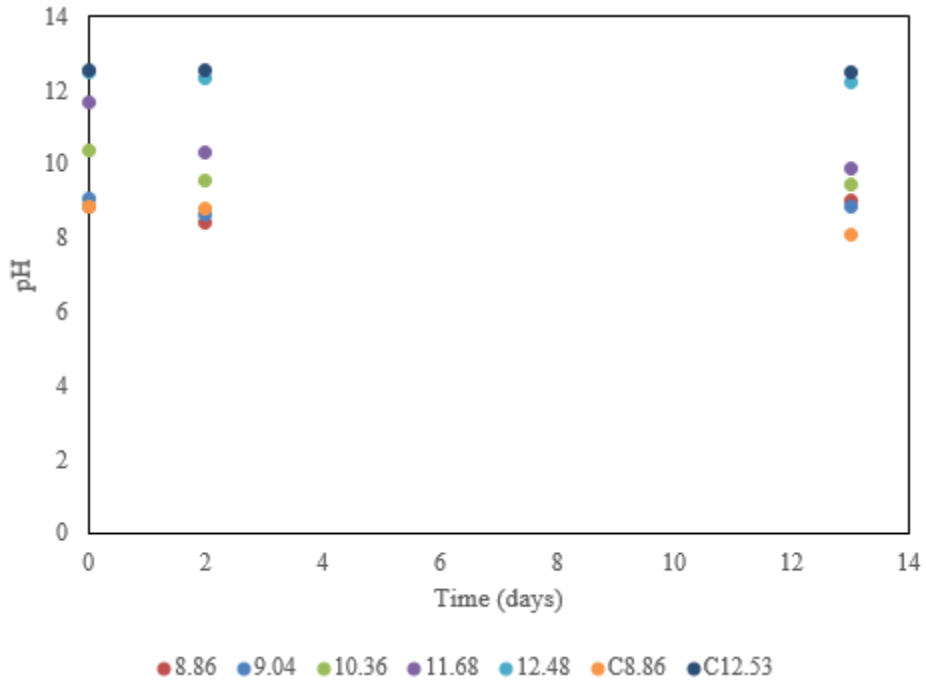

Figure 10. pH versus time in pH water/rock reactions with Oman dunite at 100°C. Data was not collected out to 70 days because the pH microelectrode was broken.

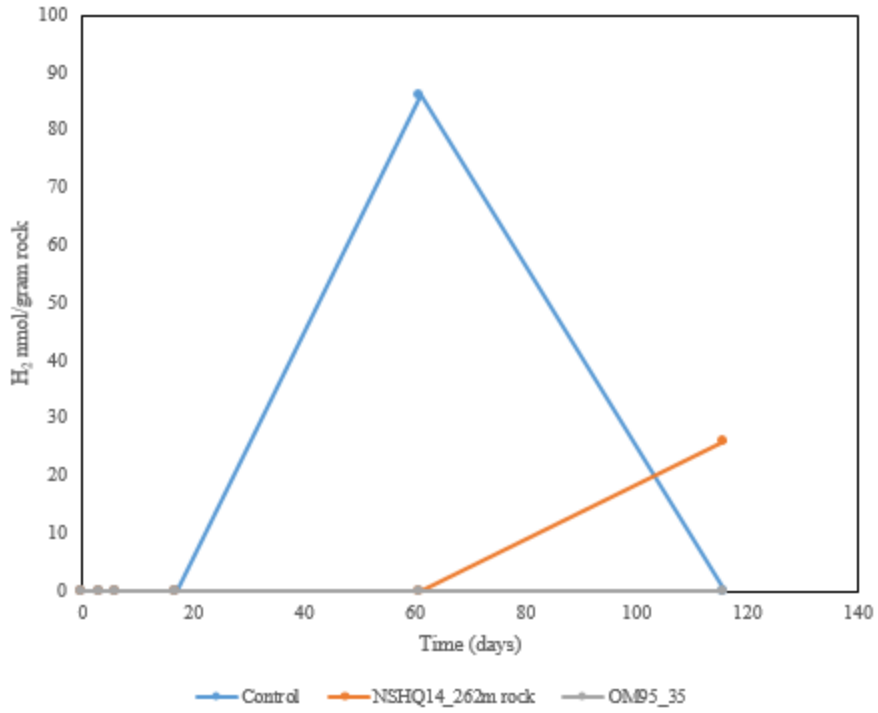

Figure 11. H_2 headspace concentrations in water/rock reactions with Oman dunite and NSHQ14_262m rock at 40°C in filtered NSHQ14 site water. The control value was run twice when the value was high, and it consistently read that value at day 60.

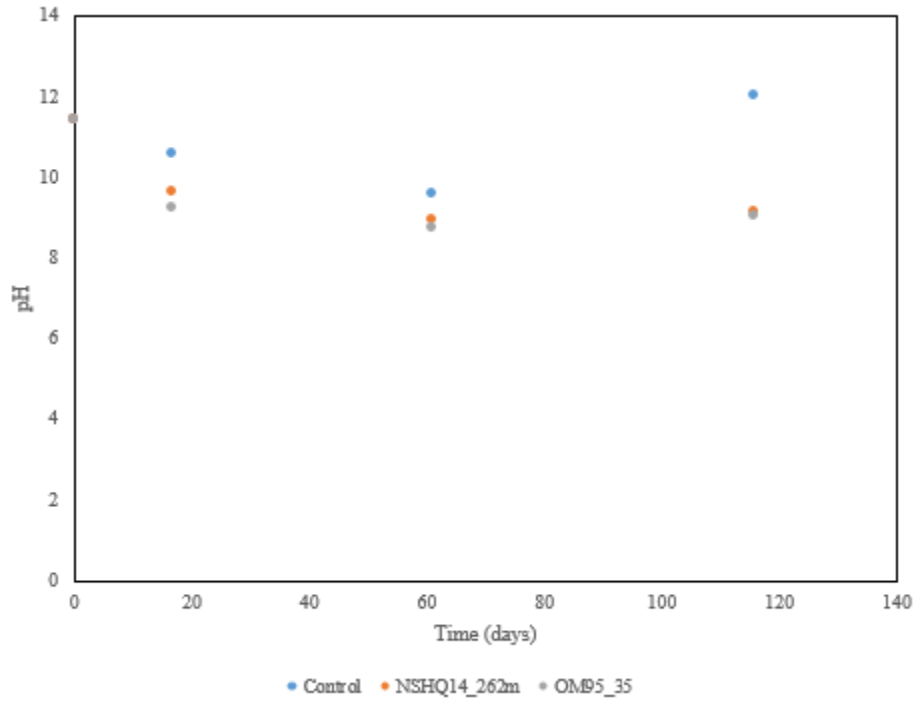

Figure 12. pH versus time in water/rock reactions with Oman dunite and NSHQ14_262m rock at 40°C.

concentrations of H_2 produced by controls. Also, when the experiments were first started, there was not an attractive alternative to allow for periodic sampling of gas and fluid. Dr. Lisa Mayhew and Hannah Miller, along with Dr. Yehor Novikov at the University of Colorado at Boulder Glass Shop, have designed a gas tight, titanium vessel that allows for repeatedly sampling of gases and fluids throughout the course of an experiment. The vessel was oxidized above 500°C to ensure none of the metal surfaces are reactive. Yehor built the system and periodically modified it based on feedback from myself after testing for leaks and functionality. The vessel is better than the current technique of conducting water/rock reactions in silica serum vials with butyl rubber stoppers because these containers leach silica into the fluids and the rubber stoppers release small amounts of H_2, and likely other uncharacterized organic materials. Although the H_2 production from rubber stoppers is small, it is an unsavory contaminant in experiments designed to measure H_2 production from water/rock reactions, not rubber stoppers. Silica leaching is particularly troublesome for serpentinization experiments, which are sensitive to silica activity, and likely changes reaction pathways and products.

The reaction vessel is constructed of titanium that has been oxidized in an oven over 500°C, coating the titanium in an oxidized, non-reactive layer (Figure 13). Additionally, the vessel does not contain plastic in contact with the sample vessel. There are 2 interlocking valve ceramic pieces in the permanent head to allow for a gas-tight seal and they are surrounded by 2 sets of o-rings to maintain the seal. These plastic o-rings are not in contact with the vessel itself and do not contribute any H_2 gas in tested control thus far. The reaction vessel consists of metal tubing capped with a permanent reaction head that can open and close with a wrench. It contains screws that can be tightened to 5 N to ensure they are properly tightened to prevent any leaks. There is also a sampling head that can be purged with N_2 and then a needle can be inserted into

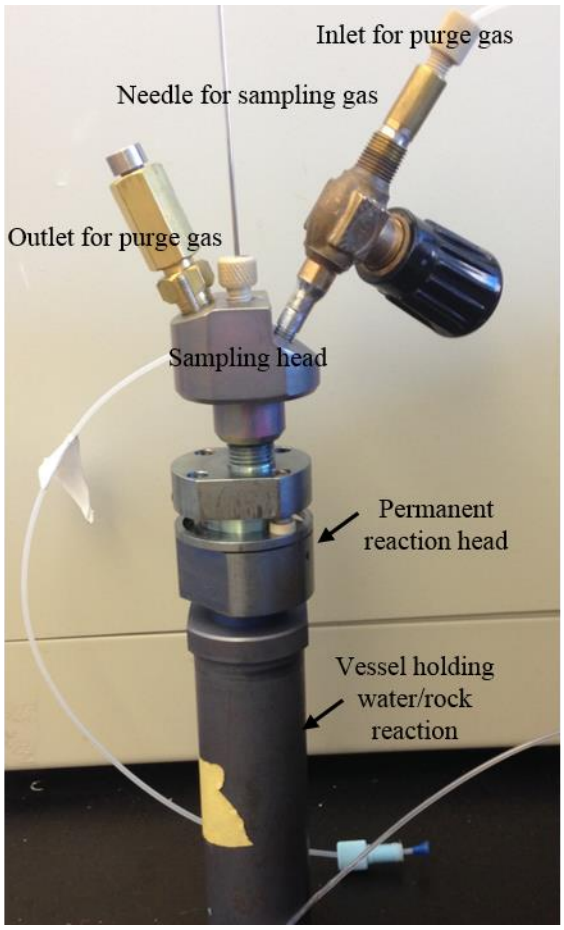

Figure 13. Image of reaction vessel showing various components.

the reaction vessel to sample gas. The protocol for using the reaction vessel is detailed in Appendix A, along with quotes for parts and labor costs.

This work has been in progress for over 3 years, and we are continually faced with leaks as the ceramic pieces break or o-rings need to be replaced. Yehor is constantly refining the vessel, but it is unclear if the vessel is viable for long-term water/rock reactions. The o-rings naturally compress over time, especially when heated to 100°C. A vessel with the functionality we envision would be a great contribution to the field of experimental water/rock reactions; however, the process has been more time-consuming and troublesome than we envisioned, and it is unclear if this vessel, as currently designed, is feasible.

Discussion

55°C and 40°C experiments

Our preliminary results indicate that water/rock reactions conducted at temperatures below 100°C do not produce steady or significant amounts of H_2. These experiments were designed to mimic the subsurface of Oman where we observe low-temperature H_2 production by reacting the Oman dunite with a pH 9 media which simulated the aqueous chemistry of subsurface fluids from well NSHQ04. Temperatures of 55 and 40°C would correspond to slightly over and under 2 km, respectively, in the subsurface with the standard geothermal gradient of 25°C/km. However, our experimental results did not align with our environmental observations of millimolar concentrations of hydrogen from subsurface, hyperalkaline wells.

Water/rock reactions below 100°C with Oman dunite may not produce hydrogen for several reasons. The formation of magnetite is kinetically inhibited, and as a consequence Fe(II)-bearing brucite forms at the expense of hydrogen production (McCollom and Bach, 2009). Also, these experiments were conducted with different media than used in chapter 3 (Table 1) that may not be conducive for destabilizing brucite, which we previously identified as a key Fe(II) reservoir leading to H_2 production. The simulated Oman pH 9 fluid and Type I fluid are much more dilute than seawater medium, which may contribute to variable brucite dissolution rates (see more detailed discussion in Miller et al. 2017). The 55° and 40°C reactions were conducted with an environmentally relevant media instead of seawater media, which yielded up to 500 nmol/gram H_2 in experiments at 100°C.

Brucite did not destabilize during the water/rock reactions at 55° and 40°C. We examined the reacted mineral grains from both 55 and 40°C experiments with Raman spectroscopy and

verified the brucite is still intermixed with serpentine by detecting a peak at 3640 cm^{-1}. As established in chapter 3, the dissolution and oxidation of Fe(II) in brucite leads to H_2 production with Oman dunite. Therefore, the presence of brucite in reacted grains indicates the tested temperatures and aqueous conditions do not destabilize brucite and consequently do not lead to hydrogen production.

The mineral assemblage increases the pH of the fluids, once the dunite is added to solution, the pH increase from 6.5 to 8.5 to 9. However, it is unclear if pH is the controlling factor in brucite destabilization and hydrogen production. We do observe increased H_2 production at 40°C with the addition of 0.1 M of $Ca(OH)_2$, which is an interesting observation that is further tested and described below.

Ionic strength experiments

Varying the ionic strength of water/rock reactions at 100°C, as controlled by $MgCl_2$, did not increase H_2 production. We predicted that high ionic strength solutions would lead to increased H_2 production based on observations of varying hydrogen production from water/rock reactions with seawater versus rainwater solutions (see Miller et al. 2017). As discussed in Miller et al. 2017, dissolution rates of brucite, the key mineral releasing Fe(II) for oxidation, are not dependent on ionic strength (Pokrovsky, 2004). However, specific ions can affect brucite dissolution, and we only modulated the ionic strength with $MgCl_2$, which may be missing the important ions promoting brucite dissolution that were present in seawater media.

Increasing the pH in the ionic strength experiments by adding $Ca(OH)_2$ led to the production of micromolar concentrations of H_2, yet it is unclear if the increased pH or addition of Ca^{2+} led to brucite dissolution. Brucite dissolution experiments have been performed with the

addition of 0.01 M Ca^{2+}, and this led to an increase in brucite dissolution at pH 4.9 (Pokrovsky, 2004). Thus, future work should try adding Ca^{2+} ions to the water/rock reactions to look for increased brucite dissolution to isolate the effects of pH and calcium ions.

After increasing the pH and measuring subsequent significant H_2 production, carbon monoxide concentrations in the headspace also increased while CO_2 concentrations decreased. Headspace CO_2 can be reduced, in the presence of H_2, to formic acid (HCOOH), which can then be dehydrated to form CO (Seewald et al., 2006). This reaction is reversible, and under sufficiently reducing conditions, additional C1 compounds like formaldehyde, methanol, and methane can be produced (Figure 14). Although we only measured C1 compounds (CO and CH_4) in these vials, carbon in serpentinizing environments can also be reduced to form alkanes (McCollom and Seewald, 2001) or solid carbonaceous material (Milesi et al., 2016). Overall, high concentrations of CO in the fluid point to carbon reduction, which is hypothesized to occur abiotically in serpentinizing environments and leads to the production of reduced carbon sources for microorganisms to metabolize (Fu et al., 2007; McCollom et al., 2010; Etiope and Sherwood Lollar, 2013). The conditions under which this CO was formed need to be further examined and constrained, as well as probing for the presence of organic acids in these fluids.

The ionic strength experiments produced millimolar amounts of hydrogen at 100°C, which is an order of magnitude more hydrogen than has been observed in our experimental low-temperature water/rock reactions thus far. We calculated that 50 micromoles of H_2 should form if all the Fe(II)-bearing brucite in 1 gram of dunite dissolves and oxidizes. The maximum observed H_2 is 2 micromoles of H_2 in the de-ionized water vial. This discrepancy is likely due to the formation of CO and possibly other organic acids that are consuming H_2. Raman spectroscopy of the grains reacted at all ionic strengths (after pH was increased with $Ca(OH)_2$ addition) shows

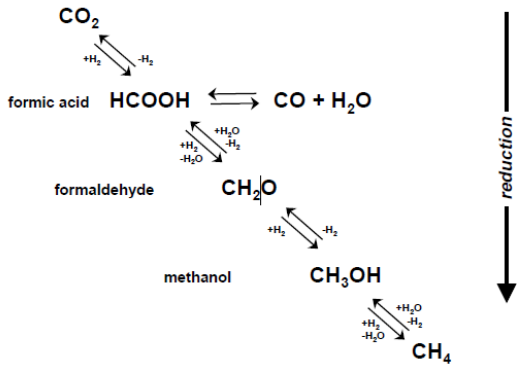

Figure 14. Seewald et al. 2006 diagram showing the redox reactions that can regulate the speciation of single carbon compounds in hydrothermal conditions.

the absence of brucite, affirming previous work showing the dissolution of Fe(II) in brucite leads to hydrogen production (Miller et al. 2017).

Overall, these experiments produced intriguing results with the extensive hydrogen generation coupled with CO generation. The experimental conditions under which these gases formed needs to be better constrained and more deeply investigated in order to better understand the reactivity of environmental samples.

pH experiments

These reactions produced half the amount of hydrogen as the RW and SW 100°C water/rock reactions. However, we used Type I media to simulate fluid percolating into the subsurface of Oman, thus the comparison is not exact due to the media differences. One hypothesis for minimal hydrogen production is that high pH solutions increase the stability of brucite, making it less likely to dissolve. Experimental results have shown that increasing pH up to 11.5 does not increase brucite solubility (Pokrovsky, 2004; Schott et al., 2009) because the rate-limiting step for brucite dissolution is breaking Mg-O bonds, which occurs through surface protonation (Oleg S. Pokrovsky, 2004). Thus, we may not have seen a pH effect in these experiments because we used NaOH to increase pH, which would not affect the stability of Fe-bearing brucite. The pH effect seen with the prior ionic strength experiments may actually be due to the addition of Ca^{2+} which may lead to the stability of a $Ca(OH)_2$ versus a $(Mg,Fe)(OH)_2$, displacing some Mg and Fe.

NSHQ14 water/rock reactions

We tried this experiment to more closely simulate the conditions in the subsurface of Oman, by reacting partially serpentinized rock recovered from 262 m depth at NSHQ14 with fluid pumped from the same well. The lack of hydrogen production suggests that the subsurface rock is not very reactive at low temperatures and under in situ conditions. Fluids in NSHQ-14 may be too closely equilibrated with the host rock to promote rapid or extensive local reaction. Instead, the hydrogen production observed in Oman may occur deeper in the subsurface or in different locations than the single well we analyzed. One possible example would be hydrologically "up-stream", where lower pH, Type I fluids undergo closed-system reaction with the peridotite.

Conclusions

Low-temperature water/rock reactions do not consistently produce H_2. Significant H_2 production is observed in water/rock reactions with high ionic strength and high pH, along with CO production and concomitant CO_2 loss. It seems that pH and/or Ca^{2+} may influence Fe(II)-bearing brucite dissolution and subsequent H_2 production, but more targeted work needs to be conducted to test this hypothesis. A reaction vessel is being developed to conduct these water/rock reactions in a more rigorous manner, but the production is slow and challenging.

References

Etiope G. and Sherwood Lollar B. (2013) Abiotic Methane on Earth. *Rev. Geophys.* **51**, 276–299.

Fu Q., Sherwood Lollar B., Horita J., Lacrampe-Couloume G. and Seyfried W. E. (2007) Abiotic formation of hydrocarbons under hydrothermal conditions: Constraints from chemical and isotope data. *Geochim. Cosmochim. Acta* **71**, 1982–1998.

McCollom T. M. and Bach W. (2009) Thermodynamic constraints on hydrogen generation during serpentinization of ultramafic rocks. *Geochim. Cosmochim. Acta* **73**, 856–875.

McCollom T. M., Lollar B. S., Lacrampe-Couloume G. and Seewald J. S. (2010) The influence of carbon source on abiotic organic synthesis and carbon isotope fractionation under hydrothermal conditions. *Geochim. Cosmochim. Acta* **74**, 2717–2740.

McCollom T. M. and Seewald J. S. (2001) A reassessment of the potential for reduction of dissolved CO2 to hydrocarbons during serpentinization of olivine. *Geochim. Cosmochim. Acta* **65**, 3769–3778.

Milesi V., McCollom T. M. and Guyot F. (2016) Thermodynamic constraints on the formation of condensed carbon from serpentinization fluids. *Geochim. Cosmochim. Acta* **189**, 391–403.

Oleg S. Pokrovsky J. S. (2004) Experimental study of brucite dissolution and precipitation in aqueous solutions: Surface speciation and chemical affinity control. *Geochim. Cosmochim. Acta* **68**, 31–45.

Oremland R. S., Marsh L. and DesMarais D. J. (1982) Methanogenesis in Big Soda Lake, Nevada: an Alkaline, Moderately Hypersaline Desert Lake. *Appl. Environ. Microbiol.* **43**, 462–468.

Schott J., Pokrovsky O. S. and Oelkers E. H. (2009) The Link Between Mineral Dissolution/Precipitation Kinetics and Solution Chemistry. *Rev. Mineral. Geochem.* **70**, 207–258.

Seewald J. S., Zolotov M. Y. and McCollom T. (2006) Experimental investigation of single carbon compounds under hydrothermal conditions. *Geochim. Cosmochim. Acta* **70**, 446–460.

CHAPTER 5

Large variability in carbon isotope fractionation by *Methanobacterium sp.* during methanogenesis at alkaline pHs

To submit for peer-review, with additional information, Spring 2017

Co-authors: Nabil Chaudhry[a], Mark E. Conrad[b], Markus Bill[b], Sebastian Kopf[a], and Alexis S. Templeton[a]

[a] Department of Geological Sciences, UCB 399, University of Colorado, Boulder, CO 80309, USA
[b]Earth Sciences Division, MS 70A-4418, E.O. Lawrence Berkeley National Laboratory, Berkeley, CA 94720, USA

Abstract

Serpentinizing environments contain millimolar concentrations of CH_4 gas; however, it is unclear if these gases have a biotic or abiotic origin. The relatively positive $\delta^{13}C$ CH_4 values of ~20 – 0‰ measured from hyperalkaline fluids in serpentinizing systems are typically assumed to indicate abiotic methane formation. However, 16S rRNA data from several serpentinizing fluids shows the presence of methanogens, and laboratory studies do not show appreciable abiotic CH_4 production under environmental conditions. Thus, it is possible that microbiology may be significantly contributing to CH_4 production in ways that cannot be easily discerned from isotope systematics. Methanogenesis at pH greater than 7 is understudied, thus this study isolated *Methanobacterium sp.* from pH 10.5 fluids from a subsurface well in the actively serpentinizing aquifer in the Samail ophiolite. Organisms were grown in a minimal media over a range of pH from 6.9-10.08 by purging with 5% H_2: 95% N_2 gas to mimic reducing subsurface fluids, with either bicarbonate or carbonate as the sole provided carbon source. The maximum and minimum fractionation factors across the pH range were 1.075 and 1.045 for $\alpha_{CO2\text{-}CH4}$ and 1.338 and 1.280 for $\alpha_{H20\text{-}CH4}$ in bicarbonate-fed cultures, respectively. The range of fractionation factors were 1.079 to 1.028 for $\alpha_{CO2\text{-}CH4}$ and 1.333 and 1.286 for $\alpha_{H20\text{-}CH4}$ in carbonate-fed cultures, respectively. The minimum carbon isotope fractionation ($\alpha_{CO2\text{-}CH4}$ of 1.029) was observed in carbonate cultures grown at pH 8.87 and 9.23, resulting in CH_4 with a $\delta^{13}C$ of -28‰, which is more positive than typically produced from methanogenesis. We are currently developing a steady-state model relating carbonate dissolution and cellular uptake of H_2CO_3 to CH_4 production to determine the processes leading to varying fractionation factors. The rate of methanogenesis at high pH decreases in both experiments, leading to an increase in carbon isotope fractionation in bicarbonate-fed experiments. However, in carbonate-fed experiments,

there is a decrease in carbon isotope fractionation, resulting in enriched $\delta^{13}C$ CH_4 as high as -28‰. This suppressed fractionation is likely the result of closed system effects caused by the slow rate of carbonate dissolution and resupply, even at slow growth rates, which progressively limits the carbon available for methanogenesis. We are developing a steady state model to quantify the processes controlling carbon fractionation during methane production, focusing on the rate of carbonate precipitation compared to carbon dioxide reduction and how these fluxes impact carbon isotope fractionation. The hydrogen isotope fractionation is similar among for both experiments and agrees with values generated by other *Methanobacterium* cultures. These combined results suggest that microbial carbonate-derived CH_4 in alkaline environments may often isotopically resemble "abiogenic" CH_4.

Introduction

Hydrogenotrophic methanogens living in hard-rock systems subsist off geologically-derived H_2 and CO_2-type substrates, which can be in the form of CO_2, formate or CO (Zeikus, 1977; Valentine et al., 2004; Madigan, 2012). It is hypothesized that these methanogens can be powered entirely by geological processes, independent of products of photosynthesis (Nealson et al., 2005). On Earth, hydrogenotrophic methanogens have been found inhabiting diverse H_2-rich rock-hosted systems: subsurface basalt aquifers in Idaho (Chapelle et al., 2002), hydrothermal vents (Proskurowski et al., 2006; Takai et al., 2008; Eecke et al., 2012), deep sediments in quartzite-hosted fractures (Moser et al., 2005), and low-temperature continental serpentinizing environments (Barnes et al., 1967; Barnes et al., 1978; Klein, Humphris, et al., 2015). Methanogens living in hard-rock systems may have been some of the earliest life forms (Sleep et al., 2004; Nealson et al., 2005; Russell et al., 2010), and there is also the potential that rocky bodies that have experienced water/rock reactions to generate H_2, such as Mars or Enceladus, may be conducive to supporting hydrogenotrophic methanogenesis (Oze, 2005; Nealson et al., 2005; Blank et al., 2009; Ehlmann et al., 2010; Kral et al., 2014; Glein et al., 2015).

Methanogens are hypothesized to subsist off geologically produced H_2 in serpentinizing systems; however, they have not been cultured from serpentinizing fluids and their metabolic strategies and ability to grow at high pHs is poorly characterized. Abundant H_2 is generated through oxidation of Fe(II)-bearing minerals in olivine, serpentine, or brucite (McCollom and Bach, 2009; Mayhew et al., 2013; Klein et al., 2013; Klein, Grozeva, et al., 2015; Miller et al., 2016). These environments oftentimes also have millimolar to micromolar concentrations of CH_4, of presumably abiotic origin based on their isotope values (Barnes et al., 1967; Barnes et al., 1978; Abrajano et al., 1990; Proskurowski et al., 2006; Etiope et al., 2011; Etiope and

Sherwood Lollar, 2013; Morrill et al., 2013). However, serpentinizing environments are oftentimes CO_2-limited. Serpentinizing fluids are hyperalkaline (pH > 10), and above pH 10.6 the most abundant carbon species is CO_3^{2-}, which is not the bioavailable form of CO_2 necessary for the first step in the biochemical conversion of CO_2 to CH_4 (Madigan, 2012; Suzuki et al., 2014). Additionally, alkaline fluids make it challenging for methanogens to maintain a proton motive force necessary to generated ATP, and their coping mechanism is unknown. Serpentinizing water/rock reactions further deprive fluids of carbon by releasing Ca^{2+} or Mg^{2+} ions in fluids, causing carbonate minerals to precipitate (Barnes et al., 1967). Microbes can use calcium carbonate for carbon fixation as shown by H_2-utilizing Betaproteobacteria *Serpentinomonas* (Suzuki et al., 2014). It is hypothesized that subsurface methanogens also rely on carbonate minerals for catabolism and anabolism (Kral et al., 2014). Another viable carbon source for hydrogenotrophic methanogenesis in hyperalkaline fluids is formate, which can be abiotically generated when high concentrations of H_2 reduce carbon (McCollom and Seewald, 2003; Lang et al., 2010).

Microbial production of CH_4 through methanogenesis generates a unique range of $\delta^{13}C$ and δD CH_4 values (Schoell, 1980; Whiticar, 1999; Valentine et al., 2004; Etiope, 2009; Etiope and Sherwood Lollar, 2013). This allows scientists to make predictions about microbial activity by investigating the isotopic signature of CH_4 in natural systems. Microbial CO_2 reduction and acetate fermentation generate CH_4 with a $\delta^{13}C$ of -110 to -45‰ and a δD ranging from -375 to -150‰ (Whiticar, 1999; Valentine et al., 2004; Etiope et al., 2013). Biotic, abiotic, and thermogenic CH_4 from a variety of environments on Earth has been isotopically characterized (Whiticar, 1999; Etiope et al., 2013). Isotopic partitioning of CH_4 based on formation mechanism gives insight into geochemical and geomicrobiological processes such as identifying natural gas

deposits and characterizing analog methanogenesis habitats on Earth of astrobiological significance (Blank et al., 2009; Etiope et al., 2013).

Alkaliphilic methanogens have been cultured from soda lakes and subsurface fluids, however, their CH_4 isotope values are understudied (Oremland et al., 1982; Worakit et al., 1986; Kiene et al., 1986; Mathrani et al., 1988; Kohl et al., 2016). Methanogens grown in sediment incubations from Big Soda Lake in Nevada metabolized methanol to produce a $\delta^{13}C_{CH4}$ value of -113.5 to -118.2‰ at pH 9.7 (Oremland et al., 1982). *Methanohalophilu zhilinae* was isolated from Bosa Lake in Egypt and grown at an optimal pH of 9.2 (Mathrani et al., 1988) and *Methanobacterium alcaliphilum* was isolated and grown at an optimal pH of 8-9 (Worakit et al., 1986). However, these methanogens isolated from saline, alkaline soda lakes generally utilize methyl groups for catabolism (Kiene et al., 1986), not hydrogen and CO_2-type substrates as would be expected in serpentinizing environments. *Methanobacterium subterraneum* is a hydrogenotrophic alkaliphilic methanogen that was isolated from granitic groundwater from a depth of 420 m and grows at an optimal pH of 7.8-8.8 at 35°C with H_2 and CO_2 or formate to make CH_4 (Kotelnikova et al., 1998). Unfortunately, there is not carbon or hydrogen isotope information available.

Hydrogenotrophic methanogens have been identified with 16S rRNA sequencing from alkaline, serpentinizing fluids (Blank et al., 2009; Suzuki et al., 2013; Woycheese et al., 2015; Kohl et al., 2016; Miller et al., 2016), but there are no laboratory cultures isolating the methanogens to quantify their carbon and hydrogen fractionation factors. Kohl et al. (2016) enriched pH 11 surface fluids from the Cedars ophiolite for methanogens, and reported a range of $\delta^{13}C_{CH4}$ values ranging from -77.4 to -92.9‰ using bicarbonate, acetate, and formate as

carbon sources (Morrill et al., 2014; Kohl et al., 2016). However, there is not any available sequence information to identify what methanogen is responsible for the fractionation.

It is important to understand the isotopic behavior of microbially-produced CH_4 under alkaline conditions because CH_4 is ubiquitous in serpentinizing environments (Abrajano et al., 1990; Etiope et al., 2011; Etiope et al., 2011; Etiope and Sherwood Lollar, 2013; Szponar et al., 2013). CH_4 captured from hyperalkaline serpentinizing fluids in the Philippines, Canada, Turkey, Oman, Lost City hydrothermal field and New Zealand has $\delta^{13}C_{CH4}$ values ranging from approximately -35 to -5‰ and are proposed to originate from abiogenic oxidation of carbon under reducing conditions (Abrajano et al., 1990; Proskurowski et al., 2006; Etiope et al., 2011; Etiope et al., 2011; Etiope and Sherwood Lollar, 2013; Szponar et al., 2013). The abiogenic methane hypothesis is not only based on the $\delta^{13}C_{CH4}$ values, but also measurements of increasingly negative $\delta^{13}C$ values from C_2 to C_5 alkanes (Proskurowski et al., 2008; Etiope et al., 2011). There is an acknowledged partial microbial contribution to the CH_4 in Lost City and the Cedars serpentinizing systems (Proskurowski et al., 2008; Bradley and Summons, 2010; Morrill et al., 2013). However, it is unlikely that microbial activity alone explains the high concentrations of CH_4 and isotopic signatures of C_{2+} alkanes (Proskurowski et al., 2008; Bradley and Summons, 2010). Yet, this above-mentioned inverse carbon isotope trend is not universally diagnostic for abiogenic methane (McCollom et al., 2010) and rates and amounts of microbially-produced CH_4 are unconstrained. Methanogens have been sequenced from Lost City, Oman, and the Philippines (Brazelton et al., 2006; Woycheese et al., 2015; Miller et al., 2016), so their presence should not be ignored in assessing the origin of CH_4 in serpentinizing systems.

Subsurface fluids from the Samail ophiolite in Oman contain millimolar concentrations of methane with the most positive $\delta^{13}C_{CH4}$ values seen from a serpentinizing system, +2.4 and

+3‰, with δD_{CH4} values of -205 and -232‰, respectively (Barnes et al., 1967; Kelemen and Matter, 2008; Kelemen et al., 2011; Miller et al., 2016). There is debate about the origin of the methane, with Miller et al. (2016) considering the origin to be likely a combination of abiotic and microbial processes, while Etiope (2016) asserts it is unlikely that microbial production or consumption of methane could fractionate the methane to such a large extent and instead the methane is likely sourced by abiotic reduction of underlying Permian carbonates. *Methanobacterium spp.* and *Methylococcus spp.* have been detected with 16S rRNA sequencing in the fluids, thus Miller et al. (2016) did not want to discount microbial contribution to the CH_4.

To investigate the carbon and hydrogen fractionation of CH_4 imparted by microbial activity in the subsurface Samail aquifer, we collected subsurface, hyperalkaline (pH 10.5) fluids, rich in H_2 and CH_4, from well NSHQ04 from an actively serpentinizing peridotite aquifer in the Samail ophiolite (Barnes et al., 1967; Kelemen and Matter, 2008; Kelemen et al., 2011; Miller et al., 2016). Fluids were collected in January 2014 by filtering 5-10 L of fluid onto a 2 µm filter, then immersing the filter in site water in a 100 mL anaerobic silica serum vial and amending with hydrogen, carbon sources and other mineral components. From these fluids, we successfully cultured *Methanobacterium sp.* in a synthetic medium formulated to mimic site water. *Methanobacterium sp*. is present in several serpentinizing environments (Blank et al., 2009; Suzuki et al., 2013; Woycheese et al., 2015; Miller et al., 2016). This species is mesophilic, forms long rods, and utilizes CO_2 as a substrate, although it may also utilize CO and formate. We grow it at 40°C in the lab and did not observe any growth at 55°C. The culture is not pure, but we suppress bacterial growth with an antibiotic cocktail. This study grows *Methanobacterium sp.* from pHs of 7 to 12, with bicarbonate ($NaHCO_3$) and carbonate ($CaCO_3$)

as respective carbon sources, to determine the carbon isotope fractionation factor of CO_2-CH_4 at alkaline pHs.

Methods

In January 2014, a shallow submersible pump was used to collect water from 18 meters depth in well NSHQ04. Fluids (~5-10L) from the well were pumped and filtered through 0.2µm Sterivex inline filters to recover enhanced biomass. These filters were then put in a 100 mL silica serum vial and filled with site water then capped to maintain the anaerobic site environment. The vials were acid washed, autoclaved and baked at 400°C in a muffle furnace prior to field work. *Methanobacterium* was sequentially isolated from NSHQ04 fluids through successive transfers into new vials, first growing for 6 generations in site water with 80% H_2:20% CO_2, 0.1 mL Fe(III) oxides, 1 mL 100 mM formate, and 1 mL Oman rock crushings, then inoculating in DSMZ medium 141 (Supplemental Tables 1&2), a specific formulation for methanogens. Eventually, *Methanobacterium* grew in a synthetic NSHQ04 medium (16 mM NaCl, 6 mM $CaCl_2$, 0.0013 mM H_4SiO_4, 0.007 mM $MgSO_4$*$7H_2O$, 0.4 K_2SO_4, 0.01 KNO_3, 0.001 NaF, 0.028 NaBr, 4.13 mM cysteine).

Methanogens were grown with 90 mL of medium in 100 mL silica serum vials with butyl rubber stoppers; the headspace was purged with 95% N2: 5% H2 and slightly overpressurized. Cultures were either grown with 10 mM $NaHCO_3$ or 10 mM $CaCO_3$, the later was oversaturated in the fluid so did not fully dissolve. 0.9 mL of trace vitamins and elements for DSMZ medium 141 were added. Additionally, 1.8 mL of filter sterilized antibiotic mixture was added, containing 5 mg penicillin, 5 mg streptomycin, and 50 uL ampicillin. We were unable to culture a pure culture despite multiple efforts at dilution-to-extinction, therefore there are some bacterial species living with the methanogens that are suppressed by antibiotics. Their presence does not seem to affect methane production, as we can clearly see the effect of a complex consortium in similar cultures containing *Methanobacterium* that is not evident here (Appendix C).

16S rRNA sequencing

The microbial analyses were conducted as described previously (Bowers et al., 2013; Emerson et al., 2015). DNA was extracted from one quarter of each of the filter samples using the MoBio PowerSoil kit. The V4-V5 region of the 16S rRNA gene was PCR amplified in triplicate reactions using the 515f/806r primer pair. The primers contained the appropriate Illumina adapters and the reverse primer contains a 12-bp error-correcting barcode unique to each sample. The triplicate reactions were composited, amplicon concentrations were determined using the PicoGreen dsDNA assay, and the amplicons from all samples were pooled together in equimolar concentrations. Sequencing was conducted on an Illumina MiSeq at the University of Colorado Genomics Core Facility following the 2 × 250 bp paired-end protocol. Quality filtering of reads and processing of the reads was conducted as described in (Barberán et al., 2015). After demultiplexing, reads were quality filtered at an equivalent sequencing depth (6000 reads per sample) and clustered into phylotypes using the UPARSE pipeline (52)(Edgar, 2013). Reads were assigned to phylotypes at the ≥97% sequence similarity threshold and phylotype taxonomy was determined using the RDP classifier with a confidence threshold of 0.5 (Wang et al., 2007) trained on the Greengenes 13_8 database (McDonald et al., 2012).

Experimental set-up

9 vials at a range of pHs (6.5, 7, 8.5, 9.7, 10.12, 10.38, 10.83, 11.51, 11.94) were amended with CaCO3 and 9 similar vials were inoculated with $NaHCO_3$. There were also control vials of each carbon source to allow for isotopic analysis of DIC pools. Vials were inoculated with 2 mL from a successfully growing culture in an identical medium. Gas concentrations were

initially monitored daily, then weekly or biweekly once it was evident growth was slow. Once CH4 levels were >0.01 mM, 5 mL of headspace gas was sampled and injected into a vacuum purged 7 mL vial, and then overpressurized with 3 mL of He gas. Samples were sent to Lawrence Berkeley National Lab for isotopic analysis.

Instrumental techniques

To determine H_2 and CH_4 concentrations the gases exsolved from the well fluids, we used a SRI 8610C gas chromatograph (GC) with a 2 m by 1 mm ID micropacked ShinCarbon ST column with N_2 as the carrier gas. 0.5 mL of gas was sampled from the headspace of serum vials sealed with blue rubber stoppers and was injected into a sampling port on the GC. H_2 was measured with a thermal conductivity detector (TCD), and a flame ionization detector (FID) was concurrently used to measure CH_4. The detection limit is 10 ppm with an analytical error of 5%.

Stable isotope analyses were conducted at the Center for Isotope Geochemistry at the Lawrence Berkeley National Laboratory. The isotopic compositions of H_2 and CH_4 were analyzed using a Thermo Scientific GC Trace Gas Ultra system connected to a Thermo Scientific Delta V Plus Mass Spectrometer (IRMS). Gas samples were injected into a 6-port valve (the loop size varied from 5L to 250 L depending on the concentration of the analyte in the sample) bypassing the inlet of the GC. After flushing with at least 3 times the volume of the loop, the sample was injected into the GC where the gases were separated chromatographically on an HP-molesieve fused silica capillary column (30 m x 0.320 mm). For H_2, after the samples went through the GC, they were passed through a combustion furnace at room temperature and then into the IRMS. Reproducibility of these analyses is ±2.5‰ (1σ), as determined by repeated analyses of a laboratory gas standard. Carbon isotope ratios of CH_4 were analyzed using the

same system with the combustion furnace (a capillary ceramic tube loaded with Ni, Cu, and Pt wires) set at 1030 °C where the CH_4 was converted to CO_2. Produced water was removed, and the carbon isotope ratio of the resulting CO_2 was measured in the IRMS. The reproducibility of these analyses is ±0.2‰. For hydrogen isotopes of CH_4, the sample was passed through a pyrolysis furnace at 1450 °C and the resulting H_2 gas measured with the IRMS. The reproducibility of these analyses is ± 5‰.

Steady state model

Isotopic fractionation modeling was performed in R, a software environment for statistical computing and graphics (R Development Core Team, 2008). Equations were solved in Mathematica (Wolfram Research, Inc., 2017).

Results

Experimental results

Headspace CH_4 concentrations in $NaHCO_3$ and $CaCO_3$ cultures were measured over time (Figure 1). For the vials amended with $NaHCO_3$, the lower pH cultures (<9) produced over 0.04 mM CH_4 within the first 11-21 days of growth, whereas the higher pH cultures did not produce 0.04 mM CH_4 until 37-97 days, and the highest pH vials, 10.99 and 11.73 never made measurable CH_4. For the vials amended with $CaCO_3$, the lower pH cultures (<8) produced >0.04 mM of CH_4 in only 8 days. The vials greater than pH 9 grew more slowly and did not produce >0.04 mM CH_4 until 45-98 days. The NaHCO3 and CaCO3 experiments stopped generating CH_4 once headspace concentrations stabilized at ~0.08 mM, due to consuming all headspace H_2. Headspace gas was sampled once the cultures produced >0.04 mM CH_4 to ensure quality data for isotopic analysis. Thus, after initial sampling, there is oftentimes a slight dip in measured CH_4 concentrations, but it is does not appear to significantly alter methanogenesis. The pH was initially measured in concert with headspace CH_4 concentrations, with 9 values total for both $NaHCO_3$ and $CaCO_3$ vials spanning from 6.87-11.85. The values were constant over the first month of growth, thus, pH was measured less as growth continued. The initial and final pH values are shown in Table 1. Vials that initially had pH values under 8 experienced a slight pH increase as *Methanobacterium* grew, whereas vials that initially had pH values >8 experienced a pH decrease as methanogenesis occurred.

The isotopic value of $\delta^{13}C_{CH4}$ produced by *Methanobacterium* was measured over the range of pHs (Figure 2). The $\delta^{13}C$ of the $NaHCO_3$ is -3.83‰ and $CaCO_3$ is -0.10‰. As pH increases in $NaHCO_3$-fed cultures, from 7.20 to 10.08, the $\delta^{13}C_{CH4}$ becomes more negative,

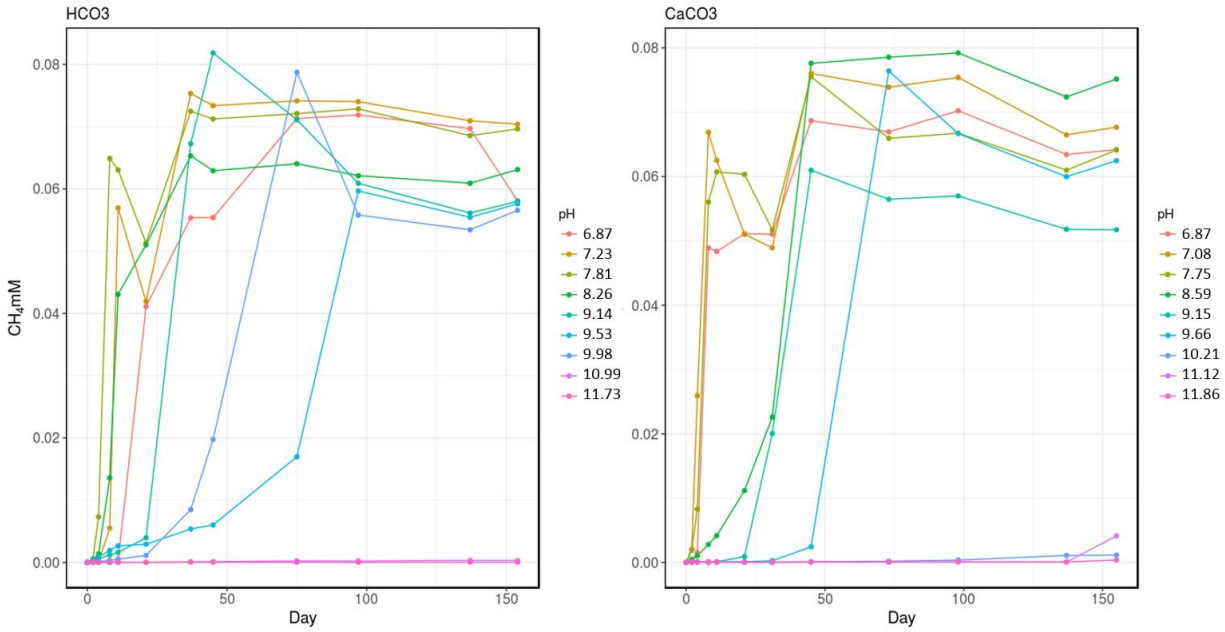

Figure 1. CH_4 concentrations (mM) over time for cultures of *Methanobacterium sp.* grown over a range of pHs with either $CaCO_3$ or HCO_3^- as a carbon source. pH values listed are the initial pH of the medium on Day 0 of the growth experiment.

Table 1. Initial and final pH values of *Methanobacterium* cultures grown with HCO_3 or $CaCO_3$ as carbon source.

pH HCO3 cultures									
	1	2	3	4	5	6	7	8	9
Day 0	6.87	7.23	7.81	8.26	9.14	9.53	9.98	10.99	11.73
Day 156	7.92	7.72	7.95	8.20	8.86	9.36	9.69	10.85	11.28
pH CaCO3 cultures									
	1	2	3	4	5	6	7	8	9
Day 0	6.87	7.08	7.75	8.59	9.15	9.66	10.21	11.12	11.85
Day 156	7.56	7.44	7.72	8.54	8.41	8.81	9.20	10.03	11.34

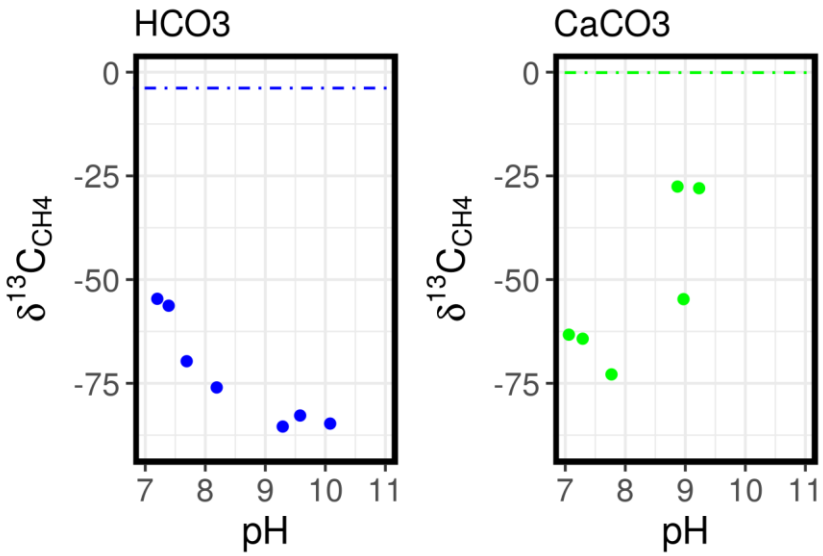

Figure 2. pH vs $\delta^{13}C$ CH_4 for cultures of Methanobacterium grown with either HCO_{3-} (green) or $CaCO_3$ (blue) carbon sources. pH corresponds to the pH of the medium when the CH_4 was sampled. Dashed blue line shows the initial $\delta^{13}C$ of the $NaHCO_3$ (-3.83‰) and dashed green line shows the initial $\delta^{13}C$ of $CaCO_3$ (-0.10‰).

decreasing from -55 to -85‰. $CaCO_3$-fed cultures do not follow the same trend with pH. The initial values of $\delta^{13}C_{CH4}$, -63 to -73‰, from pH 7.06 to 7.77, are more negative than those of HCO_3, -55 to -70 from pH 7.20 to 7.69. Then, at pH 8.87, 8.97 and 9.23, the $\delta^{13}C_{CH4}$ becomes more positive, -55, -28, and -28‰, respectively, as compared to $\delta^{13}C$ values of -76 to -85‰ in similar pH ranges with HCO_3 experiments. The CH_4 was sampled after the concentration in the headspace exceeded 0.04 mM, roughly during the middle of the exponential growth phase because CH_4 values stabilized at 0.08 mM. Measurements of the isotopic values of CH_4 at 0.08 mM are ongoing, which should correspond to the total methane made during the full growth phase. The pH values reported reflect the pH of the vials at the time of CH_4 sampling.

The initial δD H_2O is -108‰ in NSHQ04 medium and the δD H_2 is currently being measured. The δD of CH_4 for cultures growing with $CaCO_3$ and HCO_3 was also measured (Figure 3). $NaHCO_3$-fed cultures had a tight range of values, from δD of CH_4 -399 to -446‰. $CaCO_3$-fed cultures also displayed a similar range of values, from δD of CH_4 -394 to -441‰.

Hydrogen and carbon fractionation factor calculations for $NaHCO_3$ vials

In order to truly compare isotope variations amongst different species of methanogens, it is necessary to calculate apparent fractionation factors for $\alpha_{CO2\text{-}CH4}$ and $\alpha_{H2O\text{-}CH4}$ based on experimental data. This can be done with the following equation (Valentine et al., 2004):

$$\delta^{13}C_{CH4} = \delta^{13}C\ H_2CO_{3(aq)} + \varepsilon_{CO2\text{-}CH4}(1\text{-}f)[\ln(1\text{-}f)]/f \qquad \text{(Equation 1)}$$

where f is the fraction of bioavailable carbon consumed relative to initial bioavailable carbon. To accurately calculate f in $NaHCO_3$ experiments, the concentrations of the carbon species ($H_2CO_{3(aq)}$, HCO_3^-, and CO_3^{2-}) had to be calculated at the pH of each vial (Figures 4 and 5). Carbon speciation was calculated using a pKa_1 of 6.296 and pKa_2 of 10.220 (Benjamin, 2002).

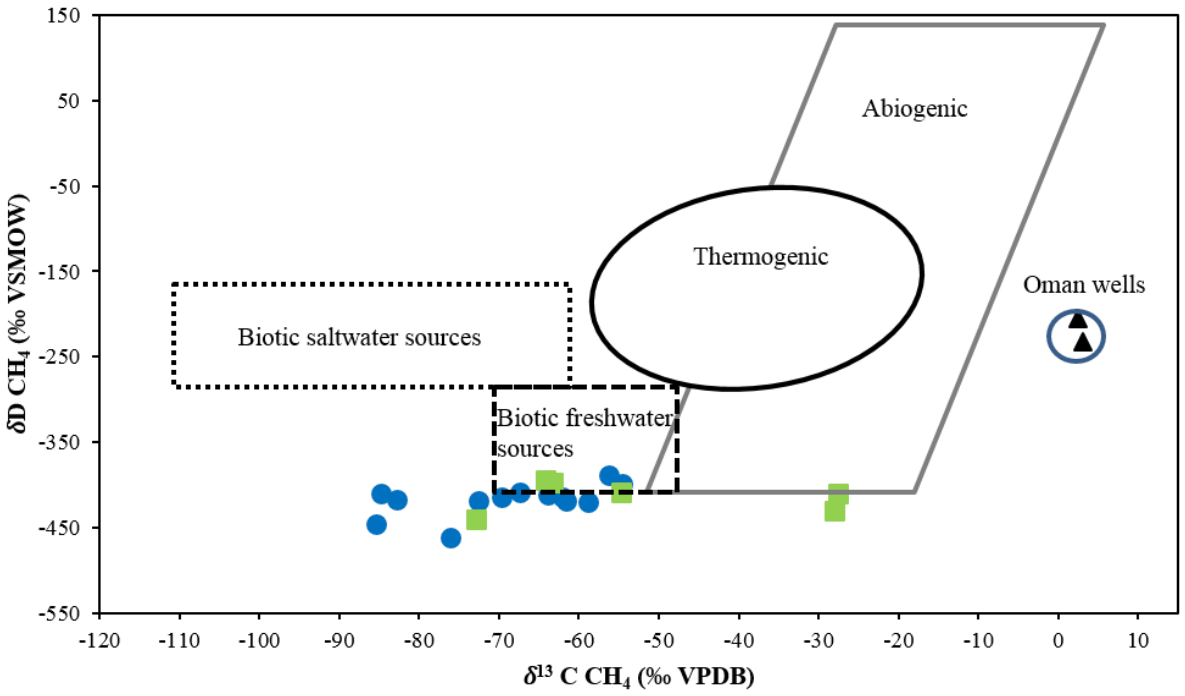

Figure 3. Based on Etiope et al. (2011), the δD and δ^{13}C CH_4 diagram includes isotope values for *Methanobacterium* grown over a range of pHs with $CaCO_3$ (green boxes) and HCO_3 (blue circles) as carbon sources. Isotope values for Oman wells NSHQ04 and NSHQ14 from January 2014 are in black triangles. The fields for various methane isotope values are general approximations based on (Whiticar, 1999; Valentine et al., 2004; Etiope and Sherwood Lollar, 2013) and do not represent the full range of diversity of these values, but serve as a general representation of these values.

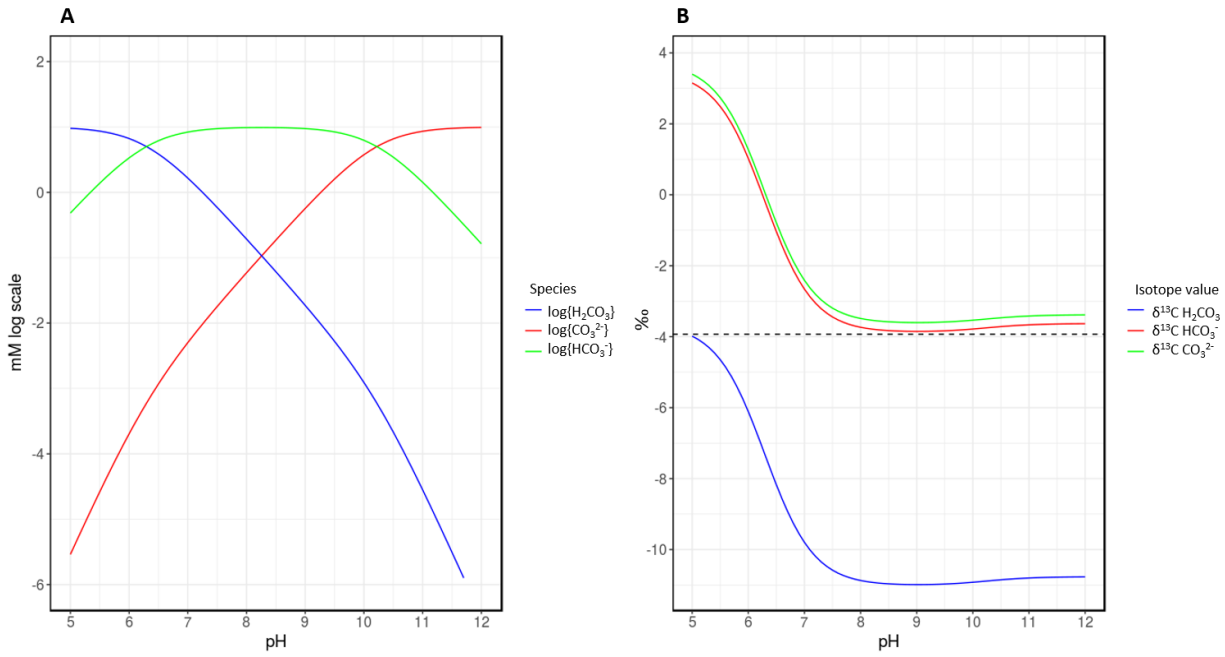

Figure 4. Speciation of carbon species over range of pH in vials supplied with $NaHCO_3$ (A), isotopic values of carbon species over range of pH (B), dashed line shows isotopic value of $NaHCO_3$ added to medium (-3.83‰)

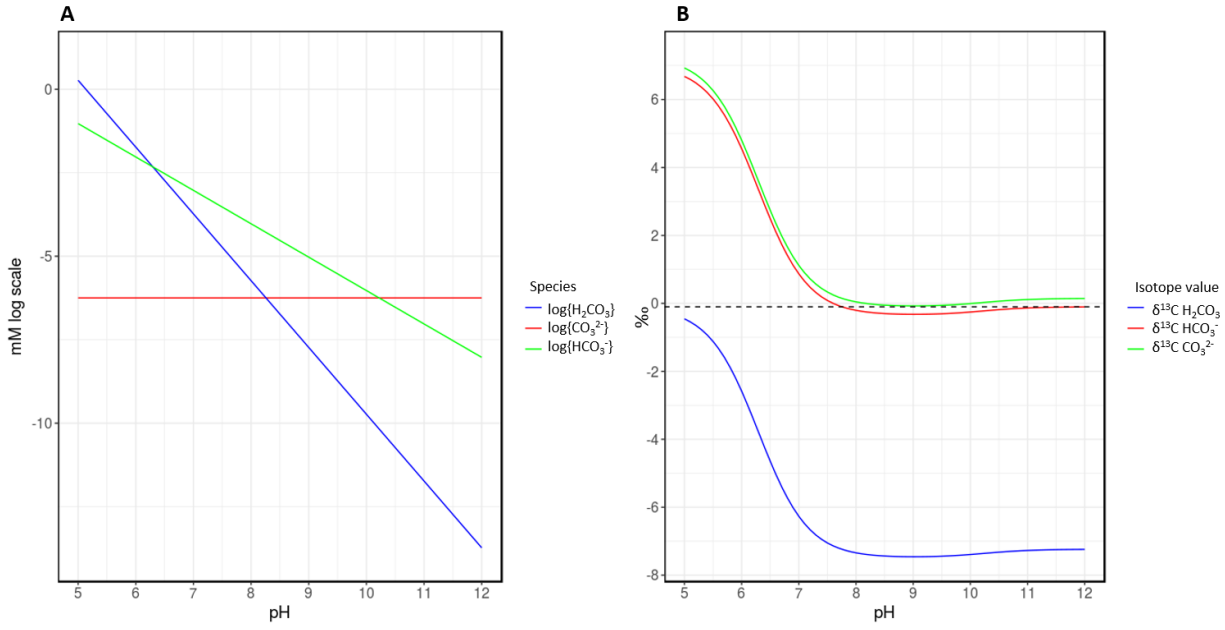

Figure 5. Speciation of carbon species over range of pH in vials supplied with $CaCO_3$ (A), isotopic values of carbon species over range of pH (B), dashed line shows isotopic value of $CaCO_3$ added to medium (-0.10‰).

The amount of carbon consumed was estimated by the concentrations of CH_4 produced in the vials. We assumed that one mole of CO_2 produces one mole of CH_4, based on the methanogenesis equation:

$$4H_2 + CO_2 = CH_4 + 2H_2O \qquad \text{(Equation 2)}$$

The $NaHCO_3$ vials contained a total of 10 mM bioavailable carbon (total aqueous carbon species) because all of the bicarbonate dissolved into the solution. The amount of CH_4 produced (at the time of sampling CH_4 for isotope values) over the total 10 mM of carbon in the vials is listed in Table 2. The f value is small, thus an approximation of equation 1 can also be used to get similar results:

$$\alpha_{CO2\text{-}CH4} = \delta^{13}C_{C02} + 1000 \,/\, \delta^{13}C_{CH4} + 1000 \qquad \text{(Equation 3)}$$

However, results are reported from the calculation with equation 1 to rigorously calculate carbon and hydrogen fractionation factors.

Carbon speciation of the dissolved inorganic carbon pool results in varying isotopic values based on pH. The unspeciated $\delta^{13}C$ of the $NaHCO_3$ is -3.83‰. The predicted isotope composition of each dissolve carbon species at each pH can be quantitatively calculated based on the following equations (Mook, 1986):

$$^{13}\varepsilon\,(CO_{2aq}\text{-}HCO_3^-{}_{aq}) = -9866/T + 24.12‰ \qquad \text{(Equation 4)}$$

$$^{13}\varepsilon\,(CO_3^{2-}{}_{aq}\text{-}HCO_3^-{}_{aq}) = -867/T + 2.52‰ \qquad \text{(Equation 5)}$$

$$\delta^{13}C_{HCO3-} = \delta^{13}C_{\Sigma CO2} - (\varepsilon_{(CO2aq\text{-}HCO3\text{-}aq)}[CO_2] + \varepsilon_{(CO32\text{-}aq\text{-}HCO3\text{-}aq)}[CO_3^{2-}]) \,/\, [\Sigma CO_2] \qquad \text{(Equation 6)}$$

$$\delta^{13}C_{CO2} = \delta^{13}C_{HCO3-} + \varepsilon(CO_{2aq}\text{-}HCO_3^-{}_{aq}) \qquad \text{(Equation 7)}$$

$$\delta^{13}C_{CO32-} = \delta^{13}C_{HCO3-} + \varepsilon(CO_3^{2-}{}_{aq}\text{-}HCO_3^-{}_{aq}) \qquad \text{(Equation 8)}$$

Table 2. Fractionation factor calculations. We are assuming the fraction of water consumed was negligible when calculating $\alpha_{H2O\text{-}CH4,}$ so we used 10^{-12} for the calculations. The fraction of carbonate consumed in the CaCO3 experiments cannot be quantified with our current data, so we just calculate an apparent fractionation factor as described in the text. * $\delta^{13}C$ CO_2 values are calculated from Mook (50) calculations of isotopic values for carbon speciation as shown in Figures 5 and 6. Cultures did not produce sufficient CH_4 at high pHs to measure isotopic values of CH_4.

						$\delta^{13}C$ HCO_3	-3.83
	HCO_3						
pH	$\delta^{13}C$ CH_4	δD CH_4	*$\delta^{13}C$ CO_2	fraction of 10 mM bicarbonate consumed		$\alpha_{CO2\text{-}CH4}$	$\alpha_{H2O\text{-}CH4}$
6.92	-54.6	-399.3	-10.20		4.11E-03	1.045	1.291
7.12	-56.3	-388.2	-10.48		5.69E-03	1.046	1.280
7.71	-69.7	-413.9	-10.74		6.49E-03	1.059	1.306
8.45	-76.0	-461.2	-10.92		4.31E-03	1.065	1.353
9.24	-85.4	-446	-10.98		8.18E-03	1.075	1.338
9.55	-82.77	-418.0	-10.96		1.70E-03	1.072	1.310
10.08	-84.72	-410.3	-10.91		7.87E-03	1.074	1.302
				Average		1.062	1.312
						$\delta^{13}C$ $CaCO_3$	-0.1
	$CaCO_3$						
pH	$\delta^{13}C$ CH_4	δD CH_4	*δ13C CO2	fraction of 10 mM carbonate consumed		$\alpha_{CO2\text{-}CH4}$	$\alpha_{H2O\text{-}CH4}$
7.11	-63.3	-397.7	-6.48	--		1.069	1.290
7.2	-64.3	-394.4	-6.82	--		1.069	1.286
7.93	-72.9	-441	-7.26	--		1.079	1.333
8.97	-54.7	-409	-7.46	--		1.058	1.301
8.87	-27.6	-410	-7.46	--		1.028	1.302
9.23	-27.98	-431.0	-7.46	--		1.029	1.323
				Average		1.055	1.306

with T in Kelvin. Our experiments were cultured at 40°C, thus the value for T was 313.15 K. The resulting isotopic composition of each part of the DIC pool based on pH and carbon species is shown in Figure 4.

The fractionation between δD H_2O and δD CH_4 was also calculated. Equation 1 was modified accordingly, replacing $\delta^{13}C_{CH4}$ with δD_{CH4} and $\delta^{13}C$ $H_2CO_{3(aq)}$ with δD H_2O. The original δD H_2O measured at -108‰ in NSHQ04 medium. The amount of H_2O consumed during the reaction is assumed to be negligible compared to the total available H_2O in the vials, thus f is set at 10^{-12} in the calculations.

The fractionation factor calculations for HCO_3 vials are summarized in Table 2. The $\alpha_{CO2\text{-}CH4}$ for HCO_3 vials varies from 1.046 – 1.076, and $\alpha_{H2O\text{-}CH4}$ varies from 1.281 – 1.354. This calculation is only based on one time point, but an additional time point from each vial will also be assessed. The fraction of carbonate consumed assumes that for every one mole of CH_4 produced, one mole of carbonate was consumed.

Hydrogen and carbon fractionation factor calculations for $CaCO_3$ vials

It is straightforward to calculate the amount of bioavailable carbon in $NaHCO_3$ vials because it is soluble in the medium. However, $CaCO_3$ is not fully soluble in the medium across the range of pHs, thus the total aqueous carbon pool varies over orders of magnitude across the range of experimental pH. At any given pH, the $CaCO_3$ vials instead have a fixed concentrations of CO_3^{2-} based on the solubility of $CaCO_3$ in NSHQ04 medium that already contains 6 mM Ca^{2+}:

$$K_{sp}\ CaCO_3 = 10^{-8.4} = [Ca^{2+}\text{ in medium} + x][x] \qquad \text{(Equation 9)}$$

where x is the moles of $CaCO_3$ dissolved, more specifically the equilibrium moles of CO_3^{2-} and moles of Ca from the dissolving carbonate. When this equation is solved, x is $10^{-6.25}$, or 0.57 µM, and the resulting speciation of all aqueous carbon species can be calculated based on this fixed amount of CO_3^{2-} (Figure 5). However, this assesses the initial equilibrium of the solution, which will then be perturbed when methanogens are present and utilizing $H_2CO_{3(aq)}$, because this drives further $CaCO_3$ dissolution. Total $CaCO_3$ dissolution could be quantified by measuring Ca^{2+} in the fluid. However, there is already 6 mM in the medium, so the micromolar concentrations of Ca^{2+} released by carbonate dissolution would not be detectable.

In order to quantify the amount of bioavailable carbon in the $CaCO_3$ experiments, we need to know the rate of calcite dissolution and the extent to which the methanogens consumed the bioavailable carbon. Because this is not feasible with the experimental set-up, we instead use simplified equation 3 to calculate a fractionation factor, which assumes f is very small. This may not be a valid assumption for this experiment, but it does allow us to calculate an apparent fractionation factor and will be discussed more below. The $\alpha_{CO2\text{-}CH4}$ for $CaCO_3$ vials varies from 1.028 – 1.079, and $\alpha_{H2O\text{-}CH4}$ varies from 1.286 – 1.333.

Gibbs Free Energy calculations

We calculated how much energy is available to the methanogens at the time the headspace gas was sampled for isotope measurements.

$$\Delta G = \Delta G^o + RT\ln Q \qquad \text{(Equation 10)}$$

ΔG^o is defined as -131 kJ/mol at STP and pH 7, R (ideal gas constant) is 8.314e-3 kJ/mol*K, T is temperature in Kelvin 313.15 K (40°C), and Q is defined as:

$$Q = \{H_2O\}^2\{CH_4\}/\{CO_2\}\{H_2\}^4 \qquad \text{(Equation 11)}$$

where {H_2O} = 1, and all the species the gas concentrations are calculated in their aqueous form, determined by using a dimensionless Henry's constant of 0.035 for CH_4 and 0.019 for H_2 (Sander 2015), calculated at 25°C. To be rigorous, the final manuscript will calculate the activities of each species taking into account the ionic strength of the solution.
The Gibbs free energy results for both $NaHCO_3$ and $CaCO_3$ experiments are shown in Figure 6.

For the $NaHCO_3$ experiment, the Gibbs free energy calculation shows decreasing energy for CH_4 formation as pH increases, and ~pH 9.5-10 the reaction is no longer thermodynamically favorable. For methanogenesis to proceed, the Gibbs free energy of reaction cannot be positive under the environmental conditions, thus there must be an error in the gas concentrations used to make this calculation. This is likely due to a poor H_2 calibration on the gas chromatograph. The GC was well calibrated to a CH_4 standard, but we were not intending to measure the H_2 as closely as the CH_4 concentrations so sufficient care was not taken to ensure accurate concentration. For the $CaCO_3$ experiment, there is a similar trend in decreasing Gibbs free energy as the pH increases, however, overall, the energetics are less favorable than in the $NaHCO_3$ experiment. This calculation also suffers from some Gibbs free energy values that are greater than 0, likely due to H_2 measurement inconsistencies.

Steady state model for $NaHCO_3$ carbon fractionation

We have generated a steady state model to describe the carbon isotope fractionation during CH_4 production from a source of $NaHCO_3$ (Figure 7), which assumes there is a nearly inexhaustible source of carbon for the microorganisms. The bioavailable aqueous carbon species that diffuses into the cell is H_2CO_3, which is already fractionated according to equations 4-8 presented above. The process of diffusion does not impart a carbon fractionation, but the rates of

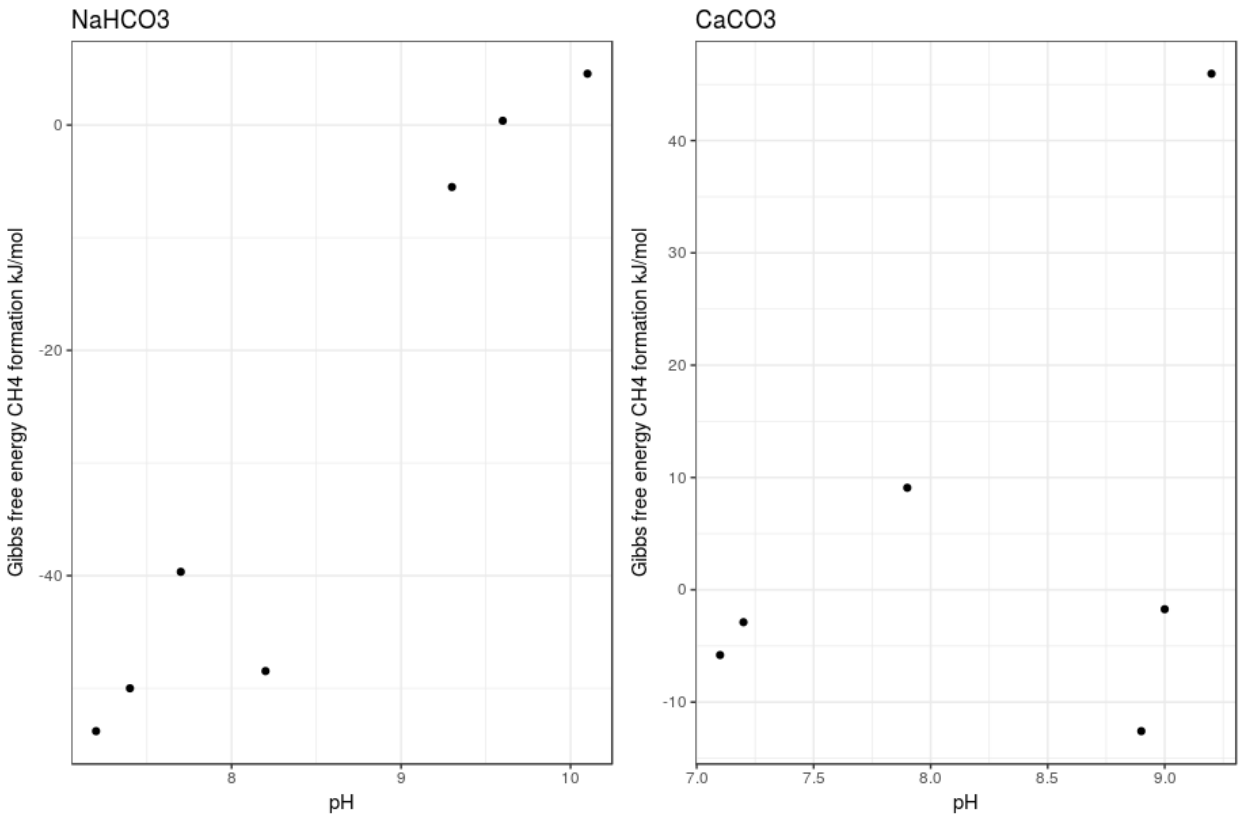

Figure 6. Gibbs free energy calculations for $NaHCO_3$ and $CaCO_3$ experiments at the time headspace gas was extracted for isotope analysis.

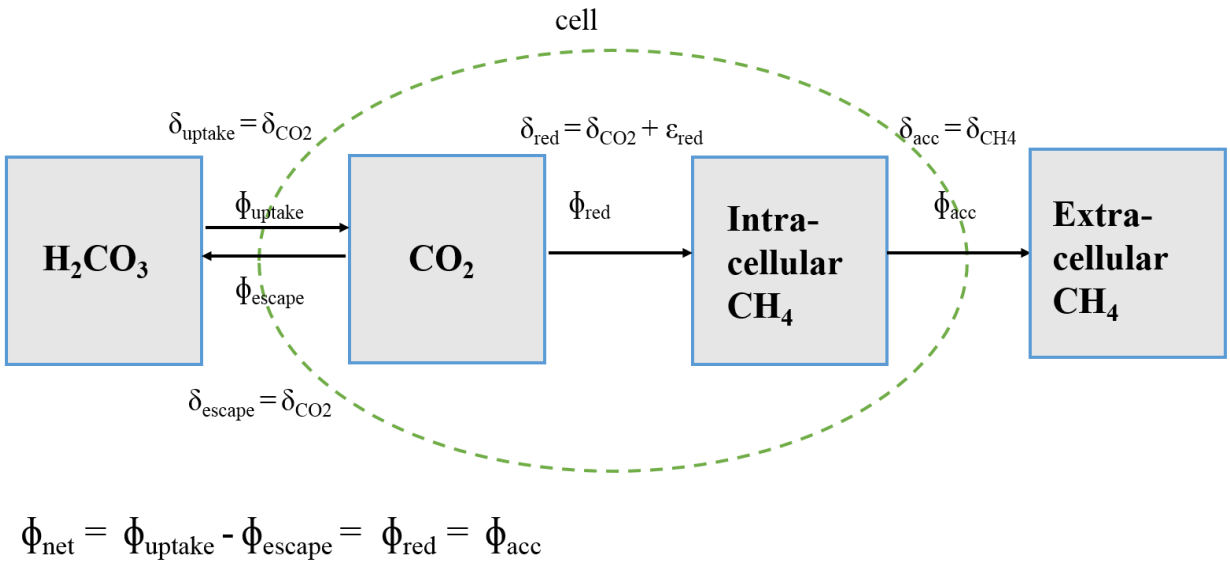

$$\phi_{net} = \phi_{uptake} - \phi_{escape} = \phi_{red} = \phi_{acc}$$

Figure 7. Steady state model of carbon isotope fractionation for $NaHCO_3$ experiments.

CO_2 uptake and escape from the cell do need to be considered. Only the process of CO_2 reduction imparts a large isotope signal according to this simple model. The initial value of $\delta^{13}C_{H2CO3}$ depends on pH, as demonstrated above. Thus, solving this model yields the simple equation:

$$\delta^{13}C_{CH4} = \delta^{13}C_{H2CO3} + \varepsilon_{red} \quad \text{(Equation 12)}$$

$$\varepsilon_{CH4\text{-}H2CO3} = \delta^{13}C_{H2CO3} - \delta^{13}C_{CH4} \quad \text{(Equation 13)}$$

The $\delta^{13}C_{CH4}$ values across a range of pH are shown in Figure 8, they decrease with pH, reaching a minimum around pH 9, and then slightly increasing.

Steady state model for $CaCO_3$ experiments

The $NaHCO_3$ model does not encompass the complexity of the rock-buffered system in the $CaCO_3$ experiments. As described above, the concentrations of bioavailable carbon are determined by the rates of carbonate dissolution and precipitation, which in turn affects the carbon isotope fractionation (Figure 9). Calcium carbon dissolves into the fluid, transforming into an inorganic carbon (DIC) pool. This forward flux of carbonate dissolution is countered by carbonate precipitation. At low pH, $CaCO_3$ dissolution rates are enhanced, whereas at higher pH, carbonate precipitation increases at higher pH. The CO_2 portion of the DIC pool diffuses into and out of the cell, which is associated with a carbon isotope fractionation. Some fraction of this CO_2 is reduced to produce intracellular CH_4, with another carbon isotope fractionation, and then that CH_4 diffuses out of the cell into the fluid, which is then measured in the form of headspace CH_4 in the vial.

The model calculates $\varepsilon_{CO2\text{-}CH4}$ values, as well as $\delta^{13}C_{CH4}$ values, as calculated using Mathematica and determining mass balance around each node:

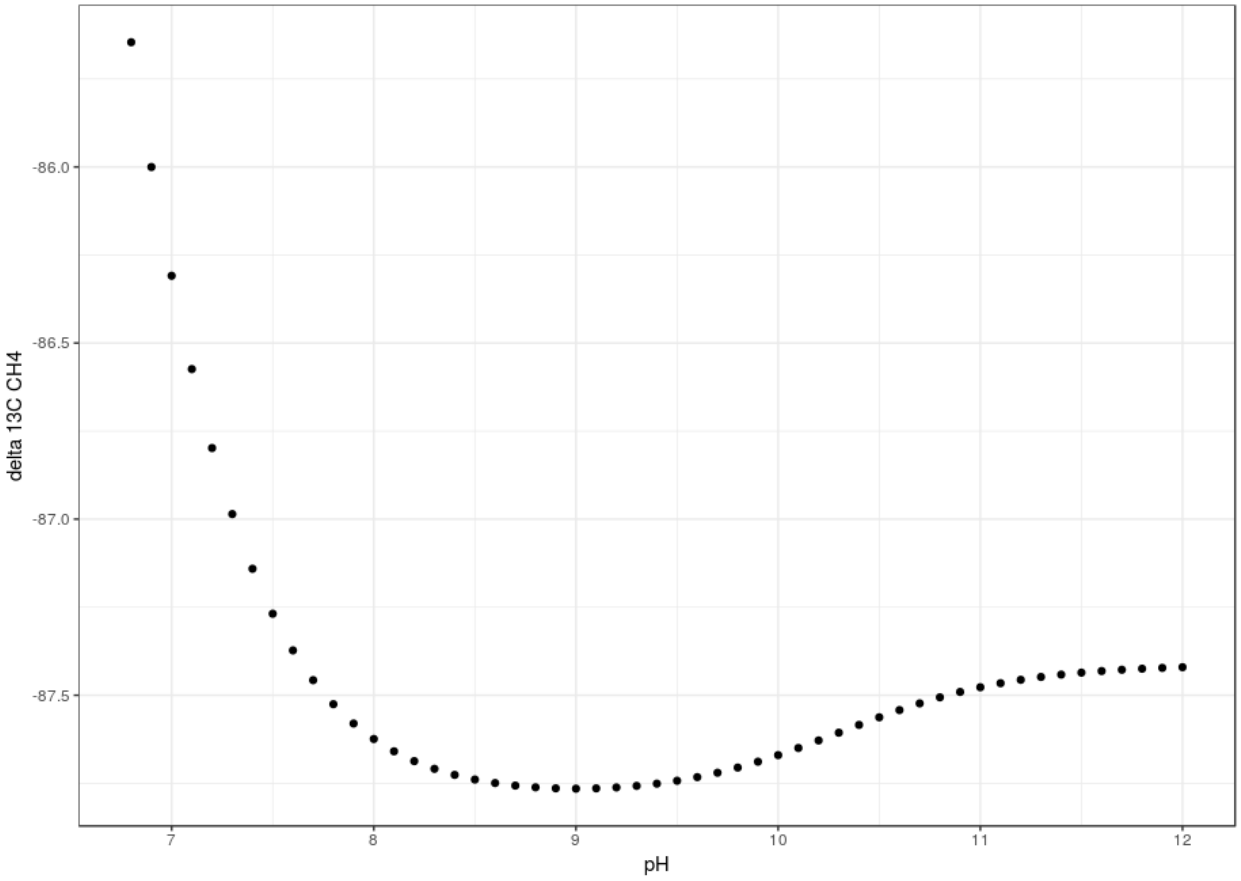

Figure 8. Modeled $\delta^{13}C$ CH_4 values versus pH, showing a maximum fractionation around 9, and then slight increase at higher pH.

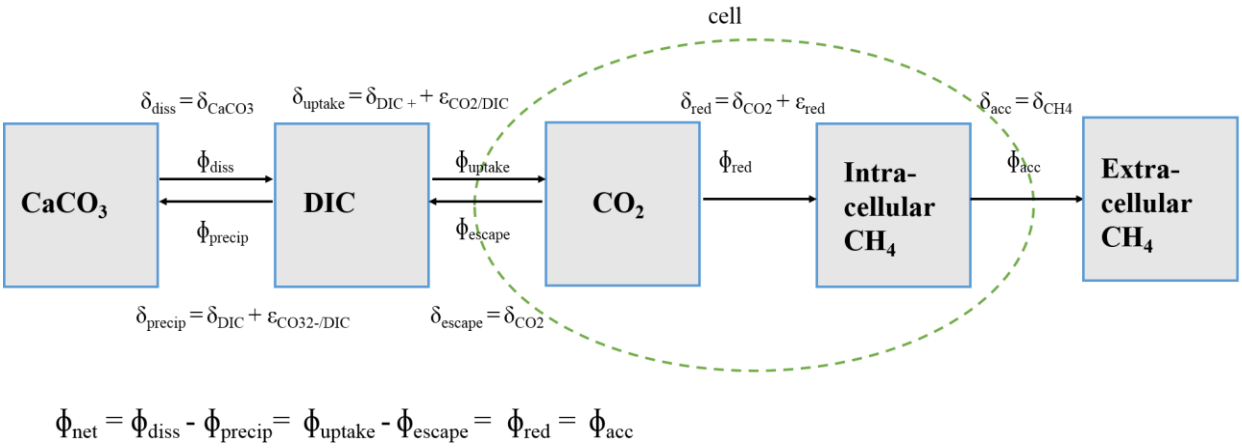

$$\phi_{net} = \phi_{diss} - \phi_{precip} = \phi_{uptake} - \phi_{escape} = \phi_{red} = \phi_{acc}$$

Figure 9. Steady state model documenting the various carbon fluxes and isotope changes in the $CaCO_3$ experiments. Calcium carbon dissolves into the inorganic carbon (DIC) pool, and then the CO_2 portion of the DIC diffuses into the cell, where it is converted into intracellular CH_4 and then diffuses into the extracellular CH_4 pool which is measured in the headspace gas.

$$\varepsilon(\mathrm{CaCO3}-\mathrm{CH4}) \rightarrow ((-f\mathrm{precip}*\varepsilon(\mathrm{CO2}-\mathrm{DIC})-f\mathrm{esc}*\ f\mathrm{precip}*\ \varepsilon(\mathrm{CO2}-\mathrm{DIC})+ f\mathrm{precip}*\ \varepsilon_{\mathrm{CO32-DIC}}+f\mathrm{esc}*f\mathrm{precip}*\ \varepsilon(\mathrm{CO32}-\mathrm{DIC})-f\mathrm{esc}*\ f\mathrm{precip}*\ \varepsilon\mathrm{red}))\ /\ (((1+ f\mathrm{esc})(1+f\mathrm{precip}))) \quad \text{(Equation 14)}$$

$$\delta\mathrm{CH4} \rightarrow (((1+f\mathrm{esc})((1+f\mathrm{precip})*\delta\mathrm{CaCO3}+f\mathrm{precip}\ (\varepsilon(\mathrm{CO2}-\mathrm{DIC})-\varepsilon(\mathrm{CO32}- \mathrm{DIC})))+f\mathrm{esc}*\ f\mathrm{precip}*\ \varepsilon\mathrm{red}))\ /\ (((1+f\mathrm{esc})(1+f\mathrm{precip}))) \quad \text{(Equation 15)}$$

with the parameters:

$$f_{esc}=\phi_{esc}/\phi_{red} \quad \text{(Equation 16)}$$

$$f_{precip}=\phi_{precip}/\phi_{red} \quad \text{(Equation 17)}$$

$\varepsilon_{CO2\text{-}DIC}$ is the fractionation between the original $CaCO_3$ carbon source and the bioavailable form of carbonate, H_2CO_3, which diffuses into the cell. $\varepsilon_{CO3\text{-}DIC}$ is the fractionation of the CO_3^{2-} portion of the carbon pool when it back-precipitates as a carbonate mineral at high pHs. ε_{red} is the average maximum observed fractionation in the experiments, which we define as -75‰.

We initially inputted a theoretical range of f_{esc} and f_{precip} values to determine the range of fractionation factors that the model would predict (Figure 10). We also explore where our experimental values for several of the reaction steps fit into the model. Suppressed fractionation, with ε of ~30 per mil, are observed over a small range of f_{esc} and f_{precip} values. When the rate of precipitation is slow relative to the rate of reduction, and f_{precip} is small, there is suppressed fractionation. Similarly, when the rate of CO_2 escape from the cell is low relative to the rate of reduction, and f_{esc} is small, there is also suppressed fractionation. Large fractionation occurs when the rate of reduction is slow compared to rates of precipitation and escape.

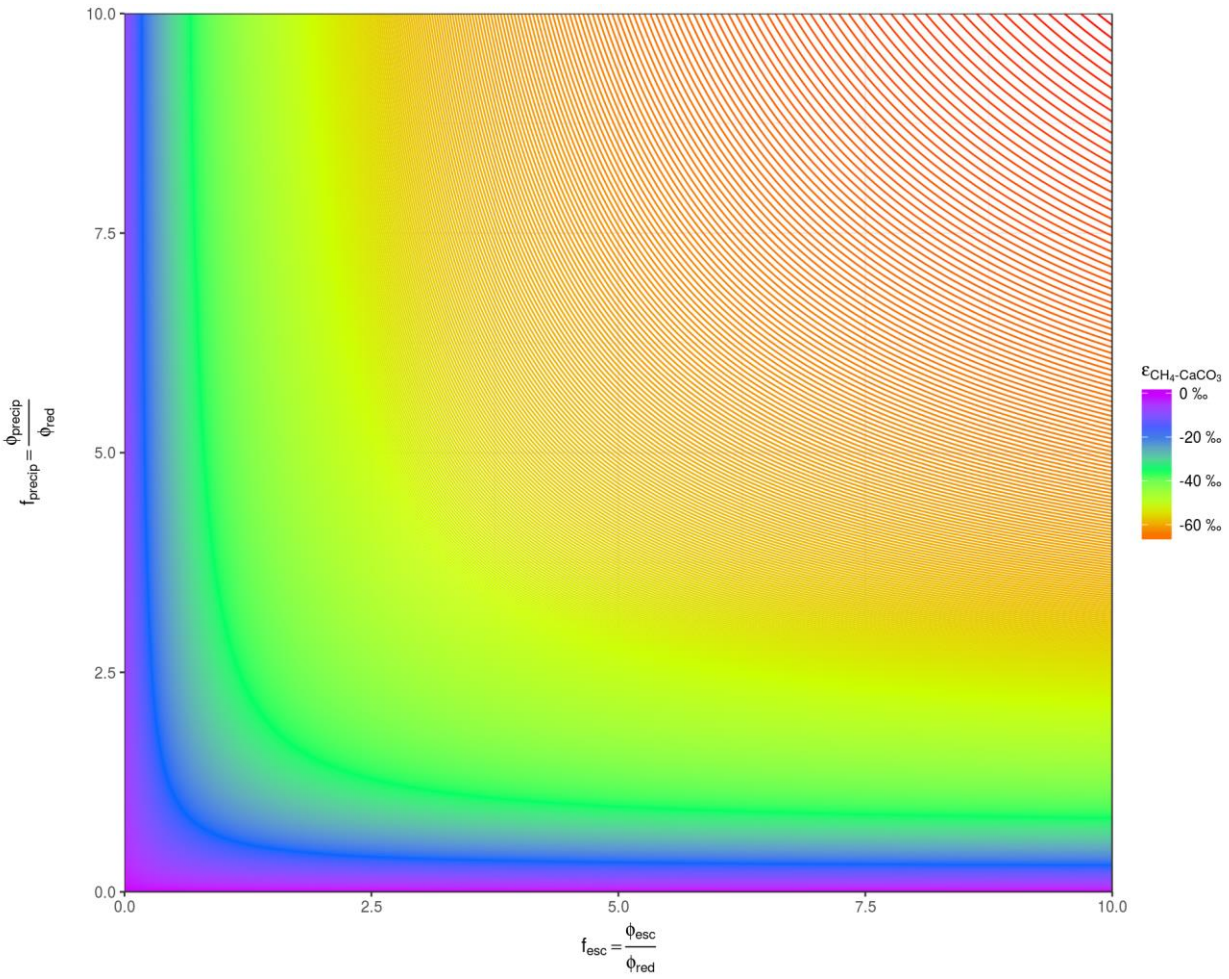

Figure 10. Range of $\varepsilon(\mathrm{CaCO3} - \mathrm{CH4})$ values obtained from varying f_{esc} and f_{precip} parameters.

Discussion

Methanobacterium fractionation factors as a function of carbon source

Methanobacterium sp. is the first methanogen isolated from actively serpentinizing fluids, and it can be grown in a defined minimal laboratory medium. It has been detected in serpentinite fluids in the Del Puerto ophiolite, the Cedars, the Zambales ophiolite and the Samail ophiolite (Blank et al., 2009; Suzuki et al., 2013; Woycheese et al., 2015; Miller et al., 2016). Methanogens living in alkaline, serpentinizing fluids are delivered fluxes of micromolar to millimolar H_2, where this H_2 may have been produced by low-temperature water/rock reactions. These methanogens, which drive CO_2 reduction by H_2, may represent one of the most primitive microbial life forms on Earth. Additionally, they may be producing some of the methane also commonly observed in serpentinizing fluids. Although an unidentified methanogen from the Cedars was enriched by Kohl et al. (2016), it was not successfully grown and propagated in a synthetic medium. Manipulating the growth of this *Methanobacterium sp.* isolate allows us to learn more about CH_4 production in not only the hyperalkaline aquifer in the Samail ophiolite, but in all hyperalkaline aquifers. This laboratory culture allows us to evaluate the growth dynamics and pH ranges under which *Methanobacterium sp.* grows more directly than with 16S rRNA or genomic studies of the fluids.

Methanobacterium produces ~0.08 mM of CH_4 growing from pH 6.87 to 9.98 in $NaHCO_3$ experiments and from pH 6.87 to 9.66 in $CaCO_3$ experiments. The CH_4 concentrations plateau at 0.08 mM due to H_2-limitation. Although serpentinizing fluids in Oman contain mM concentrations of H_2 (Barnes et al., 1978; Neal and Stanger, 1983), other sites such as the Zambales ophiolite, Lost City, and the Cedars ophiolite contain µM or lower concentrations of

H_2 (Abrajano et al., 1990; Proskurowski et al., 2008; Morrill et al., 2013). Thus, H_2-limitation may be environmentally relevant in serpentinizing locations, which in turn affects the overall amount of CH_4 generated.

Total CH_4 generation not only relies on H_2 availability, but also on the amount of bioavailable carbon in the environment. Serpentinizing fluids typically contain low concentrations of dissolved inorganic carbon (Barnes et al., 1967; Neal and Stanger, 1984). Fluids lose carbon when carbonate minerals rapidly precipitate in the alkaline Ca^{2+}-rich fluids (Barnes et al., 1978; Kelemen and Matter, 2008; Kelemen et al., 2011). Also, the reducing environment created by high concentrations of H_2 produces reduced carbon species such as formate (McCollom and Seewald, 2003; Lang et al., 2010; McCollom et al., 2010; Bradley and Summons, 2010; Etiope et al., 2011). Thus, there is oftentimes not abundant bioavailable carbon for microbial life to easily extract from fluids. We simulate abundant carbon availability in the HCO_3 experiments and carbon limited conditions in the $CaCO_3$ experiments to probe the diverse environments in which methanogens grow under alkaline conditions.

$NaHCO_3$ carbon isotope fractionation

The carbon isotope fractionation between CO_2 and CH_4 increases as pH increases in $NaHCO_3$ experiments. Across pH 7.20 - 10.08, the carbon isotope fractionation increases from 1.046 to 1.075. Additionally, as the fractionation increases, the rate of methane production decreases. We hypothesize these changes are caused by physiological adaptations to living at high pH. As pH increases, it is more challenging to maintain a proton motive force, which causes organisms to expend more energy to produce ATP, which in turn leads to slower growth rates. Additionally, the energetics for methane production become less favorable as pH increases

because there is less bioavailable carbon. This is shown in the Gibbs free energy calculations (Figure 6).

We generated a simple steady state model that shows that the resulting $\delta^{13}C_{CH4}$ is entirely dependent on the constant value of ε_{red} associated with methanogenesis and the starting isotopic composition of the bioavailable carbon. However, it does not explain the observed $\delta^{13}C_{CH4}$ values that range from -50 to -80‰ over a similar pH range. Thus, there must be another factor that needs to be considered.

The possibility of enzymatic reversibility cannot be ignored when considering carbon isotope fractionation associated with methanogenesis (Valentine et al., 2004; Thauer, 2011; Scheller et al., 2013). Methyl-coenzyme M reductase (MCR) is responsible for methane production in methanogens, and it is hypothesized that anaerobic methane oxidizers are simply using this enzyme in reverse to oxidize methane (Scheller et al., 2013). Although methanogens have not been shown to operate MCR in reverse, it is predicted to occur when the system is at thermodynamic equilibrium (Zyakun, 1996). Valentine et al. (2004) proposed that the Gibbs free energy controls the magnitude of reversibility, which is primarily controlled by H_2 partial pressure. Experiments by Valentine et al. (2004) show that abundant H_2 leads to larger Gibbs Free Energy values and less carbon fractionation, whereas limited H_2 leads to smaller Gibbs Free Energy values approaching zero and larger expressed carbon fractionation. Our calculations for the $NaHCO_3$ experiments show that at higher pH, the Gibbs Free Energy decreases, due to both H_2 and carbon limitation.

As the experiments approach Gibbs free energy values of 0, they approach thermodynamic equilibrium. This suppresses kinetic equilibrium effects, and instead leads to maximum expressed carbon fractionation, which Zyakun (1996) predicts to be 100‰ for

methanogenesis. The increasingly negative $\delta^{13}C_{CH4}$ values as pH increases shows the experiments are approaching thermodynamic equilibrium, which correspond to the Gibbs free energy calculations.

$CaCO_3$ carbon isotope fractionation

The fractionation between CO_2 and CH_4 in $CaCO_3$ experiments does not follow the same trend as seen in HCO_3 experiments. Across pH 7.06 – 8.97, the fractionation varies from 1.069 to 1.079, which is similar to the HCO_3 experiments. Yet, there is overall larger fractionation at lower pH. Then at pH 8.87 and 9.23, there is markedly suppressed fractionation. Although the $CaCO_3$ experiments also follow a trend of decreasing Gibbs free energy as pH increases, they show suppressed fractionation, which cannot be explained in a similar manner as the NaHCO3 experiments.

The suppressed fractionation is likely due to slow rates of carbonate dissolution and subsequent re-precipitation at alkaline pHs. Rates of carbonate dissolution decrease as pH increases (Chou et al., 1989), which limits the amount of bioavailable carbon. Additionally, thermodynamically, less carbonate should dissolve at higher pHs, irrespective of rate. Due to a limited carbon pool, *Methanobacterium* is consuming nearly all of the ~-7‰ CO_2, which suppresses the observed isotope effect. We investigated this with the CaCo3 steady state model, which shows that when carbon is limiting in the system, there is suppressed fractionation. However, carbon can be limiting due to slow rates of mineral dissolution, or slow rates of diffusion across the cell membrane, which leads to suppressed fractionation.

It is important to note that this model assumes that the methanogenesis reaction is irreversible and that the CH_4 quickly diffuses out of the cell into the extracellular pool. We

believe the last step of methanogenesis is sufficiently thermodynamically inhibited that it will not proceed in reverse. Additionally, we were unable to solve the model with experimental data and instead entered theoretical numbers. To better test the model in the future, we need to quantify the number of cells in the vials to calculate a cell specific rate of CO_2 reduction. It is also necessary to measure the concentrations of the DIC pool throughout the experiment, because we are estimating the amount of carbon species assuming the system is at equilibrium, thus assuming a maximum amount of carbon. We need to quantify extent of carbonate dissolution, and also need to investigate if there is reversibility.

Comparing fractionation factors to the literature

It is worthwhile to visualize the combined carbon and hydrogen CH_4 isotope values produced by *Methanobacterium* at alkaline pH in a wider perspective. Figure 3 shows the $\delta^{13}C$ and δD of CH_4 produced by a variety of abiotic and biotic processes (e.g. biotic CH_4 produced in freshwater and saltwater environments, thermogenic and abiotic CH_4 in various environments). The data were compiled by a variety of authors (Whiticar, 1999; Valentine et al., 2004; Etiope and Sherwood Lollar, 2013), and the isotopic values of CH_4 collected from subsurface hyperalkaline wells (NSHQ14 and NSHQ04) in Oman is added for comparison (Miller et al., 2016). When we add *Methanobacterium* values to this figure, the majority of the $\delta^{13}C_{CH4}$ isotope values plot in the biotic freshwater range, which is oftentimes associated with acetate fermentation (Whiticar, 1999; Etiope et al., 2011). The other main field plotted shows methane from biotic saltwater sources, which is oftentimes associated with CO_2-reduction (Whiticar, 1999; Etiope et al., 2011). *Methanobacterium* was isolated from a freshwater, hyperalkaline aquifer, yet it performs CO_2-reduction. It could be predicted that the CH_4 isotope values would

plot in both the freshwater, acetate fermentation, and saltwater, CO_2-reduction fields. We instead see points in mostly freshwater fields, but it is important to consider that the δD_{H2O} from the fluids is -1.5‰ for NSHQ04, whereas laboratory medium fluid is -108‰, which could account for the low δD_{CH4} values. Some of the $\delta^{13}C_{CH4}$ isotope values from $NaHCO_3$-fed cultures are more negative than typically seen in freshwater environments, but is consistent with saltwater, CO2-reducing environments. Also, some of the $CaCO_3$-fed cultures have such positive $\delta^{13}C$ CH_4 values that they plot in the abiogenic CH_4 field. Although this figure does not take into account the isotopic signature of the original carbon source for methanogenesis, it does provide a general framework to evaluate CH_4 isotopic values in light of their possible formation mechanisms.

Additionally, we compare the fractionation factors for *Methanobacterium* growing at alkaline pH to other known laboratory culture studies of methanogens producing CH_4 (Table 1). The maximum CO_2-CH_4 fractionation factors vary from 1.025 to 1.095 across a variety of studies (Games et al., 1978; Balabane et al., 1987; Whiticar, 1999; Chasar et al., 2000; Chidthaisong et al., 2002; Kohl et al., 2016). The maximum $\alpha_{CO2\text{-}CH4}$ is 1.076 in this study, falling on the slightly higher end of values. There is less data available for $\alpha_{H2O\text{-}CH4,}$ and the range is much broader from 1.16 – 1.86; our calculated $\alpha_{H2O\text{-}CH4}$ is 1.354, in the middle of the range. Thus, *Methanobacterium* growing at high pH does not have significantly different hydrogen isotopic fractionation factors than other methanogens.

Previous work by Kohl et al. with enrichment cultures of methanogens from the Cedars yields similar fractionation factors to this paper. The $\alpha_{CO2\text{-}CH4}$ varies from 1.068-1.078, and there was a maximum $\alpha_{H2O\text{-}CH4}$ of 1.50. These cultures were isolated from a carbonate sediment slurry from a hyperalkaline spring in reducing site fluids, then buffered at a pH of 11-12 and fed bicarbonate (Kohl et al., 2016). Kohl et al. acknowledged that further culture experiments with

methanogens at high pH are needed to understand isotope systematics of microbially produce CH_4 in serpentinizing environments. It is unclear why this study does not report suppressed carbon fractionation at alkaline pHs. The methanogens are not identified as *Methanobacterium*, thus a species difference could account for varying carbon fractionation. Additionally, the organisms were fed bicarbonate, thus they may not have been carbon limited at these high pHs.

Environmental relevance

These findings show varying carbon availability in high pH fluids leads to different carbon isotope fractionation. Thus, when looking at methane isotope values from natural environments, it is important to infer the source of carbon for methanogenesis. As we have observed, abundant bicarbonate leads to increased carbon fractionation at high pH. However, if methanogens are instead utilizing carbonate-derived carbon at high pH, we expect to see smaller than usual carbon isotope effects. The $\delta^{13}C_{CH4}$ produced under these conditions falls into the traditionally interpreted "abiogenic" methane field in Figure 3. However, not all hyperalkaline environments are carbon starved, e.g. soda lakes, or fluids that are in contact with atmospheric CO_2. When interpreting CH_4 isotopes from hyperalkaline environments, we need to consider the carbon source and availability.

For example, subsurface alkaline fluids Oman contain little dissolved inorganic carbon, but there are widespread carbonate veins in the peridotite (Kelemen et al., 2011). Thus, a likely source of carbon for methanogenesis is from slowly dissolving carbonate minerals, which we can predict would lead to suppressed carbon fractionation. Yet, the methane carbon isotope values from Oman, 2.4 and 3‰, are more positive than feasible through methanogenesis alone based on the assumption methanogens are deriving carbon from subsurface carbonates. Subsurface

carbonate veins from Oman have $\delta^{13}C_{VPDB}$ values ranging from -1.48 to -7.05‰ (Clark and Fontes, 1990; Kelemen and Matter, 2008; Kelemen et al., 2011; Mervine et al., 2014; Miller et al., 2016), thus if all dissolving carbonate were converted to CH_4, the $\delta^{13}C_{CH4}$ values could reach the same values as this DIC pool, but not more positive. Thus another mechanism in addition to, or besides, methanogenesis, must be invoked, which will be discussed in more detail later.

Etiope et al. (2011, 2013, etc.) have characterized the carbon and hydrogen isotope values of CH_4 from many serpentinizing locations, and typically classifies these values as dominantly abiotic based on $\delta^{13}C_{CH4,}$ δD_{CH4} and analyzing higher chain alkane isotopes and abundances. In light of our current work, we urge scientists to look at this data with a more critical eye and not automatically assume abiotic mechanisms are dominant based on isotope values. In order to definitively prove the case for abiotic versus biotic methane sources, it is necessary to have targeted laboratory culturing experiments and well-conducted abiotic methane production tests to show the feasibility of abiotic methane production under environmental conditions. Both of these need to be coupled with isotope measurements.

CH_4 production and subsequent oxidation

The small carbon isotope effect observed at high pH with $CaCO_3$ as a carbon source has interesting implications for carbon isotope values (2.4 and 3‰) obtained from subsurface hyperalkaline wells in Oman (Figure 3). It is apparent that methanogenesis by *Methanobacterium* does not generate the positive $\delta^{13}C_{CH4}$ values seen in the subsurface wells. If carbonate reduction were quantitative in these experiments, the resulting CH_4 would only reach ~-7‰. However, it is worthwhile to explore the effect of anaerobic methane oxidation on the most positive observed microbial $\delta^{13}C_{CH4}$ values of -28‰.

Progressive anaerobic methane oxidation of microbially produced CH_4 was modeled assuming a closed, irreversible system with Rayleigh distillation (see chapter 5). The initial $\delta^{13}C$ and δD values of the CH_4 were -27.6‰ and -410‰, respectively, based on values from *Methanobacterium* cultures. This model assumes *Methanobacterium* is growing at high pH with carbon limitation. This CH_4 is then oxidized by an unknown methane oxidizer using alternative electron acceptors (e.g. possibly sulfate) rather than O_2. The model is unidirectional with the consumption of CH_4 to CO_2 without additional or concurrent CH_4 production. The equations used were as follows:

$$\delta A = \delta A_o + \varepsilon * lnfa \text{ (Equation 18)}$$

$$\delta B = \delta A_o - \varepsilon * \frac{fa}{1-fa} * lnfa \text{ (Equation 19)}$$

where $\varepsilon = (\alpha - 1)*1000$, fa = fraction of the material that is CH_4, and δA_o is the initial value of CH_4 in the system, where δB refers to the isotopic composition of CO_2 in the system. The fractionation factors used in the model ranged from $\alpha_{CH4/CO2}$ = 1.012 – 1.039 and $\alpha_{CH4/H2O}$ = 1.109 – 1.315 (Holler et al., 2009). These values were obtained from measuring CH_4 consumed by enrichment cultures of anaerobic sea sediments and are some of the few experimental values provided for anaerobic methane oxidation. However, there is a wide range of fractionation factors possible for anaerobic methane oxidation, and the mechanisms leading to these discrepancies are unknown, but the values proposed by Holler et al. align with fractionation factor estimates proposed by other authors (Valentine et al., 2004; Conrad, 2005).

Minimum and maximum carbon and hydrogen fractionation factors were applied to methane isotope values from this study to show that although methanogenesis itself cannot generate positive $\delta^{13}C$ and δD values seen in subsurface fluids in Oman, subsequent methane oxidation of microbially produced methane could lead to these values (Figure 11). The most

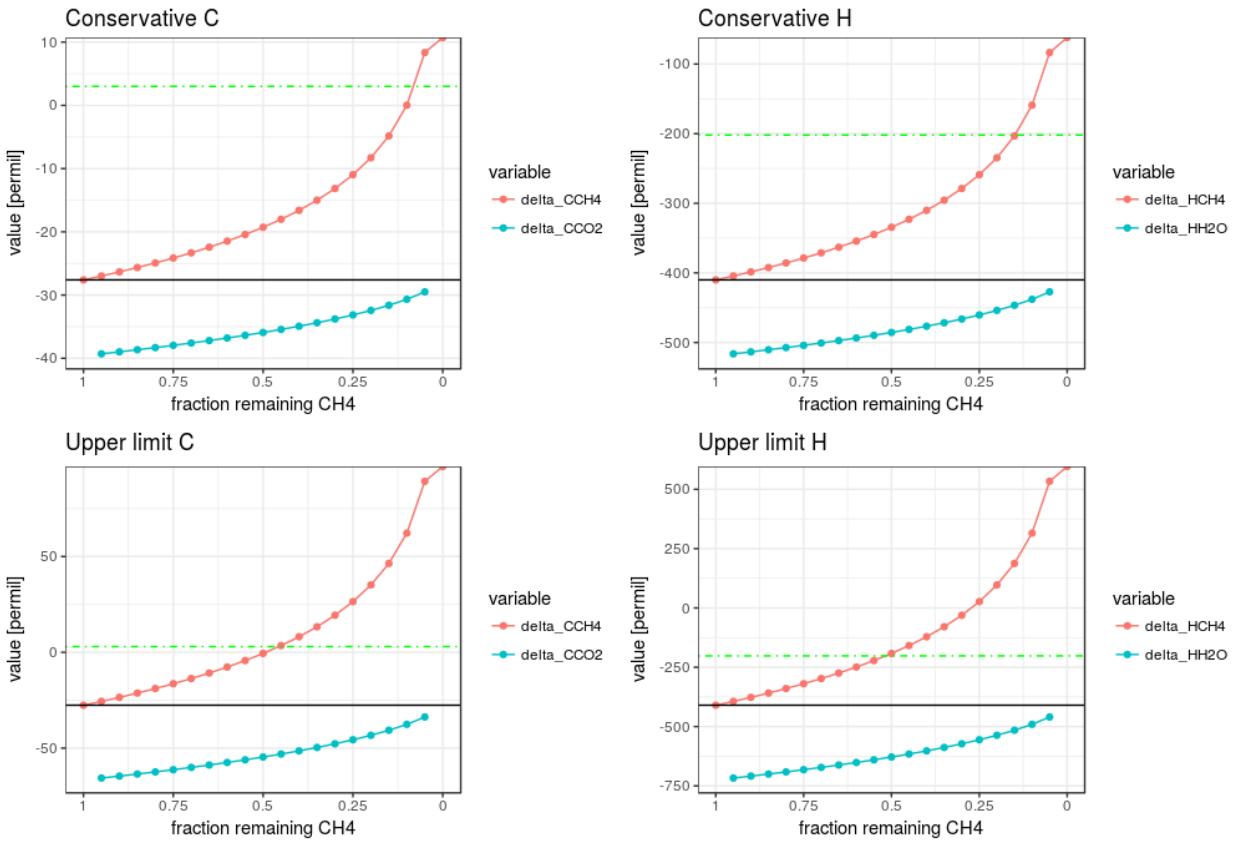

Figure 11. Modeling changes in $\delta^{13}C$ and δD of CH_4 during oxidation as vary the fractionation factors. Initial value of $\delta^{13}C$ is -27.6‰ and δD is -410‰, as indicated by solid black lines. Conservative C $\alpha_{CH4/CO2}$ is 1.012 and upper limit C $\alpha_{CH4/CO2}$ is 1.039. Conservative H $\alpha_{CH4/H2O}$ is 1.109 and upper limit H $\alpha_{CH4/H2O}$ is 1.315. Fractionation factors are taken from Holler et al. (2009). Dashed green lines indicate the $\delta^{13}C$ and δD values (+3‰ and -200‰, respectively) that have been measured from subsurface fluids rich in CH4 in a Oman hyperalkaline serpentinite aquifer.

conservative $\alpha_{CH4/CO2}$ 1.012 for $\delta^{13}C$ would produce the maximum measured $\delta^{13}C$ of 3‰ when >75% of the original CH_4 was consumed. However, if the 1.039 carbon isotope fractionation factor is applied, the residual $\delta^{13}C_{CH4}$ value of +3‰ is achieved by consuming only slightly over 50% of the original CH_4. The δD_{CH4} models are similar. The initial δD of -415.3‰ is increased during oxidation along a steeper slope than $\delta^{13}C_{CH4}$. In order to obtain δD values measured in subsurface wells from Oman, -200‰, >75% of the CH_4 would be consumed in the upper limit case, where $\alpha_{CH4/CO2}$ is 1.039. In the conservative case ($\alpha_{CH4/CO2}$ is 1.012). ~50% of the CH_4 would be consumed to get the desired δD.

Formate or CO as carbon sources for methanogenesis

Methanogens that utilize CO_2-substrates oftentimes can also grow with formate or carbon monoxide as a carbon source (Madigan, 2012). We are currently culturing *Methanobacterium sp.* with 10 mM of formate at pH 7.88 and 9.30 to investigate if it will produce CH_4, and if it does, what the resulting isotopic values are. As discussed in the introduction, formate is an environmentally relevant carbon source in serpentinizing systems, making this an interesting test that merits further study. Similarly, future work should focus on CO utilization by methanogens.

Conclusions

This paper provides CO_2-CH_4 and H_2O-CH_4 fractionation factors for *Methanobacterium sp.* growing at alkaline pH with both sodium bicarbonate and calcium carbonate. The hydrogen fractionation factors of *Methanobacterium* in both experiments are similar, with an average $\alpha_{H2O\text{-}CH4}$ of 1.309. The carbon fractionation factors of organisms consuming $NaHCO_3$ increases with increasing pH, resulting in increasingly negative $\delta^{13}C$ CH_4 that reach values as low as -85‰ permil. A trend of increased carbon isotope fractionation correlated with pH is true for $CaCO_3$ experiments up to pH ~8.8 as well. However, there is a sharp transition at pH 8.87 and 9.23 in carbonate-fed experiments, where carbon fractionation is suppressed and $\delta^{13}C$ CH_4 increases by 45‰. This results in $\delta^{13}C_{CH4}$ values of -28‰, which is a more positive $\delta^{13}C_{CH4}$ value than typically observed in methanogenesis. However, this only occurs when $CaCO_3$ is a carbon source for methanogenesis at high pH, and the extent and rate of carbonate dissolution is dictating carbon availability.

The fractionation factors and modeling allow us to predict the expected $\delta^{13}C_{CH4}$ values in high pH environments. If bioavailable carbon is not limited and *Methanobacterium* is growing slowly in fluids >pH 9, the resulting CH_4 produced by methanogenesis would show large carbon fractionation and be ~-70‰ more negative than the source carbon. It is possible the carbon fractionation would be larger in higher pH fluids when dissolved H_2, CO_2 and methane are close to thermodynamic equilibrium, giving rise to CH_4 depleted in ^{13}C up to -100‰ relative to the initial carbon source as predicted by Zyakun (1996), yet this remains to be tested. If carbon is derived from carbonate mineral dissolution at pH >9, then the resulting carbon fractionation is expected to be suppressed. This is caused by microbes consuming nearly all of the bioavailable carbon and appears to be limited by the rate of carbon dissolution at high pH. Additionally, the

carbon and isotope values observed in this laboratory study allow us to model the effects of methane oxidation under high pH and carbon-limited conditions. It is possible to oxidize ~50% of CH_4 with a $\delta^{13}C_{CH4}$ values of -28‰ to produce a $\delta^{13}C_{CH4}$ of +2‰ as measured from subsurface wells in Oman.

Methane isotope compositions aid in predicting the source of CH_4 in an environment, but as this study shows, it is necessary to understand the carbon source for methanogenesis. There is evidence of modern-day CH_4 on Mars that may indicate microbial activity or a favorable environment for microbial activity (Chen P, 2015). The search for CH_4 on other planets highlights the importance of understanding C and H fractionation during methanogenesis, with an emphasis on tracking the isotopic systematics of the source carbon to the final CH_4 product to robustly indicate microbial activity. We were not successful in growing the methanogens above pH 10.23, thus future work focusing on hyperalkaline pH isotope systematics would be helpful. Future genomic analysis of *Methanobacterium sp*. would also give insight into understanding how *Methanobacterium* copes with high pH when generating a proton motive force.

Acknowledgements

We would like to thank the Fierer lab at the University of Colorado at Boulder for their sequencing help. This research was funded by the Department of Energy (DE-SC0006886) and the NASA Astrobiology Institute (Cooperative Agreement NNA15BB02A).

References

Abrajano T. A., Sturchio N. C., Kennedy B. M., Lyon G. L., Muehlenbachs K. and Bohlke J. K. (1990) Geochemistry of reduced gas related to serpentinization of the Zambales ophiolite, Philippines. *Appl. Geochem.* **5**, 625–630.

Balabane M., Galimov E., Hermann M. and Létolle R. (1987) Hydrogen and carbon isotope fractionation during experimental production of bacterial methane. *Org. Geochem.* **11**, 115–119.

Barberán A., Ladau J., Leff J. W., Pollard K. S., Menninger H. L., Dunn R. R. and Fierer N. (2015) Continental-scale distributions of dust-associated bacteria and fungi. *Proc. Natl. Acad. Sci.* **112**, 5756–5761.

Barnes I., LaMarche V. C. and Himmelberg G. (1967) Geochemical Evidence of Present-Day Serpentinization. *Science* **156**, 830–832.

Barnes I., O'Neil J. R. and Trescases J. J. (1978) Present day serpentinization in New Caledonia, Oman and Yugoslavia. *Geochim. Cosmochim. Acta* **42**, 144–145.

Benjamin M. M. (2002) *Water Chemistry*., Waveland Press, Inc., Long Grove, Illinois.

Blank J. G., Green S. J., Blake D., Valley J. W., Kita N. T., Treiman A. and Dobson P. F. (2009) An alkaline spring system within the Del Puerto Ophiolite (California, USA): A Mars analog site. *Planet. Space Sci.* **57**, 533–540.

Bowers R. M., Clements N., Emerson J. B., Wiedinmyer C., Hannigan M. P. and Fierer N. (2013) Seasonal Variability in Bacterial and Fungal Diversity of the Near-Surface Atmosphere. *Environ. Sci. Technol.* **47**, 12097–12106.

Bradley A. S. and Summons R. E. (2010) Multiple origins of methane at the Lost City Hydrothermal Field. *Earth Planet. Sci. Lett.* **297**, 34–41.

Brazelton W. J., Schrenk M. O., Kelley D. S. and Baross J. A. (2006) Methane- and Sulfur-Metabolizing Microbial Communities Dominate the Lost City Hydrothermal Field Ecosystem. *Appl. Environ. Microbiol.* **72**, 6257–6270.

Chapelle F. H., O'Neill K., Bradley P. M., Methé B. A., Ciufo S. A., Knobel L. L. and Lovley D. R. (2002) A hydrogen-based subsurface microbial community dominated by methanogens. *Nature* **415**, 312–315.

Chasar L. S., Chanton J. P., Glaser P. H. and Siegel D. I. (2000) Methane Concentration and Stable Isotope Distribution as Evidence of Rhizospheric Processes: Comparison of a Fen and Bog in the Glacial Lake Agassiz Peatland Complex. *Ann. Bot.* **86**, 655–663.

Chen P Y. Y. (2015) Methane on Mars. *J. Astrobiol. Outreach* **3**. Available at: http://esciencecentral.org/journals/methane-on-mars-2332-2519-1000125.php?aid=38624 [Accessed June 28, 2016].

Chidthaisong A., Chin K.-J., Valentine D. L. and Tyler S. C. (2002) A comparison of isotope fractionation of carbon and hydrogen from paddy field rice roots and soil bacterial enrichments during CO2/H2 methanogenesis. *Geochim. Cosmochim. Acta* **66**, 983–995.

Chou L., Garrels R. M. and Wollast R. (1989) Comparative study of the kinetics and mechanisms of dissolution of carbonate minerals. *Chem. Geol.* **78**, 269–282.

Clark I. D. and Fontes J.-C. (1990) Paleoclimatic reconstruction in northern Oman based on carbonates from hyperalkaline groundwaters. *Quat. Res.* **33**, 320–336.

Conrad R. (2005) Quantification of methanogenic pathways using stable carbon isotopic signatures: a review and a proposal. *Org. Geochem.* **36**, 739–752.

Edgar R. C. (2013) UPARSE: highly accurate OTU sequences from microbial amplicon reads. *Nat. Methods* **10**, 996–8.

Eecke H. C. V., Butterfield D. A., Huber J. A., Lilley M. D., Olson E. J., Roe K. K., Evans L. J., Merkel A. Y., Cantin H. V. and Holden J. F. (2012) Hydrogen-limited growth of hyperthermophilic methanogens at deep-sea hydrothermal vents. *Proc. Natl. Acad. Sci.* **109**, 13674–13679.

Ehlmann B. L., Mustard J. F. and Murchie S. L. (2010) Geologic setting of serpentine deposits on Mars: SERPENTINE ON MARS. *Geophys. Res. Lett.* **37**, n/a-n/a.

Emerson J. B., Keady P. B., Brewer T. E., Clements N., Morgan E. E., Awerbuch J., Miller S. L. and Fierer N. (2015) Impacts of Flood Damage on Airborne Bacteria and Fungi in Homes after the 2013 Colorado Front Range Flood. *Environ. Sci. Technol.* **49**, 2675–2684.

Etiope G. (2009) Natural emissions of methane from geological seepage in Europe. *Atmos. Environ.* **43**, 1430–1443.

Etiope G., Ehlmann B. L. and Schoell M. (2013) Low temperature production and exhalation of methane from serpentinized rocks on Earth: A potential analog for methane production on Mars. *Icarus* **224**, 276–285.

Etiope G., Schoell M. and Hosgörmez H. (2011) Abiotic methane flux from the Chimaera seep and Tekirova ophiolites (Turkey): Understanding gas exhalation from low temperature serpentinization and implications for Mars. *Earth Planet. Sci. Lett.* **310**, 96–104.

Etiope G. and Sherwood Lollar B. (2013) Abiotic Methane on Earth. *Rev. Geophys.* **51**, 276–299.

Games L. M., HayesRobert J. M. and Gunsalus P. (1978) Methane-producing bacteria: natural fractionations of the stable carbon isotopes. *Geochim. Cosmochim. Acta* **42**, 1295–1297.

Glein C. R., Baross J. A. and Waite Jr. J. H. (2015) The pH of Enceladus' ocean. *Geochim. Cosmochim. Acta* **162**, 202–219.

Holler T., Wegener G., Knittel K., Boetius A., Brunner B., Kuypers M. M. M. and Widdel F. (2009) Substantial 13C/12C and D/H fractionation during anaerobic oxidation of methane by marine consortia enriched in vitro. *Environ. Microbiol. Rep.* **1**, 370–376.

Kelemen P. B. and Matter J. (2008) In situ carbonation of peridotite for CO2 storage. *Proc. Natl. Acad. Sci.* **105**, 17295–17300.

Kelemen P. B., Matter J., Streit E. E., Rudge J. F., Curry W. B. and Blusztajn J. (2011) Rates and Mechanisms of Mineral Carbonation in Peridotite: Natural Processes and Recipes for Enhanced, in situ CO2 Capture and Storage. *Annu. Rev. Earth Planet. Sci.* **39**, 545–576.

Kiene R. P., Oremland R. S., Catena A., Miller L. G. and Capone D. G. (1986) Metabolism of Reduced Methylated Sulfur Compounds in Anaerobic Sediments and by a Pure Culture of an Estuarine Methanogen. *Appl. Environ. Microbiol.* **52**, 1037–1045.

Klein F., Bach W. and McCollom T. M. (2013) Compositional controls on hydrogen generation during serpentinization of ultramafic rocks. *Lithos* **178**, 55–69.

Klein F., Grozeva N. G., Seewald J. S., McCollom T. M., Humphris S. E., Moskowitz B., Berquó T. S. and Kahl W.-A. (2015) Experimental constraints on fluid-rock reactions during incipient serpentinization of harzburgite. *Am. Mineral.* **100**, 991–1002.

Klein F., Humphris S. E., Guo W., Schubotz F., Schwarzenbach E. M. and Orsi W. D. (2015) Fluid mixing and the deep biosphere of a fossil Lost City-type hydrothermal system at the Iberia Margin. *Proc. Natl. Acad. Sci.*, 201504674.

Kohl L., Cumming E., Cox A., Rietze A., Morrissey L., Lang S. Q., Richter A., Suzuki S., Nealson K. H. and Morrill P. L. (2016) Exploring the metabolic potential of microbial communities in ultra-basic, reducing springs at The Cedars, CA, USA: Experimental evidence of microbial methanogenesis and heterotrophic acetogenesis. *J. Geophys. Res. Biogeosciences* **121**, 2015JG003233.

Kotelnikova S., Macario A. J. and Pedersen K. (1998) Methanobacterium subterraneum sp. nov., a new alkaliphilic, eurythermic and halotolerant methanogen isolated from deep granitic groundwater. *Int. J. Syst. Bacteriol.* **48**, 357–367.

Kral T. A., Birch W., Lavender L. E. and Virden B. T. (2014) Potential use of highly insoluble carbonates as carbon sources by methanogens in the subsurface of Mars. *Planet. Space Sci.* **101**, 181–185.

Lang S. Q., Butterfield D. A., Schulte M., Kelley D. S. and Lilley M. D. (2010) Elevated concentrations of formate, acetate and dissolved organic carbon found at the Lost City hydrothermal field. *Geochim. Cosmochim. Acta* **74**, 941–952.

Madigan M. T. (2012) *Brock biology of microorganisms*., Benjamin Cummings, San Francisco.

Mathrani I. M., Boone D. R., Mah R. A., Fox G. E. and Lau P. P. (1988) Methanohalophilus zhilinae sp. nov., an alkaliphilic, halophilic, methylotrophic methanogen. *Int. J. Syst. Bacteriol.* **38**, 139–142.

Mayhew L. E., Ellison E. T., McCollom T. M., Trainor T. P. and Templeton A. S. (2013) Hydrogen generation from low-temperature water–rock reactions. *Nat. Geosci.* **6**, 478–484.

McCollom T. M. and Bach W. (2009) Thermodynamic constraints on hydrogen generation during serpentinization of ultramafic rocks. *Geochim. Cosmochim. Acta* **73**, 856–875.

McCollom T. M., Lollar B. S., Lacrampe-Couloume G. and Seewald J. S. (2010) The influence of carbon source on abiotic organic synthesis and carbon isotope fractionation under hydrothermal conditions. *Geochim. Cosmochim. Acta* **74**, 2717–2740.

McCollom T. M. and Seewald J. S. (2003) Experimental constraints on the hydrothermal reactivity of organic acids and acid anions: I. Formic acid and formate. *Geochim. Cosmochim. Acta* **67**, 3625–3644.

McDonald D., Price M. N., Goodrich J., Nawrocki E. P., DeSantis T. Z., Probst A., Andersen G. L., Knight R. and Hugenholtz P. (2012) An improved Greengenes taxonomy with explicit ranks for ecological and evolutionary analyses of bacteria and archaea. *ISME J.* **6**, 610–8.

Mervine E. M., Humphris S. E., Sims K. W. W., Kelemen P. B. and Jenkins W. J. (2014) Carbonation rates of peridotite in the Samail Ophiolite, Sultanate of Oman, constrained through 14C dating and stable isotopes. *Geochim. Cosmochim. Acta* **126**, 371–397.

Miller H. M., Matter J. M., Kelemen P., Ellison E. T., Conrad M. E., Fierer N., Ruchala T., Tominaga M. and Templeton A. S. (2016) Modern water/rock reactions in Oman hyperalkaline peridotite aquifers and implications for microbial habitability. *Geochim. Cosmochim. Acta* **179**, 217–241.

Mook W. G. (1986) 13C in atmospheric CO2. *Neth. J. Sea Res.* **20**, 211–223.

Morrill P. L., Brazelton W. J., Kohl L., Rietze A., Miles S. M., Kavanagh H., Schrenk M. O., Ziegler S. E. and Lang S. Q. (2014) Investigations of potential microbial methanogenic and carbon monoxide utilization pathways in ultra-basic reducing springs associated with present-day continental serpentinization: the Tablelands, NL, CAN. *Front. Microbiol.* **5**. Available at: http://www.ncbi.nlm.nih.gov/pmc/articles/PMC4230201/ [Accessed January 6, 2015].

Morrill P. L., Kuenen J. G., Johnson O. J., Suzuki S., Rietze A., Sessions A. L., Fogel M. L. and Nealson K. H. (2013) Geochemistry and geobiology of a present-day serpentinization site in California: The Cedars. *Geochim. Cosmochim. Acta* **109**, 222–240.

Moser D. P., Gihring T. M., Brockman F. J., Fredrickson J. K., Balkwill D. L., Dollhopf M. E., Lollar B. S., Pratt L. M., Boice E., Southam G., Wanger G., Baker B. J., Pfiffner S. M., Lin L.-H. and Onstott T. C. (2005) Desulfotomaculum and Methanobacterium spp. Dominate a 4- to 5-Kilometer-Deep Fault. *Appl. Environ. Microbiol.* **71**, 8773–8783.

Neal C. and Stanger G. (1984) Calcium and magnesium hydroxide precipitation from alkaline groundwaters in Oman, and their significance to the process of serpentinization. *Miner. Mag* **48**, 237–241.

Neal C. and Stanger G. (1983) Hydrogen generation from mantle source rocks in Oman. *Earth Planet. Sci. Lett.* **66**, 315–320.

Nealson K. H., Inagaki F. and Takai K. (2005) Hydrogen-driven subsurface lithoautotrophic microbial ecosystems (SLiMEs): do they exist and why should we care? *Trends Microbiol.* **13**, 405–410.

Oremland R. S., Marsh L. and DesMarais D. J. (1982) Methanogenesis in Big Soda Lake, Nevada: an Alkaline, Moderately Hypersaline Desert Lake. *Appl. Environ. Microbiol.* **43**, 462–468.

Oze C. (2005) Have olivine, will gas: Serpentinization and the abiogenic production of methane on Mars. *Geophys. Res. Lett.* **32**. Available at: http://doi.wiley.com/10.1029/2005GL022691 [Accessed February 7, 2014].

Proskurowski G., Lilley M. D., Kelley D. S. and Olson E. J. (2006) Low temperature volatile production at the Lost City Hydrothermal Field, evidence from a hydrogen stable isotope geothermometer. *Chem. Geol.* **229**, 331–343.

Proskurowski G., Lilley M. D., Seewald J. S., Olson E. J., Früh-Green G. L., Lupton J. E., Sylva S. P. and Kelley D. S. (2008) Abiogenic hydrocarbon production at Lost City hydrothermal field. *Science* **319**, 604–607.

R Development Core Team (2008) *R: A language and environment for statistical computing*., R Foundation for Statistical Computing, Vienna, Austria. Available at: http://www.R-project.org.

Russell M. J., Hall A. J. and Martin W. (2010) Serpentinization as a source of energy at the origin of life: Serpentinization and the emergence of life. *Geobiology* **8**, 355–371.

Scheller S., Goenrich M., Thauer R. K. and Jaun B. (2013) Methyl-Coenzyme M Reductase from Methanogenic Archaea: Isotope Effects on the Formation and Anaerobic Oxidation of Methane. *J. Am. Chem. Soc.* **135**, 14975–14984.

Schoell M. (1980) The hydrogen and carbon isotopic composition of methane from natural gases of various origins. *Geochim. Cosmochim. Acta* **44**, 649–661.

Sleep N. H., Meibom A., Fridriksson T., Coleman R. G. and Bird D. K. (2004) H2-rich fluids from serpentinization: geochemical and biotic implications. *Proc. Natl. Acad. Sci. U. S. A.* **101**, 12818–12823.

Suzuki S., Ishii S., Wu A., Cheung A., Tenney A., Wanger G., Kuenen J. G. and Nealson K. H. (2013) Microbial diversity in The Cedars, an ultrabasic, ultrareducing, and low salinity serpentinizing ecosystem. *Proc. Natl. Acad. Sci.* **110**, 15336–15341.

Suzuki S., Kuenen J. G., Schipper K., van der Velde S., Ishii S., Wu A., Sorokin D. Y., Tenney A., Meng X., Morrill P. L., Kamagata Y., Muyzer G. and Nealson K. H. (2014) Physiological and genomic features of highly alkaliphilic hydrogen-utilizing Betaproteobacteria from a continental serpentinizing site. *Nat. Commun.* **5**. Available at: http://www.nature.com/ncomms/2014/140521/ncomms4900/full/ncomms4900.html [Accessed November 19, 2014].

Szponar N., Brazelton W. J., Schrenk M. O., Bower D. M., Steele A. and Morrill P. L. (2013) Geochemistry of a continental site of serpentinization, the Tablelands Ophiolite, Gros Morne National Park: A Mars analogue. *Icarus* **224**, 286–296.

Takai K., Nakamura K., Toki T., Tsunogai U., Miyazaki M., Miyazaki J., Hirayama H., Nakagawa S., Nunoura T. and Horikoshi K. (2008) Cell proliferation at 122°C and

isotopically heavy CH4 production by a hyperthermophilic methanogen under high-pressure cultivation. *Proc. Natl. Acad. Sci.* **105**, 10949–10954.

Thauer R. K. (2011) Anaerobic oxidation of methane with sulfate: on the reversibility of the reactions that are catalyzed by enzymes also involved in methanogenesis from CO2. *Curr. Opin. Microbiol.* **14**, 292–299.

Valentine D. L., Chidthaisong A., Rice A., Reeburgh W. S. and Tyler S. C. (2004) Carbon and hydrogen isotope fractionation by moderately thermophilic methanogens1. *Geochim. Cosmochim. Acta* **68**, 1571–1590.

Wang Q., Garrity G. M., Tiedje J. M. and Cole J. R. (2007) Naive Bayesian classifier for rapid assignment of rRNA sequences into the new bacterial taxonomy. *Appl. Environ. Microbiol.* **73**, 5261–7.

Whiticar M. J. (1999) Carbon and hydrogen isotope systematics of bacterial formation and oxidation of methane. *Chem. Geol.* **161**, 291–314.

Worakit S., BOONE D. R., MAH R. A., ABDEL-SAMIE M.-E. and El-Halwagi M. M. (1986) Methanobacterium alcaliphilum sp. nov., an H2-utilizing methanogen that grows at high pH values. *Int. J. Syst. Bacteriol.* **36**, 380–382.

Woycheese K. M., Meyer-Dombard D. R., Cardace D., Argayosa A. M. and Arcilla C. A. (2015) Out of the dark: transitional subsurface-to-surface microbial diversity in a terrestrial serpentinizing seep (Manleluag, Pangasinan, the Philippines). *Front. Microbiol.* **6**. Available at: http://journal.frontiersin.org/Article/10.3389/fmicb.2015.00044/abstract [Accessed May 21, 2015].

Zeikus J. G. (1977) The biology of methanogenic bacteria. *Bacteriol. Rev.* **41**, 514–541.

Zyakun A. M. (1996) Potential of 13C/12C variations in bacterial methane in assessing origin of environmental methane. Available at: http://archives.datapages.com/data/specpubs/memoir66/25/0341.htm [Accessed December 15, 2016].

CHAPTER 6

Conclusions and Future Work

Research in the geomicrobiology of serpentinizing systems has rapidly increased since the discovery in the early 2000s of low-temperature serpentinization in Lost City. Technological advancements make it possible to easily, quickly, and cheaply sequence small amounts of 16S rRNA, so it is now possible to look for signs of life in these, and other, extreme environments on Earth. Searching for geologic reactions that fuel life not only helps constrain the limits of life on Earth, but it gives insight into possible locations on other rocky bodies in our Solar System where microbial life may be found.

Overall, this dissertation focuses on water/rock reactions leading to hydrogen production in the Samail ophiolite. All experimental and analytical work was conducted with partially serpentinized peridotite from both the surface and subsurface of the Samail ophiolite. Fe(II)-bearing brucite is a key reactive mineral that can quickly destabilize to produce hydrogen and Fe(III)-bearing minerals, such as magnetite, under low-temperatures and fluid compositions similar to those found in shallow serpentinizing aquifers. These observations on the reactivity of Fe(II)-bearing brucite are relevant for any system with partially serpentinized rock, however, it is important to note these reactions occur over short time scales. Additionally, this work investigates methanogenic microbial activity that may subsist off geologically-produced hydrogen. CH_4 is found in mM concentrations in subsurface fluids from the Samail ophiolite, and it has d13C values as positive as +3‰. The source of the CH_4 is presumed to be abiotic based off its isotope values, however, we wanted to investigate the possibility of methanogenesis in these fluids. *Methanobacterium spp.* was isolated from subsurface hyperalkaline fluids in Oman and the isotope values of the CH_4 produced over a range of alkaline pHs were measured to calculate carbon and hydrogen fractionation factors. The resulting wide range of carbon fractionation factors over alkaline pHs and under varying carbon limitation increases the range of

biotic carbon isotope values in serpentinizing systems. However, as with most studies, the more we learn about serpentinizing environments, the more questions we have. Thus, this conclusion muses on several of the previously discussed topics and provides input about future fruitful research topics.

Water/rock reactions

1. *Hydrogen*

The heart of this work surrounds hydrogen production from water/rock reactions. I made the discovery that the dissolution of Fe(II)-bearing brucite can drive hydrogen production at low temperatures in partially serpentinized rocks, yet the controlling factors for this reaction are still unconstrained. There seems to be increased hydrogen production when $Ca(OH)_2$ is added to solution. However, I was unable to consistently reproduce results to synthesize a cohesive hypothesis. I think future work should focus on systematically increasing Ca^{2+} levels in solution to look for an effect on rate and extent of H_2 production. Future work should also focus on factors that increase the rate of brucite dissolution, which is likely affected by aqueous silica concentrations. It is valuable to understand what controls H_2 production at low temperatures because it constrains what geochemical conditions may lead to high concentrations of H_2, and potential associated microbial life.

2. *Iron*

Along with Dr. Lisa Mayhew and Eric Ellison, I have worked to advance our synchrotron capabilities to quantify the ratio of Fe^{III}/Fe_{total} in silicates. This technique involves mapping the pre-edge features of Fe-spectra with a high resolution, and then comparing the pre-edge centroids

and intensities to know standards to determine $Fe^{III}/Fe_{total.}$ This is a powerful tool to quantify the extent of Fe mineral oxidation with an error of ~10% on the scale of ~2 μm, whereas before we were merely qualitative in defining relative oxidation states of minerals. Future work can more exactly pinpoint Fe-oxidation changes in minerals due to water/rock reaction. However, my experimental work has continually been challenged by small extent of mineral reaction. I believe conducting water/rock reactions with an isotope tracer of reaction would be a helpful tool to look at small-scale reactions. For example, it is unclear if Fe-bearing serpentine is dissolving and re-precipitating with a different Fe^{III}/Fe_{total} ratio under low-temperature laboratory experiments. It could be useful to spike the solution with an oxygen 17 or 18 label and then track its presence in minerals to assess new mineral formation. Oxygen seems like the ideal isotope tracer because it would be presumably incorporated into new serpentine, brucite, or magnetite, which all are predicted to form during low-temperature serpentinization reactions. This would be a large undertaking with significant method development phases and would probably be best accomplished using secondary ion mass spectrometry (SIMS) so spatial changes could be observed and paired with changes in Fe^{III}/Fe_{total} ratios obtained from synchrotron work.

3. Carbon

A common theme in studying water/rock reactions in serpentinizing systems is the transformation of carbon. Carbon may be sequestered into carbonate minerals, which could be engineered to mitigate the effects of global warming (Kelemen and Matter, 2008) Additionally, inorganic carbon in the form of aqueous CO_2 or carbonate may convert to CH_4 or higher chain alkanes, formate, acetate or solid carbonaceous material, which can then be utilized by microbes

(McCollom and Seewald, 2001; Pasini et al., 2013; McCollom, 2016). However, the geochemical constraints determining these transformations are not well defined.

CH_4 is present in many serpentinizing environments (Barnes et al., 1978; Abrajano et al., 1990; Proskurowski et al., 2006; Lang et al., 2010; Morrill et al., 2014; Miller et al., 2016), and it is of great interest to know whether CH_4 can form abiotially at 100°C or below. Our experiments do not show abiotic formation of CH_4 at 100°C, yet CH_4 has been observed as a product in water/rock reaction experiments at 30, 50 and 70°C in previous studies (Neubeck et al., 2011; Okland et al., 2014). It is unclear if such CH_4 formed as the result of Fischer-Tropsch type (FTT) reactions or was released from fluid inclusions or the butyl stoppers used in the experiment. FTT reactions are kinetically inhibited at less than 200°C and usually require the presence of a mineral catalyst like awaruite even at high temperatures (Berndt et al., 1996; McCollom and Seewald, 2001). It has been suggested that at temperatures <50°C, CH_4 production is possible in the presence of catalysts such as ruthenium, rhodium, or chromium minerals commonly found in serpentinites (Etiope et al., 2013). However, although magnetite and chromite were present during our experiments, and H_2 was produced in the presence of CO_2, we did not observe detectable CH_4.

The presence of formate and acetate both in environmental fluids and experimental water/rock reaction fluids is intriguing because it is unclear how it forms at low temperatures, and is also an excellent fuel source for subsurface microorganism. What are the specific reactions leading to their formation if they are abiotically produced? Is a mineral catalyst required? Acetate formation in our 100°C water/rock reactions is enigmatic. Acetate, propionate, and butyrate formation have been modeled from 0-350°C, and are thermodynamically favored when cold, oxidized seawater rich in bicarbonate mixes with hot, reduced hydrothermal fluids

(Shock and Schulte, 1998). Yet the more complex carboxylic acids, such as acetate, propionate, and butyrate may be more difficult to synthesize under our laboratory conditions because our batch water/rock reactions do not have a compositional gradient characterized by disequilibrium between two fluids. Lever (2012) assessed the thermodynamics of biotic acetate formation from H_2-CO_2 and H_2-formate in the temperature ranges in which life has been found. It is feasible that acetate formation may be thermodynamically favorable at the micromolar $H_{2(aq)}$ concentrations achieved in our experiments at 100°C. However, a mechanistic pathway for acetate formation in the absence of biology is not yet known, and experimental studies assessing low-temperature acetate formation need to be conducted.

In future work, to truly understand carbon cycling in water/rock reactions leading to H_2 production, we suggest that the conversion of bicarbonate species into organic acids (and potential carbonaceous solids) be rigorously tested using a $NaH^{13}CO_3$ tracer (McCollom and Seewald, 2001). All of the added carbon would be labeled, and the incorporation of the label into organic acids could be measured by HPLC methods, which were not available to us during this study. In addition, the mechanism of CO_2-reduction should be assessed, in particular whether or not mineral catalysts, such as the relict chromites and newly formed magnetite, are required to promote the conversion of CO_2 to low molecular weight organic acids as has often been invoked for higher temperature organic synthesis reactions in peridotites (Shock and Schulte, 1998; McDermott et al., 2015).

Another outstanding question is why don't we observe carbonate formation in the water/rock experiments? Carbonates are predicted to form as Type I fluids percolate into the subsurface and become out of equilibrium with the atmosphere, precipitating Mg^{2+}, Ca^{2+}, and $HCO3^-$, reducing the overall oxygen fugacity of the fluids until H_2-producing reactions can occur

to generate Type II fluids (Kelemen and Matter, 2008; Kelemen et al., 2011). Carbon veins are pervasive throughout the Oman ophiolite (Kelemen and Matter, 2008; Kelemen et al., 2011), under what conditions do they precipitate? Large-scale geologic carbonation may be an effective way to sequester large amounts of atmospheric CO_2 and mitigate the effects of global warming, and the Samail ophiolite in Oman has been proposed as a site where this is occurring naturally. Research into mineral carbonation has shown that the rate-limiting step is the dissolution of silicate minerals, calcium carbonates precipitate quickly (Daval et al., 2009), but magnesite precipitates more slowly (Pokrovsky and Schott, 1999). However, I have yet to see carbonate formation during water/rock reactions with a partially serpentinized dunite. Carbonation likely occurs before H_2 production when fluids are transiting from an oxic to anoxic stage, do H_2-rich fluids cause carbonate dissolution and the subsequent reduction of carbon species to form CH_4 or formate? Can we experimentally simulate mineral carbonation with partially serpentinized peridotite from Oman? Ongoing work about this topic is being conducted in other laboratories, but I think it is worthwhile to note that my laboratory water/rock experiments did not show carbonate precipitation with <1 bar P_{CO2}, and under reducing conditions.

Microbial CH_4 production and consumption

Although CH_4 in serpentinizing environments is oftentimes assumed to have abiotic origins based on its carbon and hydrogen isotope values, it is possible that CH_4 is produced by microbial activity due to the presence of methanogens and methanotrophs in these environments. Our cultures of *Methanobacterium* isolated from sitewater in Oman produce CH_4 with $\delta^{13}C$ values as positive as -28‰. If this CH_4 were then partially oxidized by methanotrophs, the $\delta^{13}C$ value of the residual CH_4 could easily approach +2‰, as observed in fluids from Oman.

Although I tried to grow consortia from subsurface fluids that would show this isotope value progression, the work has not come to fruition. I have not identified the key nutrients to stimulate the desired methane consortia growth, and it is challenging to work with small amounts of site water and small concentrations of produced and consumed CH_4. It is also unclear if the CH4 is oxidized anaerobically or if there are low amounts of oxygen present to sustain an aerobic methanotroph. Future work should focus on specifically enriching for *Methylococcus* from fluids from Oman, and then inoculating those organisms into *Methanobacterium* lab cultures and analyzing the resultant CH_4 isotope values over time. Additionally, once *Methylococcus* is successfully isolated in a lab culture, it would be worthwhile to investigate the lowest levels of O_2 it can tolerate or if another electron acceptor such as nitrate or sulfate can be used in lieu of O_2. Also, constraining the carbon and hydrogen fractionation factors of *Methylococcus* would be help to interpret CH_4 seen in serpentinizing fluids.

The rates and extent of microbial activity in the subsurface of Oman are still unconstrained; it is unclear if these methane-cycling microbes are abundant enough to account for all of the CH_4 seen in subsurface fluids in Oman. Thus, more work needs to be conducted to look at *in situ* rates of methanogenesis and methanotrophy, as well as looking at all the relevant gases present in the fluids to see if there is an overall microbial or abiotic trend.

There are also additional questions surrounding the laboratory *Methanobacterium* culture isolated from Oman. Why doesn't it grow at pH 11 in the laboratory when 16S rRNA shows its presence in pH 11 fluids in Oman? Am I missing key nutrients in the growth medium that prevents *Methanobacterium* from growing at higher pHs, or is the growth rate so slow that I cannot currently quantify it?

Overall

This combined spectroscopic analysis of environmental samples with experimental work that revealed the importance of Fe(II)-bearing brucite as an unstable mineral that can quickly oxidize and form H_2 gas. We also investigated the potential origin of the unique CH_4 isotope values found in the Samail ophiolite by quantifying the production of CH_4 and $\delta^{13}C_{CH4}$ produced by *Methanobacterium*, isolated from subsurface fluids in Oman, across a wide range in pH and with $NaHCO_3$ and $CaCO_3$ as carbon sources. Although there are still outstanding questions about carbon isotope fractionation at high pH and under carbon limitation, this work has increased the understanding of the range of isotope values produced by *Methanobacterium* in serpentinizing environments. The interplay between geologic processes and microbial ones is complex, but hydrogen produced by water/rock reactions is an important electron donor for microbial life. This geologically derived H_2 likely fuels methanogenic activity in serpentinizing systems, and the carbon isotope values of microbially produced methane may mistakenly be interpreted as abiotic if the organisms are growing in alkaline conditions under carbon limitation.

CUMULATIVE REFERENCES

Abrajano T. A., Sturchio N. C., Kennedy B. M., Lyon G. L., Muehlenbachs K. and Bohlke J. K. (1990) Geochemistry of reduced gas related to serpentinization of the Zambales ophiolite, Philippines. *Appl. Geochem.* **5**, 625–630.

Anderson R. T., Chapelle F. H. and Lovley D. R. (1998) Evidence Against Hydrogen-Based Microbial Ecosystems in Basalt Aquifers. *Science* **281**, 976–977.

Andreani M., Muñoz M., Marcaillou C. and Delacour A. (2013a) μXANES study of iron redox state in serpentine during oceanic serpentinization. *Lithos* **178**, 70–83.

Andreani M., Muñoz M., Marcaillou C. and Delacour A. (2013b) μXANES study of iron redox state in serpentine during oceanic serpentinization. *Lithos* **178**, 70–83.

Bach W. (2016) Some Compositional and Kinetic Controls on the Bioenergetic Landscapes in Oceanic Basement. *Extreme Microbiol.*, 107.

Bach W. and Edwards K. J. (2003) Iron and sulfide oxidation within the basaltic ocean crust: implications for chemolithoautotrophic microbial biomass production. *Geochim. Cosmochim. Acta* **67**, 3871–3887.

Bach W., Garrido C. J., Paulick H., Harvey J. and Rosner M. (2004) Seawater-peridotite interactions: First insights from ODP Leg 209, MAR 15°N. *Geochem. Geophys. Geosystems* **5**, Q09F26.

Bach W., Paulick H., Garrido C. J., Ildefonse B., Meurer W. P. and Humphris S. E. (2006) Unraveling the sequence of serpentinization reactions: petrography, mineral chemistry, and petrophysics of serpentinites from MAR 15°N (ODP Leg 209, Site 1274). *Geophys. Res. Lett.* **33**. Available at: http://doi.wiley.com/10.1029/2006GL025681 [Accessed May 19, 2015].

Balabane M., Galimov E., Hermann M. and Létolle R. (1987) Hydrogen and carbon isotope fractionation during experimental production of bacterial methane. *Org. Geochem.* **11**, 115–119.

Balch W. E., Fox G. E., Magrum L. J., Woese C. R. and Wolfe R. S. (1979) Methanogens: reevaluation of a unique biological group. *Microbiol. Rev.* **43**, 260–296.

Barberán A., Ladau J., Leff J. W., Pollard K. S., Menninger H. L., Dunn R. R. and Fierer N. (2015) Continental-scale distributions of dust-associated bacteria and fungi. *Proc. Natl. Acad. Sci.* **112**, 5756–5761.

Barnes I., LaMarche V. C. and Himmelberg G. (1967) Geochemical Evidence of Present-Day Serpentinization. *Science* **156**, 830–832.

Barnes I. and O'Neil J. R. (1969) The Relationship between Fluids in Some Fresh Alpine-Type Ultramafics and Possible Modern Serpentinization, Western United States. *Geol. Soc. Am. Bull.* **80**, 1947–1960.

Barnes I., O'Neil J. R. and Trescases J. J. (1978) Present day serpentinization in New Caledonia, Oman and Yugoslavia. *Geochim. Cosmochim. Acta* **42**, 144–145.

Beal E. J., House C. H. and Orphan V. J. (2009) Manganese- and Iron-Dependent Marine Methane Oxidation. *Science* **325**, 184–187.

Béarat H., McKelvy M. J., Chizmeshya A. V. G., Gormley D., Nunez R., Carpenter R. W., Squires K. and Wolf G. H. (2006) Carbon Sequestration via Aqueous Olivine Mineral Carbonation: Role of Passivating Layer Formation. *Environ. Sci. Technol.* **40**, 4802–4808.

Benjamin M. M. (2002) *Water Chemistry*., Waveland Press, Inc., Long Grove, Illinois.

Berndt M. E., Allen D. E. and Seyfried W. E. (1996) Reduction of CO2 during serpentinization of olivine at 300 °C and 500 bar. *Geology* **24**, 351–354.

Blank J. G., Green S. J., Blake D., Valley J. W., Kita N. T., Treiman A. and Dobson P. F. (2009) An alkaline spring system within the Del Puerto Ophiolite (California, USA): A Mars analog site. *Planet. Space Sci.* **57**, 533–540.

Boetius A., Ravenschlag K., Schubert C. J., Rickert D., Widdel F., Gieseke A., Amann R., Jørgensen B. B., Witte U. and Pfannkuche O. (2000) A marine microbial consortium apparently mediating anaerobic oxidation of methane. *Nature* **407**, 623–626.

Boston P. J., Ivanov M. V. and P. McKay C. (1992) On the possibility of chemosynthetic ecosystems in subsurface habitats on Mars. *Icarus* **95**, 300–308.

Bottinga Y. (1969) Calculated fractionation factors for carbon and hydrogen isotope exchange in the system calcite-carbon dioxide-graphite-methane-hydrogen-water vapor. *Geochim. Cosmochim. Acta* **33**, 49–64.

Boudier F., Baronnet A. and Mainprice D. (2010) Serpentine Mineral Replacements of Natural Olivine and their Seismic Implications: Oceanic Lizardite versus Subduction-Related Antigorite. *J. Petrol.* **51**, 495–512.

Bowers R. M., Clements N., Emerson J. B., Wiedinmyer C., Hannigan M. P. and Fierer N. (2013) Seasonal Variability in Bacterial and Fungal Diversity of the Near-Surface Atmosphere. *Environ. Sci. Technol.* **47**, 12097–12106.

Bradley A. S. and Summons R. E. (2010) Multiple origins of methane at the Lost City Hydrothermal Field. *Earth Planet. Sci. Lett.* **297**, 34–41.

Brazelton W. J., Morrill P. L., Szponar N. and Schrenk M. O. (2013) Bacterial Communities Associated with Subsurface Geochemical Processes in Continental Serpentinite Springs. *Appl. Environ. Microbiol.* **79**, 3906–3916.

Brazelton W. J., Nelson B. and Schrenk M. O. (2012) Metagenomic Evidence for H2 Oxidation and H2 Production by Serpentinite-Hosted Subsurface Microbial Communities. *Front. Microbiol.* **2**. Available at: http://www.frontiersin.org/Journal/10.3389/fmicb.2011.00268/full [Accessed January 30, 2014].

Brazelton W. J., Schrenk M. O., Kelley D. S. and Baross J. A. (2006) Methane- and Sulfur-Metabolizing Microbial Communities Dominate the Lost City Hydrothermal Field Ecosystem. *Appl. Environ. Microbiol.* **72**, 6257–6270.

Bruni J., Canepa M., Chiodini G., Cioni R., Cipolli F., Longinelli A., Marini L., Ottonello G. and Vetuschi Zuccolini M. (2002) Irreversible water–rock mass transfer accompanying the generation of the neutral, Mg–HCO3 and high-pH, Ca–OH spring waters of the Genova province, Italy. *Appl. Geochem.* **17**, 455–474.

Butler R. and Banerjee S. (1975) Theoretical Single-Domain Grain Size Range m Magnetite and Titanomagnetite. *J. Geophys. Res.*, 4049–4058.

Cardace D. and Hoehler T. M. (2009) Serpentinizing Fluids Craft Microbial Habitat. *Northeast. Nat.* **16**, 272–284.

Cardace D., Meyer-Dombard D. R., Woycheese K. M. and Arcilla C. A. (2015) Feasible metabolisms in high pH springs of the Philippines. *Front. Microbiol.* **6**. Available at: http://journal.frontiersin.org/Article/10.3389/fmicb.2015.00010/abstract [Accessed May 21, 2015].

Chapelle F. H., O'Neill K., Bradley P. M., Methé B. A., Ciufo S. A., Knobel L. L. and Lovley D. R. (2002) A hydrogen-based subsurface microbial community dominated by methanogens. *Nature* **415**, 312–315.

Chasar L. S., Chanton J. P., Glaser P. H. and Siegel D. I. (2000) Methane Concentration and Stable Isotope Distribution as Evidence of Rhizospheric Processes: Comparison of a Fen and Bog in the Glacial Lake Agassiz Peatland Complex. *Ann. Bot.* **86**, 655–663.

Chavagnac V., Ceuleneer G., Monnin C., Lansac B., Hoareau G. and Boulart C. (2013) Mineralogical assemblages forming at hyperalkaline warm springs hosted on ultramafic rocks: A case study of Oman and Ligurian ophiolites. *Geochem. Geophys. Geosystems* **14**, 2474–2495.

Chavagnac V., Monnin C., Ceuleneer G., Boulart C. and Hoareau G. (2013) Characterization of hyperalkaline fluids produced by low-temperature serpentinization of mantle peridotites in the Oman and Ligurian ophiolites. *Geochem. Geophys. Geosystems* **14**, 2496–2522.

Chen P Y. Y. (2015) Methane on Mars. *J. Astrobiol. Outreach* **3**. Available at: http://esciencecentral.org/journals/methane-on-mars-2332-2519-1000125.php?aid=38624 [Accessed June 28, 2016].

Chidthaisong A., Chin K.-J., Valentine D. L. and Tyler S. C. (2002) A comparison of isotope fractionation of carbon and hydrogen from paddy field rice roots and soil bacterial enrichments during CO2/H2 methanogenesis. *Geochim. Cosmochim. Acta* **66**, 983–995.

Chou L., Garrels R. M. and Wollast R. (1989) Comparative study of the kinetics and mechanisms of dissolution of carbonate minerals. *Chem. Geol.* **78**, 269–282.

Clark I. D. and Fontes J.-C. (1990) Paleoclimatic reconstruction in northern Oman based on carbonates from hyperalkaline groundwaters. *Quat. Res.* **33**, 320–336.

Coey J. M. D., Ballet O., Moukarika A. and Soubeyroux J. L. (1981) Magnetic properties of sheet silicates; 1:1 layer minerals. *Phys. Chem. Miner.* **7**, 141–148.

Coleman R. G. (1981) Tectonic setting for ophiolite obduction in Oman. *J. Geophys. Res. Solid Earth* **86**, 2497–2508.

Conrad R. (2005) Quantification of methanogenic pathways using stable carbon isotopic signatures: a review and a proposal. *Org. Geochem.* **36**, 739–752.

Crespo-Medina M., Twing K. I., Kubo M. D. Y., Hoehler T. M., Cardace D., McCollom T. and Schrenk M. O. (2014) Insights into environmental controls on microbial communities in a continental serpentinite aquifer using a microcosm-based approach. *Front. Microbiol.* **5**. Available at: http://www.ncbi.nlm.nih.gov/pmc/articles/PMC4231944/ [Accessed September 1, 2015].

Daval D., Martinez I., Corvisier J., Findling N., Goffé B. and Guyot F. (2009) Carbonation of Ca-bearing silicates, the case of wollastonite: Experimental investigations and kinetic modeling. *Chem. Geol.* **265**, 63–78.

Debret B., Andreani M., Muñoz M., Bolfan-Casanova N., Carlut J., Nicollet C., Schwartz S. and Trcera N. (2014) Evolution of Fe redox state in serpentine during subduction. *Earth Planet. Sci. Lett.* **400**, 206–218.

Dewandel B., Lachassagne P., Boudier F., Al-Hattali S., Ladouche B., Pinault J.-L. and Al-Suleimani Z. (2005) A conceptual hydrogeological model of ophiolite hard-rock aquifers in Oman based on a multiscale and a multidisciplinary approach. *Hydrogeol. J.* **13**, 708–726.

Downs R. T. (2006) The RRUFF Project: an integrated study of the chemistry, crystallography, Raman and infrared spectroscopy of minerals. In *Program and Abstracts of the 19th General Meeting of the International Mineralogical Association in Kobe, Japan* pp. O03-13.

Dunlop D. J. (1973) Superparamagnetic and single-domain threshold sizes in magnetite. *J. Geophys. Res.* **78**, 1780–1793.

Eberl D. D. (2003) *User Guide to RockJock - A Program for Determining Quantitative Mineralogy from X-Ray Diffraction Data*., U.S. Geological Survey. Available at: http://pubs.er.usgs.gov/publication/ofr200378 [Accessed January 29, 2016].

Edgar R. C. (2013) UPARSE: highly accurate OTU sequences from microbial amplicon reads. *Nat. Methods* **10**, 996–8.

Eecke H. C. V., Butterfield D. A., Huber J. A., Lilley M. D., Olson E. J., Roe K. K., Evans L. J., Merkel A. Y., Cantin H. V. and Holden J. F. (2012) Hydrogen-limited growth of hyperthermophilic methanogens at deep-sea hydrothermal vents. *Proc. Natl. Acad. Sci.* **109**, 13674–13679.

Ehlmann B. L., Mustard J. F. and Murchie S. L. (2010) Geologic setting of serpentine deposits on Mars: SERPENTINE ON MARS. *Geophys. Res. Lett.* **37**, n/a-n/a.

Elmaleh A., Tarantino S. C., Zema M., Devouard B. and Fialin M. (2012) The low-temperature magnetic signature of Fe-rich serpentine in CM2 chondrites: Comparison with terrestrial cronstedtite and evolution with the degree of alteration. *Geochem. Geophys. Geosystems* **13**, Q05Z42.

Emerson J. B., Keady P. B., Brewer T. E., Clements N., Morgan E. E., Awerbuch J., Miller S. L. and Fierer N. (2015) Impacts of Flood Damage on Airborne Bacteria and Fungi in Homes after the 2013 Colorado Front Range Flood. *Environ. Sci. Technol.* **49**, 2675–2684.

Espinosa A., Serrano A., Llavona A., Morena J. J. de la, Abuin M., Figuerola A., Pellegrino T., Fernández J. F., Garcia-Hernandez M., Castro G. R. and Garcia M. A. (2012) On the discrimination between magnetite and maghemite by XANES measurements in fluorescence mode. *Meas. Sci. Technol.* **23**, 15602.

Etiope G. (2016) Methane origin in the Samail ophiolite: Comment on "Modern water/rock reactions in Oman hyperalkaline peridotite aquifers and implications for microbial habitability." *Geochim. Cosmochim. Acta*, 217–241.

Etiope G. (2009) Natural emissions of methane from geological seepage in Europe. *Atmos. Environ.* **43**, 1430–1443.

Etiope G., Ehlmann B. L. and Schoell M. (2013) Low temperature production and exhalation of methane from serpentinized rocks on Earth: A potential analog for methane production on Mars. *Icarus* **224**, 276–285.

Etiope G. and Ionescu A. (2015) Low-temperature catalytic CO2 hydrogenation with geological quantities of ruthenium: a possible abiotic CH4 source in chromitite-rich serpentinized rocks. *Geofluids* **15**, 438–452.

Etiope G., Schoell M. and Hosgörmez H. (2011) Abiotic methane flux from the Chimaera seep and Tekirova ophiolites (Turkey): Understanding gas exhalation from low temperature serpentinization and implications for Mars. *Earth Planet. Sci. Lett.* **310**, 96–104.

Etiope G. and Sherwood Lollar B. (2013) Abiotic Methane on Earth. *Rev. Geophys.* **51**, 276–299.

Evans B. W. (2010) Lizardite versus antigorite serpentinite: Magnetite, hydrogen, and life (?). *Geology* **38**, 879–882.

Evans B. W. (2004) The Serpentinite Multisystem Revisited: Chrysotile Is Metastable. *Int. Geol. Rev.* **46**, 479–506.

Evans B. W., Kuehner S. M. and Chopelas A. (2009) Magnetite-free, yellow lizardite serpentinization of olivine websterite, Canyon Mountain complex, N.E. Oregon. *Am. Mineral.* **94**, 1731–1734.

Frost B. R. (1985) On the stability of sulfides, oxides, and native metals in serpentinite. *J. Petrol.* **26**, 31–63.

Frost B. R. and Beard J. S. (2007) On Silica Activity and Serpentinization. *J. Petrol.* **48**, 1351–1368.

Frost B. R., Evans K. A., Swapp S. M., Beard J. S. and Mothersole F. E. (2013) The process of serpentinization in dunite from New Caledonia. *Lithos* **178**, 24–39.

Fu Q., Sherwood Lollar B., Horita J., Lacrampe-Couloume G. and Seyfried W. E. (2007) Abiotic formation of hydrocarbons under hydrothermal conditions: Constraints from chemical and isotope data. *Geochim. Cosmochim. Acta* **71**, 1982–1998.

Fyfe W. S. (1974) Heats of Chemical Reactions and Submarine Heat Production. *Geophys. J. R. Astron. Soc.* **37**, 213–215.

Games L. M., HayesRobert J. M. and Gunsalus P. (1978) Methane-producing bacteria: natural fractionations of the stable carbon isotopes. *Geochim. Cosmochim. Acta* **42**, 1295–1297.

Giammar D. E., Bruant Jr. R. G. and Peters C. A. (2005) Forsterite dissolution and magnesite precipitation at conditions relevant for deep saline aquifer storage and sequestration of carbon dioxide. *Chem. Geol.* **217**, 257–276.

Girguis P. R., Orphan V. J., Hallam S. J. and DeLong E. F. (2003) Growth and Methane Oxidation Rates of Anaerobic Methanotrophic Archaea in a Continuous-Flow Bioreactor. *Appl. Environ. Microbiol.* **69**, 5472–5482.

Glein C. R., Baross J. A. and Waite Jr. J. H. (2015) The pH of Enceladus' ocean. *Geochim. Cosmochim. Acta* **162**, 202–219.

Groppo C., Rinaudo C., Cairo S., Gastaldi D. and Compagnoni R. (2006) Micro-Raman spectroscopy for a quick and reliable identification of serpentine minerals from ultramafics. *Eur. J. Mineral.* **18**, 319–329.

Guyot F., Daval D., Dupraz S., Martinez I., Ménez B. and Sissmann O. (2011) CO2 geological storage: The environmental mineralogy perspective. *Comptes Rendus Geosci.* **343**, 246–259.

Hänchen M., Prigiobbe V., Baciocchi R. and Mazzotti M. (2008) Precipitation in the Mg-carbonate system—effects of temperature and CO2 pressure. *Chem. Eng. Sci.* **63**, 1012–1028.

Hänchen M., Prigiobbe V., Storti G., Seward T. M. and Mazzotti M. (2006) Dissolution kinetics of fosteritic olivine at 90–150 °C including effects of the presence of CO2. *Geochim. Cosmochim. Acta* **70**, 4403–4416.

Hanghøj K., Kelemen P. B., Hassler D. and Godard M. (2010a) Composition and Genesis of Depleted Mantle Peridotites from the Wadi Tayin Massif, Oman Ophiolite; Major and Trace Element Geochemistry, and Os Isotope and PGE Systematics. *J. Petrol.* **51**, 201–227.

Hanghøj K., Kelemen P. B., Hassler D. and Godard M. (2010b) Composition and Genesis of Depleted Mantle Peridotites from the Wadi Tayin Massif, Oman Ophiolite; Major and Trace Element Geochemistry, and Os Isotope and PGE Systematics. *J. Petrol.* **51**, 201–227.

Hannington M. D., Jonasson I. R., Herzig P. M. and Petersen S. (1995) Physical and chemical processes of seafloor mineralization at mid-ocean ridges. *Seafloor Hydrothermal Syst. Phys. Chem. Biol. Geol. Interact.*, 115–157.

Hansen L. D., Dipple G. M., Gordon T. M. and Kellett D. A. (2005) Carbonated Serpentinite (listwanite) at Atlin, British Columbia: A Geological Analogue to Carbon Dioxide Sequestration. *Can. Mineral.* **43**, 225–239.

Haouari O., Fardeau M.-L., Cayol J.-L., Fauque G., Casiot C., Elbaz-Poulichet F., Hamdi M. and Ollivier B. (2008) Thermodesulfovibrio hydrogeniphilus sp. nov., a new thermophilic sulphate-reducing bacterium isolated from a Tunisian hot spring. *Syst. Appl. Microbiol.* **31**, 38–42.

Haroon M. F., Hu S., Shi Y., Imelfort M., Keller J., Hugenholtz P., Yuan Z. and Tyson G. W. (2013) Anaerobic oxidation of methane coupled to nitrate reduction in a novel archaeal lineage. *Nature* **500**, 567–570.

Hicks D. B., Liu J., Fujisawa M. and Krulwich T. A. (2010) F1F0-ATP synthases of alkaliphilic bacteria: Lessons from their adaptations. *Biochim. Biophys. Acta BBA - Bioenerg.* **1797**, 1362–1377.

Hoal K. O., Appleby S. K., Stammer J. G. and Palmer C. (2009) SEM-based quantitative mineralogical analysis of peridotite, kimberlite, and concentrate. *Lithos* **112**, **Supplement 1**, 41–46.

Hoehler T. M., Alperin M. J., Albert D. B. and Martens C. S. (1994) Field and laboratory studies of methane oxidation in an anoxic marine sediment: Evidence for a methanogen-sulfate reducer consortium. *Glob. Biogeochem. Cycles* **8**, 451–463.

Holland H. D. (2002) Volcanic gases, black smokers, and the great oxidation event. *Geochim. Cosmochim. Acta* **66**, 3811–3826.

Holler T., Wegener G., Knittel K., Boetius A., Brunner B., Kuypers M. M. M. and Widdel F. (2009) Substantial 13C/12C and D/H fractionation during anaerobic oxidation of methane by marine consortia enriched in vitro. *Environ. Microbiol. Rep.* **1**, 370–376.

Holloway J. R. and O'DAY P. A. (2000) Production of CO2 and H2 by Diking-Eruptive Events at Mid-Ocean Ridges: Implications for Abiotic Organic Synthesis and Global Geochemical Cycling. *Int. Geol. Rev.* **42**, 673–683.

Horibe Y. and Craig H. (1995) DH fractionation in the system methane-hydrogen-water. *Geochim. Cosmochim. Acta* **59**, 5209–5217.

Horita J. and Berndt M. E. (1999) Abiogenic Methane Formation and Isotopic Fractionation Under Hydrothermal Conditions. *Science* **285**, 1055–1057.

Hövelmann J., Austrheim H. and Jamtveit B. (2012) Microstructure and porosity evolution during experimental carbonation of a natural peridotite. *Chem. Geol.* **334**, 254–265.

Hug L. A., Castelle C. J., Wrighton K. C., Thomas B. C., Sharon I., Frischkorn K. R., Williams K. H., Tringe S. G. and Banfield J. F. (2013) Community genomic analyses constrain the distribution of metabolic traits across the Chloroflexi phylum and indicate roles in sediment carbon cycling. *Microbiome* **1**, 22.

Jacquemin M., Beuls A. and Ruiz P. (2010) Catalytic production of methane from CO2 and H2 at low temperature: Insight on the reaction mechanism. *Catal. Today* **157**, 462–466.

Jetten M. S., Stams A. J. and Zehnder A. J. (1992) Methanogenesis from acetate: a comparison of the acetate metabolism in Methanothrix soehngenii and Methanosarcina spp. *FEMS Microbiol Rev* **88**, 181–197.

Jöns N., Bach W. and Klein F. (2010) Magmatic influence on reaction paths and element transport during serpentinization. *Chem. Geol.* **274**, 196–211.

Joye S. B., Boetius A., Orcutt B. N., Montoya J. P., Schulz H. N., Erickson M. J. and Lugo S. K. (2004) The anaerobic oxidation of methane and sulfate reduction in sediments from Gulf of Mexico cold seeps. *Chem. Geol.* **205**, 219–238.

Kelemen P. B. and Hirth G. (2012) Reaction-driven cracking during retrograde metamorphism: Olivine hydration and carbonation. *Earth Planet. Sci. Lett.* **345**–**348**, 81–89.

Kelemen P. B., Hirth G., Shimizu N., Spiegelman M. and Dick H. J. (1997) A review of melt migration processes in the adiabatically upwelling mantle beneath oceanic spreading ridges. *Philos. Trans. R. Soc. Lond. Math. Phys. Eng. Sci.* **355**, 283–318.

Kelemen P. B. and Matter J. (2008) In situ carbonation of peridotite for CO2 storage. *Proc. Natl. Acad. Sci.* **105**, 17295–17300.

Kelemen P. B., Matter J., Streit E. E., Rudge J. F., Curry W. B. and Blusztajn J. (2011) Rates and Mechanisms of Mineral Carbonation in Peridotite: Natural Processes and Recipes for Enhanced, in situ CO2 Capture and Storage. *Annu. Rev. Earth Planet. Sci.* **39**, 545–576.

Kelley D. S., Karson J. A., Blackman D. K., Früh-Green G. L., Butterfield D. A., Lilley M. D., Olson E. J., Schrenk M. O., Roe K. K., Lebon G. T., Rivizzigno P. and the AT3-60 Shipboard Party (2001) An off-axis hydrothermal vent field near the Mid-Atlantic Ridge at 30° N. *Nature* **412**, 145–149.

Kiene R. P., Oremland R. S., Catena A., Miller L. G. and Capone D. G. (1986) Metabolism of Reduced Methylated Sulfur Compounds in Anaerobic Sediments and by a Pure Culture of an Estuarine Methanogen. *Appl. Environ. Microbiol.* **52**, 1037–1045.

Kim W., Suh C.-Y., Cho S.-W., Roh K.-M., Kwon H., Song K. and Shon I.-J. (2012) A new method for the identification and quantification of magnetite–maghemite mixture using conventional X-ray diffraction technique. *Talanta* **94**, 348–352.

Klein F., Bach W., Humphris S. E., Kahl W.-A., Jons N., Moskowitz B. and Berquo T. S. (2013) Magnetite in seafloor serpentinite--Some like it hot. *Geology* **42**, 135–138.

Klein F., Bach W., Jöns N., McCollom T., Moskowitz B. and Berquó T. (2009) Iron partitioning and hydrogen generation during serpentinization of abyssal peridotites from 15°N on the Mid-Atlantic Ridge. *Geochim. Cosmochim. Acta* **73**, 6868–6893.

Klein F., Bach W. and McCollom T. M. (2013) Compositional controls on hydrogen generation during serpentinization of ultramafic rocks. *Lithos* **178**, 55–69.

Klein F., Grozeva N. G., Seewald J. S., McCollom T. M., Humphris S. E., Moskowitz B., Berquó T. S. and Kahl W.-A. (2015) Experimental constraints on fluid-rock reactions during incipient serpentinization of harzburgite. *Am. Mineral.* **100**, 991–1002.

Klein F., Humphris S. E., Guo W., Schubotz F., Schwarzenbach E. M. and Orsi W. D. (2015) Fluid mixing and the deep biosphere of a fossil Lost City-type hydrothermal system at the Iberia Margin. *Proc. Natl. Acad. Sci.*, 201504674.

Kohl L., Cumming E., Cox A., Rietze A., Morrissey L., Lang S. Q., Richter A., Suzuki S., Nealson K. H. and Morrill P. L. (2016) Exploring the metabolic potential of microbial communities in ultra-basic, reducing springs at The Cedars, CA, USA: Experimental

evidence of microbial methanogenesis and heterotrophic acetogenesis. *J. Geophys. Res. Biogeosciences* **121**, 2015JG003233.

Kotelnikova S. (2002) Microbial production and oxidation of methane in deep subsurface. *Earth-Sci. Rev.* **58**, 367–395.

Kotelnikova S., Macario A. J. and Pedersen K. (1998) Methanobacterium subterraneum sp. nov., a new alkaliphilic, eurythermic and halotolerant methanogen isolated from deep granitic groundwater. *Int. J. Syst. Bacteriol.* **48**, 357–367.

Kral T. A., Birch W., Lavender L. E. and Virden B. T. (2014) Potential use of highly insoluble carbonates as carbon sources by methanogens in the subsurface of Mars. *Planet. Space Sci.* **101**, 181–185.

Kral T. A., Brink K. M., Miller S. L. and McKay C. P. (1998) Hydrogen Consumption by Methanogens on the Early Earth. *Orig. Life Evol. Biosph.* **28**, 311–319.

Kumar M. R. and Saravanan V. S. (2011) Candidate OP Phyla: Importance, Ecology and Cultivation Prospects. *Indian J. Microbiol.* **50**, 474–477.

Lafay R., Montes-Hernandez G., Janots E., Chiriac R., Findling N. and Toche F. (2012) Mineral replacement rate of olivine by chrysotile and brucite under high alkaline conditions. *J. Cryst. Growth* **347**, 62–72.

Laier T. and Nytoft H. P. (2012) Bitumen biomarkers in the Mid-Proterozoic Ilímaussaq intrusion, Southwest Greenland – A challenge to the mantle gas theory. *Mar. Pet. Geol.* **30**, 50–65.

Lang S. Q., Butterfield D. A., Schulte M., Kelley D. S. and Lilley M. D. (2010a) Elevated concentrations of formate, acetate and dissolved organic carbon found at the Lost City hydrothermal field. *Geochim. Cosmochim. Acta* **74**, 941–952.

Lang S. Q., Butterfield D. A., Schulte M., Kelley D. S. and Lilley M. D. (2010b) Elevated concentrations of formate, acetate and dissolved organic carbon found at the Lost City hydrothermal field. *Geochim. Cosmochim. Acta* **74**, 941–952.

Lever M. A. (2012) Acetogenesis in the Energy-Starved Deep Biosphere – A Paradox? *Front. Microbiol.* **2**. Available at: http://journal.frontiersin.org/article/10.3389/fmicb.2011.00284/abstract [Accessed July 6, 2016].

Lollar B. S., Onstott T. C., Lacrampe-Couloume G. and Ballentine C. J. (2014) The contribution of the Precambrian continental lithosphere to global H2 production. *Nature* **516**, 379–382.

Lorand J. (1987) A New Occurrence of Native Iron in a Serpentinized Mantle Peridotite - Maqsad, Sumail Massif, Semail Ophiolite (Southern Oman). *Comptes Rendus Acad. Sci. Ii* **304**, 703–6.

Macdonald A. H. and Fyfe W. S. (1985) Rate of serpentinization in seafloor environments. *Tectonophysics* **116**, 123–135.

Madigan M. T. (2012) *Brock biology of microorganisms*., Benjamin Cummings, San Francisco.

Malvoisin B., Brunet F., Carlut J., Rouméjon S. and Cannat M. (2012) Serpentinization of oceanic peridotites: 2. Kinetics and processes of San Carlos olivine hydrothermal alteration. *J. Geophys. Res. Solid Earth* **117**, n/a–n/a.

Malvoisin B., Carlut J. and Brunet F. (2012) Serpentinization of oceanic peridotites: 1. A high-sensitivity method to monitor magnetite production in hydrothermal experiments. *J. Geophys. Res. Solid Earth* **117**, B01104.

Marcaillou C., Muñoz M., Vidal O., Parra T. and Harfouche M. (2011) Mineralogical evidence for H2 degassing during serpentinization at 300 °C/300 bar. *Earth Planet. Sci. Lett.* **303**, 281–290.

Martens C. S. and Berner R. A. (1977) Interstitial water chemistry of anoxic Long Island Sound sediments. 1. Dissolved gases1. *Limnol. Oceanogr.* **22**, 10–25.

Mathrani I. M., Boone D. R., Mah R. A., Fox G. E. and Lau P. P. (1988) Methanohalophilus zhilinae sp. nov., an alkaliphilic, halophilic, methylotrophic methanogen. *Int. J. Syst. Bacteriol.* **38**, 139–142.

Mayhew L. E., Ellison E. T., McCollom T. M., Trainor T. P. and Templeton A. S. (2013) Hydrogen generation from low-temperature water–rock reactions. *Nat. Geosci.* **6**, 478–484.

Mayhew L. E., Webb S. M. and Templeton A. S. (2011) Microscale Imaging and Identification of Fe Speciation and Distribution during Fluid–Mineral Reactions under Highly Reducing Conditions. *Environ. Sci. Technol.* **45**, 4468–4474.

McCollom T. M. (2016) Abiotic methane formation during experimental serpentinization of olivine. *Proc. Natl. Acad. Sci.* **113**, 13965–13970.

McCollom T. M. (2013) Laboratory Simulations of Abiotic Hydrocarbon Formation in Earth's Deep Subsurface. *Rev. Mineral. Geochem.* **75**, 467–494.

McCollom T. M. and Bach W. (2009) Thermodynamic constraints on hydrogen generation during serpentinization of ultramafic rocks. *Geochim. Cosmochim. Acta* **73**, 856–875.

McCollom T. M. and Donaldson C. (2016) Generation of Hydrogen and Methane during Experimental Low-Temperature Reaction of Ultramafic Rocks with Water. *Astrobiology*. Available at: http://online.liebertpub.com/doi/abs/10.1089/ast.2015.1382 [Accessed June 6, 2016].

McCollom T. M., Klein F., Robbins M., Moskowitz B., Berquó T. S., Jöns N., Bach W. and Templeton A. (2016) Temperature trends for reaction rates, hydrogen generation, and

partitioning of iron during experimental serpentinization of olivine. *Geochim. Cosmochim. Acta* **181**, 175–200.

McCollom T. M., Lollar B. S., Lacrampe-Couloume G. and Seewald J. S. (2010) The influence of carbon source on abiotic organic synthesis and carbon isotope fractionation under hydrothermal conditions. *Geochim. Cosmochim. Acta* **74**, 2717–2740.

McCollom T. M. and Seewald J. S. (2001) A reassessment of the potential for reduction of dissolved CO2 to hydrocarbons during serpentinization of olivine. *Geochim. Cosmochim. Acta* **65**, 3769–3778.

McCollom T. M. and Seewald J. S. (2007) Abiotic Synthesis of Organic Compounds in Deep-Sea Hydrothermal Environments. *Chem. Rev.* **107**, 382–401.

McCollom T. M. and Seewald J. S. (2003) Experimental constraints on the hydrothermal reactivity of organic acids and acid anions: I. Formic acid and formate. *Geochim. Cosmochim. Acta* **67**, 3625–3644.

McDermott J. M., Seewald J. S., German C. R. and Sylva S. P. (2015) Pathways for abiotic organic synthesis at submarine hydrothermal fields. *Proc. Natl. Acad. Sci.*, 201506295.

McDonald D., Price M. N., Goodrich J., Nawrocki E. P., DeSantis T. Z., Probst A., Andersen G. L., Knight R. and Hugenholtz P. (2012) An improved Greengenes taxonomy with explicit ranks for ecological and evolutionary analyses of bacteria and archaea. *ISME J.* **6**, 610–8.

Ménez B., Pasini V. and Brunelli D. (2012) Life in the hydrated suboceanic mantle. *Nat. Geosci.* **5**, 133–137.

Mervine E. M., Humphris S. E., Sims K. W. W., Kelemen P. B. and Jenkins W. J. (2014) Carbonation rates of peridotite in the Samail Ophiolite, Sultanate of Oman, constrained through 14C dating and stable isotopes. *Geochim. Cosmochim. Acta* **126**, 371–397.

Meyer-Dombard D. R., Woycheese K. M., YargÄ±Ã§oÄŸlu E. N., Cardace D., Shock E. L., GÃ¼leÃ§al-Pektas Y. and Temel M. (2015) High pH microbial ecosystems in a newly discovered, ephemeral, serpentinizing fluid seep at YanartaÅŸ (Chimera), Turkey. *Front. Microbiol.* **5**. Available at: http://journal.frontiersin.org/article/10.3389/fmicb.2014.00723/abstract [Accessed March 7, 2015].

Milesi V., McCollom T. M. and Guyot F. (2016) Thermodynamic constraints on the formation of condensed carbon from serpentinization fluids. *Geochim. Cosmochim. Acta* **189**, 391–403.

Miller H. M. (2017) Reply to "Methane origin in the Samail ophiolite: Comment on "Modern water/rock reactions in Oman hyperalkaline peridotite aquifers and implications for microbial habitability [Geochim. Cosmochim. Acta 179 (2016) 217–241]. *Geochim. Cosmochim. Acta* **197**, 467–470.

Miller H. M., Matter J. M., Kelemen P., Ellison E. T., Conrad M. E., Fierer N., Ruchala T., Tominaga M. and Templeton A. S. (2016) Modern water/rock reactions in Oman hyperalkaline peridotite aquifers and implications for microbial habitability. *Geochim. Cosmochim. Acta* **179**, 217–241.

Moody J. B. (1976) Serpentinization: a review. *Lithos* **9**, 125–138.

Mook W. G. (1986) 13C in atmospheric CO2. *Neth. J. Sea Res.* **20**, 211–223.

Morrill P. L., Brazelton W. J., Kohl L., Rietze A., Miles S. M., Kavanagh H., Schrenk M. O., Ziegler S. E. and Lang S. Q. (2014) Investigations of potential microbial methanogenic and carbon monoxide utilization pathways in ultra-basic reducing springs associated with present-day continental serpentinization: the Tablelands, NL, CAN. *Front. Microbiol.* **5**. Available at: http://www.ncbi.nlm.nih.gov/pmc/articles/PMC4230201/ [Accessed January 6, 2015].

Morrill P. L., Kuenen J. G., Johnson O. J., Suzuki S., Rietze A., Sessions A. L., Fogel M. L. and Nealson K. H. (2013) Geochemistry and geobiology of a present-day serpentinization site in California: The Cedars. *Geochim. Cosmochim. Acta* **109**, 222–240.

Moser D. P., Gihring T. M., Brockman F. J., Fredrickson J. K., Balkwill D. L., Dollhopf M. E., Lollar B. S., Pratt L. M., Boice E., Southam G., Wanger G., Baker B. J., Pfiffner S. M., Lin L.-H. and Onstott T. C. (2005) Desulfotomaculum and Methanobacterium spp. Dominate a 4- to 5-Kilometer-Deep Fault. *Appl. Environ. Microbiol.* **71**, 8773–8783.

Mulkidjanian A. Y., Dibrov P. and Galperin M. Y. (2008) The past and present of sodium energetics: May the sodium-motive force be with you. *Biochim. Biophys. Acta BBA - Bioenerg.* **1777**, 985–992.

Muñoz M., Vidal O., Marcaillou C., Pascarelli S., Mathon O. and Farges F. (2013) Iron oxidation state in phyllosilicate single crystals using Fe-K pre-edge and XANES spectroscopy: Effects of the linear polarization of the synchrotron X-ray beam. *Am. Mineral.* **98**, 1187–1197.

Nash W. P. (1992) Analysis of oygen with the electron microprobe: Applications to hydrated glass and minerals. *American Mineralogist* **77**, 453–457.

Neal C. and Stanger G. (1984) Calcium and magnesium hydroxide precipitation from alkaline groundwaters in Oman, and their significance to the process of serpentinization. *Miner. Mag* **48**, 237–241.

Neal C. and Stanger G. (1983) Hydrogen generation from mantle source rocks in Oman. *Earth Planet. Sci. Lett.* **66**, 315–320.

Neal C. and Stanger G. (1985) Past And Present Serpentinisation of Ultramafic Rocks; An Example from the Semail Ophiolite Nappe of Northern Oman. In *The Chemistry of Weathering* (ed. J. I. Drever). Nato ASI Series. Springer Netherlands. pp. 249–275.

Available at: http://link.springer.com/chapter/10.1007/978-94-009-5333-8_15 [Accessed June 17, 2015].

Nealson K. H., Inagaki F. and Takai K. (2005) Hydrogen-driven subsurface lithoautotrophic microbial ecosystems (SLiMEs): do they exist and why should we care? *Trends Microbiol.* **13**, 405–410.

Neubeck A., Duc N. T., Bastviken D., Crill P. and Holm N. G. (2011a) Formation of H2 and CH4 by weathering of olivine at temperatures between 30 and 70 C. *Geochem. Trans.* **12**, 6.

Neubeck A., Duc N. T., Bastviken D., Crill P. and Holm N. G. (2011b) Formation of H2 and CH4 by weathering of olivine at temperatures between 30 and 70 C. *Geochem. Trans.* **12**, 6.

Neubeck A., Duc N. T., Hellevang H., Oze C., Bastviken D., Bacsik Z. and Holm N. G. (2014) Olivine alteration and H2 production in carbonate-rich, low temperature aqueous environments. *Planet. Space Sci.* **96**, 51–61.

Neubeck A., Nguyen D. T. and Etiope G. (2015) Low-temperature dunite hydration: evaluating CH4 and H2 production from H2O and CO2. *Geofluids*, n/a-n/a.

Nielsen J. L. and Nielsen P. H. (1998) Microbial Nitrate-Dependent Oxidation of Ferrous Iron in Activated Sludge. *Environ. Sci. Technol.* **32**, 3556–3561.

van Noort R., Spiers C. J., Drury M. R. and Kandianis M. T. (2013) Peridotite dissolution and carbonation rates at fracture surfaces under conditions relevant for in situ mineralization of CO2. *Geochim. Cosmochim. Acta* **106**, 1–24.

Oelkers E. H., Gislason S. R. and Matter J. (2008) Mineral Carbonation of CO2. *Elements* **4**, 333–337.

Ogasawara Y., Okamoto A., Hirano N. and Tsuchiya N. (2013) Coupled reactions and silica diffusion during serpentinization. *Geochim. Cosmochim. Acta* **119**, 212–230.

Okland I., Huang S., Dahle H., Thorseth I. H. and Pedersen R. B. (2012) Low temperature alteration of serpentinized ultramafic rock and implications for microbial life. *Chem. Geol.* **318**–**319**, 75–87.

Okland I., Huang S., Thorseth I. H. and Pedersen R. B. (2014) Formation of H2, CH4 and N-species during low-temperature experimental alteration of ultramafic rocks. *Chem. Geol.* **387**, 22–34.

Oremland R. S., Marsh L. and DesMarais D. J. (1982) Methanogenesis in Big Soda Lake, Nevada: an Alkaline, Moderately Hypersaline Desert Lake. *Appl. Environ. Microbiol.* **43**, 462–468.

Oremland R. S., Miller L. G. and Whiticar M. J. (1987) Sources and flux of natural gases from Mono Lake, California. *Geochim. Cosmochim. Acta* **51**, 2915–2929.

Orphan V. J., House C. H., Hinrichs K.-U., McKeegan K. D. and DeLong E. F. (2002) Multiple archaeal groups mediate methane oxidation in anoxic cold seep sediments. *Proc. Natl. Acad. Sci.* **99**, 7663–7668.

Oufi O., Cannat M. and Horen H. (2002) Magnetic properties of variably serpentinized abyssal peridotites. *J. Geophys. Res. Solid Earth* **107**, EPM 3-1.

Özdemir Ö. and Dunlop D. J. (2010) Hallmarks of maghemitization in low-temperature remanence cycling of partially oxidized magnetite nanoparticles. *J. Geophys. Res. Solid Earth* **115**, B02101.

Oze C. (2005) Have olivine, will gas: Serpentinization and the abiogenic production of methane on Mars. *Geophys. Res. Lett.* **32**. Available at: http://doi.wiley.com/10.1029/2005GL022691 [Accessed February 7, 2014].

Pasini V., Brunelli D., Dumas P., Sandt C., Frederick J., Benzerara K., Bernard S. and Ménez B. (2013) Low temperature hydrothermal oil and associated biological precursors in serpentinites from Mid-Ocean Ridge. *Lithos* **178**, 84–95.

Paukert A. N., Matter J. M., Kelemen P. B., Shock E. L. and Havig J. R. (2012) Reaction path modeling of enhanced in situ CO2 mineralization for carbon sequestration in the peridotite of the Samail Ophiolite, Sultanate of Oman. *Chem. Geol.* **330**–**331**, 86–100.

Petriglieri J. R., Salvioli-Mariani E., Mantovani L., Tribaudino M., Lottici P. P., Laporte-Magoni C. and Bersani D. (2015) Micro-Raman mapping of the polymorphs of serpentine. *J. Raman Spectrosc.*, n/a-n/a.

Pokrovsky O. S. and Schott J. (1999) Processes at the magnesium-bearing carbonates/solution interface. II. kinetics and mechanism of magnesite dissolution. *Geochim. Cosmochim. Acta* **63**, 881–897.

Pokrovsky O. S., Schott J. and Castillo A. (2005) Kinetics of brucite dissolution at 25°C in the presence of organic and inorganic ligands and divalent metals. *Geochim. Cosmochim. Acta* **69**, 905–918.

Pokrovsky, Oleg S. J. S. (2004) Experimental study of brucite dissolution and precipitation in aqueous solutions: Surface speciation and chemical affinity control. *Geochim. Cosmochim. Acta* **68**, 31–45.

Postec A., Quéméneur M., Bes M., Mei N., Benaïssa F., Payri C., Pelletier B., Monnin C., Guentas-Dombrowsky L., Ollivier B., Gérard E., Pisapia C., Gérard M., Ménez B. and Erauso G. (2015) Microbial diversity in a submarine carbonate edifice from the serpentinizing hydrothermal system of the Prony Bay (New Caledonia) over a 6-year period. *Front. Microbiol.* **6**. Available at:

http://www.ncbi.nlm.nih.gov/pmc/articles/PMC4551099/ [Accessed November 20, 2015].

Power I. M., Wilson S. A. and Dipple G. M. (2013) Serpentinite Carbonation for CO2 Sequestration. *Elements* **9**, 115–121.

Prigiobbe V., Costa G., Baciocchi R., Hänchen M. and Mazzotti M. (2009) The effect of and salinity on olivine dissolution kinetics at. *Chem. Eng. Sci.* **64**, 3510–3515.

Proskurowski G., Lilley M. D., Kelley D. S. and Olson E. J. (2006) Low temperature volatile production at the Lost City Hydrothermal Field, evidence from a hydrogen stable isotope geothermometer. *Chem. Geol.* **229**, 331–343.

Proskurowski G., Lilley M. D., Seewald J. S., Olson E. J., Früh-Green G. L., Lupton J. E., Sylva S. P. and Kelley D. S. (2008) Abiogenic hydrocarbon production at Lost City hydrothermal field. *Science* **319**, 604–607.

R Development Core Team (2008) *R: A language and environment for statistical computing*., R Foundation for Statistical Computing, Vienna, Austria. Available at: http://www.R-project.org.

Ravaut P., Bayer R., Hassani R., Rousset D. and Yahya'ey A. A. (1997) Structure and evolution of the northern Oman margin: gravity and seismic constraints over the Zagros-Makran-Oman collision zone. *Tectonophysics* **279**, 253–280.

Reynard B., Bezacier L. and Caracas R. (2015) Serpentines, talc, chlorites, and their high-pressure phase transitions: a Raman spectroscopic study. *Phys. Chem. Miner.* **42**, 641–649.

Rinaudo C., Gastaldi D. and Belluso E. (2003) Characterization of Chrysotile, Antigorite and Lizardite by Ft-Raman Spectroscopy. *Can. Mineral.* **41**, 883–890.

Russell M. J., Hall A. J. and Martin W. (2010) Serpentinization as a source of energy at the origin of life: Serpentinization and the emergence of life. *Geobiology* **8**, 355–371.

Russell M. J. and Martin W. (2004) The rocky roots of the acetyl-CoA pathway. *Trends Biochem. Sci.* **29**, 358–363.

Russell M. J., Nitschke W. and Branscomb E. (2013) The inevitable journey to being. *Phil Trans R Soc B* **368**, 20120254.

Saldi G. D., Daval D., Morvan G. and Knauss K. G. (2013) The role of Fe and redox conditions in olivine carbonation rates: An experimental study of the rate limiting reactions at 90 and 150°C in open and closed systems. *Geochim. Cosmochim. Acta* **118**, 157–183.

Schoell M. (1980) The hydrogen and carbon isotopic composition of methane from natural gases of various origins. *Geochim. Cosmochim. Acta* **44**, 649–661.

Schott J., Pokrovsky O. S. and Oelkers E. H. (2009) The Link Between Mineral Dissolution/Precipitation Kinetics and Solution Chemistry. *Rev. Mineral. Geochem.* **70**, 207–258.

Schrenk M. O., Brazelton W. J. and Lang S. Q. (2013) Serpentinization, Carbon, and Deep Life. *Rev. Mineral. Geochem.* **75**, 575–606.

Schuiling R. D. (2006) Mineral Sequestration of CO2 and Recovery of the Heat of Reaction. In *Macro-Engineering* (eds. V. Badescu, R. B. Cathcart, and R. D. Schuiling). Water Science and Technology Library. Springer Netherlands. pp. 21–29. Available at: http://link.springer.com/chapter/10.1007/1-4020-4604-9_2 [Accessed February 25, 2014].

Seewald J. S., Zolotov M. Y. and McCollom T. (2006) Experimental investigation of single carbon compounds under hydrothermal conditions. *Geochim. Cosmochim. Acta* **70**, 446–460.

Sekine Y., Shibuya T., Postberg F., Hsu H.-W., Suzuki K., Masaki Y., Kuwatani T., Mori M., Hong P. K., Yoshizaki M., Tachibana S. and Sirono S. (2015) High-temperature water–rock interactions and hydrothermal environments in the chondrite-like core of Enceladus. *Nat. Commun.* **6**, 8604.

Sherwood Lollar B., Frape S. K., Weise S. M., Fritz P., Macko S. A. and Welhan J. A. (1993) Abiogenic methanogenesis in crystalline rocks. *Geochim. Cosmochim. Acta* **57**, 5087–5097.

Shibuya T., Russell M. J. and Takai K. (2016) Free energy distribution and hydrothermal mineral precipitation in Hadean submarine alkaline vent systems: Importance of iron redox reactions under anoxic conditions. *Geochim. Cosmochim. Acta* **175**, 1–19.

Shibuya T., Yoshizaki M., Sato M., Shimizu K., Nakamura K., Omori S., Suzuki K., Takai K., Tsunakawa H. and Maruyama S. (2015) Hydrogen-rich hydrothermal environments in the Hadean ocean inferred from serpentinization of komatiites at 300 °C and 500 bar. *Prog. Earth Planet. Sci.* **2**, 46.

Shock E. L. and Schulte M. D. (1998) Organic synthesis during fluid mixing in hydrothermal systems. *J. Geophys. Res. Planets* **103**, 28513–28527.

Sleep N. H., Meibom A., Fridriksson T., Coleman R. G. and Bird D. K. (2004) H2-rich fluids from serpentinization: geochemical and biotic implications. *Proc. Natl. Acad. Sci. U. S. A.* **101**, 12818–12823.

Spear J. R., Walker J. J., McCollom T. M. and Pace N. R. (2005) Hydrogen and bioenergetics in the Yellowstone geothermal ecosystem. *Proc. Natl. Acad. Sci. U. S. A.* **102**, 2555–2560.

Stanger G. (1986) The hydrogeology of the Oman Mountains. Open University London.

Stein C. A., Stein S. and Pelayo A. M. (1995) Heat flow and hydrothermal circulation. *Seafloor Hydrothermal Syst. Phys. Chem. Biol. Geol. Interact.*, 425–445.

Stevens T. O. and McKinley J. P. (2000) Abiotic Controls on H $_2$ Production from Basalt−Water Reactions and Implications for Aquifer Biogeochemistry. *Environ. Sci. Technol.* **34**, 826–831.

Stevens T. O. and McKinley J. P. (1995) Lithoautotrophic Microbial Ecosystems in Deep Basalt Aquifers. *Science* **270**, 450–455.

Streit E., Kelemen P. and Eiler J. (2012) Coexisting serpentine and quartz from carbonate-bearing serpentinized peridotite in the Samail Ophiolite, Oman. *Contrib. Mineral. Petrol.* **164**, 821–837.

Suda K., Ueno Y., Yoshizaki M., Nakamura H., Kurokawa K., Nishiyama E., Yoshino K., Hongoh Y., Kawachi K., Omori S., Yamada K., Yoshida N. and Maruyama S. (2014) Origin of methane in serpentinite-hosted hydrothermal systems: The CH4–H2–H2O hydrogen isotope systematics of the Hakuba Happo hot spring. *Earth Planet. Sci. Lett.* **386**, 112–125.

Suzuki S., Ishii S., Wu A., Cheung A., Tenney A., Wanger G., Kuenen J. G. and Nealson K. H. (2013) Microbial diversity in The Cedars, an ultrabasic, ultrareducing, and low salinity serpentinizing ecosystem. *Proc. Natl. Acad. Sci.* **110**, 15336–15341.

Suzuki S., Kuenen J. G., Schipper K., van der Velde S., Ishii S., Wu A., Sorokin D. Y., Tenney A., Meng X., Morrill P. L., Kamagata Y., Muyzer G. and Nealson K. H. (2014) Physiological and genomic features of highly alkaliphilic hydrogen-utilizing Betaproteobacteria from a continental serpentinizing site. *Nat. Commun.* **5**. Available at: http://www.nature.com/ncomms/2014/140521/ncomms4900/full/ncomms4900.html [Accessed November 19, 2014].

Szponar N., Brazelton W. J., Schrenk M. O., Bower D. M., Steele A. and Morrill P. L. (2013) Geochemistry of a continental site of serpentinization, the Tablelands Ophiolite, Gros Morne National Park: A Mars analogue. *Icarus* **224**, 286–296.

Takai K., Nakamura K., Toki T., Tsunogai U., Miyazaki M., Miyazaki J., Hirayama H., Nakagawa S., Nunoura T. and Horikoshi K. (2008) Cell proliferation at 122°C and isotopically heavy CH4 production by a hyperthermophilic methanogen under high-pressure cultivation. *Proc. Natl. Acad. Sci.* **105**, 10949–10954.

Takami H., Noguchi H., Takaki Y., Uchiyama I., Toyoda A., Nishi S., Chee G.-J., Arai W., Nunoura T., Itoh T., Hattori M. and Takai K. (2012) A Deeply Branching Thermophilic Bacterium with an Ancient Acetyl-CoA Pathway Dominates a Subsurface Ecosystem. *PLoS ONE* **7**, e30559.

Tauxe L., Banerjee S. K., Butler R. F. and van der Voo R. (2014) Essentials of Paleomagnetism, 3rd Web Edition.

Telling J., Boyd E. S., Bone N., Jones E. L., Tranter M., MacFarlane J. W., Martin P. G., Wadham J. L., Lamarche-Gagnon G., Skidmore M. L., Hamilton T. L., Hill E., Jackson M. and Hodgson D. A. (2015) Rock comminution as a source of hydrogen for subglacial ecosystems. *Nat. Geosci.* **8**, 851–855.

Templeton A. S., Chu K.-H., Alvarez-Cohen L. and Conrad M. E. (2006) Variable carbon isotope fractionation expressed by aerobic CH4-oxidizing bacteria. *Geochim. Cosmochim. Acta* **70**, 1739–1752.

Tindall B. J., Sikorski J., Lucas S., Goltsman E., Copeland A., Glavina Del Rio T., Nolan M., Tice H., Cheng J.-F., Han C., Pitluck S., Liolios K., Ivanova N., Mavromatis K., Ovchinnikova G., Pati A., Fähnrich R., Goodwin L., Chen A., Palaniappan K., Land M., Hauser L., Chang Y.-J., Jeffries C. D., Rohde M., Göker M., Woyke T., Bristow J., Eisen J. A., Markowitz V., Hugenholtz P., Kyrpides N. C., Klenk H.-P. and Lapidus A. (2010) Complete genome sequence of Meiothermus ruber type strain (21T). *Stand. Genomic Sci.* **3**, 26–36.

Toft P. B., Arkani-Hamed J. and Haggerty S. E. (1990) The effects of serpentinization on density and magnetic susceptibility: a petrophysical model. *Phys. Earth Planet. Inter.* **65**, 137–157.

Valentine D. L., Chidthaisong A., Rice A., Reeburgh W. S. and Tyler S. C. (2004) Carbon and hydrogen isotope fractionation by moderately thermophilic methanogens1. *Geochim. Cosmochim. Acta* **68**, 1571–1590.

Wang Q., Garrity G. M., Tiedje J. M. and Cole J. R. (2007) Naive Bayesian classifier for rapid assignment of rRNA sequences into the new bacterial taxonomy. *Appl. Environ. Microbiol.* **73**, 5261–7.

Weyhenmeyer C. (2000) Origin and evolution of groundwaters in the alluvial aquifer of the Eastern Batinah Coastal Plain, Sultanate of Oman. *PhD Thesis Univ. Bern Switz.*

Whiticar M. J. (1990) A geochemial perspective of natural gas and atmospheric methane. *Org. Geochem.* **16**, 531–547.

Whiticar M. J. (1999a) Carbon and hydrogen isotope systematics of bacterial formation and oxidation of methane. *Chem. Geol.* **161**, 291–314.

Whiticar M. J. (1999b) Carbon and hydrogen isotope systematics of bacterial formation and oxidation of methane. *Chem. Geol.* **161**, 291–314.

Whiticar M. J. and Faber E. (1986) Methane oxidation in sediment and water column environments—Isotope evidence. *Org. Geochem.* **10**, 759–768.

Wilke M., Farges F., Petit P.-E., Brown G. E. and Martin F. (2001) Oxidation state and coordination of Fe in minerals: An Fe K-XANES spectroscopic study. *Am. Mineral.* **86**, 714–730.

Willems A., Busse J., Goor M., Pot B., Falsen E., Jantzen E., Hoste B., Gillis M., Kersters K., Auling G. and others (1989) Hydrogenophaga, a new genus of hydrogen-oxidizing bacteria that includes Hydrogenophaga flava comb. nov.(formerly Pseudomonas flava), Hydrogenophaga palleronii (formerly Pseudomonas palleronii), Hydrogenophaga pseudoflava (formerly Pseudomonas pseudoflava and "Pseudomonas carboxydoflava"), and Hydrogenophaga taeniospiralis (formerly Pseudomonas taeniospiralis). *Int. J. Syst. Bacteriol.* **39**, 319–333.

Worakit S., BOONE D. R., MAH R. A., ABDEL-SAMIE M.-E. and El-Halwagi M. M. (1986) Methanobacterium alcaliphilum sp. nov., an H2-utilizing methanogen that grows at high pH values. *Int. J. Syst. Bacteriol.* **36**, 380–382.

Worm H.-U. (1998) On the superparamagnetic—stable single domain transition for magnetite, and frequency dependence of susceptibility. *Geophys. J. Int.* **133**, 201–206.

Woycheese K. M., Meyer-Dombard D. R., Cardace D., Argayosa A. M. and Arcilla C. A. (2015) Out of the dark: transitional subsurface-to-surface microbial diversity in a terrestrial serpentinizing seep (Manleluag, Pangasinan, the Philippines). *Front. Microbiol.* **6**. Available at: http://journal.frontiersin.org/Article/10.3389/fmicb.2015.00044/abstract [Accessed May 21, 2015].

Zeikus J. G. (1977) The biology of methanogenic bacteria. *Bacteriol. Rev.* **41**, 514–541.

Zinder S. H. (1993) Physiological Ecology of Methanogens. In *Methanogenesis* (ed. D. J. G. Ferry). Chapman & Hall Microbiology Series. Springer US. pp. 128–206. Available at: http://link.springer.com/chapter/10.1007/978-1-4615-2391-8_4 [Accessed November 11, 2015].

Zyakun A. M. (1996) Potential of 13C/12C variations in bacterial methane in assessing origin of environmental methane. Available at: http://archives.datapages.com/data/specpubs/memoir66/25/0341.htm [Accessed December 15, 2016].

Appendix A

CHAPTER 2

Comment and Reply to "Methane origin in the Samail ophiolite: Comment on “Modern water/rock reactions in Oman hyperalkaline peridotite aquifers and implications for microbial habitability”" [*Geochim. Cosmochim. Acta* 179 (2016) 217–241]

Supporting Information

Miller et al. 2016 was published in GCA, then Giuseppe Etiope received a comment that we correspondingly replied to, both are detailed below:

Comment on "Modern water/rock reactions in Oman hyperalkaline peridotite aquifers and implications for microbial habitability" by Miller et al. 2016

Author: Giuseppe Etiope

Instituto Nazionale di Geofisica e Vulcanologia, Sezione Roma 2, Italy, and Faculty of Environmental Science and Engineering, Babes-Bolyai University, Cluj-Napoca, Romania

Corresponding author: giuseppe.etiope@ingv.it

Published 8 August 2016

Miller et al. (2016) report a new study of fluids in the peridotites of the Samail ophiolite in Oman related to modern serpentinization (olivine hydration), a process that can provide energy and raw materials for chemosynthetic microbial life. The authors, in particular, report an isotopic composition for methane (CH_4) in groundwater near Ibra (up to 1.4 mM) that is unusually 13C-enriched ($\delta^{13}C_{CH4}$ ~ +2.4 and +3‰ VPDB), and consider the gas origin to be uncertain, i.e., abiotic or microbial, and to be modulated by significant fractionation due to oxidation or diffusion. The purpose of this comment is to clarify and correct a few points concerning the possible origin of the $\delta^{13}C_{CH4}$ values, with the intention to promote a fruitful and constructive debate, considering the interest that there is for serpentinization and the associated formation of

various gases. The CH_4 data from Miller et al. are re-examined in a global context of gas in serpentinized peridotites and, in particular, by considering published data (isotope composition of CH_4 and concentrations of C2+ alkanes) also obtained from the Samail ophiolite, data neglected by the authors. These data significantly impact the interpretation of Miller et al. concerning the possibility that methane can be microbial. Potential isotopic fractionations by oxidation or diffusion, evaluated considering $\delta^{13}C_{CH4} - \delta D_{CH4}$ correlated variations, the occurrence of significant amounts of ethane and propane in the Oman ophiolite aquifers and Rayleigh fractionation analysis suggest that methane can hardly be considered microbial. Isotopic fractionations, however, are not necessary to explain the unusual $\delta^{13}C_{CH4}$ values: an alternative hypothesis is that methane carbon may derive from 13C-enriched carbonates occurring below the Samail ophiolite nappe, a hypothesis not considered by Miller et al.

1. THE IBRA BOREHOLE $\delta^{13}C_{CH4}$ VALUES ARE NOT THE HIGHEST OBSERVED TO DATE

A first note addresses the singularity of the $\delta^{13}C_{CH4}$ values. Miller et al. claimed (in the Abstract and on page 233) that the CH_4 they analyzed has the heaviest carbon (the most 13C-enriched) reported in the literature to date ($\delta^{13}C_{CH4} \sim +2.4$ and +3‰ VPDB). Their statement is not correct. Much more 13C-enriched CH4 values, with $\delta^{13}C_{CH4}$ up to +21‰, were reported by Potter et al. (2004) for gas measured in the German Zechstein (Permian) evaporite; this 13C enrichment was likely due to evaporation of brines.

2. GLOBAL CONTEXT AND NEGLECTED GAS GEOCHEMICAL DATA

The Samail ophiolite in Oman is one of tens of sites in the world where methane related to active serpentinization has been reported since the 1980s (e.g., Etiope and Schoell, 2014). To date, CH_4-rich hyperalkaline waters and/or gas seeps issuing from faulted peridotites have been documented in at least 16 countries (in Oman as well as in the Philippines, New Zealand, Turkey, Italy, Greece, Portugal, Spain, United States - California, Costa Rica, Japan, the United Arab Emirates, Canada, New Caledonia, Norway, and Serbia). Whenever stable C and H isotope ratios of CH4 are analyzed together, a dominant abiotic origin of the gas, related to the reduction of a C compound (generally CO_2) via Fischer–Tropsch or Sabatier reactions, has been suggested (with the exception of The Cedar springs in California that release dominantly microbial CH_4; Wang et al., 2015). At least 60 hyperalkaline springs, some displaying free gas bubbling, have been documented within the Samail ophiolite in Oman (Neal and Stanger, 1983). Fritz et al. (1992) were the first to report the stable C and H isotopic composition of CH_4 within the Samail peridotite and to propose an abiotic origin. Successive works (Sano et al., 1993; Boulart et al., 2013) also suggested inorganic reactions as the source of gas and excluded microbial origins. Recently, Etiope et al. (2015) reported a typical abiotic isotopic composition of CH4 within the Samail peridotite aquifer in the United Arab Emirates. Unfortunately, Miller et al. did not take into account all these publications, which provide a useful reference for better evaluating methane origin in the two boreholes investigated.

3. REASSESSING CH4 ORIGIN

Fig. 1 provides the new isotope data of Miller et al. (boreholes NSHQ) together with the data of Fritz et al. (1992), Sano et al. (1993), and Etiope et al. (2015) for the Samail ophiolite. Additional values are provided for all other continental serpentinization sites discovered to date.

The new Samail data of Miller et al. are actually the most 13C-enriched among the serpentinization sites and fall near the traditionally defined abiotic range. CH_4 in Oman hyperalkaline waters has a variable isotopic signature: $\delta^{13}C$ is 34‰ at Ain Al-Waddah (Sano et al., 1993) and approximately 12 to 15‰ at Nizwa and Al Khoud (Fritz et al., 1992). Miller et al. suggested that methane at Ibra, with a $\delta^{13}C_{CH4} \sim +2.4$ and +3‰, could be abiotic or microbial, since they detected some methanogens in the water. In any case Miller et al. outline that methane would be affected by extensive fractionation due to biological oxidation or diffusion, with both processes enriching the residual methane in 13C. In both cases, as the authors admit, methane should also be enriched in 2 H, a finding that was not observed. Nevertheless, in the Conclusions section, the authors kept a microbial origin hypothesis without explaining how microbial gas, even after oxidation, could have acquired a combination of ‘‘abnormal” (positive) $\delta^{13}C_{CH4}$ values and ‘‘normal” δD_{CH4} values. The wide range of $\delta^{13}C_{CH4}$ values of the Samail ophiolite fluids, now shown in Fig. 1, can be due to different carbon feedstocks, temperatures of C reduction and degree of reaction completeness (Etiope and Ionescu, 2015).

3.1. Microbial methane origin?

The microbial oxidation of methane produces $\delta^{13}C_{CH4}$– δD_{CH4} correlated variations with $\Delta H/\Delta C$ ~8–9 (Alperin et al., 1988; Feisthauer et al., 2011). ΔH and ΔC are the respective variations in δD_{CH4} and $\delta^{13}C_{CH4}$ values: when the $\delta^{13}C_{CH4}$ value increases by 1‰, the corresponding δD_{CH4} value increases by ~8–9‰. Following this trend (red arrow in Fig. 1), it is clear that NSHQ methane cannot be derived from any microbial gas (neither from thermogenic gas). It could be derived from abiotic methane, similar to that observed within the Samail ophiolite located in the United Arab Emirates (Al Farfar; Etiope et al., 2015). Such oxidation could have been favored

by stagnant water in boreholes. In order to be microbial in origin, the NSHQ methane should have experienced an oxidation with $\Delta H/\Delta C \sim 2$. To date, there are no enzymes (methane monooxygenases) known to produce such low methane isotope enrichment factors (Feisthauer et al., 2011). A non-microbial origin of methane is supported by the presence of considerable amounts of C2+ alkanes (from ethane to butane) in hyperalkaline Oman waters, with total concentrations within the extracted gas phase on the order of 10–100 ppmv (in 9 sites analysed, including springs in the Ibra area; Boulart et al., 2013). Dissolved ethane is up to 0.28 lmol/L, similar to the amounts observed in the Tableland ophiolite springs, where methane was considered nonmicrobial (Morrill et al., 2014). It is known that only trace amounts of ethane and propane can be produced by microbes and under special conditions in seafloor sediments (Formolo, 2010). Ethanogens and propanogens have never been detected in hyperalkaline waters. So, based on what we know today, and as interpreted for C2+ bearing hyperalkaline springs elsewhere (e.g. Morrill et al., 2014), the presence of C2+ hydrocarbons suggests that microbial gas, if any, is not a dominant component of the methane within the hyperalkaline waters of the Samail ophiolite.

Miller et al. also mention the possibility that NSHQ methane is isotopically fractionated due to diffusion. 13C-enrichment by gas diffusion is generally not significant in natural gas geologic systems because the main gas migration mechanism, especially in tectonized (fractured, faulted) rocks, is advection (driven by pressure gradients) and not diffusion (driven by concentration gradients). Advection may lead to molecular fractionation but not to isotopic fractionation (Etiope, 2015). Diffusion can be dominant in low permeability (non fractured) igneous rocks, shales and evaporites. The Ibra area is characterized by salt tectonics, with salt diapirs responsible for basin uplift (the Ibra Dome). Evaporites occur below the peridotite nappe,

specifically beneath the Sumeini Unit (Hopson et al., 1981; Cooper et al., 2013). Salt diapirs could act as a sort of impermeable barrier along the gas migration pathway, isotopically filtering gas whose residual component may enter the ophiolite aquifer. The hypothesis requires a complex combination of factors. However, assuming that the diffusion fractionation factor for hydrogen isotopes is an order of magnitude larger than that for carbon (Alperin et al., 1988), it is clear from Fig. 1 that the original gas must always be abiotic. For any type of fractionation, then, a rapid check of Rayleigh fractionation shows that in order to get 1.4 mM CH4 with $\delta^{13}C_{CH4}$ ~+3‰ from a supposed microbial $\delta^{13}C_{CH4}$ < 60‰ (e.g. like The Cedars springs), the original microbial CH4 amount would have been very large, 2–3 orders of magnitude above concentrations typically observed in hyperalkaline springs.

Basically, we cannot exclude that there may be a fraction of microbial methane in the NSHQ gas, but multiple lines of evidence suggest that this component should not be relevant.

3.2. Heavy carbon sources

Looking for potential CH_4 precursors (carbon feedstock), Miller et al. did not find formate or other organic acids that are assumed to have a role in CH_4 genesis in hyperalkaline fluids. However, the authors did find carbonates within the peridotite drill cuttings, with d13C values ranging from 1.48 to 7.05‰. These values are lighter than $\delta^{13}C_{CH4}$, suggesting, as the authors indicate, that these carbonates cannot be the carbon feedstock even if the entire dissolved inorganic carbon pool was converted to methane under extreme carbon limitation. The authors assumed, then, that further $\delta^{13}C$ enrichment by methane diffusion or oxidation is required to explain the positive $\delta^{13}C_{CH4}$ values. This possibility has been discussed above, based on Fig. 1. However, such secondary, post-genetic, alteration processes would not be necessary in order to

explain the positive $\delta^{13}C_{CH4}$ values. In fact, Miller et al. did not consider the possibility that methane carbon may derive from 13C-enriched Permian carbonates belonging to the Hawasina, Sumeini, or Saih Hatat formations occurring below the Samail ophiolite nappe. In particular, the Coquina and Reefal Limestone units (Wadi Wasit block) typically yield marine Permian values from +2 to +4‰ (e.g., Richoz et al., 2010), isotopic values that are similar to those of NSHQ CH_4. These Permian carbonates also outcrop in many places at the margin of the Semail block and are in lateral tectonic contact with the ophiolite in the Ibra zone (Hopson et al., 1981). Therefore, Permian carbonates could be effective sources of 13C-enriched CO_2 (allochthonous in the studied system) that can then be reduced to CH_4, likely with H_2 generated by peridotite serpentinization. Low temperature (<100°C) CO_2-H_2 reactions may be catalyzed by platinum group elements, such as ruthenium, which are particularly abundant in the Ibra chromitites (Etiope and Ionescu, 2015 and references therein). Alternatively, we cannot exclude that the dissolved CH_4 at Ibra derives from magmatic or post-magmatic fluid inclusions in the peridotite.

4. MISQUOTATIONS

Finally, two minor notes regarding references and data misquotation. Miller et al. wrote: ‘‘Platinum group metal inclusions, including Ru and Rh, are found in chromites (e.g., Jacquemin et al., 2010). Platinum group metals in chromites in Oman could be catalyzing low temperature methane formation and leading to a heavy $\delta^{12}C_{CH4}$ signature, but there are no experimental data to confirm this hypothesis”. To be precise, Jacquemin et al. (2010) did not reference chromites or any other rock. A correct reference for the ruthenium-chromite link would be Etiope and Ionescu (2015), which also reports experimental data supporting the hypothesis of low temperature methane production catalyzed by ruthenium. In their Table 2, Miller et al. report $\delta^{2}H$ values of

H_2 (-40 to -50‰) for The Cedar springs (California) with a reference from Morrill et al. (2013). The authors likely confused the δ^2H values with those of water, H_2O (-40‰). Morrill et al. (2013) did not report any isotopic data for H_2.

References

Alperin, M.J., Reeburgh, W.S., Whiticar, M.J. (1988) Carbon and hydrogen isotope fractionation resulting from anaerobic methane oxidation. *Global Biogeoch. Cycles,* **2**, 219-288.

Boulart C, Chavagnac V, Monnin C, Delacour A, Ceuleneer G, Hoareau G (2013) Differences in gas venting from ultramafic-hosted warm springs: the example of Oman and Voltri ophiolites. *Ofioliti,* **38**,143–156

Cooper D.J.W., Ali M.Y., Searle M.P., Al-Lazki A.I. (2013) Salt intrusions in Jabal Qumayrah, northern Oman Mountains: Implications from structural and gravity investigations. *GeoArabia,* **18**, 141-176.

Etiope G. (2015). *Natural Gas Seepage. The Earth's hydrocarbon degassing*. Springer, pp. 199.

Etiope G., Ionescu A. (2015) Low-temperature catalytic CO2 hydrogenation with geological quantities of ruthenium: a possible abiotic CH4 source in chromitite-rich serpentinized rocks. *Geofluids,* **15**, 438-452.

Etiope G., Judas J., Whiticar M.J. (2015) Occurrence of abiotic methane in the eastern United Arab Emirates ophiolite aquifer. *Arab. J. Geosci.*, **8**, 11345-11348

Etiope G., Vadillo I., Whiticar M.J., Marques J.M. , Carreira P.M., Tiago I., Benavente J., Jiménez P., Urresti B. (2016) Abiotic methane seepage in the Ronda peridotite massif, southern Spain. *Appl. Geochemistry,* **66**, 101-113

Feisthauer S., Vogt C., Modrzynski J., Szlenkier M., 203 Krüger M., Siegert M., Richnow R.-R. (2011). Different types of methane monooxygenases produce similar carbon and hydrogen isotope fraction patterns during methane oxidation. *Geochim. Cosmochim. Acta,* **75**, 1173-1184.

Formolo M (2010) The microbial production of methane and other volatile hydrocarbons. In: Kenneth N (ed) *Timmis handbook of hydrocarbon and lipid microbiology*, Springer, New York. pp 113–126

Fritz P, Clark ID, Fontes J-C, Whiticar MJ, Faber E (1992) Deuterium and 13C evidence for low temperature production of hydrogen and methane in a highly alkaline groundwater environment in Oman. In: Kharaka YK, Maest AS (eds), *Proceedings of 7th Int symp water–rock interaction: low temperature environments*, vol 1. Balkema, Rotterdam, pp 793–796

Hopson C.A., Coleman R.G., Gregory R.T., Pallister J.S., Bailey E.H. (1981) Geologic section through the Samail Ophiolite and associated rocks along a Muscat-Ibra transect, Southeastern Oman Mountains. *J. Geoph. Res.*, **86**, 2527-2544.

Miller H.M., Matter J.M., Kelemen P., Ellison E.T., Conrad M.E., Fierer N., Ruchala T., Tominaga M., Templeton A.S. (2016) Modern water/rock reactions in Oman hyperalkaline peridotite aquifers and implications for microbial habitability. *Geochim. Cosmochim. Acta,* **179**,

217-241.

Morrill P.L., Kuenen J.G., Johnson O.J., Suzuki S., Rietze A., Sessions A.L., Fogel M.L., Nealson K.H. (2013) Geochemistry and geobiology of a present-day serpentinization site in California: the Cedars. *Geochim. Cosmochim. Acta* **109**, 222–240.

Morrill P.L., Brazelton W.J., Kohl L., Rietze A., Miles S.M., Kavanagh H., Schrenk M.O., Ziegler S.E., Lang S.Q. (2014) Investigations of potential microbial methanogenic and carbon monoxide utilization pathways in ultra-basic reducing springs associated with present-day continental serpentinization: The Tablelands, NL, CAN. *Front. Microbiol*., **5**, 1–13

Neal C. and Stanger G. (1983) Hydrogen generation from mantle source rocks in Oman. *Earth Planet. Sci. Lett.* **66**, 315–320.

Potter J., Siemann M.G., Tsypukov M. (2004) Large-scale carbon isotope fractionation in evaporites and the generation of extremely 13238 C-enriched methane. *Geology*, **32**, 533-536.

Richoz S., Krystyn L., Baud A., Brandner R., Horacek M., Mohtat-Aghai P. (2010) Permian–Triassic boundary interval in the Middle East (Iran and N. Oman): Progressive environmental change from detailed carbonate carbon isotope marine curve and sedimentary evolution. *J. Asian Earth. Sci.*, **39**, 236-253.

Sano Y., Urabe A., Wakita H. and Wushiki H. (1993) Origin of hydrogen-nitrogen gas seeps, Oman. *Appl. Geochem.*, **8**, 1-8.

Wang, D.T., Gruen, D.S., Sherwood Lollar, B., Hinrichs, K.-U., Stewart, L.C., Holden, J.F., Hristov, A.N., Pohlman, J.W., Morrill, P.L., Konneke, M., Delwiche, K.B., Reeves, E.P., Sutcliffe, C.N., Ritter, D.J., Seewald, J.S., McIntosh, J.C., Hemond, H.F., Kubo, M.D., Cardace,D., Hoehler, T.M., Ono, S. (2015) Nonequilibrium clumped isotope signals in microbial methane. *Science*, **348**, 428-431.

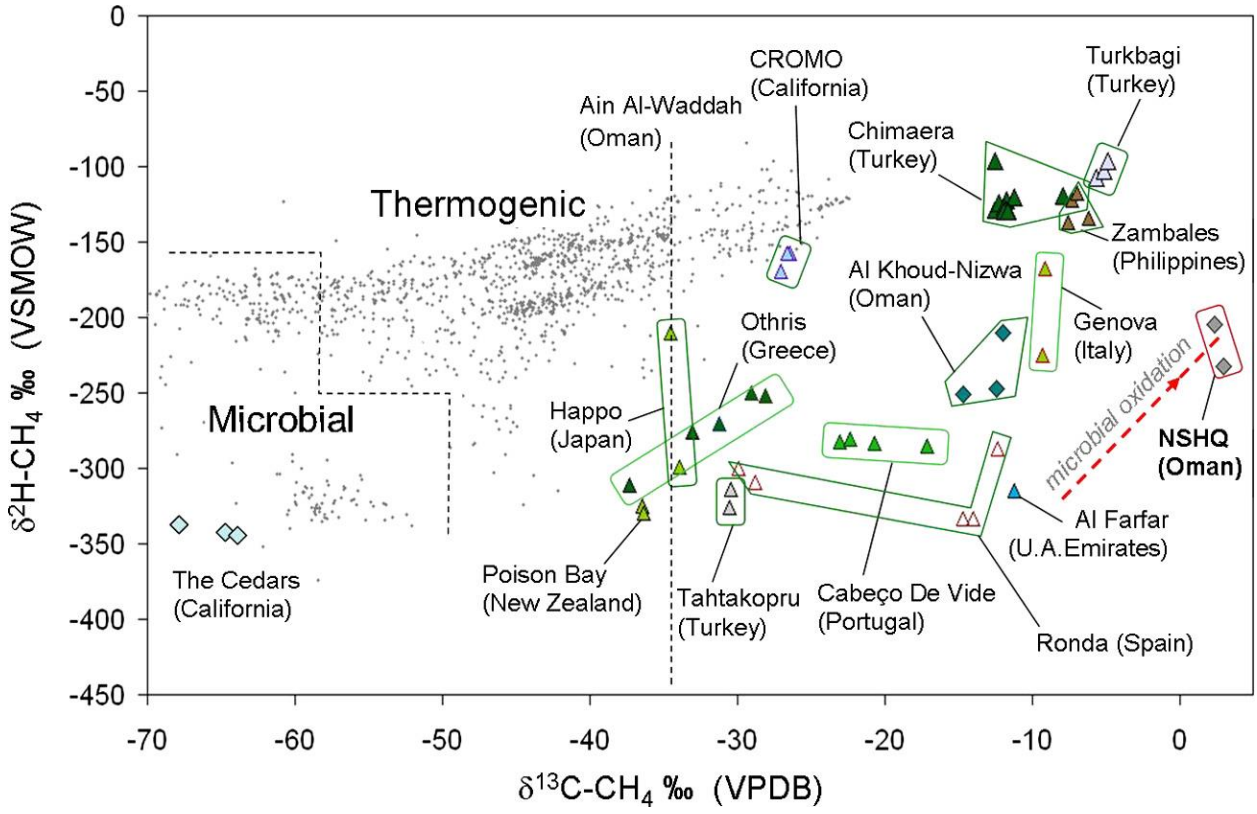

Fig. 1. The deuterium and carbon isotope ratios of methane reported by Miller et al. (2016) (NSHQ) as compared to other sites located within the Samail ophiolite (Oman and United Arab Emirates), land-based serpentinization sites worldwide, and global data-sets of biotic (microbial and thermogenic) gas (data from Etiope and Schoell, 2014; Wang et al., 2015; Etiope et al., 2016). Only d13C was analysed for the Ain Al-Waddah spring (vertical dashed line; Sano et al., 1993). The red arrow shows the microbial oxidation trend (d13CCH4–d2HCH4 correlated variations with DH/DC _ 8–9), as explained in the text. (For interpretation of the references to colour in this figure legend, the reader is referred to the web version of this article.)

Reply to ‘‘Methane origin in the Samail ophiolite: Comment on‘Modern water/rock reactions in Oman hyperalkaline peridotite aquifers and implications for microbial habitability’”[Geochim. Cosmochim. Acta 179 (2016) 217–241]

Authors: Hannah M. Miller, Ju¨rg M. Matter, Peter Kelemen, Eric T. Ellison,
Mark Conrad, Noah Fierer, Tyler Ruchala, Masako Tominaga,
Alexis S. Templeton

Published 16 November 2016

We thank Dr. Giuseppe Etiope for his comment and the opportunity to further discuss why we consider the origin of the methane detected in subsurface fluids obtained from a peridotite aquifer in Oman to be enigmatic.

The central focus of Miller et al. (2016) was the characterization of the fluids and dissolved gases recovered from 300 meter wells drilled into peridotite at two locations near Ibra. Microscale geochemical analyses of rock chips recovered during drilling gave further insight into the aqueous geochemistry measurements. These samples allowed us to analyze the extent of modern peridotite hydration and secondary mineralization in light of potential hydrogen-generating reactions. Additionally, biomass was recovered from the fluids, and 16S rRNA showed the presence of methanogens and methanotrophs. These methane-cycling microbes may be modulating the isotopic signature of CH_4 found in the wells; thus, we do not feel comfortable rejecting the hypothesis that microbial activity contributes to the unusual isotopic signature of CH_4 in the wells without further investigation.

The comment by Etiope (2016) is entirely directed towards the interpretation of the two methane $\delta^{13}C$ and δD values reported. Miller et al. (2016) simply hypothesized about possible origins of the CH_4 and offered several potential processes, both abiotic and biotic, which could contribute to the positive $\delta^{13}C$ observed in the CH_4. We recognize this is a complex topic because numerous physical, chemical and biological processes likely modulate the residence time and reaction histories of the fluids that were sampled, as well as the concentrations and isotopic composition of the gases. We are now conducting more comprehensive studies to understand the coupled abiotic and biological processes that may give rise to hydrogen and methane cycling, whereas Miller et al. (2016) simply presented novel data and discussed potential processes leading to the positive $\delta^{13}C$ CH_4. With the framework that identifying the origin of the methane was only a small portion of Miller et al. (2016), we will reply to Etiope's comment and engage in further debate.

Etiope (2016) makes the point that the $\delta^{13}C$ CH_4 values found in subsurface Oman boreholes are the most positive $\delta^{13}C$ values from a serpentinization site reported so far, but not the heaviest values reported in the literature as we asserted. We regret our error in the original paper and were interested to read the Potter et al. 2004 paper. However, Miller et al. (2016) did provide a global context for the $\delta^{13}C$ CH_4 values measured near Ibra and gave examples of methane isotopic measurements from crystalline bedrock and/or serpentinization sites in the Zambales ophiolite, Lost City, Canadian Shield, and Cedars ophiolite. Additionally, Figure 2 showed how the $\delta^{13}C$ values of dissolved methane samples at wells NSHQ04 and NSHQ14 compare to CH_4 isotopic measurements from various sites around the world as presented in Etiope's extensive body of work on the subject (Etiope et al., 2013). Etiope (2016) has now contributed an excellent visual representation for several additional sites (see Figure 1).

The methane isotopic compositions reported in Miller et al. (2016) do differ strongly from known isotopic compositions of biogenic methane. Currently, only abiogenic pathways are known to produce isotopically heavy methane values with $\delta^{13}C$ values > -25‰ (Etiope and Schoell, 2014).

Etiope (2016) proposes that the heavy $\delta^{13}C$ of the NSHQ04 and NSHQ14 methane could be due to the reduction of isotopically heavy dissolved inorganic carbon derived from Permian carbonates underlying the ophiolite. However, the geology of the Ibra area does not support this hypothesis. The aquifer intersected by wells NSHQ04 and NSHQ14 is in a relatively well-defined hydrological catchment area that does not contain any Coquina and Reefal Limestone (Permian) outcrops. The Hawasina sediments (including carbonates) do underlie the ophiolite, and they do have carbon isotope ratios that are heavier, >0.5‰, (Weyhenmeyer, 2000) than the carbonate veins, -0.12 to -9.64‰ and DIC in alkaline spring waters in the peridotite, -11.66 to -23.67‰ (Kelemen et al., 2011). If the Hawasina-derived carbonate is transferred into the peridotite aquifer, there should be an enrichment in the DIC $\delta^{13}C$, which is not observed. The peridotites and the Hawasina sediments are hydrologically separated by the metamorphic sole at the base of the ophiolite, which acts as a barrier to fluid exchange. This is supported by the occurrence of many springs along this contact, where large changes in hydraulic conductivity occur.

Fluid exchange between the Permian carbonates and the groundwater in NSHQ04 and NSHQ14 is considered unlikely. Weyhenmeyer et al. (2002) measured $^{87}Sr/^{86}Sr$ isotopes of groundwater samples in the Samail ophiolite that varied from 0.7080 to 0.7088, which showed that the fluid chemistry was only affected by water/rock reactions with tertiary gravels and carbonate veins in the peridotite. Similarly low $^{87}Sr/^{86}Sr$ values have been measured by co-author Juerg Matter for

fluids in NSHQ04 (0.705642) and in NSQH14 (0.707587). Underlying allochthonous metasediments of the Hawasina Group have a more radiogenic strontium isotope ratio >0.7100, including values as high as 0.7189 (Weyhenmeyer et al., 2002; Falk and Kelemen, 2015). Although, low-grade portions of the metamorphic sole do have $^{87}Sr/^{86}Sr$ values as low as 0.7061 (Falk and Kelemen, 2015), which allows the possibility that NSHQ14 fluids may have interacted with fluids in contact with the metamorphic sole. However, the proposal that carbon is transferred from water/rock interaction in the Hawasina carbonate sediments into the peridotite aquifer is unlikely.

Etiope (2016) also hypothesizes that the CH_4 migration pathways could be affected by salt diapirs in the area. However, the wells are north of the Ibra salt dome, and the observations of Cooper et al. 2013 are not directly relevant; this study refers to a region in northern Oman, not in the Tayin Massif where the wells are situated.

We agree with Etiope and Schoell (2014) that CH_4 production is prevalent in hyperalkaline fluids hosted in serpentinites, such as the Type II fluids sampled in this study at NSHQ14 and NSHQ04. We also agree that methane likely forms through low temperature CO_2-reduction pathways that are abiotically catalyzed. Several works have invoked FTT or Sabatier reactions as an abiotic source of CH_4 in sites of active serpentinization. However, the reaction mechanism has not yet been directly constrained in low-temperature serpentinizing systems. Thus we caution against labelling these gasses as strictly abiotic. Such statements are too exclusive of physical and biological processes that may modulate CH_4 gas concentrations and isotopic signatures, and they prevent continued evaluation of the reaction pathways operating in such aquifers.

We reiterate that the coupled δD and $\delta^{13}C$ isotopic compositions of the methane is most consistently interpreted as abiogenic according to empirically defined isotope fields (Etiope et

al., 2013), as well as in Figure 1 (Etiope 2016). Miller et al. (2016) and Etiope (2016) both agree that when the methane originally formed, the $\delta^{13}C$ was probably not as positive as is measured in our samples. Any action that significantly shifts the isotopic composition of the δD and $\delta^{13}C$ of the methane will require significant loss and distillation, such as diffusion or oxidation. This would imply extensive methane consumption given the millimolar concentrations of dissolved methane measured in the deep well fluids. If methane does undergo significant aerobic biological oxidation in the shallow subsurface, we agree that the $\delta H/\delta C$ for methanotrophy will impart a steep slope due to the strong kinetic fractionation imparted by methane monooxygenase during the irreversible breaking of the C-H bond (Wang et al., 2016). If we use the current $\delta^{13}C$ and δD of the CH_4 detected in wells NSHQ04 and NSHQ14 and trace backwards to a potential initial isotopic composition, those projected values will fall within a field empirically defined as abiotic, as shown by Etiope (2016). Therefore, we concur that abiotic C reduction may well be the most likely mechanism of CH_4 formation, as originally discussed by Miller et al. (2016).

However, we do not know the original $\delta^{13}C$ and δD CH_4 and we do not have sufficient data points to define the field of possible CH_4 isotopic compositions in the aquifer; therefore, we also consider alternative processes that may have generated methane with unexpected initial isotopic compositions. Miller et al. (2016) aimed to characterize the water/rock reactions in the hyperalkaline aquifer that could sustain microbial life in the subsurface. The paper discussed how CH_4 is relevant, because it can be both a product of methanogenesis and/or a potential electron donor for microbes in the subsurface. The aqueous geochemistry of the wells is favorable for anaerobic oxidation of methane (AOM) with sulfate, Fe(III)-oxides or nitrate as suitable electron acceptors. During AOM under energy-limited conditions, it is considered that CH_4 is cycled under conditions of greater reversibility which could permit hydrogen exchange

between C□4 and H_2O. Such reversible exchange would reset the methane □D towards an equilibrium value with cellular water during C-H bond breakage and reassembly (see Wang et al. 2016). Thus, progressive consumption of methane could generate a shallower slope of □H/□C under well conditions reported in Miller et al. (2016), leading to preferential □^{13}C enrichment.

Diffusion should not be ignored in this system. Etiope (2016) suggests the gases would be transported via advective flow. However, we are not sampling near a fault contact delivering fluids or gases to the surface. Below 50 meters, the peridotite aquifer has low permeability (Dewandel et al., 2005). Fluids are stored over long residence times, and the surface of the unconfined water table is located a few tens of meters below the land surface (Paukert, 2014). We can then assume some loss of H_2 and CH_4 through diffusive gas transport, but it is important to note that currently, there is not sufficient data to support either diffusive or advective transport. If we consider the isotopic effects derived from the diffusion of $^{12}CH_4$, $^{13}CH_4$ and $^{12}CH_3D$, independent of oxidation processes, we would predict a very shallow slope for □H/□C for diffusive loss of CH_4 alone (Alperin et al., 1988).

We are currently studying 15 wells in the Samail ophiolite of Oman that tap into gabbro and peridotite-hosted subsurface fluids. By capturing methane from a greater number of geochemical, hydrological and biological conditions, and applying a greater focus on the molecular composition of the full suite of hydrocarbons, we should be able to better unravel the sources of CH_4, possible mixing of CH_4 sources, and processes that contribute to CH_4 turnover and loss. We are also now working with cultures of methanogenic and methane consuming organisms cultivated from well NSHQ04 in Oman that will permit greater scrutiny of the processes controlling the observed isotopic composition of CH_4. The discussion in Miller et al. (2016), Etiope (2016) and this reply highlight some of the critical processes to be deciphered in

the coupling between low-temperature geochemical and biological processes in the H_2 and CH_4 rich fluids commonly found in ophiolites. Although we cannot yet definitively pinpoint the CH_4 origins in the Oman aquifer, it will certainly require further research into both biotic and abiotic processes. We are excited that this work has generated interest in the scientific community, and this debate should continue to fruitfully evolve.

References

Alperin M. J., Reeburgh W. S. and Whiticar M. J. (1988) Carbon and hydrogen isotope fractionation resulting from anaerobic methane oxidation. *Glob. Biogeochem. Cycles* **2**, 279–288.

Dewandel B., Lachassagne P., Boudier F., Al-Hattali S., Ladouche B., Pinault J.-L. and Al-Suleimani Z. (2005) A conceptual hydrogeological model of ophiolite hard-rock aquifers in Oman based on a multiscale and a multidisciplinary approach. *Hydrogeol. J.* **13**, 708–726.

Etiope G., Ehlmann B. L. and Schoell M. (2013) Low temperature production and exhalation of methane from serpentinized rocks on Earth: A potential analog for methane production on Mars. *Icarus* **224**, 276–285.

Etiope G. and Schoell M. (2014) Abiotic Gas: Atypical, But Not Rare. *Elements* **10**, 291–296.

Falk E. S. and Kelemen P. B. (2015) Geochemistry and petrology of listvenite in the Samail ophiolite, Sultanate of Oman: Complete carbonation of peridotite during ophiolite emplacement. *Geochim. Cosmochim. Acta* **160**, 70–90.

Kelemen P. B., Matter J., Streit E. E., Rudge J. F., Curry W. B. and Blusztajn J. (2011) Rates and Mechanisms of Mineral Carbonation in Peridotite: Natural Processes and Recipes for Enhanced, in situ CO2 Capture and Storage. *Annu. Rev. Earth Planet. Sci.* **39**, 545–576.

Miller H. M., Matter J. M., Kelemen P., Ellison E. T., Conrad M. E., Fierer N., Ruchala T., Tominaga M. and Templeton A. S. (2016) Modern water/rock reactions in Oman hyperalkaline peridotite aquifers and implications for microbial habitability. *Geochim. Cosmochim. Acta* **179**, 217–241.

Paukert A. (2014) Mineral carbonation in Mantle Peridotite of the Samail Ophiolite, Oman: Implications for permanent geological carbon dioxide capture and storage. Columbia University. Available at: http://yly-mac.gps.caltech.edu/ReprintsYLY/A_RecentPapers/yung%20chen%202015%20methane-on-mars-2332-2519-1000125.pdf [Accessed June 28, 2016].

Wang D. T., Welander P. V. and Ono S. (2016) Fractionation of the methane isotopologues 13CH4, 12CH3D, and 13CH3D during aerobic oxidation of methane by Methylococcus capsulatus (Bath). *Geochim. Cosmochim. Acta* **192**, 186–202.

Weyhenmeyer C. E., Burns S. J., Waber H. N., Macumber P. G. and Matter A. (2002) Isotope study of moisture sources, recharge areas, and groundwater flow paths within the eastern Batinah coastal plain, Sultanate of Oman. *Water Resour. Res.* **38**, 1184.

Appendix B

CHAPTER 3

Low temperature hydrogen production during experimental hydration of partially-serpentinized dunite

Supporting Information

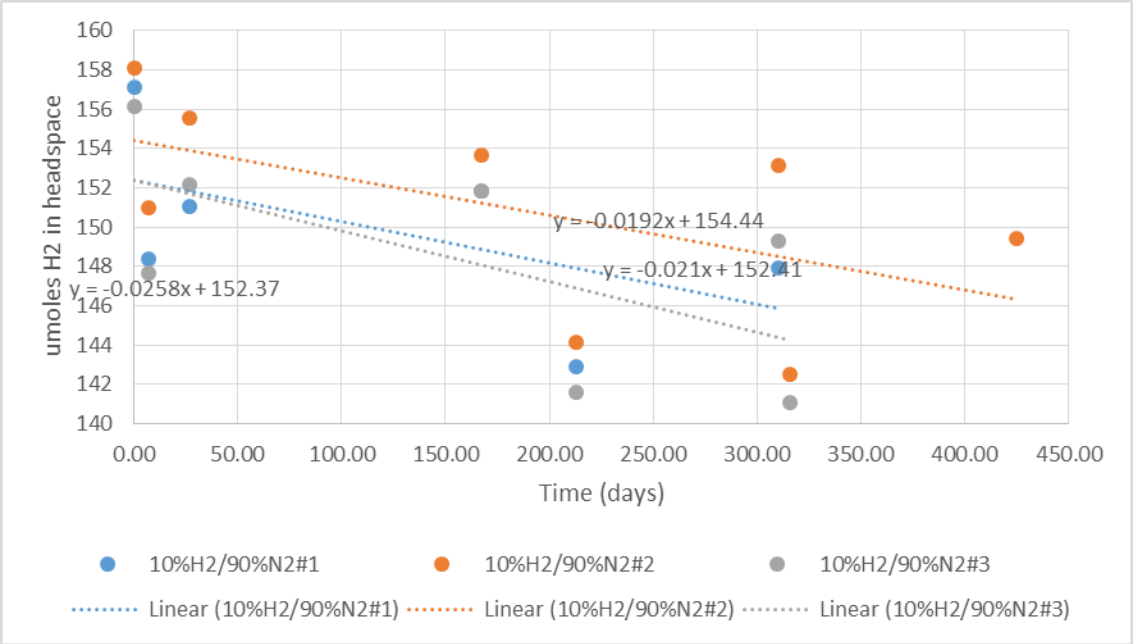

Supplementary Figure 1. Testing butyl rubber stoppers in serum vials for leaking H_2 gas. The figure shows H_2 headspace measurements over time. Regressing the data gives a slope of approximately 20 nanomoles/day H_2 loss. However, our experiments only have a maximum of 2.4 µmoles of H_2 in the headspace and fluid versus 158 µmoles tested below, thus we scaled the rate of H_2 diffusion down: (2.4 µmoles*0.00192 µmoles/day) / 158 µmoles = 0.29 nmoles/day or approximately 1 nanomole per day, which is negligible.

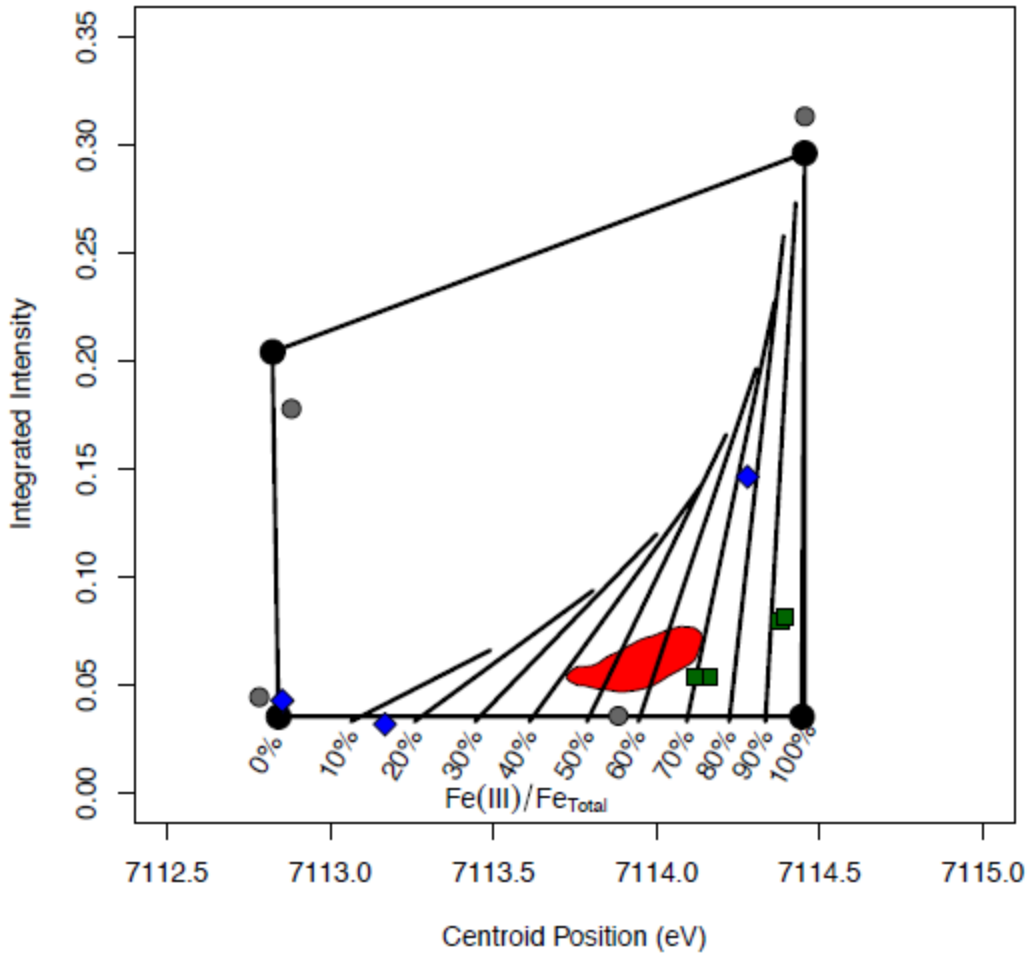

Supplementary Figure 2. Diagram depicting Fe(III) percent of Fe total as determined by calibration of Fe K-edge of pre-edge XANES centroid and intensity. Red area depicts range of variation of Fe(III) % in initial serpentine in the unreacted dunite, as determined by multiple energy pre-edge mapping of unreacted thin section. Green squares show Fe(III) % of newly precipitated serpentine in RW media. Equivalent data could not be acquired for newly precipitated serpentine in SW media due to contamination by small olivine grains and the Fe-poor nature of the precipitate. The small grey squares show the values of the standards used to tether the variogram (samples donated by Manuel Munoz, (Wilke et al., 2001; Andreani et al., 2013), along with blue diamonds used to verify the calibration (Bourdelle et al., 2013).

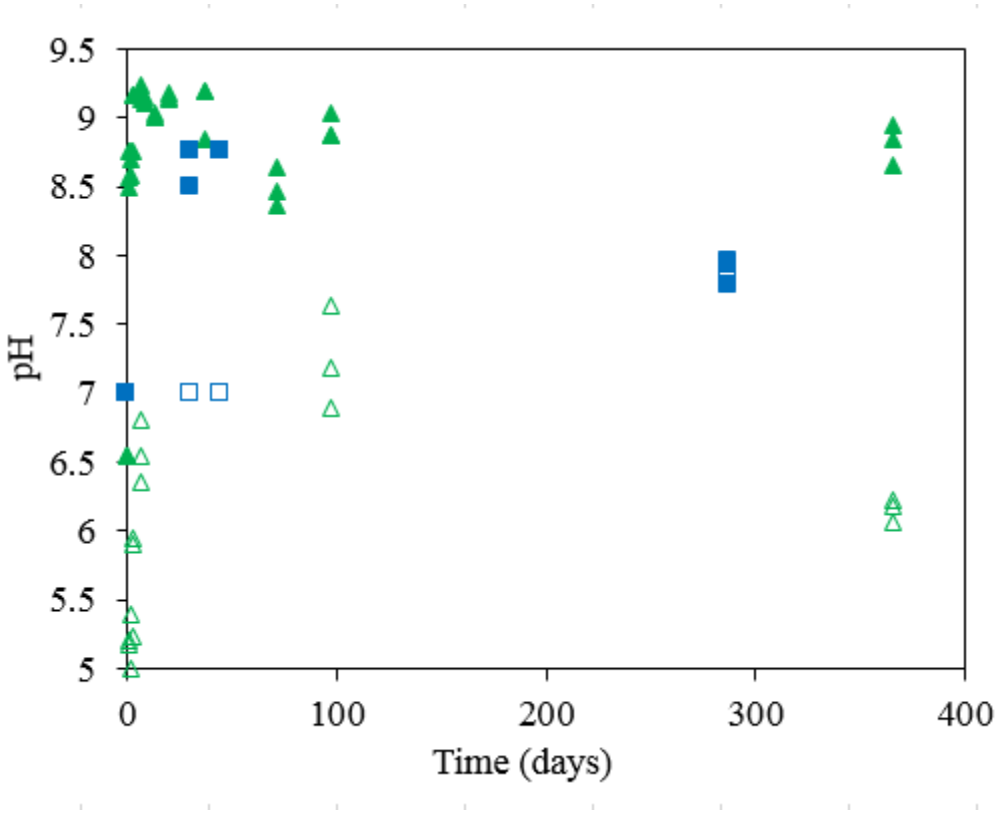

Supplementary Figure 3. pH of water/rock reactions: SW media (blue squares) and RW media (green triangles). Controls are corresponding open symbols. pH increases to 9 after 24 hours of reaction and then slowly declines.

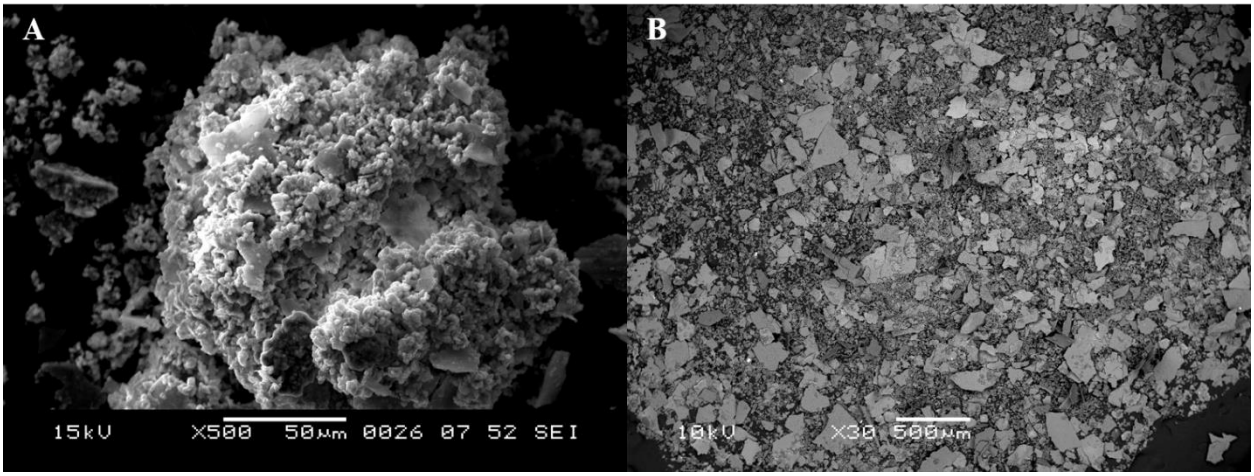

C.

	RW serpentine non-quantitative Weight %	**SW serpentine non-quantitative Weight %**
C (carbon coated)	27.38	52.84
O	32.72	30.21
Mg	10.62	7.64
Al	1.94	0.61
Si	25.56	7.00
Fe	1.79	0.97
Cl	--	0.73

Supplementary Figure 4. SEM images of precipitated serpentine forming during water/rock reactions. A: Serpentine forming in RW media. B: Serpentine forming in SW media C: Weight % of elements (collected with EDS and carbon coated) in serpentine formed during RW and SW media water/rock reactions. Carbon concentrations reflect carbon coating plus any carbon that may be in the minerals.

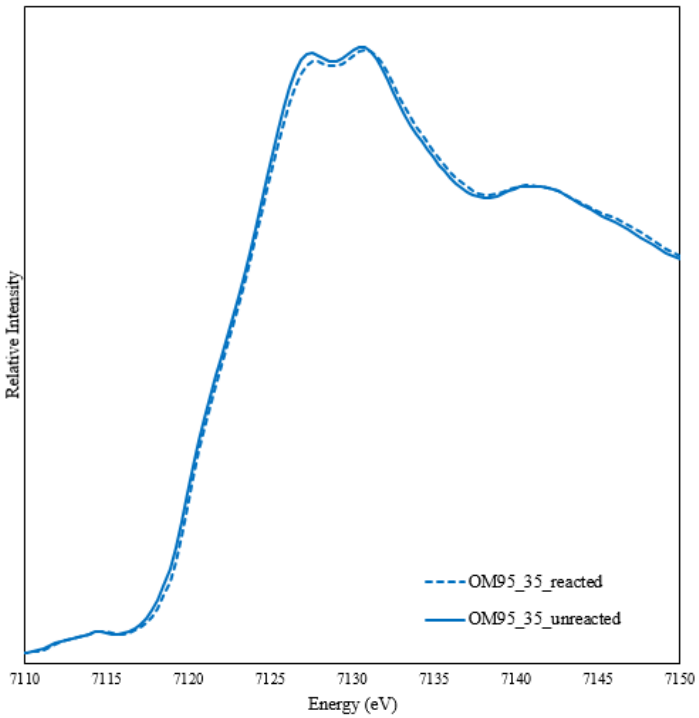

Minerals	Serpentine	Olivine	Magnetite	Brucite	Pyroxene	Sum	Energy shift	R factor
Unreacted Oman dunite	0.43	0.46	0.00	0.07	0.02	0.99	0.38	2.47E-05
RW reacted dunite	0.45	0.45	0.00	0.05	0.03	0.99	0.26	8.00E-05

Supplementary Figure 5. Bulk Fe K-edge XANES spectra of homogenized powders of unreacted and reacted grains from the RW experiments. Linear-combination fits with Fe XANES model spectra (e.g. Mayhew et al., 2011) of minerals known to be present (olivine, pyroxene, brucite, magnetite, and serpentine) show that serpentine and olivine equally make up the majority of the mineralogy in both the unreacted and RW reacted mineralogy, and there are not significant Fe-mineralogy changes post-reaction. The changes in bulk Fe speciation are small and due to the large number of Fe-bearing phases present, the bulk Fe XANES data is relatively insensitive to noted mineralogical changes, and the fits do not suggest increased magnetite and decreased brucite. The energy shift shows how the energy (eV) of the spectrum was adjusted to fit the model spectra. The model serpentine spectra include 6 different serpentine spectra from various environments and with various Fe-contents. Brucite models include 2 spectra also, the rest of the model minerals just have one representative spectrum. The R factor provides a metric for how well the fit accounts for the variability of the spectrum; for example, <1% of the spectrum is not explained by the fit.

Supplementary Table 1. Si release by serum vials measured at 100°C in artificial SW medium.

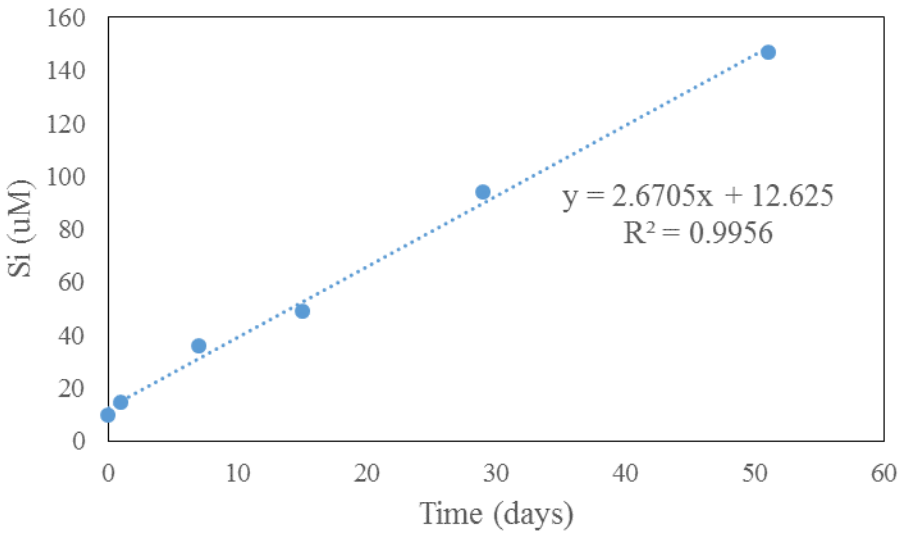

Supplementary Table 2. Carbonate quantification in unreacted and reacted samples, along with isotopic signature of evolved CO_2.

	Estimated carbonate weight %	**$d^{13}C$ (‰ VPDB)**	**$d^{13}O$ (‰ VPDB)**
Unreacted dunite	0.24	-7.14	-7.28
SW_reacted	0.11	-19.26	-18.41
RW_reacted	0.24	-22.06	-21.35

Supplementary Table 3. Average lengths of olivine grains as measured with ImageJ (Rasband, 1997) on pictures of grain mounts for unreacted, RW reacted (275 days) and SW reacted dunite (111 days). 45 grains were analyzed for each sample.

(μm)	Unreacted	SW reacted	RW reacted
Maximum length	257	231	250
Minimum length	23	50	38
Average length	99	109	109
Standard deviation	43	42	42

Supplementary Table 4. Summary of Fe(II) sources and Fe(III) sinks in the 100°C water/rock reactions, along with subsequent calculations of H_2 production compared to experimental observations. *assuming 50% of Fe in serpentine is Fe(II)

Fe(II) sources

Mineral	Mineral formula	Total mineral mass (g/mol)	wt% Fe(II) in mineral	wt % mineral in dunite	total wt% Fe(II) in 5 grams of reacting dunite	grams Fe(II) in reactant	moles Fe(II) in reactant
Olivine	$(Mg_{1.8}Fe_{0.2})SiO_4$	147.02	8.0	51	3.8E-02	1.9E-01	3.4E-03
Serpentine*	$Mg_{2.96}Fe_{0.24}Si_{1.76}O_5(OH)_4$	282.83	3.0	43	1.1E-02	5.6E-02	1.0E-03
Brucite	$(Mg_{0.86}Fe_{0.14})OH_2$	63.37	14	6.0	8.4E-03	4.2E-02	7.5E-04
					Total Fe(II) unreacted dunite	**2.9E-01**	**5.2E-03**

Fe(III) sinks

		Total mineral mass	wt % Fe(III) in mineral	wt % mineral generated in reaction	total wt% Fe(III) in 5 grams of reacted dunite	grams Fe(III)	moles Fe(III) generated
Magnetite	$Fe^{2+}Fe^{3+}Fe^{3+}O_4$	231.55	48	0.0003	1.4E-04	7.2E-04	1.3E-05
Serpentine	$(MgFe)_3Si_2O_5(OH)_4$	don't have electron microprobe data					

H_2 production via $3Fe(OH)_2 = Fe_3O_4 + H_2 + 2H_2O$

Maximum moles H_2 measured in SW	Theoretical moles Fe(III) generated	Theoretical moles Fe(II) consumed	Theoretical % Fe(II) reacted	Calculated H_2 generation from magnetite produced	Calculated moles H_2 generation from brucite consumed	H_2 sink in small weight molecular compounds
2.33E-06	4.66E-06	6.99E-06	1.35E-03	6.48E-06	2.51E-04	1.90E-06

Supplementary Table 5. Table shows carbon mass balance calculations (in moles) based on headspace concentrations of CO_2 in the RW and SW experiments and the sink of carbon in the form of organic acids and aqueous CO_2. Carbonate was not detected forming in the reactions and no organic carbon was measured with combustion techniques.

	SW experiment	RW experiment
Carbon sources		
Initial headspace CO_2 (moles)	1.7E-04	2.9E-04
Final headspace CO_2 (moles)	1.0E-06	4.1E-05
Carbon consumed		
Headspace CO_2 consumed (moles)	1.7E-04	2.5E-04
Aqueous CO_2 consumed (moles)	1.4E-04	2.1E-04
Carbon sinks		
Final aqueous total[CO_2] (moles)	8.8E-07	3.5E-06
[HCO_3^-] at pH 9 (moles)	8.4E-07	3.3E-06
CO_2 consumed by organic acids (moles)	1.9E-06	4.6E-06
Carbon mass balance		
Missing C (moles)	1.4E-04	2.0E-04
Mass of missing C (grams)	1.7E-03	2.4E-03

Appendix C

CHAPTER 4

Effects of pH, ionic strength, and temperature on hydrogen production from partially serpentinized Oman dunite

Supporting Information

Reaction vessel

This appendix summarizes efforts to create and test a new reaction vessel for conducting water/rock reactions. The deficiencies of the silica serum vials with butyl rubber stoppers are detailed in chapter 3. As a result, Dr. Lisa Mayhew and I have been working with Dr. Yehor Novikov to design a better vessel that allows for periodical gas, liquid, and mineral sampling without any H_2 or silica contamination. Lisa started working with Yehor on the design in late 2012, and I took over the project in January 2014. Progress has been slow and leaking is a pervasive problem.

Efforts to get the reaction vessel working:

January 2014: Lisa had done some testing work and seemed optimistic that I could start an experiment with the reaction vessel. Before she left, she gave Yehor the sampling head with some suggestions to change the design.

May 2014: Yehor gave me a new model, and I tested one vessel with EM medium as a control and the other with EM and Fe(0) to practice measuring H_2 from the new set-up. I ran these experiments at 100°C. Seemed to work fine but want to have another vessel so I can have a DI water control.

July 2014: Yehor made another permanent reaction head so we can have 3 working reaction vessels. I want to have a vessel to run a DI water control. The process of giving the vessel to Yehor and asking him to make more or make modifications is slow.

October 2014: Started a DI water reaction vessel experiment to ensure there is no H_2 contamination. I also added 0.391 grams of Fe filings to another vessel to test reproducibility of H_2 production. When close valve on sampling head, get slow leak out of supposedly airtight

valve…not sure if I should be concerned about this because it is unlikely to negatively affect sampling. Brought the problem up to Yehor and he thinks it will be an easy fix.

November 2014: Ran Fe(0) and DIW test for a week to make sure that not having any leaks; Fe(0) permanent head leaks, getting fixed now (only 1 out of 3 of the permanent heads is leaking). DIW test is going well, no H_2 production after over a month and doesn't appear to be leak of any gas or fluid

January 2015: I started an experiment with labeled $NaH^{13}CO_3$ and OM95_35 with N_2 in the headspace to understand carbon cycling in water/rock reactions without any contaminants, as well as verify H2 production occurs in a vessel without a butyl stopper. These experiments leaked, along with the expensive labeled $NaH^{13}CO_3$. I gave the vessels to Yehor, and he worked on figuring out the source of the leak and re-designing the vessels to fix it.

February 2015: Frustrated with reaction vessel, need to talk to Yehor about continual leaks, having troubles getting Fe-oxides cleaned completely out of the vessel, it is tricky to clean (this was before realized could put it in acid bath)

April 2015: Yehor needs to replace the plastic fitting inside the reaction vessel because they wear out over time, concerning realization. Best solution is to keep the vessel standing upright so it doesn't get mineral stuck in the fittings which can compromise them, it is challenging to replace the plastic part but Yehor ran a pressure test with the vial in water and the new fittings looked good

May 2015: Need to try something new with the reaction vessel – Yehor says "there is no precedent…it is a shot in the dark"

June 2015: Yehor is optimistic, he made 3 of the new permanent heads to test, thinks one complete vessel will cost $100

July 2015: Newly designed reaction vessel from Yehor, ran 3 blanks with Type 1 media, purged N_2:CO_2 at 100°C for 3 days before made initial gas measurement, laying on side in oven so can check for leaking

August 2015: No H_2 after tested with Type 1 media at 100°C for 3 weeks, no leaking, Lisa ordered thicker tubing so we can make larger vessels so can hold 5 grams of rock and 35 mL of fluid, ready to start ^{13}C labeled experiment

September 2015: LEAKS, I opened to start new experiment (N2:CO2, 100C, OM9535) and there was no fluid left when I originally put in 20mL of Type I media purged with N2:CO2, didn't observe a leak in the first month that I was measuring gas, so happens over time

Lisa took it into Yehor this week and the problem is probably due to the elastomer O-rings compressing, can tighten screws to fix this. We need to periodically tighten these screws (every time sample or every 2 weeks) with a torque screw driver – valve top should NOT turn just by hand without a wrench

- Bought a 5263A43 $96 torque screw driver from McMaster with 5263A324 blade, Yehor is adding 2 extra holes on vessel head so can tighten when vessel is closed
- Looking into replacing the O-ring with metal springs so can get a sustained seal without re-tightening

October 2015: Testing 2 vials purged with N2:CO2 and EM media, I shake them after filling to make sure there is no liquid leaking, tighten the screws to 5N every time use the vessel, or every 2 weeks if letting them sit

November 2015: It is problematic if you suck up some H_2O into the syringe because the water vapor makes the GC measurements seemingly inaccurate. One of the vessels might have shown some H2, but when measured it the next week was gone, not convinced doesn't leak

December 2015: I have been testing 2 reaction vessels since 10/26. I added 18mL of EM media and purged with N2:CO2, measured them 4 or 5 times, and made sure to tighten the screws at least every 2 weeks and every time after I used the vessel. Here are some troubling things I have found:

1) I observed some leaking (by observing white precipitates in the oven), but I thought it may have just been due to the fact that I accidentally drew up some liquid when gas sampling and it was user error, not the actual vessel. However, when I opened the vessel and measured the fluid remaining, I only had 10mL in a vessel I originally put 18 mL in. Not good. This vessel did retain CO2, but obviously small amounts of liquid leaked. The other vessel had the same 18mL of fluid it originally did.

2) One of the vessels had H2 in the headspace - but only every other week/sporadically, it was not consistent. This was not the vessel that was leaking. I suspect it is from zero valent iron I didn't properly clean out before...but I am not sure.

3) The liquid from both vessels had some black chunks in it, so I doubt it was completely clean before I started my experiments. This is a significant problem I have with the reaction vessel - I cleaned both of them multiple times with dilute HCl (I was under the impression we shouldn't put them in the acid bath for fear of rusting) and scraped around with various devices trying to get every nook and cranny, but it is really difficult to see if you are getting everything out even when shining a flashlight in there. I thought I cleaned everything out, but it is so hard to tell.

Yehor fixed the vessels, I soaked in HCl bath for 20 minutes (they don't fit in the sonicator well) and hopefully should be clean, testing again with 18mL of EM and purged with N2:CO2, going to make sure don't leak and the solution comes out clean

Definitely haven't leaked after ~3 weeks of testing, gas levels seem good too

Larger vessels are complete from Yehor, will conduct a short test with these, but will use the same permanent head as have already tested, so should be good

January 2016: Now have 75mL reaction vessels 20mL ones and tops work well – tested for a month with no leaking, had 18mL at start and end of experiment, kept constant CO2 levels

- Testing 35mL of EM media in 75mL vessels purged with N2:CO2, everything is designed the same, just ensuring that these permanent heads work and are designed properly
- Having trouble completely getting rid of O2 in the vessel when initially purging because not really an outlet valve…Lisa suggests purging for half an hour
- 75mL vessels seem to somewhat leak where the permanent head attaches, not sure if I am not putting them on tightly enough, talking to Yehor
- Also get some CO and CH4 made, but no H2, not sure what that means…

February 2016: Need a stronger vice to securely close the reaction vessels so they don't leak, he has one in his building, but Paul REFUSES to let us secure one in our lab. Problem still not solved.

- Want to start new experiments with 0.1M Ca(OH)2 powder mixed with grams of OM95_35, tracking pH over time, will have 2 vessels with rock + OH, one with just rock, and one with just fluid
- Use EM media and purge with N2
- Save some powder to characterize beforehand with the Ca mixed in

- Track H2 and pH over time, then look to see if brucite goes away over time
- Looking to start this soon, just waiting on the vice situation

April 2016: Started reaction vessel experiments, replicates aren't the same, had to get long enough needles to sample the fluid 8", all of the vessels appear to have a small O2 peak one the GC which is disturbing, either leaking or didn't purge properly

May 2016: EM control has an H2 peak, bad, 2 of them seem to leak sometimes, after measured EM control 5 days after saw H2 peak it was gone, trying purging the sampling head for 10 minutes now, fear I am getting some sort of leaching of something or haven't properly cleaned vials?

Currently: Yehor fixing leak problem, worried about cleaning or if they somehow leach something, maybe need to do a test with MilliQ and EM and make sure fluid chemistry stays constant.

Protocol for working with the reaction vessel (August 2016)

Starting an experiment

1. Start with a clean reaction vessel by soaking the bottom of the reaction vessel in the acid bath for 10 minutes. Do not soak the permanent or sampling head in the acid bath. Then rinse 3 times with MilliQ water and allow to dry (in the oven if want to expedite the process). Need to muffle at 550C?? Need to ask Yehor if we can
2. Add reaction substrate (e.g. Fe0, peridotite, etc.) to vessel while the permanent head is off of the vessel. Add fluid that has already been purged with N2 (or headspace gas of interest) and quickly put permanent head onto vessel. Yehor recommends not filling the vessel more than 75% full with media so that it will not become overpressurized (2 different volume vessels)

3. MUST tighten permanent head with a wrench and in a strong, non-moving vice. Need to tighten the permanent head, but not overtighten, don't need to apply much pressure, just make sure head is firmly on the vessel.
4. Attach sampling head to the vessel – make sure this is snug but only finger tight.
5. Open the valve on the permanent head with a wrench (which direction?). Open the inlet valve on the sampling head (large knob) and twist the outlet valve open (small knob). Attach a piece of small plastic tubing to the outlet and put this in a container with water to ensure that gas is exiting through the outlet. Put the 8"? gassing needle into the top of the sampling head through a tan threaded-stopper with an o-ring until it slides into the reaction vessel itself – cap with a 1mL syringe to prevent gas from escaping.
6. Turn on N2 gas so it is purging through the sampling head and through the reaction vessel body. Verify gas is flowing by looking for bubbles in water container – if don't see anything tighten stoppers, increase gas flow rate, or open valves more. Keep the gas purging for 20 minutes (need to verify the time) to completely clear the vessel of any O2. *not sure if this step is effectively removing all O2…
7. After 20 minutes, close the outlet valve so the vessel can get over-pressurized slightly. Then move the long needle up so it is no longer in the reaction vessel, and close the permanent reaction vessel head with a wrench. Tighten the 4 screws on the permanent head with the 5N screwdriver until it pops.
8. The vessel is now ready for incubation. It is good to test the tightness of the seal by allowing the vessel to lay on their side while incubating because then, with a sufficiently salty medium, you can generally see if it is leaking by the formation of salt precipitates.

Gas sampling:

For steps 1-4 make sure the main valve into the reaction vessel is CLOSED!!

1. Attach sampling head to the vessel – make sure this is snug but only finger tight
2. Start purging sampling head with N2, open outlet valve and put 8” gassing needle into top slot with the GC 1mL syringe with the green and red stopper on top to seal the sampling head except for the outlet valve. Place tubing for outlet valve in a container with water and look for bubbles to ensure that gas is moving through the system. This is to purge the air out of the sampling head, which is likely 0.5mL of space.
3. Set the regulator on the purge gas supply to a low pressure that still allows gas bubbles to come out of the outlet tubing, around 5 psi. You need to know this exact pressure to calculate the dilution of N2 gas we are putting into the reaction vessel when we sample.
4. Move the piston of the syringe up and down to force gas through the sampling head. Then fill the syringe to 0.5mL with purge gas and close the outlet valve on the sampling head. Now hold the system closed for ~20 seconds to allow the sampling head to get to 5 psi of N2 gas in all the dead space. ?any reason to close the stopper on the syringe?
5. Now that the dead space is purged with 5 psi gas, turn off the gas flow into the sampling head and close that valve. Open the permanent reaction head with a wrench and slide the sampling needle into the reaction vessel. Empty the syringe of the 0.5mL of N2 gas, then pump the syringe valve a couple of times to allow the gases to equilibrate, then sample 0.5mL of gas inside the reaction vessel, hold for 5 seconds, then close valve on syringe. Pull the gassing needle up out of the reaction vessel, then use the wrench to close the permanent head. Use the 5N screwdriver to tighten the screws. *If pressure in the reaction vessel is less than that of the sampling head, the max dilution would be 10% because if we have 5mL of headspace and allow 0.5mL of deadspace in, or if the reaction vessel pressure is larger than that of the sampling head, gas will expand to fill the extra space but the maximum dilution will be less than 10%. *
6. Inject sample into GC and put reaction vessel back in oven.

Calculating actual gas concentration in reaction vessel from dilution

There is 350 uL of dead space in sampling head, **calculate dilution factor** based off how much fluid in reaction vessel and how much headspace:

- $V_2 = V_1 (P_1/P_2)$
- V_1 : deadspace volume, 0.350mL; P_1 : pressure in sampling head, 12.2psi (atmospheric in Boulder) + pressure of N_2 coming out of tank (5psi), 17.2 psi; P_2 : atmospheric pressure in Boulder, 12.2psi
- V_2: volume of gas introduced into vessel each time sample, plus 0.5mL N_2 in purged needle
- Dilution factor = V_2/ headspace in reaction vessel (vessel is 25mL, back calculate headspace from fluid add)

Example calculation: To assess the quality and consistency of my results, I calculated the dilution factor following the procedure Yehor outlined V2 = V1*(P1/P2) so V2 = 0.5ml *(20psi/15psi)=0.667ml = volume of introduced purge gas. I decided to fill my sampling syringe with 0.5ml of purge gas that I then inject into the vessel to compensate for the 0.5ml of sample that I remove for measuring H2. Clearly, this also contributes to diluting the headspace. So, I add a total of 1.167ml purge gas to the 7ml headspace which should dilute the headspace by 16.7% each time I take a sample if I've done my math correctly.

University of Colorado
CIRES/Chemistry Instrument Design Facility
CIRES Rm. 318
Boulder, CO 80309-0216
Ph: 303-735-4727 Fax: 303-492-1149
web: http://cires.colorado.edu/IIDF/

Quotation

DATE:9/18/2015

To:Lisa Mayhew,
University of Colorado - Boulder
Department of Geological Sciences
2200 Colorado Ave. UCB 399

SALESPERSON	QUOTE NUMBER	PO NUMBER	F.O.B. POINT	TERMS
YN	15326		Destination	Net 30

Quantity	Description	Unit Price	Amount
-	Machining time, 13hr for 4 vessels	$82.00	$1066
4	Titanium alloy 2 rod 1.5"OD, 3.3" long	$31.47	$125.90
4	016 FEP O-ring McMaster 9319K16	$4.24	$16.96
4	021 FEP O-ring McMaster 9319K144	$4.24	$16.96
4	Kohler RGP77005-RP ceramic disks	$14.47	$57.88
8	Fasteners and PEEK washers	$4.54	$36.30
	Total	$330	$1320

Appendix D

CHAPTER 5

Large variability in carbon isotope fractionation by *Methanobacterium sp.* during methanogenesis at alkaline pHs

Supporting Information

Positive $\delta^{13}C$ CH_4 isotopic values produced by consortia from Oman

This appendix details how I have enriched several different methane-cycling consortia from subsurface hyperalkaline fluids in the Samail ophiolite and monitored the resultant carbon and hydrogen isotope values of the methane. These consortia were cultured under a variety of conditions, but all derive from subsurface fluids pumped from well NSHQ04. Consortia produced methane with a $\delta^{13}C_{CH4}$ that varied between 12.2 to -65‰. However, these consortia do not grow the same when transferred and grown under identical conditions, or even when growth is re-stimulated when adding nutrients. This results in varying amounts of methane produced and consumed, which gives rise to variable $\delta^{13}C_{CH4}$ values. While it appears that methane production and consumption by microbes in fluids from Oman can lead to unique carbon isotope values, we cannot yet point to the mechanism or organism behind the process. Future work needs to focus on isolating the methane-oxidizing organism(s), determining their mechanism of methane oxidation and quantifying their carbon isotope fractionation factors.

Introduction

Subsurface fluids collected from wells NSHQ04 and 14 in the Samail ophiolite in Oman contain millimolar concentrations of dissolved methane; this methane exhibits the most positive $\delta^{13}C_{CH4}$ values sampled from a serpentinizing site, -2.4 and -3‰. However, the origin of these methane in these fluids and the carbon source and formation pathway is unknown (Etiope, 2016; Miller et al., 2016). Initial 16S rRNA sequencing of DNA obtained from filtering 5-10 liters of subsurface fluid onto a 2 µm filter show well fluid (NSHQ04) contains methanogens (*Methanobacterium sp.)*, as well as methanotrophs (*Methylococcus sp.*, Miller et al., 2016). However, 16S rRNA sequencing only indicates the presence or absence of organisms, it does not give insight into the

in-situ geochemical or biological activity occurring in the subsurface. The role of microbial activity in influencing the isotopic composition of the dissolved methane in Oman needs to be assessed.

Methane is an abundant gas in serpentinizing aquifers, and it is inferred to form via abiogenic oxidation through analysis of the gas isotopic composition, since the methane exhibits a range of δD (~-350 to -100‰) and $\delta^{13}C$ (~-40 to -10‰) isotopic values distinct from common biogenic or thermogenic sources of methane (Etiope and Sherwood Lollar, 2013; Etiope et al., 2013; Etiope and Schoell, 2014). Fischer-Tropsch type or Sabatier reactions are oftentimes cited as the mechanism behind abiogenic methane formation in serpentinizing systems. These reactions can generate CH_4 through C1 compound reduction in the presence of NiFe-alloys from 200-400°C (Horita and Berndt, 1999). However, natural mineral catalysts like chromite or magnetite have not been unequivocally shown to catalyze CH_4 formation at temperatures <100°C in the laboratory (Neubeck et al., 2011; McCollom, 2013). Despite inconclusive evidence for abiogenic CH_4 formation under near-surface conditions, this is the generally accepted origin of CH_4 in serpentinizing environments.

Conversely, it is possible that microbial activity exerts an effect on the observed isotopic values of CH_4 in serpentinizing environments. Methanogenesis generally enriches the methane pool in ^{12}C, leading to more negative CH4 values than the carbon source the organisms consumed, which is discussed in detail in Chapter 5. However, methanotrophs selectively consume ^{12}C and leave behind CH_4 enriched in ^{13}C Aerobic bacterial methanotrophs have an $\alpha_{CH4\text{-}CO2}$ of 1.003 to 1.039 (Templeton et al., 2006), which leads to more positive values of $\delta^{13}C_{CH4}$ than observed from methanogenesis. Anaerobic methane oxidation likely yields similar fractionation factors with $\alpha_{CH4\text{-}CO2}$ values ranging from 1.0088-1.038 (Alperin et al., 1988; Martens et al., 1999;

Holler et al., 2009). Methane from the Cedars, an ophiolite system in California, is likely a mixture of microbial and abiogenic gas based on its $\delta^{13}C_{CH4}$ of -68‰ and its high CH_4/C_2 ratio (Morrill et al., 2013). However, methane from other ophiolite systems, Lost City, Chimaera, Zambales, Samail, and the eastern United Arab Emirates ophiolite, have $\delta^{13}C_{CH4}$ values more positive than -50‰ (Etiope et al., 2011; Etiope et al., 2013; Etiope et al., 2015; Miller et al., 2016), which is an atypical isotopic indicator of microbial activity.

The hypothesis that microorganisms are producing the isotopic signature of methane in ophiolite systems has not been seriously explored because it seems unlikely based on previous isotopic observations of microbial methane. However, the suppressed carbon fractionation factors for methanogens detailed in chapter 5 under carbon limitation at high pH make this hypothesis more feasible. Also, recent observations of CH_4 in subsurface wells in Oman associated with methane-producing and methane-oxidizing microorganisms question the traditional wisdom (Etiope, 2016; Miller et al., 2016).

Experiments

To test the hypothesis that microbial activity gives rise to the positive $\delta^{13}C_{CH4}$ observed in Oman, we stimulated diverse anaerobic microbial consortia using fluids from well NSHQ04 and investigated the microbial cycling of CH_4. We measured methane production and consumption while looking at the associated isotopic signature of CH_4. Various amendments were added to NSHQ04 fluid (Table 1) to encourage a diverse microbial consortia to grow in an attempt to closely mimic subsurface conditions. The headspace of each vial was flushed of residual site CH_4 using 80% H_2:20% CO_2 or 100% N_2 gas to ensure that the subsequently sampled isotopes of CH_4 were not from the original fluid, but instead reflected isotopic compositions resulting from

microbial activity. Initially, we randomly sampled CH_4 from enrichment cultures, to determine which cultures were producing methane and then looking for a positive $\delta^{13}C_{CH4}$ similar to that measured in the environment. When some consortia produced positive $\delta^{13}C_{CH4}$ values, we tried to discern the key nutrients and microorganisms responsible. This was not straightforward because 16S rRNA sequencing showed different bacterial species from consortia that produced similar positive $\delta^{13}C_{CH4}$ values, and there was no predominant methane-consuming organism present. In addition, when cultures exhibiting positive $\delta^{13}C_{CH4}$ values were transferred to new experimental vials to reinitiate growth and CH_4 production, the new generations cultured in the same way as their successful predecessors yielded different extents of CH_4 production, consumption and CH_4 isotopic values.

Results

We enriched ~20 consortia that produced $\delta^{13}C_{CH4}$ values ranging from 12.2‰ to -65‰. The $\delta^{13}C$ isotopic values for consortia are plotted against values for *Methanobacterium* isolated from the same fluids show significant overlap in $\delta^{13}C$ values, with an overall trend towards more positive $\delta^{13}C_{CH4}$ values in the consortia versus the relatively pure *Methanobacterium* cultures (Figure 1). Consortia growth was erratic, and it was challenging to determine the ideal growth conditions for methane producers and consumers. The growth conditions that led to the most positive $\delta^{13}C_{CH4}$ values are detailed in Table 1; they were not similar. Unfortunately, only consortia 05_gen1 and A1_gen1 had sufficient concentrations of CH_4 to also measure δD of CH_4, and those values were -262.3 and -382‰. The δD of subsurface fluids NSHQ04 is -15‰, and the δD of H_2 gas from Oman is 680‰. To give these values more environmental context, the $\delta^{13}C$ and δD values from *Methanobacterium* over a range of pHs (chapter 5) and consortia producing

a positive $\delta^{13}C$ of CH_4 are shown in Figure 2. There are more $\delta^{13}C$ isotope values from consortia (Figure 1) than shown in Figure 2 because it was challenging to measure corresponding δD values with small sample concentrations. The enrichment consortia have a wider spread of $\delta^{13}C$ and δD values than those produced by *Methanobacterium* cultures. One enrichment consortia, 05_gen1, has very similar isotope values to those of the CH_4 from wells in Oman.

During consortia growth, we have observed the reduction of orange Fe(III)-oxides to black Fe-minerals. Sulfate reduction was also measured in several vials. However, the consumption of Fe-oxides and sulfate cannot be directly linked to methane oxidation because H_2 was also present in the vials, and thus H_2-utlizing Fe-reducers and sulfate reducers may also be active. Fluids and mineral particles were also stained with Syto9 and observed under a microscope. Auto-fluorescing methanogens were observed, along with other cells and spores. Sometimes methanogens aggregated on mineral particles, but this was not a universal observation.

The methane concentrations of the consortia were monitored to investigate methane cycling. Most of the consortia produced enough CH_4 to saturate the gas chromatograph after about one month (>2 μmol/mL). However, these consortia yielded $\delta^{13}C_{CH4}$ values of -68 to -30‰, similar to *Methanobacterium* values. A few vials never became fully saturated with CH_4 (0.01 – 2 μmol/mL). These vials with low methane concentrations generally had a positive $\delta^{13}C_{CH4}$ value (Table 1). Unfortunately, sampling gas for isotopic analysis appears to perturb the consortia. Sampling generally requires 5 mL of gas from a 35 mL vial with 20 mL of headspace, which unfortunately changes the methane concentrations quite drastically, as can be seen in Figure 3. Oftentimes, sampling CH_4 appears to spur the production of more CH_4. Unfortunately, we do not have corresponding isotope data to each gas chromatograph time point due to sample volume limitations.

16S rRNA sequencing was conducted to gain insight into the microorganisms mediating these isotope fractionations (see chapter 2 for methods). Unfortunately, the consortia are complex with no clear bacterial or archaeal methane-oxidizing microorganisms dominating the population. Sequencing results for 05_gen1 reveal that *Methanobacterium* dominates the archaeal population and order Thermoanaerobacterales, family SRB2 dominates the bacterial population (Table 2). The consortium was sequenced with both archaeal primers (519F – 958R) and bacterial primers (515F – 806R); thus, it is hard to assess relative abundance of archaea to bacteria. However, sequencing of A1_gen1 enrichment shows archaeal *Methanobacterium* dominating, while the most abundant bacterial species was *Vulcanobacillus*, although 1% *Methylococcus* was detected. Once again, the archaea and bacteria were sequenced with different primers. N2form_gen1 contains *Methanobacterium*, with the main bacterial sequencing pointing to *Cupriavidus*. SO4_gen1 only contained *Cupriavidus*, despite the presence of CH_4 in the headspace. HCO3_gen 1 contains *Methanobacterium* with the main bacterial genus Effusibacillus. Thus, for the culturing efforts conducted, there are varying dominant microbial populations associated with positive $\delta^{13}C$ of CH_4 values. Sequencing shows the presence of *Methanobacterium*, a CH_4-producing organism, but there is no clear methane-consuming partner.

Discussion

Anaerobic consortia from subsurface hyperalkaline well NSHQ04 produce methane with a positive $\delta^{13}C$ of CH_4, sometimes similar to the highly enriched isotopic values of CH_4 measured from subsurface wells in the Samail ophiolite.

Growth conditions and microbial species

The growth conditions and 16S rRNA of consortia associated with positive $\delta^{13}C_{CH4}$ values vary. However, some trends do emerge. All consortia are grown in site water directly pumped from subsurface fluids in NSHQ04; they do not grow in artificial media. With regards to the microbes present, *Methanobacterium* is present in most consortia. *Methylococcus* is present in one consortium, which is surprising because *Methylococcus* is an aerobic bacteria and the consortium it was sequenced from was under anaerobic conditions in silica serum vials with butyl rubber stoppers, purged with 80%H_2:20%CO_2. Bacterial communities are diverse across the consortia. This is not surprising because the vials are rich in various electron donors and acceptors that can provide a range of organisms with abundant energy. DNA was not extracted concurrently with the shift to positive $\delta^{13}C_{CH4}$ values because there was insufficient CH_4 to sample continually. Thus, we sampled DNA at various growth stages of the consortia when the methane-cycling organisms may no longer be active or dominating.

Isotope systematics

The evolution of anaerobic methane oxidation of microbially produced CH_4 was modeled assuming a closed, irreversible system with Rayleigh distillation (see chapter 5). This model shows that the oxidation of methane produced by *Methanobacterium* cultures can lead to isotope values observed in subsurface fluids from Oman. This would have to be verified by growing cultures in the laboratory that displayed the same isotope fractionation, however, it does show the theoretical possibility of paired methanogenic and methanotrophic activity leading the anomalously positive $\delta^{13}C$ and δD values under alkaline pHs and carbon limitation.

Challenges

There are many challenges with the experimental set-up. The consortia are slow growing, and they only produce positive $\delta^{13}C_{CH4}$ values (-13 to 12.2‰) when incubated in site water from NSHQ04. A positive $\delta^{13}C_{CH4}$ has not been observed from *Methanobacterium* cultures growing in a synthetic medium that has been amended with antibiotics to suppress bacterial activity. As a result of the consortia only growing in site water, we are sample-limited and cannot grow these cultures in mass quantities. Additionally, the detection limit for CH4 using the GC-MS is ~0.02 µmol/mL, which makes it challenging to measure small concentrations of CH_4 where we suspect constant CH_4-cycling is producing positive $\delta^{13}C$ of CH_4. Sampling headspace gas for isotopic analyses slows the growth rate of the cultures and may lead to different isotopic effects than what is observed in the field system, thus it would be ideal to sample <1 mL of headspace gas. Also, it is challenging to identify the operative methane-cycling organisms through DNA extraction. We cannot label a specific methane-oxidizing species with a probe associated with a ^{13}C carbon label because we do not know what organism to target with the probe. Perhaps technique like RNA-SIP (stable isotope protocol) are feasible in this system, but rates of growth are slow, and thus it is likely ^{13}C labels would diffuse throughout the consortia. The biggest challenge is reproducibility – new cultures cannot be spurred to consistently make CH_4 with positive $\delta^{13}C$ values, and even old cultures cannot be coaxed to do so multiple times.

Conclusions

Enrichment consortia from well NSHQ04 generate CH_4 with a positive $\delta^{13}C$ of CH_4, with some values similar to CH_4 collected from the field. The isotopic signature is not produced solely through methane production by *Methanobacterium*, but in a consortia that grows in fluid from well NSHQ04 that is amended with either Fe-oxides, sulfate or formate. It is unclear if there is

concurrent CH_4 production and consumption in the consortia; the continual geochemical and isotope measurements necessary to verify this process are challenging because they require large volumes of gas from a small headspace. Also, it is important to perform these experiments without any H_2 present to ensure we are observing direct oxidation of CH_4. Despite the uncertainty regarding the organisms responsible and the exact isotopic progression leading to isotopically unusual CH4, the observations from these consortia provide an important window into methane cycling in the hyperalkaline Oman ophiolite and should generate vigourous debate about the ongoing interpretation of "abiogenic" methane isotopic values in serpentinizing systems.

References

Alperin M. J., Reeburgh W. S. and Whiticar M. J. (1988) Carbon and hydrogen isotope fractionation resulting from anaerobic methane oxidation. *Glob. Biogeochem. Cycles* **2**, 279–288.

Etiope G. (2016) Methane origin in the Samail ophiolite: Comment on "Modern water/rock reactions in Oman hyperalkaline peridotite aquifers and implications for microbial habitability." *Geochim. Cosmochim. Acta*, 217–241.

Etiope G., Ehlmann B. L. and Schoell M. (2013) Low temperature production and exhalation of methane from serpentinized rocks on Earth: A potential analog for methane production on Mars. *Icarus* **224**, 276–285.

Etiope G., Judas J. and Whiticar M. J. (2015) Occurrence of abiotic methane in the eastern United Arab Emirates ophiolite aquifer. *Arab. J. Geosci.* **8**, 11345–11348.

Etiope G. and Schoell M. (2014) Abiotic Gas: Atypical, But Not Rare. *Elements* **10**, 291–296.

Etiope G., Schoell M. and Hosgörmez H. (2011) Abiotic methane flux from the Chimaera seep and Tekirova ophiolites (Turkey): Understanding gas exhalation from low temperature serpentinization and implications for Mars. *Earth Planet. Sci. Lett.* **310**, 96–104.

Etiope G. and Sherwood Lollar B. (2013) Abiotic Methane on Earth. *Rev. Geophys.* **51**, 276–299.

Holler T., Wegener G., Knittel K., Boetius A., Brunner B., Kuypers M. M. M. and Widdel F. (2009) Substantial 13C/12C and D/H fractionation during anaerobic oxidation of methane by marine consortia enriched in vitro. *Environ. Microbiol. Rep.* **1**, 370–376.

Horita J. and Berndt M. E. (1999) Abiogenic Methane Formation and Isotopic Fractionation Under Hydrothermal Conditions. *Science* **285**, 1055–1057.

Martens C. S., Albert D. B. and Alperin M. J. (1999) Stable isotope tracing of anaerobic methane oxidation in the gassy sediments of Eckernforde Bay, German Baltic Sea. *Am. J. Sci.* **299**, 589–610.

McCollom T. M. (2013) Laboratory Simulations of Abiotic Hydrocarbon Formation in Earth's Deep Subsurface. *Rev. Mineral. Geochem.* **75**, 467–494.

Miller H. M., Matter J. M., Kelemen P., Ellison E. T., Conrad M. E., Fierer N., Ruchala T., Tominaga M. and Templeton A. S. (2016) Modern water/rock reactions in Oman hyperalkaline peridotite aquifers and implications for microbial habitability. *Geochim. Cosmochim. Acta* **179**, 217–241.

Morrill P. L., Kuenen J. G., Johnson O. J., Suzuki S., Rietze A., Sessions A. L., Fogel M. L. and Nealson K. H. (2013) Geochemistry and geobiology of a present-day serpentinization site in California: The Cedars. *Geochim. Cosmochim. Acta* **109**, 222–240.

Neubeck A., Duc N. T., Bastviken D., Crill P. and Holm N. G. (2011) Formation of H2 and CH4 by weathering of olivine at temperatures between 30 and 70 C. *Geochem. Trans.* **12**, 6.

Templeton A. S., Chu K.-H., Alvarez-Cohen L. and Conrad M. E. (2006) Variable carbon isotope fractionation expressed by aerobic CH4-oxidizing bacteria. *Geochim. Cosmochim. Acta* **70**, 1739–1752.

Table 1. Growth conditions for NSHQ04 consortia generating positive $\delta^{13}C$ of CH_4 values.

Sample name	CH_4 $\delta^{13}C_{VPDB}$ (‰)	δD_{CH4} (‰)	Days growing	Nutrients added	Headspace, medium	Vitamins and minerals	pH, T (°C)
A1_gen1	12.2	-382	59	1 mL 100 mM formate, 0.1 mL Fe(III) oxides, 1 mL Oman dunite crushings	80% H2:20%CO2; site water		6.55, 40
N2formate_gen1	-7.07	bd	123	1 mL 100 mM formate	100%N2, site water		8.45, 40
HCO3_gen1	-13.55	bd	63	1mL 24 mM NaHCO3, 50 uL Fe(III) oxides	100%N2, site water	50 µL formulation for DSMZ 141	7.79, 40
05_gen1	1.05	-262.3	428	1 mL 100 mM formate, 0.1 mL Fe(III) oxides, 1 mL Oman dunite crushings	80% H2:20%CO2; site water		7.53, 40
SO4_gen1	-12.75	bd	318	1mL 100 mM formate, 0.1 mL Fe(III) oxides, 1 mL Oman dunite crushings, 1 mL 50 mM MgSO4	80% H2:20%CO2; site water		NA, 40

Table 2. 16S rRNA sequencing results for 5 consortia producing positive $\delta^{13}C$ of CH_4. If archaea and bacteria were sequenced with different primers, that is indicated. OTUs with abundance 5% and over are noted. If an OTU less than 5% is listed, that is to show the presence of *Methanobacterium* or *Methylococcus*.

HCO3_gen1 $\delta^{13}C$ of CH_4: -13.55‰ δD CH_4: bd

16S rRNA Archaea; 519F-958R

Percent OTUs	*Domain*	*Phyla*	*Class*	*Order*	*Family*	*Genus*
54%	Archaea	Euryarchaeota	Methanobacteria	Methanobacteriales	Methanobacteriaceae	Methanobacterium
2%	Archaea	Thaumarchaeota	Soil_Crenarchaeotic_Group(SCG)	Unknown_Order	Unknown_Family	Candidatus_Nitrososphaera

16S rRNA Bacteria; 515F-806R

48%	Bacteria	Firmicutes	Bacilli	Bacillales	Alicyclobacillaceae	Effusibacillus
10%	Bacteria	Firmicutes	Clostridia	Clostridiales	Family_XVIII	Family_XVIII_unclassified
6%	Bacteria	Firmicutes	Bacilli	Bacillales	Bacillaceae	Bacillus
5%	Bacteria	Firmicutes	Bacilli	Bacillales	Alicyclobacillaceae	Effusibacillus

05_gen1 $\delta^{13}C$ of CH_4: 1.05‰ δD CH_4: -262.3‰

16S rRNA Archaea; 519F-958R

Percent OTUs	*Domain*	*Phyla*	*Class*	*Order*	*Family*	*Genus*
38%	Archaea	Euryarchaeota	Methanobacteria	Methanobacteriales	Methanobacteriaceae	Methanobacterium
5%	Archaea	Thaumarchaeota	Soil_Crenarchaeotic_Group(SCG)	Unknown_Order	Unknown_Family	Candidatus_Nitrososphaera
5%	Archaea	Thaumarchaeota	Soil_Crenarchaeotic_Group(SCG)	uncultured_crenarchaeote	uncultured_crenarchaeote_unclassified	uncultured_crenarchaeote_unclassified

16S rRNA Bacteria; 515F-806R

20%	Bacteria	Firmicutes	Clostridia	Thermoanaerobacterales	SRB2	SRB2_unclassified
11%	Bacteria	Firmicutes	Clostridia	Clostridiales	Christensenellaceae	Christensenellaceae_uncultured
10%	Bacteria	Firmicutes	Clostridia	Halanaerobiales	Halobacteroidaceae	Halobacteroidaceae_unclassified

A1_gen1 $\delta^{13}C$ of CH_4: 12.2‰ δD CH_4: -382‰

16S rRNA Archaea; 519F-958R

Percent OTUs	*Domain*	*Phyla*	*Class*	*Order*	*Family*	*Genus*
59%	Archaea	Euryarchaeota	Methanobacteria	Methanobacteriales	Methanobacteriaceae	Methanobacterium

16S rRNA Bacteria; 515F-806R

22%	Bacteria	Firmicutes	Bacilli	Bacillales	Bacillaceae	Vulcanibacillus
13%	Bacteria	Firmicutes	Clostridia	Clostridiales	Clostridiaceae_1	Clostridiaceae_1_unclassified
7%	Bacteria	Deinococcus-Thermus	Deinococci	Thermales	Thermaceae	Meiothermus
1%	Bacteria	Proteobacteria	Gammaproteobacteria	Methylococcales	Methylococcaceae	Methylococcus

SO4_gen1 $\delta^{13}C$ of CH_4: -12.75‰ δD CH_4: bd

16S rRNA; 515F-806R

Percent OTUs	*Domain*	*Phyla*	*Class*	*Order*	*Family*	*Genus*
71%	Bacteria	Proteobacteria	Betaproteobacteria	Burkholderiales	Oxalobacteraceae	Cupriavidus

N2form_gen1 $\delta^{13}C$ of CH_4: -7.07‰ δD CH_4: bd

16S rRNA; 515F-806R

Percent OTUs	*Domain*	*Phyla*	*Class*	*Order*	*Family*	*Genus*
73%	Bacteria	Proteobacteria	Betaproteobacteria	Burkholderiales	Oxalobacteraceae	Cupriavidus
3%	Archaea	Euryarchaeota	Methanobacteria	Methanobacteriales	Methanobacteriaceae	Methanobacterium

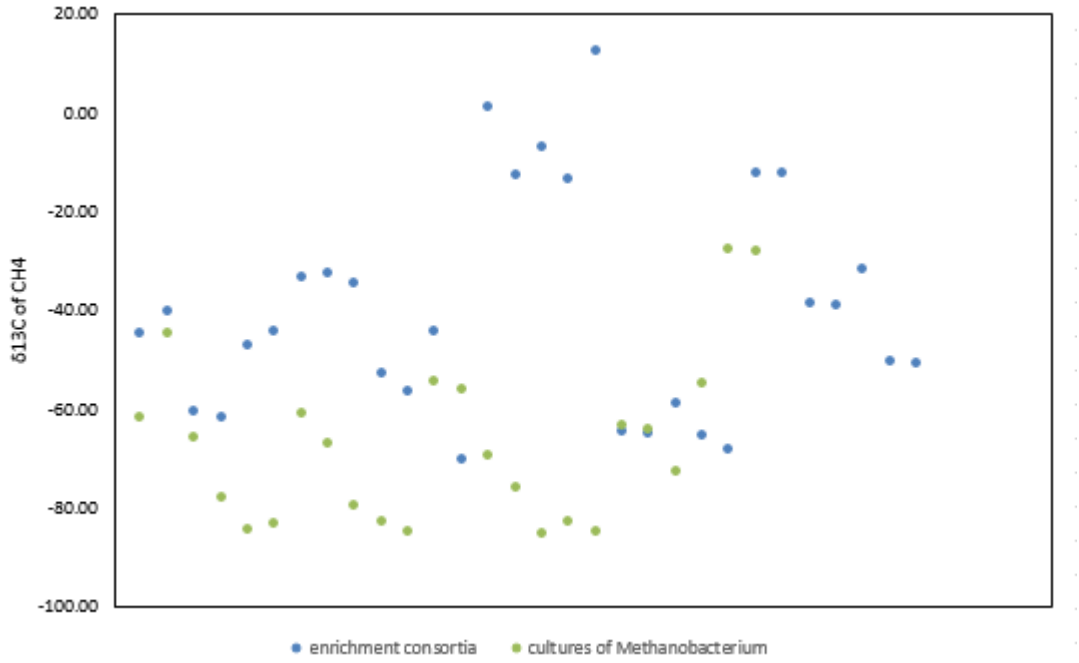

Figure 1. Blue circles show positive $\delta^{13}C$ of CH_4 values measured from NSH04 site water enrichment consortia grown under various conditions detailed in Table 1. Green circles $\delta^{13}C$ of CH_4 values generated by *Methanobacterium*, isolated from NSHQ04 site water.

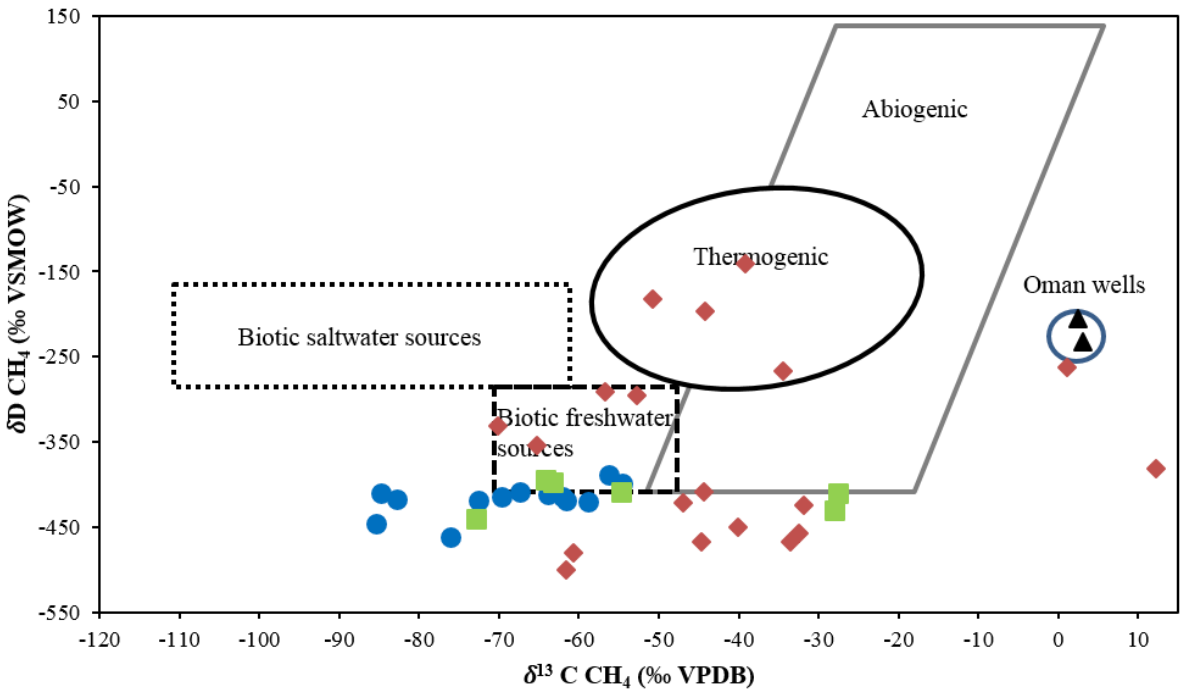

Figure 2. Diagram showing traditional range of $\delta^{13}C$ and δD CH_4 isotopes, adopted from Etiope and Whiticar. Green squares show CH_4 isotope data from Methanobacterium growing with CaCO3 as carbon source, blue circles show Methanobacterium growing with NaHCO3 as a carbon source. Red diamonds show CH_4 isotope values from various NSHQ04 consortia. There are more $\delta^{13}C$ isotope values from consortia than shown in the figure, but there are not corresponding δD values due to small sample concentrations. Black triangles represent CH_4 sampled from wells NSHQ04 and NSHQ14 in January 2014 (Miller et al. 2016). The fields denoted (e.g. thermogenic, abiogenic, etc.) represent average values from the literature, thus slight deviations outside these fields should not be considered significant.

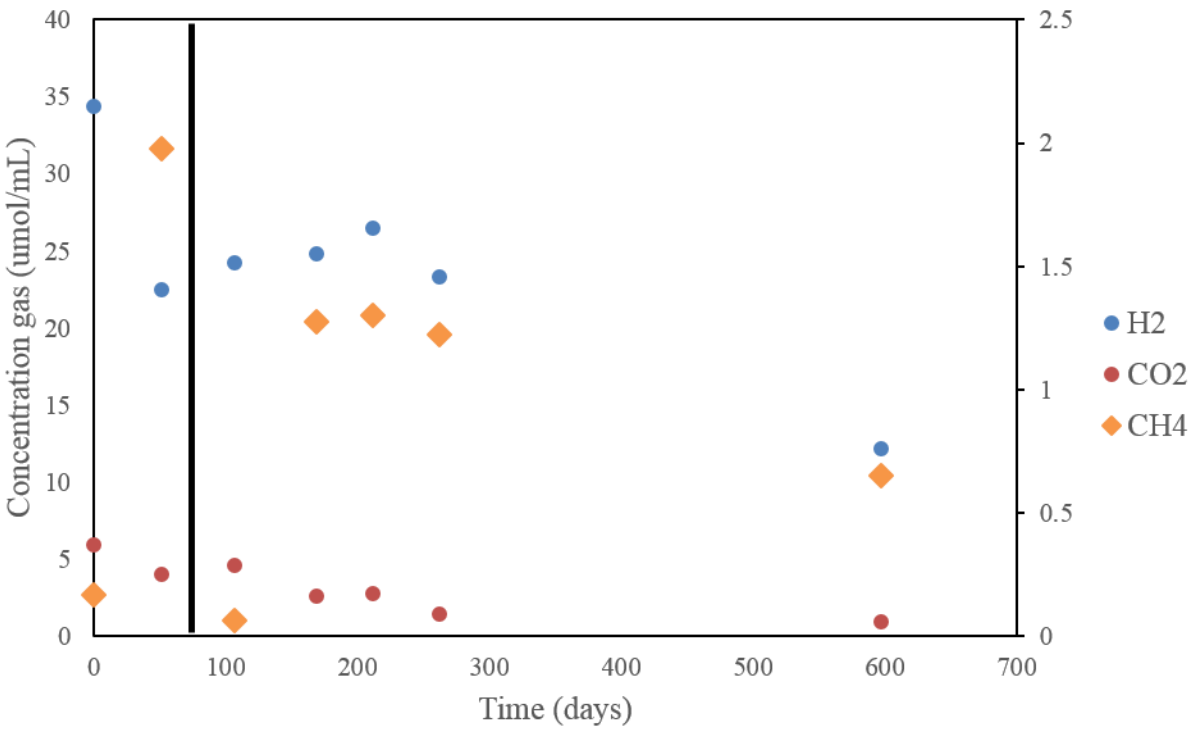

Figure 3. Gas concentrations (µmol/mL) of enrichment A1_gen1 over lifetime of experiment. Black line indicates where gas was sampled for isotopic analysis, resulting in lower CH_4 concentrations. Concentrations of CH_4 eventually rebound after gas sampling, and H_2 and CO_2 concentrations do not seem affected by sampling.